

e-ISSN 1308-8459

Official Publication of the Turkish Society of Anatomy and Clinical Anatomy

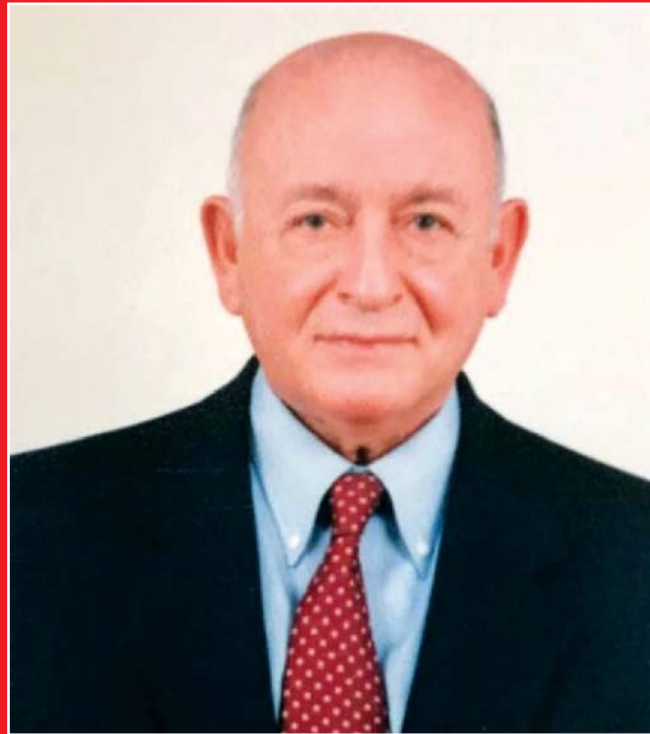
<https://dergipark.org.tr/tr/pub/anatomy>

anatomy

An International Journal of Experimental and Clinical Anatomy

Volume 15 / Issue 1 / April 2021

Published three times a year



deomed®

anatomy

An International Journal of Experimental and Clinical Anatomy

Official Publication of the Turkish Society of Anatomy and Clinical Anatomy

Aim and Scope

Anatomy, an international journal of experimental and clinical anatomy, is a peer-reviewed journal published three times a year with an objective to publish manuscripts with high scientific quality from all areas of anatomy. The journal offers a forum for anatomical investigations involving gross, histological, developmental, neurological, radiological and clinical anatomy, and anatomy teaching methods and techniques. The journal is open to original papers covering a link between gross anatomy and areas related with clinical anatomy such as experimental and functional anatomy, neuroanatomy, comparative anatomy, modern imaging techniques, molecular biology, cell biology, embryology, morphological studies of veterinary discipline, and teaching anatomy. The journal is currently indexing and abstracting in TUBITAK ULAKBIM Turkish Medical Index, Proquest, EBSCO Host, Index Copernicus and Google Scholar.

Publication Ethics

Anatomy is committed to upholding the highest standards of publication ethics and observes the principles of Journal's Publication Ethics and Malpractice Statement which is based on the recommendations and guidelines for journal editors developed by the Committee on Publication Ethics (COPE), Council of Science Editors (CSE), World Association of Medical Editors (WAME) and International Committee of Medical Journal Editors (ICMJE). For detailed information please visit the online version of the journal which is available at <https://dergipark.org.tr/tr/pub/anatomy>

Authorship

All persons designated as authors should have participated sufficiently in the work to take public responsibility for the content of the manuscript. Authorship credit should be based on substantial contributions to (1) conception and design or analysis and interpretation of data, (2) drafting of the manuscript or revising it for important intellectual content and, (3) final approval of the version to be published. The Editor may require the authors to justify assignment of authorship. In the case of collective authorship, the key persons responsible for the article should be identified and others contributing to the work should be recognized with proper acknowledgment.

Copyright

Copyright © 2021, by the Turkish Society of Anatomy and Clinical Anatomy, TSACA. All rights reserved. No part of this publication may be reproduced, stored or transmitted in any form without permission in writing from the copyright holder beforehand, exceptionally for research purpose, criticism or review. The publisher and the Turkish Society of Anatomy and Clinical Anatomy assume no liability for any material published in the journal. All statements are the responsibility of the authors. Although all advertising material is expected to conform ethical standards, inclusion in this publication does not constitute a guarantee or endorsement of the quality or value of such product or of the claims made of it by its manufacturer. Permission requests should be addressed to the publisher.

Publisher

Deomed Publishing
Gür Sok. No:7/B Kadıköy, İstanbul, Turkey
Phone: +90 216 414 83 43 (Pbx) / Fax: +90 216 414 83 42
www.deomed.com / e-mail: medya@deomed.com

deomed®

Publication Information

Anatomy (e-ISSN 1308-8459) as an open access electronic journal is published by Deomed Publishing, İstanbul, for the Turkish Society of Anatomy and Clinical Anatomy, TSACA. Due the Press Law of Turkish Republic dated as June 26, 2004 and numbered as 5187, this publication is classified as a periodical in English language.

Ownership

On behalf of the Turkish Society of Anatomy and Clinical Anatomy, Ahmet Kağan Karabulut, MD, PhD; Konya

Editor-in-Chief

Nihal Apaydin, MD
Department of Anatomy,
Faculty of Medicine, Ankara University,
06100, Sıhhiye, Ankara, Turkey
Phone: 0090 312 595 82 48
e-mail: napaydin@gmail.com; napaydin@medicine.ankara.edu.tr

Administrative Office

Güven Mah. Güvenlik Cad. Onlar Ap. 129/2 Aşağı Ayrancı, Ankara
Phone: +90 312 447 55 52-53

Submission of Manuscripts

Manuscripts should be submitted at our manuscript submission and information portal <https://dergipark.org.tr/en/pub/anatomy>

Categories of Articles

- **Original Articles** describe substantial original research that falls within the scope of the Journal.
- **Teaching Anatomy** section contains regular or all formats of papers which are relevant to comparing teaching models or to introducing novel techniques, including especially the own experiences of the authors.
- **Reviews** section highlights current development in relevant areas of anatomy. The reviews are generally invited; other prospective authors should consult with the Editor-in-Chief.
- **Case Reports** include new, noteworthy or unusual cases which could be of help for basic notions and clinical practice.
- **Technical Note** articles cover technical innovations and developments with a specific technique or procedure or a modification of an existing technique. They should be sectioned like an original research article but not exceed 2000 words.
- **Viewpoint** articles give opinions on controversial topics or future projections, some of these are invited.
- **Historical View** category presents overview articles about historical sections from all areas of anatomy.
- **Terminology Zone** category is a platform for the articles which discuss some terminological controversies or opinions.

The categories above are peer-reviewed. They should include abstract and keywords. There are also categories including Letters to the Editor, Book Reviews, Abstracts, Obituary, News and Announcements which do not require a peer review process.

For detailed instructions concerning the submission of manuscripts, please refer to the Instructions to Authors.

Advertising and Reprint Requests

Please direct to publisher. e-mail: medya@deomed.com

Honorary Editor

Doğan Akşit, Ankara, Turkey

Founding Editors

Salih Murat Akkın, Gaziantep, Turkey

Hakan Hamdi Çelik, Ankara, Turkey

Former Editors-in-Chief and Advising Editors

Salih Murat Akkın (2007-2013)
Gaziantep, Turkey

Gülgün Şengül (2014-2019)
Izmir, Turkey

Editor-in-Chief

Nihal Apaydın, Ankara, Turkey

Editors

Zeliha Kurtoğlu Olgunus, Mersin, Turkey

Luis Puelles, Murcia, Spain

Mustafa F. Sargon, Ankara, Turkey

Gülgün Şengül, Izmir, Turkey

Shane Tubbs, Birmingham, AL, USA

Emel Ulupınar, Eskişehir, Turkey

Associate Editors

Vaclav Baca, Prague, Czech Republic

Çağatay Barut, Istanbul, Turkey

Jon Cornwall, Dunedin, New Zealand

Ayhan Cömert, Ankara, Turkey

Mirela Eric, Novi Sad, Serbia

Georg Feigl, Graz, Austria

Quentin Fogg, Melbourne, Australia

David Kachlik, Prague, Czech Republic

Marko Korschake, Innsbruck, Austria

Scott Lozanoff, Honolulu, HI, USA

Levent Sarıkçıoğlu, Antalya, Turkey

Cristian Stefan, Boston, MA, USA

İlkan Tatar, Ankara, Turkey

Trifon Totlis, Thessaloniki, Greece

Executive Board of Turkish Society of Anatomy and Clinical Anatomy

Esat Adıgüzel (President)

Çağatay Barut (Vice President)

Zeliha Kurtoğlu Olgunus (Vice President)

Piraye Kervancıoğlu (Secretary General)

Ayhan Cömert (Treasurer)

İlke Ali Gürses (Vice Treasurer)

Nadire Ünver Doğan (Member)

Scientific Advisory Board

Peter H. Abrahams
Cambridge, UK

Halil İbrahim Açar
Ankara, Turkey

Marian Adamkov
Martin, Slovakia

Esat Adıgüzel
Denizli, Turkey

Mustafa Aktekin
Istanbul, Turkey

Mahindra Kumar Anand
Gujarat, India

Serap Arbak
Istanbul, Turkey

Alp Bayramoğlu
Istanbul, Turkey

Brion Benninger
Lebanon, OR, USA

Susana Biasutto
Cordoba, Argentina

Dragica Bobinac
Rijeka, Croatia

David Bolender
Milwaukee, WI, USA

Eric Brenner
Innsbruck, Austria

Mustafa Büyükmumcu
Konya, Turkey

Richard Halti Cabral
Sao Paulo, Brazil

Safiye Çavdar
Istanbul, Turkey

Katharina D'Herde
Ghent, Belgium

Fabrice Duparc
Rouen, France

Behice Durgun
Adana, Turkey

İzzet Duyar
Istanbul, Turkey

Mete Ertürk
Izmir, Turkey

Reha Erzurumlu
Baltimore, MD, USA

Ali Firat Esmir
Ankara, Turkey

António José Gonçalves Ferreira
Lisboa, Portugal

Christian Fontaine
Lille, France

Figen Gövsa Gökmen
Izmir, Turkey

Rod Green
Bendigo, Australia

Bruno Grignon
Nancy Cedex, France

Nadir Gülekon
Ankara, Turkey

Mürvet Hayran
Izmir, Turkey

David Heylings
Norwich, UK

Lazar Jelev
Sofia, Bulgaria

Samet Kapakin
Erzurum, Turkey

Ahmet Kağan Karabulut
Konya, Turkey

S. Tuna Karahan
Ankara, Turkey

Simel Kendir
Ankara, Turkey

Piraye Kervancıoğlu
Gaziantep, Turkey

Hee-Jin Kim
Seoul, Korea

Necdet Kocabiyik
Ankara, Turkey

Cem Kopuz
Samsun, Turkey

Mustafa Ayberk Kurt
Istanbul, Turkey

Marios Loukas
Grenada, West Indies

Veronica Macchi
Padua, Italy

Petru Matusz
Timisoara, Romania

Ali Mirjalili
Auckland, New Zealand

Bernard Moxham
Cardiff, Wales, UK

Konstantinos Natsis
Thessaloniki, Greece

Lia Lucas Neto
Lisbon, Portugal

Helen Nicholson
Dunedin, New Zealand

Davut Özbağ
Malatya, Turkey

P. Hande Özdinler
Chicago, IL, USA

Adnan Öztürk
Istanbul, Turkey

Mehmet Hakan Öztürk
Mersin, Turkey

Friedrich Paulsen
Erlangen, Germany

Wojciech Pawlina
Rochester, MN, USA

Tuncay Veysel Peker
Ankara, Turkey

Vid Persaud
Winnipeg, MB, Canada

David Porta
Louisville, KY, USA

Jose Ramon Sanudo
Madrid, Spain

Tatsuo Sato
Tokyo, Japan

Mohammadali M. Shoja
Birmingham, AL, USA

Ahmet Sinav
Istanbul, Turkey

Takis Skandalakis
Athens, Greece

Isabel Stabile
Malta

Vildan Sümbüloğlu
Gaziantep, Turkey
(*Biostatistics*)

Muzaffer Şeker
Konya, Turkey

Erdoğan Şendemir
Bursa, Turkey

İbrahim Tekdemir
Ankara, Turkey

Hironubu Tokuno
Tokyo, Japan

Mehmet İbrahim Tuğlu
Manisa, Turkey

Selçuk Tunalı
Ankara, Turkey

Uğur Türe
Istanbul, Turkey

Aysun Uz
Ankara, Turkey

Mehmet Üzel
Istanbul, Turkey

Ivan Varga
Bratislava, Slovakia

Tuncay Varol
Manisa, Turkey

Stephanie Woodley
Otago, New Zealand

Bülent Yalçın
Ankara, Turkey

Gazi Yaşargil
Istanbul, Turkey

Hiroshi Yorifuji
Gunma, Japan

Anatomy, an international journal of experimental and clinical anatomy, is the official publication of the Turkish Society of Anatomy and Clinical Anatomy, TSACA. It is a peer-reviewed e-journal that publishes scientific articles in English. For a manuscript to be published in the journal, it should not be published previously in another journal or as full text in congress books and should be found relevant by the editorial board. Also, manuscripts submitted to Anatomy must not be under consideration by any other journal. Relevant manuscripts undergo conventional peer review procedure (at least three reviewers). For the publication of accepted manuscripts, author(s) should reveal to the Editor-in-Chief any conflict of interest and transfer the copyright to the Turkish Society of Anatomy and Clinical Anatomy, TSACA.

In the Materials and Methods section of the manuscripts where experimental studies on humans are presented, a statement that informed consent was obtained from each volunteer or patient after explanation of the procedures should be included. This section also should contain a statement that the investigation conforms with the principles outlined in the appropriate version of 1964 Declaration of Helsinki. For studies involving animals, all work must have been conducted according to applicable national and international guidelines. Prior approval must have been obtained for all protocols from the relevant author's institutional or other appropriate ethics committee, and the institution name and permit numbers must be provided at submission.

Anatomical terms used should comply with Terminologia Anatomica by FCAT (1998).

No publication cost is charged for the manuscripts but reprints and color printings are at authors' cost.

Preparation of manuscripts

During the preparation of the manuscripts, uniform requirements of the International Committee of Medical Journal Editors, a part of which is stated below, are valid (see ICMJE). Uniform requirements for manuscripts submitted to biomedical journals. Updated content is available at www.icmje.org. The manuscript should be typed double-spaced on one side of a 21x29.7 cm (A4) blank sheet of paper. At the top, bottom and right and left sides of the pages a space of 2.5 cm should be left and all the pages should be numbered except for the title page.

Manuscripts should not exceed 15 pages (except for the title page). They must be accompanied by a cover letter signed by corresponding author and the Conflicts of Interest Disclosure Statement and Copyright Transfer Form signed by all authors. The contents of the manuscript (original articles and articles for Teaching Anatomy category) should include: 1- Title Page, 2- Abstract and Keywords, 3- Introduction, 4- Materials and Methods, 5- Results, 6- Discussion (Conclusion and/or Acknowledgement if necessary), 7- References

Title page

In all manuscripts the title of the manuscript should be written at the top and the full names and surnames and titles of the authors beneath. These should be followed with the affiliation of the author. Manuscripts with long titles are better accompanied underneath by a short version (maximum 80 characters) to be published as running head. In the title page the correspondence address and telephone, fax and e-mail should be written. At the bottom of this page, if present, funding sources supporting the work should be written with full names of all funding organizations and grant numbers. It should also be indicated in a separate line if the study has already been presented in a congress or likewise scientific meeting. Other information such as name and affiliation are not to be indicated in pages other than the title page.

Abstract

Abstract should be written after the title in 100–250 words. In original articles and articles prepared in IMRAD format for Teaching Anatomy category the abstract should be structured under sections Objectives, Methods, Results and Conclusion. Following the abstract at least 3 keywords should be added in alphabetical order separated by semicolons.

References

Authors should provide direct references to original research sources. References should be numbered consecutively in square brackets, according to the order in which they are first mentioned in the manuscript. They should follow the standards detailed in the NLM's Citing Medicine, 2nd edition (Citing medicine: the NLM style guide for authors, editors, and publishers [Internet]. 2nd edition. Updated content is available at www.ncbi.nlm.nih.gov/books/NBK7256). The names of all contributing authors should be listed, and should be in the order they appear in the original reference. The author is responsible for the accuracy and completeness of references. When necessary, a copy of a referred article can be requested from the author. Journal names should be abbreviated as in *Index Medicus*. Examples of main reference types are shown below:

- **Journal articles:** Author's name(s), article title, journal title (abbreviated), year of publication, volume number, inclusive pages
 - *Standard journal article:* Sargon MF, Celik HH, Aksit MD, Karaagaoglu E. Quantitative analysis of myelinated axons of corpus callosum in the human brain. *Int J Neurosci* 2007;117:749–55.

- *Journal article with indication article published electronically before print:* Sengul G, Fu Y, Yu Y, Paxinos G. Spinal cord projections to the cerebellum in the mouse. *Brain Struct Funct* Epub 2014 Jul 10. DOI 10.1007/s00429-014-0840-7.
- **Books:** Author's name(s), book title, place of publication, publisher, year of publication, total pages (entire book) or inclusive pages (contribution to a book or chapter in a book)
 - *Entire book:*
 - *Standard entire book:* Sengul G, Watson C, Tanaka I, Paxinos G. Atlas of the spinal cord of the rat, mouse, marmoset, rhesus and human. San Diego (CA): Academic Press Elsevier; 2013. 360 p.
 - *Book with organization as author:* Federative Committee of Anatomical Terminology (FCAT). Terminologia anatomica. Stuttgart: Thieme; 1998. 292 p.
 - *Citation to a book on the Internet:* Bergman RA, Afifi AK, Miyauchi R. Illustrated encyclopedia of human anatomic variation. Opus I: muscular system [Internet]. [Revised on March 24, 2015] Available from: <http://www.anatomyatlases.org/AnatomicVariants/AnatomyHP.shtml>
 - *Contribution to a book:*
 - *Standard reference to a contributed chapter:* Potten CS, Wilson JW. Development of epithelial stem cell concepts. In: Lanza R, Gearhart J, Blau H, Melton D, Moore M, Pedersen R, Thomson J, West M, editors. Handbook of stem cell. Vol. 2, Adult and fetal. Amsterdam: Elsevier; 2004. p. 1–11.
 - *Contributed section with editors:* Johnson D, Ellis H, Collins P, editors. Pectoral girdle and upper limb. In: Standing S, editor. Gray's anatomy: the anatomical basis of clinical practice. 29th ed. Edinburgh (Scotland): Elsevier Churchill Livingstone; 2005. p. 799–942.
 - *Chapter in a book:*
 - *Standard chapter in a book:* Doyle JR, Botte MJ. Surgical anatomy of the hand and upper extremity. Philadelphia (PA): Lippincott Williams and Wilkins; 2003. Chapter 10, Hand, Part 1, Palmar hand; p. 532–641.

Illustrations and tables

Illustrations and tables should be numbered in different categories in the manuscript and Roman numbers should not be used in numbering. Legends of the illustrations and tables should be added to the end of the manuscript as a separate page. Attention should be paid to the dimensions of the photographs to be proportional with 10x15 cm. Some abbreviations out of standards can be used in related illustrations and tables. In this case, abbreviation used should be explained in the legend. Figures and tables published previously can only be used when necessary for a comparison and only by giving reference after obtaining permission from the author(s) or the publisher (copyright holder).

Author Contribution

Each manuscript should contain a statement about the authors' contribution to the Manuscript. Please note that authorship changes are no longer possible after the final acceptance of an article.

List each author by the initials of names and surnames and describe each of their contributions to the manuscript using the following terms:

- Protocol/project development
- Data collection or management
- Data analysis
- Manuscript writing/editing
- Other (please specify briefly using 1 to 5 words)

For example: NBA: Project development, data collection; AS: Data collection, manuscript writing; STR: Manuscript writing

Funding: information that explains whether and by whom the research was supported.

Conflicts of interest/Competing interests: include appropriate disclosures.

Ethics approval: include appropriate approvals or waivers. Submitting the official ethics approval by whom the research was approved, including the approval date, number or code is necessary.

If the submission uses cadaveric tissue, please acknowledge the donors in an acknowledgement at the end of the paper.

Control list

- Length of the manuscript (max. 15 pages)
- Manuscript format (double space; one space before punctuation marks except for apostrophes)
- Title page (author names and affiliations; running head; correspondence)
- Abstract (100–250 words)
- Keywords (at least three)
- References (relevant to *Index Medicus*)
- Illustrations and tables (numbering; legends)
- Conflicts of Interest Disclosure Statement and Copyright Transfer Form
- Cover letter

All manuscripts must contain the following declaration sections. These should be placed before the reference list at the end of the manuscript.

What 2021 takes and what it brings

Nihal Apaydın¹⁻⁴ 

¹Department of Anatomy, Ankara University School of Medicine, Ankara, Turkey

²Department of Multidisciplinary Neuroscience, Institute of Health Sciences, Ankara University, Ankara, Turkey

³Brain Research Center (AU-BAUM), Ankara University, Ankara, Turkey

⁴Neuroscience and Neurotechnology Center of Excellence (NÖROM), Ankara, Turkey

Anatomy 2021;15(1):iii ©2021 Turkish Society of Anatomy and Clinical Anatomy (TSACA)

Dear Colleagues,

2021 took away a very precious person from us. Earlier this year, we received the news of a falling star from our Turkish Anatomy Society; Professor Doğan Taner... Our professor's contributions to the Anatomy and Medicine cannot be repayable, but we would like to dedicate our first issue of 2021 to his memory in order to express even a little bit of our loyalty towards him. On this occasion, I would like to thank Prof. Dr. Deniz Demiryürek for his contributions to the editorial process in the articles written on Prof. Taner's behalf and also his anchoring and directorship in the video interviews. Thanks to him, I believe that the name of our teacher and mentor Doğan will always be remembered and will be immortal for our journal readers.

Like last year; this year had also started under the influence of the COVID-19 pandemic. I am extremely happy and proud to be able to publish the works of academics who did not stop their education and research activities under the shadow of the pandemic. We yet don't know what 2021 will bring to us; but I hope that the days when we can work more effectively and with higher motivation are ahead and hope that all the post-

poned studies will be implemented soon. In this context, I am pleased to announce the 2 congresses that will be held online this year as well.

The first is the 16th EACA and 12th ISCAA Joint Congress. This congress will be held online on 14–16 September 2021, under the presidency of Professor Raffaele De Caro, using the technical infrastructure of the University of Padova. You can follow the detailed information about the congress on the updated website <https://neuroscienze.unipd.it/eaca-iscaa>. The deadline for abstract submission is June 30, 2021.

The second is the XXII National Anatomy Congress, which will be held online between 13–17 October with the joint contributions of Gazi University and Yüksek İhtisas University Medical Faculties Anatomy Departments. The main theme of the Congress will be “Anatomy and Technology”. You can follow detailed information and current developments about the congress, on the congress website “<https://anatomikongresi2021.gazi.edu.tr/>”. The deadline for submission is August 15, 2021.

Hope to see you in healthy days.

With my deepest regards.

ORCID ID:

N. Apaydin 0000-0002-7680-1766

Correspondence to: Nihal Apaydın, MD, PhD

Department of Anatomy, Ankara University School of Medicine, Sıhhiye 06100 Ankara, Turkey

Phone: +90 312 595 82 48

e-mail: napaydin@gmail.com

Conflict of interest statement: No conflicts declared.

deomed®

This is an open access article distributed under the terms of the Creative Commons Attribution-NonCommercial-NoDerivs 4.0 Unported (CC BY-NC-ND4.0) Licence (<http://creativecommons.org/licenses/by-nc-nd/4.0/>) which permits unrestricted noncommercial use, distribution, and reproduction in any medium, provided the original work is properly cited. *How to cite this article:* Apaydın N. What 2021 takes and what it brings. Anatomy 2021;15(1):iii.

Investigation of the moderate toxicity of agricultural pesticides cyantraniliprole, boscalid and spiromesifen *in vitro* using neurotoxicity screening test

Emine Müge Karakayalı¹ , Duygu Kekeç¹ , Tuna Önal² , İbrahim Tuğlu² 

¹Department of Medical Microbiology, School of Medicine, İzmir Democracy University, İzmir, Turkey

²Department of Histology and Embryology, School of Medicine, Manisa Celal Bayar University, Manisa, Turkey

Abstract

Objectives: Although industrial products used as agricultural pesticides are considered safe, they are likely to lead to chronic problems due to their long-term effects. The neurotoxicity screening test (NST) is a method based on the inhibition of neurite extension of neurons that do not die with toxic effects. In this study, we aimed to investigate the moderate neurotoxic effects and reveal the potential dangers of agricultural pesticides *in vitro* using NST.

Methods: Cyantraniliprole, boscalid and spiromesifen were used as agricultural pesticides on the mouse neuroblastoma cell line N2a. Neurite extension of neurons was performed by taking them into the proliferation medium followed by the differentiation medium. Cell viability and proliferation were analyzed using the MTT test. The percentage of neurite inhibition was calculated by measuring neurite outgrowth by NST. Oxidative stress was analyzed by NOS staining with h-score and apoptosis was shown using the apoptotic index in TUNEL staining.

Results: Cyantraniliprole, boscalid and spiromesifen at high concentrations caused neurite inhibition, decreased proliferation and reduced the viability of cultured neurons. These agricultural pesticides were found to be significantly moderate toxic for neurons by increasing oxidative stress and apoptosis.

Conclusion: We conclude neurite inhibition may be important in early recognition for detecting and preventing the neurotoxic effect of pesticides, and NST is an important *in vitro* test that can predict the long-term effects of neurotoxic agents. In the present study, we observed cyantraniliprole, boscalid and spiromesifen had moderate neurotoxic effects in varying degrees using NST. This means that pesticides may behave toxic even in permissible limits for chronic exposure.

Keywords: agricultural pesticide; apoptosis; environmental toxicity; MTT, neurotoxicity screening test

Anatomy 2021;15(1):1–10 ©2021 Turkish Society of Anatomy and Clinical Anatomy (TSACA)

Introduction

Agricultural pesticides are neglected in terms of their effect on environmental pollution due to their increasing use and their being considered safe. Environmental pollution caused by agricultural pesticides at acceptable doses does not seem to be a problem. However, in the long-term use, their slow accumulation may lead to moderate neurotoxic effects that can be observed in the long term.^[1,2] In the present study, the moderate neurotoxic effects of agricultural pesticides such as cyantraniliprole (CP), boscalid (BC) and spiromesifen (SM) were investigated *in vitro*.

CP is a new second-generation ryanodine receptor insecticide. Its pesticidal effect is through unregulated activation of insect ryanodine receptor channels. This effect causes internal calcium store depletion and disorganized muscle contraction, paralysis and death of the insect.^[1,3] A previous study used inhalation IC₅₀ dose as 5.2 mg/l for the rat.^[4]

BO is a fungicide in agriculture and detected in both environments and agricultural products. BO is thought to be safe for neurotoxic effects. BO induced developmental

defects related to oxidative stress with alteration of ATPase activity in zebrafish embryos.^[5] Moreover, BO also caused disruption of motion and locomotor function in larval fish.^[6,7] These results provide a warning for its residues in environment and agricultural products. It was also shown that BO was neurotoxic for primary cultured cortical neurons at low level of exposure for several days at doses 0.1 and 100 μM for 7 days.^[5] Moreover, another study showed that BO was also toxic to human lymphocytes.^[7]

SM is novel insecticide belonging to the chemical class of tetronic and tetramic acid derivatives. It is very effective on *Bemisia tabaci* around the world.^[8,9] SM was toxic for rat hepatocytes at 3 mg/kg.^[3] However, there was no toxic signs in acute, subchronic and chronic neurotoxicity in rats. The long-term rat studies revealed no indications for neurotoxic or immunotoxic potential of SM.^[3]

The neurotoxicity screening test (NST) is a method based on neurite prolongation after the application of differentiation medium to neuronal cell line.^[10] After they acquire neuron characteristics, neurite prolongation inhibition occurs in cells that do not die as a result of the direct toxic effect. With the NST, products likely to have a moderate neurotoxic effect in the long term are detected.^[11-13] While the direct neurotoxic effect leads to the occurrence of decreased proliferation and necrosis, the moderate indirect neurotoxic effect which takes a long time to act induces apoptosis and neurite inhibition. Free radicals, which increase oxidative stress due to toxic effects, and intracellular signal communication are the mechanisms used in the emergence of these findings.^[14-16] In this study, the moderate toxic effects of various agricultural pesticides whose safety has been proven and toxic effects are minimum were investigated with the NST.

N2a line neuronal cells are from mouse neuroblastoma.^[14,17] These neuron-like cells have been used in studies for neuronal differentiation, axonal growth, signaling pathway and neurotoxicity.^[18] N2a cells express neuronal characteristics with the presence of neurofilaments and large amounts of microtubular proteins after differentiation. They differentiate to neurons through serum deprivation with dibutyryl cyclic adenosine monophosphate (dbcAMP) in culture medium.^[18]

Safe agricultural pesticide may have some moderate toxic effect such as neurite inhibition and apoptosis before they die from toxic effect.^[14] These signs are more important in chronic use. Many studies show that they have potential neurotoxicity due to chronic exposure to low doses of pesticides. Most of these works used cell culture model for chronic exposure to evaluate possible environmental toxic compounds by alterations in the

sensitivity of nerve cells to subsequent acute exposure. N2a neuroblastoma cells in culture were grown in the presence of various pesticides or herbicides for appropriated time.^[4] Extension of neurite-like structures was measured by light microscopy and quantitative image analysis at IC50 level.^[17] It is possible to see their potential toxicity in chronic exposure by this method.^[4,11,14,19,20]

Materials and Methods

Supplies and Chemicals

The mouse neuroblastoma (N2a) cells (cell line: 89121404) were obtained [The European Collection of Authenticated Cell Cultures (ECACC)].^[10] All the chemicals used in the experiment were obtained from Sigma (St. Louis, MO, USA). While the tissue culture flasks and culture plates were obtained from Falcon / Fred Baker (Runcorn, Cheshire, England), gentamicin was obtained from Ibrahim Etem (20 mg Genta[®] bulb, Ibrahim Etem, Istanbul, Turkey).^[7,10]

Cell Culture

In all the experiments, different agricultural pesticides were investigated in terms of their effects on the differentiated and undifferentiated culture cells. Pesticides were dissolved in DMSO at final concentration for IC50 doses. Differentiated and undifferentiated cells were incubated with the pesticides for a further 24 hours. Neuroblastoma cells in culture medium containing 5% fetal calf serum, 5% horse serum, 25 $\mu\text{g}/\text{mL}$ gentamicin, 1% penicillin / streptomycin solutions (10,000 U/10 mg), Glutamax-1 and high glucose Dulbecco Modified Eagle (DMEM) were incubated at 37°C in a humid environment including 5% CO₂.^[21,22]

Cell Viability

To calculate the cell viability and growth, the MTT experiment, reduction of 3- (4,5-dimethylthiazol-2-yl) - 2,5-diphenyltetrazolium bromide to a purple formazan product was used.^[16] Three wells of the 96-well culture dish were used for the evaluation of each pesticide concentration. Cell densities of $5 \times 10^4/\text{mL}$ prepared per well were used. Pesticide-free cell medium (100 μL) was used as the positive control, while cell and pesticide-free medium was used as the negative control. Cells were previously treated with the indicated concentrations for 24 and 48 hours. During the last 4 hours of the culture period tested, cells were incubated with the MTT at 37°C in a humidified environment including 5% CO₂. The medium was then changed, by adding 200 μL of dimethyl sulfoxide (DMSO, Sigma-Aldrich) to each well to dissolve the formazan salts. Absorbance was determined at 570 nm in a UV-spec-

trophotometer multi-plate reader (Versa Max, Molecular Device, Sunnyvale, CA, USA).^[15,16,19,20,23–25]

Cell Differentiation and Neurite Outgrowth

To measure neurite outgrowth, N2a cells were placed in the proliferation medium in 24-well culture plates at a cell density of 15,000 cells/mL. Twenty-four hours later, cells were induced to differentiate and produce neurites in the presence of pesticides using the following method.^[10,18] The culture medium in each well was changed to the medium containing no serum but 0.5 mM dibutyl cyclic AMP. To measure neurite growth, pesticides at IC50 concentrations were added. Cells were incubated for a further 24 hours. Cells fixed with phosphate buffered saline (PBS) with 4% (w/v) paraformaldehyde for 10 minutes were then stained with Coomassie for 3 minutes.^[26] Blue cell dye (0.6% [w/v] Coomassie Brilliant Blue G, 10% [v/v] acetic acid, 10% [v/v] methanol and 80% [v/v] PBS) was washed with the PBS. Two blinded observers took the photographs of samples by using an Olympus BX-40 (Olympus, Tokyo, Japan) light microscope with a video camera (JVC-TK-C 601, Tokyo, Japan) for digital imaging. The analysis of the images was performed using the Image-Pro Plus image analyzer (5.1.259, Bioscience Technology, Bethesda, MD, USA). Ten different areas with approximately 10 cells were selected for pesticides and controls.^[7] By automatically measuring the total neurite length (in pixels) for cells in each area, the results were expressed as the average neurite length per cell.^[1,10,12,21]

Oxidative Stress

Cells were immunostained for e-NOS and i-NOS to evaluate levels of the oxidative stress. After application of OC at IC50 dose, the cells were fixed in the 4% paraformaldehyde for 30 min and washed in the PBS three times for 5 min each. Permeabilization was performed using 0.1% Triton X-100 (A4975; AppliChem, Darmstadt, Germany) at 4°C for 15 min, and cells were washed with the PBS. Endogenous peroxidase activity was inhibited using 3% hydrogen peroxide for 5 min. Cells were washed with the PBS and incubated with anti-eNOS rabbit polyclonal antibody (RB-1711-P1; Neomarkers, Fremont, CA, USA) diluted 1:100 and anti-i-NOS rabbit polyclonal antibody (RB-1605-P; Neomarkers) diluted 1:100 for 18 h at 4°C. The cells were washed three times for 5 min each in the PBS, treated with biotin-streptavidin hydrogen peroxidase secondary antibody (Invitrogen-Histostain Plus Bulk Kit®, 85-9043; Invitrogen) for 30 min. After washing with PBS three times for 5 min each, cells were incubated with diaminobenzidine (DAB) (00-2020; Zymed, Burlingame CA, USA) for 5 min for immunolabeling, then counterstained with Mayer's haematoxylin (72804E; Microm,

Walldorf, Germany). Cells were covered with mounting medium (AML060; Scytek, Logan, UT; USA) and photographed using an Olympus light microscope (BX40; Tokyo, Japan). Control samples were processed identically except that the primary antibody was omitted. The immunostaining was repeated three times. The two blinded observers scored the immunostaining as 0, no staining; 1, weak staining; 2, moderate staining; 3, moderate-strong staining; 4, strong staining; 5, very strong staining. The H-score then was calculated using the following formula: H-score = Pi intensity of staining + 1, where Pi is the percentage of stained cells for each intensity varying from 0 to 100%.^[1,21]

TUNEL Assay

Terminal deoxynucleotidyl transferase-biotin nick end labelling (TUNEL) using the DeadEnd™ Colorimetric TUNEL system (Promega, Madison, WI, USA) was used to detect apoptotic cells. After the application, the cells were fixed in 4% paraformaldehyde for 30 min and rinsed three times in the PBS for 5 min. Then the cells were incubated with 20 µg/mL Proteinase K. for 10 min and washed three times again in the PBS for 5 min. For endogenous activity inhibition, the cells were treated with 3% hydrogen peroxide and rinsed in the PBS. Afterward, the cells which were treated with the equilibration buffer for 5 min incubated with Tdt-enzyme for 60 at 37°C than were proceeded with 2×SCC solution for 15 min and then washed three times in the PBS for 5 min. The streptavidin peroxidase procedure was performed for 45 min, after which the cells were rinsed in the PBS and incubated with DAB; Mayer's haematoxylin was performed for counterstaining. The cells were than rinsed in distilled water and mounted in the mounting medium. TUNEL-positive staining was evaluated by two blind observers, under Olympus BX40 light microscope. Apoptotic index was calculated as the sum of the percentages of positively labelled cells. For TUNEL staining, each section was counted for 100 TUNEL-positive cells from the randomly chosen fields. Observers rated the percentage of apoptotic cells as 0: no apoptosis, 1: 1%–10% apoptosis, 2: 11%–25% apoptosis, 3: 26%–50% apoptosis, 4: 51%–75% apoptosis, and 5: more than 75% apoptosis.^[2,21,27,28] The apoptotic index was counted as the percentage of the apoptotic cells relative to the total cell number.

Statistical Analysis

The results were analysed using the GraphPad (GraphPad Software, San Diego, CA, USA) and one-way ANOVA with Tukey post hoc testing and presented as mean±SEM.^[2,20,21] Statistical significance was defined as p≤0.05 or p≤0.001.

Results

N2a cells were taken into the culture medium and incubated for 24 hours to proliferate. In the second 24 hours after proliferation, N2a cells were taken to the differentiation medium for neurite elongation. Neurite elongation was shown using Coomassie staining (**Figure 1**). The IC50 doses of the pesticides administered in the proliferation stage and determined by the MTT were as follows: 38.44 μM for CP, 55.66 μM for BO and 8.12 μM for SM (**Figure 2a**).

Neurite inhibitions of differentiated cells after the second 24 hours of application were as follows: 78.94 \pm 6.48 % for CP, 86.94 \pm 7.74% for BO, and 62.22 \pm 5.25% for SM (**Figure 2b**). Compared to the controls, pesticides were observed to have significant neurite inhibition as neurotoxic effects ($p < 0.05$).

At IC50 doses, the iNOS and eNOS expressions of the cells were determined to increase both in the proliferation stage and in the neuritis inhibition stage after differentiation (**Figure 3**). Moreover, H score levels which increased significantly ($p < 0.05$) due to oxidative stress. There was significantly more toxic effect for SM compared to those of BO ($p < 0.001$) and CP ($p < 0.05$) in eNOS h-score. Similarly, SM was showed significantly ($p < 0.001$) more toxic effect for BO ($p < 0.01$) and CP ($p < 0.05$) in iNOS h-score. Neurotoxic effect of BO and CP didn't differ significantly (**Figure 4**).

At IC50 doses, it was observed in TUNNEL labeling of cells that the apoptotic index increased both in the proliferation stage and in the neurite inhibition stage after differentiation (**Figure 3**). It was also observed that the apoptotic index increased significantly ($p < 0.05$) due to toxic

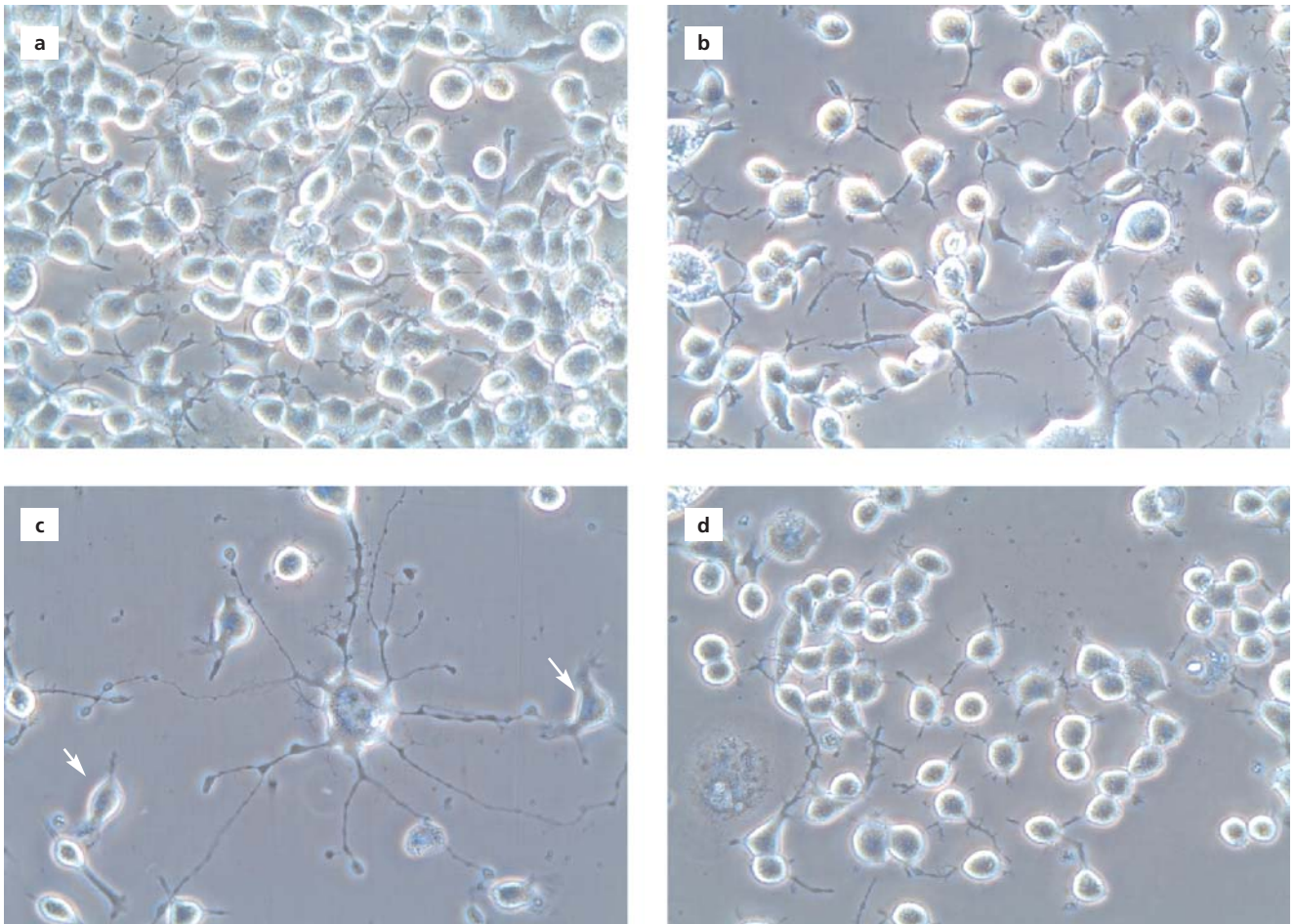


Figure 1. (a) N2a cells were taken into the culture medium and incubated for 24 hours to proliferate; (b, c) In the second 24 hours after proliferation, N2a cells were taken to the differentiation medium for neurite elongation; (d) There was neurite inhibition after application of pesticide. Coomassie staining; $\times 200$.

agents. SM caused more apoptosis than BO ($p < 0.01$) and CP ($p < 0.05$) shown by TUNEL staining (Figure 4).

Due to the neurotoxic effect of the cells, when the phase, light and electron microscope images were examined, decrease in cell volume, chromatin condensation, cytoplasmic vacuoles and fragmentations were observed as the signs of cell death. It was observed that the cells

made cytoplasmic projections in the form of lamellipodia (Figure 5).

Discussion

Widely used in agriculture, synthetic pesticides control harmful pests and prevent crop yield losses and product damage. These may have undesirable effects to health and

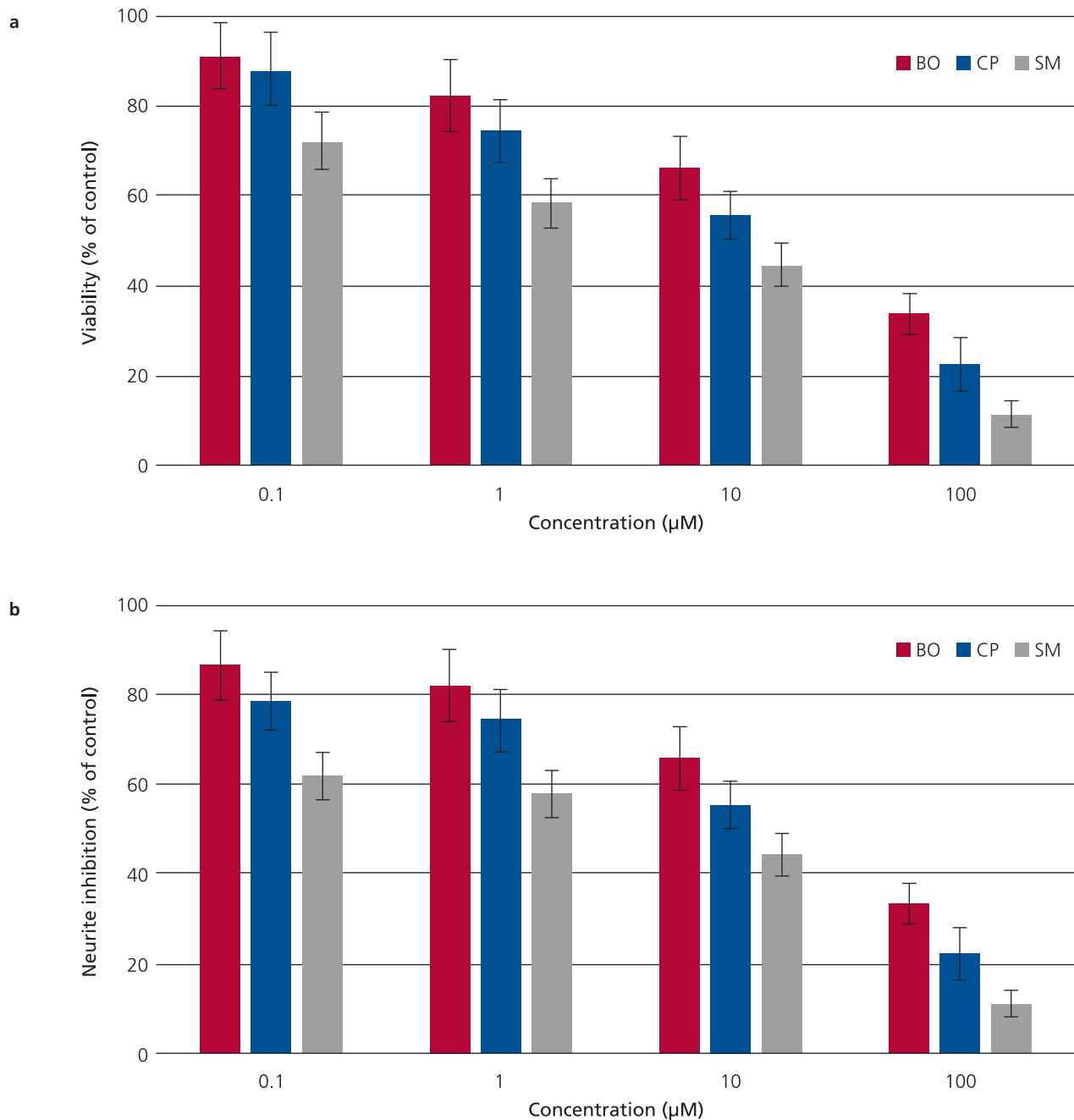


Figure 2 (a) The IC₅₀ doses of the pesticides administered in the proliferation stage and determined by MTT; (b) Neurite inhibitions of differentiated cells after the second 24 hours of application were determined by NST.

environment, due to their high biological activity and, in certain cases, long persistence in the nature.^[4] Environmental pollution caused by agricultural pesticides and resulting health problems are not fully known. The

neurotoxic effect that agricultural pesticides can show in adults can be much more serious and problematic in children in the developmental period. This effect, called developmental neurotoxicity, is thought to be much more

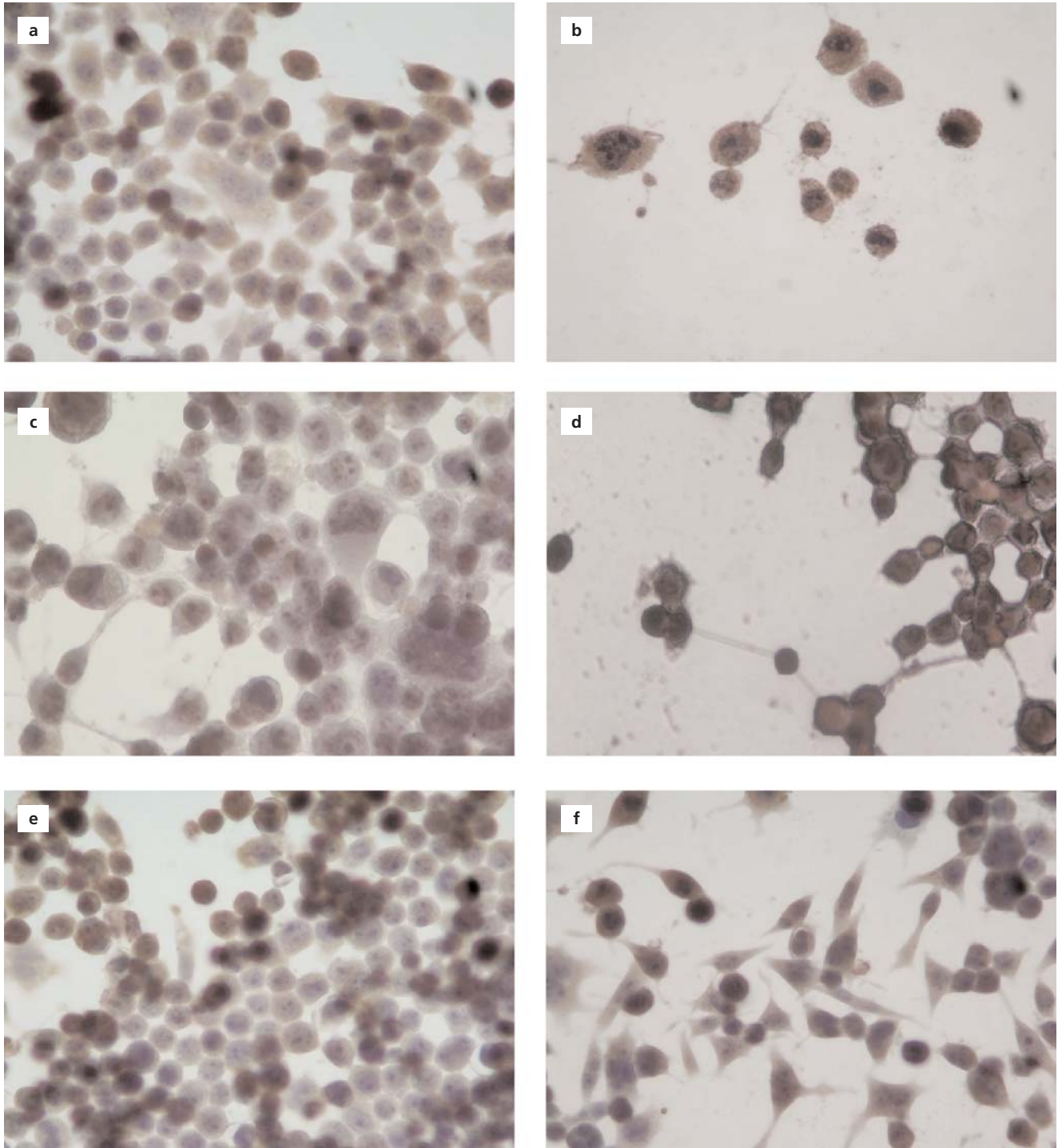


Figure 3. (a-f) At IC50 doses, the eNOS and iNOS expressions of the cells were shown by immunocytochemistry; $\times 200$.

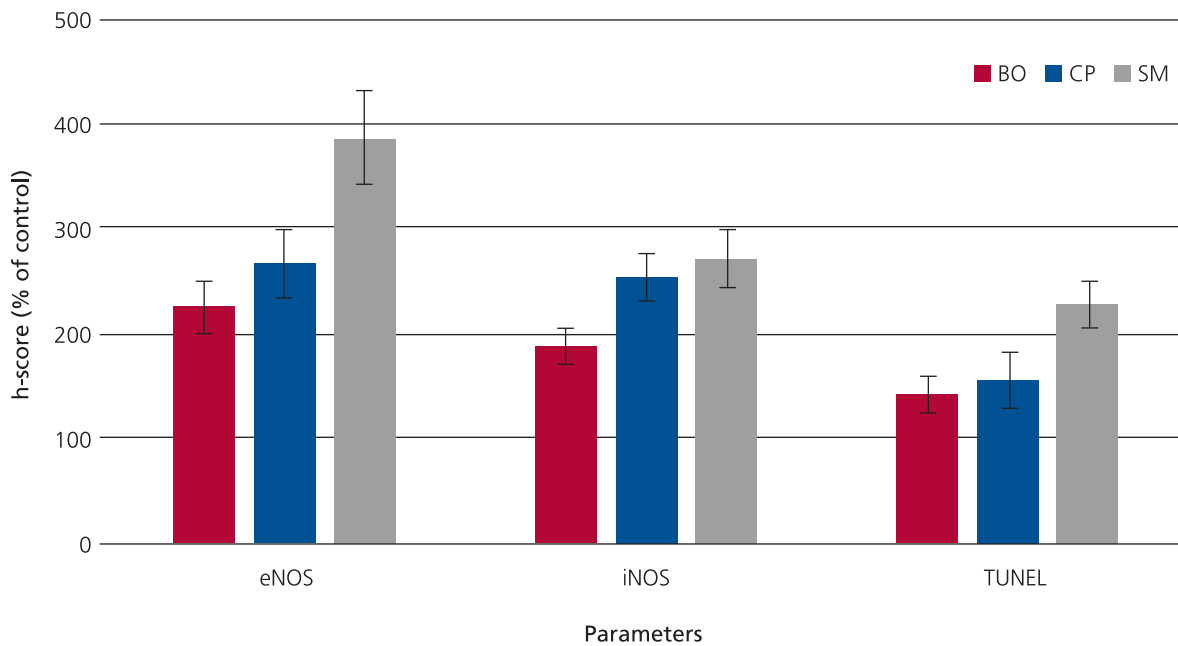


Figure 4. Oxidative stress was determined by h-score and apoptosis was determined by apoptotic index for the effect of the pesticide.

severe and irreversible. This is important in terms of developing diagnostic tests to investigate and prevent environmental pollution-related public health problems. Classical toxicity methods performed for this purpose are important for acute and effective toxicity. However, methods that can be used in terms of chronic toxicity are not many and one of them is neurite inhibition. In this method, due to the inhibition of the neuron's classical elongation ability, a moderate toxic effect is detected when the cell is alive. The onset of degeneration of the neuron exposed to toxic effect occurs with the disruption of the synapse and the loss of the tropic factor support. If toxic effect develops slowly, neurite prolongation is inhibited. This condition is associated with microtubules and neurofilament proteins. To demonstrate this moderate neurotoxic effect for agricultural pesticides, we used MTT for proliferation and cell survival, immunohistochemistry for oxidative stress and TUNEL for apoptosis. We showed that the moderate neurotoxicity had a proliferative effect as the MTT value decreased, and an oxidative stress effect as the h-score of NOS increased and that it was associated with TUNEL labeling through apoptosis.

The increasing use of agricultural industrial products poses a significant threat to environmental pollution. Despite all the rules and measures taken according to European data, hundreds of pesticides are still widely used. The dose of pesticides in one out of every twenty food

items is more than the accepted level. Pesticides adversely affect children's development and in urine analysis, this toxic effect has been shown to be at varying degrees. Pesticides' contribution to environmental pollution is seen by detecting their presence in rivers, groundwater, soil, air, plants, and human and animal tissues proves pesticides' contribution to environmental pollution. Despite all the precautions taken, their toxic effects are observed, and the

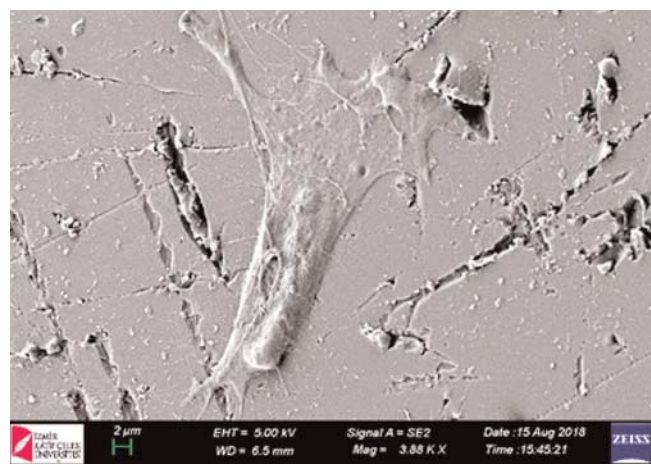


Figure 5. SEM images from proliferation, differentiation, neurite extension and apoptosis. There was decrease in cell volume, chromatin condensation, cytoplasmic vacuoles and fragmentations were observed as the signs of cell death.

brain and neurons are the most critical organs among possible target organs.^[15] Therefore, different agricultural product that we were investigated for moderate toxicity from environmental pollution could be very important to human health.

It is more meaningful to reveal their possible effects in the culture environment due to the difficulties in conducting *in vivo* studies, and ethical concerns. While exposure lasting ≥ 90 days is considered chronic in *in vivo* toxicity, its equivalent in the culture medium is the cell's undergoing neurite inhibition before it dies, which can be demonstrated with a three-day culture study.^[15] In a study conducted to investigate developmental neurotoxicity, it was found that neurite elongation was inhibited in PC12 cell line at non-toxic concentrations of a pesticide species. Dithiocarbamate fungicides were found to cause copper-dependent oxidative stress and neurotoxic effect with ROS production due to mitochondrial dysfunction. In addition, glutamate was thought to lead to a neurotoxic effect by affecting vesicular transport. It has been shown that apoptotic cell death due to toxic effect occurs due to intracellular calcium. It was also found that peripheral neuropathy and parkinsonism-like extrapyramidal effects occurred in toxicity-induced chronic exposure.^[23] In the neuron degenerated by toxic factors such as fungal pesticides, disruption of synapse, affection of perineurium, and decrease in trophic factors occur. The extent of the damage is related to the severity, time and continuity of the toxic agent. Neurotoxic effect occurs rapidly or slowly and affects the cell at different levels. Inhibition of neurite elongation is seen with a slow progressing moderate neurotoxic effect, and it occurs by the impairment of axonal transport. It is thought that the neurotoxic effect due to agricultural antifungal pesticides occurs in a similar way in our experiments. In a study in which the neurotoxic effects of agricultural pesticides were investigated in the culture environment, it was shown that they had a moderate neurotoxic effect related to dose and duration, consistent with our culture results.

It was determined that mitochondrial respiration complex and similarly the electron carrier ubiquinone or coenzyme Q were among the mechanisms used. Decreased ATP production and mitochondrial membrane depolarization were shown to cause cell death via increased cytosolic calcium. It was found that the different action mechanism shown in this way in cortical neurons cultured with new fungicides exerts a neurotoxic effect in relation to calcium channels. It was thought that calcium channel blockers would have a neuroprotective effect in this sense. Half of the cells were found to be viable despite the extended exposure times. In a comparison, that neurons were exposed to toxic effect in less concentrations than were lymphocytes indicated the importance of the nervous system in terms of

health problems. It was observed that the delayed neurotoxic effect seen especially in organophosphates occurs clinically, similar to its occurrence as in the culture medium.^[24] In many cases, this condition results with neuropathy. Excitotoxicity and neuroinflammation are seen in alcohol-induced neurotoxic effect and are associated with proinflammatory cytokines. It was understood that oxidative stress and apoptosis mechanisms were used in the moderate neurotoxic effect that occurred here.^[2] Similar mechanisms were determined in the neurotoxic effect of glutamate. It has been reported that the neuroprotective effect of many different pesticides occurs through caspase 3 inhibition, and that neural damage due to decreased apoptosis is regressed. There are studies indicating that antioxidant-effective drugs similarly reduce neuron damage with calcium dependent mechanisms and that this situation is observed in the clinic situation.^[5,15] Similar to these experiments, we found apoptosis in our neurons due to agricultural products which may related to calcium metabolism.

There are studies investigating the responses of differentiated and undifferentiated cells in neuronal cell lines to demonstrate the neurotoxic effect. The response seen in differentiated cells against the neurotoxic effect shown by MTT, which is caused by the proliferation of undifferentiated cells, may be a different mechanism demonstrated by morphological and enzymatic methods. In a study, the neurotoxic effect for cylindrospermopsin was observed with changes in the form of acetylcholine esterase and apoptosis. The increase in oxidative stress causing apoptosis has been shown to be associated with changes in acetylcholine esterase activity. In addition, the authors thought that the clinical response of the *in vitro* neurotoxicity was related to the transition of the toxic agent to the blood-brain barrier.^[28,29] The neurotoxic effect of agricultural products on the factors other than the target is important. The toxic effect of imidacloprid used to protect wheat on worms and the related environmental pollution has been shown in many studies.^[22,27] These studies indicated that apoptotic neurons due to agricultural products depend on acetylcholine esterase related alterations.

In earlier studies, it was shown that the morphology of cell size, shape and neurite lengths might change by substrate type and microscope. It was clear after proper staining, that the thin cell processes extending on the tissue culture surface showed classical neuronal behavior. We observed that the overall cell shape evolved to the direction of neurons, with several narrow extensions and cytosol appears more evenly extending all around its edges. Therefore, neuron-like cells kept their characteristics under tSEM examination. The cell adhesion and number of cells were sufficient to examine the ultrastructure of the neurons.^[11,26]

Conclusion

Neurite inhibition may be important in early recognition for detecting and preventing the neurotoxic effect of pesticides. NST is an important *in vitro* test that can predict the long-term effects of neurotoxic agents. In the present study, antifungals used as pesticides were shown to have moderate neurotoxic effects in varying degrees. This means that pesticides may behave toxic in permitted limits for chronic exposure. In further studies, it will be possible to demonstrate other neurotoxic factors and to test antioxidant and antiapoptotic neuroprotective agents that can reduce neural damage. Thus, the potential of using neuroprotective agents in the clinic will increase the quality of life of patients.

Conflict of Interest

The authors declare that they have no known competing financial interests or personal relationships that could have appeared to influence the work reported in this paper.

Author Contributions

EMK: design, analysis, revising the draft, approval of the final version of the manuscript; TÖ & DK: data collection; İT: analysis, design, revising the draft, approval of the final version of the manuscript.

Ethics Approval

No ethics approval needed.

Funding

This research did not receive any specific grant from funding agencies in the public, commercial, or non-profit sectors.

References

- Yoshida M, McGregor D. Cyantraniliprole. In Pesticide residues in food 2013. Joint FAO/WHO Meeting on Pesticide Residues. Report of the Joint Meeting of the FAO Panel of Experts on Pesticide Residues in Food and the Environment and the WHO Core Assessment Group on Pesticide Residues. Geneva, Switzerland, September 17–26 2013. Rome: FAO; 2014. p. 131–76.
- EFSA Panel on Nutrition, Novel Foods and Food Allergens (NDA); Truck D, Castenmiller J, De Henauw S, Hirsch-Ernst KI, Kearney J, Maciuk A, Mangelsdorf I, McArdle HJ, Naska A, Pelaez C, Pentieva K, Siani A, Thies F, Tsbouri S, Vinceti M, Cubadda F, Frenzel T, Heinonen M, Marchelli R, Neuhauser-Berthold M, Poulsen M, Prieto Maradona M, Schlatter JR, van Loveren H, Verwer E, Knutsen HK. Scientific Opinion on the safety of dried yellow mealworm (*Tenebrio molitor* larva) as a novel food pursuant to regulation (EU) 2015/2283. EFSA NDA Panel (EFSA Panel on Nutrition, Novel Foods and Food Allergens). EFSA J 2021;19(1):e06343.1–29.
- European Food Safety Authority (EFSA). Conclusion on the peer review of the pesticide risk assessment of the active substance spiromesifen. EFSA J 2007;5(7):e105.1–69.
- European Food Safety Authority (EFSA). Conclusion on the peer review of the pesticide risk assessment of the active substance cyantraniliprole. EFSA J 2014;12899.e03814.1–249.
- Regueiro J, Olguín N, Simal-Gándara J, Suñol C. Toxicity evaluation of new agricultural fungicides in primary cultured cortical neurons. Environ Res 2015;140:37–44.
- El Merhie A, Salerno M, Toccafondi C, Dante S. Neuronal-like response of N2a living cells to nanoporous patterns of thin supported anodic alumina. Colloids Surf B Biointerfaces 2019;178:32–7.
- Wang H, Meng Z, Liu F, Zhou L, Su M, Meng Y, Zhang S, Liao X, Cao Z, Lu H. Characterization of boscalid-induced oxidative stress and neurodevelopmental toxicity in zebrafish embryos. Chemosphere 2020;238:124753.
- Çayır A, Coskun M, Coskun M. Micronuclei, nucleoplasmic bridges, and nuclear buds induced in human lymphocytes by the fungicide signum and its active ingredients (boscalid and pyraclostrobin). Environ Toxicol 2014;29:723–32.
- Bielza P, Moreno I, Belando A, Grávalos C, Izquierdo J, Nauen R. Spiromesifen and spirotriamat resistance in field populations of Bemisia tabaci Gennadius in Spain. Pest Manag Sci 2019;75:45–52.
- McLean WG, Holme AD, Janneh O, Southgate A, Howard CV, Reed MG. The effect of benomyl on neurite outgrowth in mouse N2A and human SH-SY5Y neuroblastoma cells *in vitro*. Neurotoxicology 1998;19:629–32.
- Smith SL, Sadler CJ, Dodd CC, Edwards G, Ward SA, Park BK, McLean WG. The role of glutathione in the neurotoxicity of artemisinin derivatives in vitro. Biochem Pharmacol 2001;15:409–16.
- Vural K, Tuglu MI. Neurotoxic effect of statins on mouse neuroblastoma NB2a cell line. Eur Rev Med Pharmacol Sci 2011;15:985–91.
- Ferrari E, Cardinale A, Picconi B, Gardoni F. From cell lines to pluripotent stem cells for modelling Parkinson's disease. J Neurosci Methods 2020;340:108741.
- Axelrad JC, Howard CV, McLean WG. Interactions between pesticides and components of pesticide formulations in an *in vitro* neurotoxicity test. Toxicology 2002;173:259–68.
- Voorhees JR, Rohlman DS, Lein PJ, Pieper AA. Neurotoxicity in preclinical models of occupational exposure to organophosphorus compounds. Front Neurosci 2017;10:590.
- Vural K, Seyrek O. The neuroprotective effect of pioglitazone on NB2a mouse neuroblastoma cell culture. Kafkas Üniversitesi Veteriner Fakültesi Dergisi 2019;25:1–8.
- Klebe RJ, Chen T, Ruddle FH. Mapping of a human genetic regulator element by somatic cell genetic analysis. Proc Natl Acad Sci USA 1970;66:1220–7.
- LePage KT, Dickey RW, Gerwick WH, Jester EL, Murray TF. On the use of neuro-2a neuroblastoma cells versus intact neurons in primary culture for neurotoxicity studies. Crit Rev Neurobiol 2005;17:27–50.
- Lee MK, Nikodem VM. Differential role of ERK in cAMP-induced Nurr1 expression in N2A and C6 cells. Neuroreport 2004;15:99–102.
- Axelrad JC, Howard CV, McLean WG. The effects of acute pesticide exposure on neuroblastoma cells chronically exposed to diazinon. Toxicology 2003;185:67–78.

21. Mete M, Aydemir I, Ünlü Ünsal Ü, Duransoy YK, Tuğlu İM, Selçuki M. Neuroprotective effects of bone marrow-derived mesenchymal stem cells and conditioned medium in mechanically injured neuroblastoma cells. *Turk J Med Sci* 2016;46:1900–7.
22. Sachana M, Flaskos J, Alexaki E, Glynn P, Hargreaves AJ. The toxicity of chlorpyrifos towards differentiating mouse N2a neuroblastoma cells. *Toxicol In Vitro* 2001;15:369–72.
23. Bjørling-Poulsen M, Andersen HR, Grandjean P. Potential developmental neurotoxicity of pesticides used in Europe. *Environ Health* 2008;7:50.
24. Hargreaves AJ, Sachana M, Flaskos J. The use of differentiating N2a and C6 cell lines for studies of organophosphate toxicity. In: Aschner M, Suñol C, Bal-Price A, editors. *Neuromethods*, Vol 56: Cell culture techniques. New York (NY): Springer; 2011. p. 269–91.
25. Bilir EK, Tutun H, Sevin S, Kismali G, Yarsan E. Cytotoxic effects of *Rhododendron ponticum* L. extract on prostate carcinoma and adenocarcinoma cell line (DU145, PC3). *Kafkas Üniversitesi Veteriner Fakültesi Dergisi* 2018;24:451–7.
26. Lau K, McLean WG, Williams DP, Howard CV. Synergistic interactions between commonly used food additives in a developmental neurotoxicity test. *Toxicol Sci* 2006;90:178–87.
27. Qi Y, Cao X, Abd El-Aty AM, Ma C, Li H, Jiang Z, She Y, Wang S, Wang J, Yang S. A magnetic zeolitic imidazolate framework nanohybrid for fast and efficient extraction of clothianidin, imidacloprid, acetamiprid, and thiacloprid in water. *J Nanosci Nanotechnol* 2019;19:3310–8.
28. Damalas CA, Koutroubas SD. Farmers' exposure to pesticides: toxicity types and ways of prevention. *Toxics* 2016;4:1.
29. Hinojosa MG, Gutiérrez-Praena D, Prieto AI, Guzmán-Guillén R, Jos A, Cameán AM. Neurotoxicity induced by microcystins and cylindrospermopsin: a review. *Sci Total Environ* 2019;10:668:547–65.

ORCID ID:

E. M. Karakayalı 0000-0001-5779-4102; D. Kekeç 0000-0003-2192-2058;
T. Önal 0000-0002-3650-4046; I. Tuğlu 0000-0002-0569-8415

**Correspondence to:** Müge Karakayalı, MD

Department of Medical Microbiology, School of Medicine,
Izmir Democracy University, Izmir, Turkey
Phone: +90 532 507 62 96
e-mail: muge.karakayali@idu.edu.tr

Conflict of interest statement: No conflicts declared.

This is an open access article distributed under the terms of the Creative Commons Attribution-NonCommercial-NoDerivs 4.0 Unported (CC BY-NC-ND4.0) Licence (<http://creativecommons.org/licenses/by-nc-nd/4.0/>) which permits unrestricted noncommercial use, distribution, and reproduction in any medium, provided the original work is properly cited. *How to cite this article:* Karakayalı EM, Kekeç D, Önal T, Tuğlu İ. Investigation of the moderate toxicity of agricultural pesticides cyantraniliprole, boscalid and spiromesifen *in vitro* using neurotoxicity screening test. *Anatomy* 2021;15(1):1–10.

***In silico* transcriptomic analysis of ascending colon cancer unearths known and novel genes and gene sets regard to characteristic features of colon cancer**

Can Türk 

Department of Medical Microbiology, Faculty of Medicine, Lokman Hekim University, Ankara, Turkey

Abstract

Objectives: Colon cancer emerges as a serious health problem in both men and women. Cancers in the colon have different genotypes and phenotypes according to the anatomical region. Tumors in ascending colon are usually diagnosed later, but it is more malignant than the descending and transverse colon, and the survival rates of patients are lower than other regions. The purpose of this study was to determine significantly high or low expressed genes in the ascending colon tumors by comparing all genome information obtained from cancer samples of ascending, transverse and descending colon. In concordance with all this information, another aim of the study was to identify the pathways to which the genes obtained from the colon in the large intestine and to determine their relationship with each other and to correlate them with the characteristics of cancer.

Methods: Gene expression values for three subtypes of colon cancer as ascending, transverse, and descending were obtained from GEO (Gene Expression Omnibus) (GSE41258). Data included a total of 47 ascending, 18 transverse and 31 descending colon cancer patient samples. Linear regression analysis was performed to determine differentially expressed genes. Gene Cluster 3.0 was used in order to cluster the genes hierarchically. In addition to linear regression and hierarchical clustering, network analysis with multivariable genes was performed in Cytoscape application 3.8.2 using GeneMANIA. GSEA 4.1.0 (Gene Set Enrichment Analysis) was performed to understand the different genes among the specified groups.

Results: As a result of these analyses, it was determined that there were 85 genes with high expression and 139 genes with low expression in the ascending colon tumor samples. It has been shown that these genes can differentiate tumor samples in the ascending colon better than tumor samples in other colon regions.

Conclusion: Our findings are important for understanding the genome of ascending colon tumors; if these findings are confirmed *in vitro* and clinically, it may have potential to be revealed that the identified genes also have biomarker properties for tumors in the ascending colon.

Keywords: ascending colon; descending colon; transcriptomic analysis; transverse colon

Anatomy 2021;15(1):11–25 ©2021 Turkish Society of Anatomy and Clinical Anatomy (TSACA)

Introduction

The large intestine is approximately 1.5–2 meters long and consists of caecum, colons and rectum. The rectum is the last part before the anus and this part is also known as the area where feces is stored. On the other hand, the colon, forms the large part of the large intestine. Colon cancers basically occur as a result of an abnormality in this part. Studies carried out at the molecular level show

that the formation of colon cancer occurs through a complex mechanism influenced by many factors. Genetic factors trigger the formation of colon cancer cells as well as the effects of lifestyle factors such as smoking and eating habits. Studies show that mainly CIMP (CpG island methylator phenotype), MSI (microsatellite instability), and additionally, CIN (chromosomal instability) mechanisms play a role in cancer development.^[1–4]

It has been shown that approximately 20% to 30% of patients with colon cancer have abnormalities in the CIMP pathway. Hypermethylation in the promoter sequences of the cell plays an essential role in the pattern of gene expression. Basically, CpG dinucleotide sequences are known to locate in this promoter region. The trigger for colon cancer cells is that sequences are not hypermethylated properly. In addition, this imprecision also affects critical cell mechanisms such as apoptosis, invasion, angiogenesis, cell cycle regulation, DNA adhesion and repair.^[1-5]

According to statistical studies, MSI is responsible for 15% of colon cancers. MSI occurs due to DNA incompatibility, is involved in the process of DNA replication, mutations in some genes involved in the mechanism. These mutations generally inactivate the functions of genes. It plays an essential role in the protein synthesis of MMR genes. These proteins cause a decrease in polymerase function for to recognize and correct these defects, resulting in anomalies occurring on the microsatellite during replication. Mutations that arise because of the function of the recovery system accumulate and trigger formation of colon cancer cells.^[1-4,6]

Colon cancer is a common type of cancer among gastrointestinal cancers worldwide. The prevalence of colon cancer varies depending on age. I.e., while it is 1.6% in the 50–60 age group, it is known that this rate increases up to 3% over the age of 70. In addition, studies show that the incidence of colon cancer may vary depending on gender. It has been shown that the incidence rate in women is higher than in men.^[7-10]

Considering the mechanism of colon cancer, the importance can be seen more clearly. Basically; CIN, MSI, and CIMP play critical roles on colon cancer. Abnormalities caused by these mechanisms increase mutagenic activity in tumor suppressors and oncogenes. Critically, these mutations lead to an increase in the number of cancer stem cells, which play an important role in the onset of tumor formation. In addition, the acceleration of mutation accumulation also accelerates the epigenetic change of cells.^[1,7-10]

Importantly, the characteristics and effects of colon cancer may vary according to anatomical regions. It consists of three main anatomical parts, respectively, ascending colon, transverse colon and descending colon. Generally, about 45% of colon cancer is located in the left colon region. However, in recent years, studies have showed that right colon (cecum and ascending colon) cancers have reached the rate of up to 25% and the reasons for this increase include the increase of the popula-

tion over the age of 65 and the different colon segments in terms of embryonic development. There are studies showing that comorbid conditions that increase with age and excessive fatty diet may increase right colon cancer, and excessive protein diet may increase left colon cancer. In addition, among the reasons for the decrease in the occurrence of left colon cancers, more effective use of screening programs and removal of existing polyps at an early stage may be effective.^[11-14]

Studies have shown that cancer consisting of different parts of the colon has different characteristics. In general, tumors occurring in the right region are more malignant and the survival rate of patients is lower. However, the effective functionality of the lymph nodes can improve this survival rate.^[15] Another study shows that patients with colon cancer in the right region do not respond well to chemotherapy treatment. However, the same study states that immunotherapy treatment may be a better option. The main reason for this is the high level of antigenic load of tumor cells formed in these regions.

As supported, separately evaluating the formation and effect of tumors occurring in different types and regions plays a critical role for the treatment to be determined.^[16] In this study, the genes responsible for the characteristics of the cancers that occur in the ascending section and having different expression values compared to the cancer in other colon regions and the pathways in which these genes are involved were determined by *in silico* analysis.

Materials and Methods

Data Collection and Normalization

Gene expression values for three subtypes of colon cancer as ascending, transverse, and descending, respectively, were obtained from (Gene Expression Omnibus) (GSE41258, <https://www.ncbi.nlm.nih.gov/geo/query/acc.cgi?acc=GSE41258>).^[17]

GSE41258 data includes a total of 47 ascending, 18 transverse and 31 descending colon cancer patient samples. In the data gene expressions profiled by array-based. Sample codes and anatomic locations used within this data are shown in **Appendix 1**. The obtained raw data were normalized by RMA (Robust Multi-Array) normalization algorithm in R 3.6.1.^[18]

Linear Regression Analysis

Linear regression analysis was performed to determine differentially expressed genes. Student's t-test (p-value) was calculated among the ascending, and transverse and ascending, and descending groups, and as a result of this

analysis, genes with $p < 0.05$ were selected. The analysis continued with the genes expressing these genes significantly in both groups.

Hierarchical Clustering

Gene Cluster 3.0 application^[19] was applied in order to cluster the determined statistically significant genes hierarchically. This clustering is based on Euclidean distance with a similarity metric limit for both genes and sequences, as well as the full link aggregation method. This methodology supports differentiating and distinguishing statistically highly variable genes.

Network and Pathway Analysis

In addition to linear regression and hierarchical clustering, network analysis with multivariable genes was performed in Cytoscape application 3.8.2^[20] using GeneMANIA.^[21] This app helps to better understand the correlation of statistically significant and highly variable genes by showing genetic interaction and their co-expression. Cytoscape also allows to illuminate the link between identified genes and even with each other.

In addition, the online DAVID: Bioinformatics Resources Tool was used to understand the respective pathways of these genes.^[22,23] This tool allows to show the proper pathway linked to these genes.

Gene Set Enrichment Analysis (GSEA)

GSEA 4.1.0 (Gene set enrichment analysis) was performed to understand the different genes among the specified groups.^[24] In this study, gene set enrichment analysis was performed among the ascending colon cancer patient groups and transverse colon cancer patient groups, ascending colon cancer patient groups and decreasing colon cancer patient groups. GSEA was performed by gene expression of GSE41258 data. As a result of gene set enrichment analysis, the enriched pathways and the most important and associated genes are determined by comparing the ascending and transverse and ascending and descending groups and their gene expression levels.

Results

After the normalization process of the data obtained was completed, the analyzes were continued with a total of 13,432 genes (21,225 Probe Sets). Ascending tumor samples were compared with transverse and descending tumor samples. When the genes belonging to ascending and transverse colon cancer were encountered, it was determined that a total of 1035 genes were expressed differently. This number was determined as 1531 when the

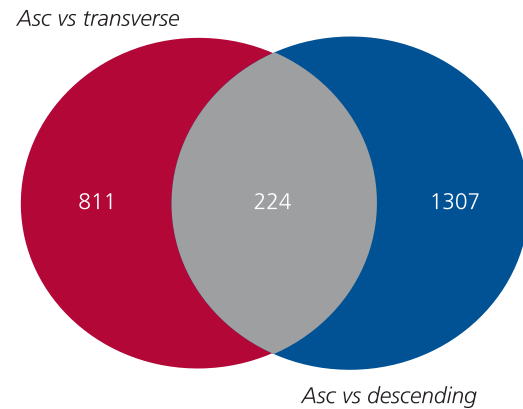


Figure 1. Linear regression analysis between the ascending (Asc) and transverse and Asc and descending groups showed expression of 224 common and statistically significant genes in both groups.

increasing and decreasing subgroups were compared. 224 genes were found in common in these two groups (**Figure 1**). **Appendix 2** includes t-test p-values ($p < 0.05$), which expressed statistically significant.

Then, upregulated genes in the ascending cohort and downregulated in the transverse and descending cohorts, and vice versa, were identified. *I.e.*, while *MLH3* and *APC* genes have a higher expression value when compared to other subgroups (**Figure 2a**), and *BAX* and *PMS2* genes are expressed lower (**Figure 2b**). The statistically significant genes cluster colon cancer subtypes (ascending, transverse and descending) in a hierarchical manner are shown in **Figure 3**.

Network analysis was performed to understand the network link between these 50 genes that are upregulated in ascending colon cancer and down-regulated in transverse and descending colon cancer, and vice versa. The connecting line between genes illuminates the network of these genes. The thickness of the binding line determines the binding strength of the respective genes. The thickest lines show that it has been determined that the connection between these genes has been determined by studying more precisely. In addition, the black nodes indicate the target genes given by the authors. On the other hand, gray nodes show genes associated with genes determined by GeneMANIA application in Cytoscape. The co-expression of genes is shown in **Figure 4a** and the genetic interaction between these genes is shown in **Figure 4b**. The genes that are available in the Online Mendelian Inheritance in Man (OMIM) database in the DAVID application and are statistically significantly up or down regulated in the ascending colon tumor subtype are shown in **Table 1**.

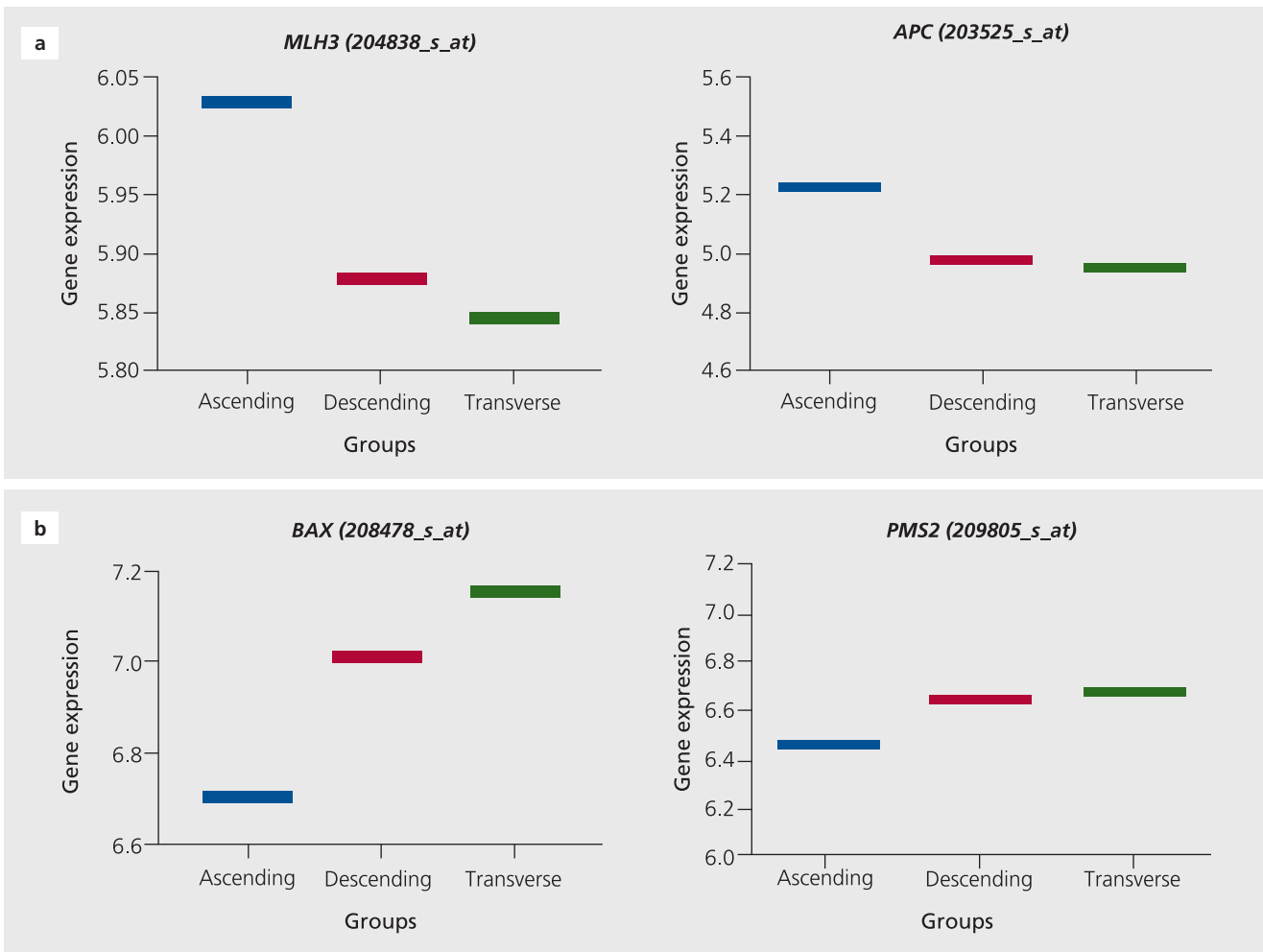


Figure 2. (a) Expression profile of the MLH3, APC, BAX and PMS2 genes. (a) MHL3 and APC significantly upregulated in ascending colon cancer compared to transverse and descending colon cancers; (b) BAX and PMS2 genes significantly down-regulated in ascending colon cancer compared to transverse and descending colon cancers. Numbers near the genes are Probe Set IDs; (Probe Set ID: The identifier that refers to a set of probe pairs selected to represent expressed sequences on an array).

As a result of GSEA, it was determined that a total of 11 gene sets were enriched in the ascending tumor type, while 6 gene sets were not enriched in the same group (Appendix 3).

Among these SPLICEOSOMAL_SNRNP_ASSEMBLY and TRANSITION_METAL_ION_HOMEOSTASIS contain the most gene sets. Therefore, they can be consid-

Table 1

The major 4 genes that are determined from OMIM database in the DAVID program and the diseases associated with these genes.

Gene symbols	OMIM disease
<i>APC, WNT signaling pathway regulator (APC)</i>	Colorectal cancer, somatic, Hepatoblastoma, somatic, Desmoid disease, hereditary, Adenomatous polyposis coli, Brain tumor-polyposis syndrome 2, Gardner syndrome, Gastric cancer, somatic, Adenoma, periampullary, somatic
<i>BCL2 associated X, apoptosis regulator (BAX)</i>	Colorectal cancer, somatic, T-cell acute lymphoblastic leukemia, somatic
<i>PMS1 homolog 2, mismatch repair system component (PMS2)</i>	Mismatch repair cancer syndrome, Colorectal cancer, hereditary nonpolyposis, type 4
<i>mutL homolog 3 (MLH3)</i>	Colorectal cancer, somatic, Endometrial cancer, susceptibility to, Colorectal cancer, hereditary nonpolyposis, type 7

ered to have a more important roles. SPLICEOSOMAL_SNRNP_ASSEMBLY is enriched in ascending colon tumor (Figure 5a), while the TRANSITION_METAL_ION_HOMEOSTASIS gene set is enriched in transverse and descending colon cancer (Figure 5b).

Discussion

Studies have intensified in the early 2000s to reveal the molecular differences of tumors in the right and left colon regions. In a comprehensive study by Guinney et al.^[25] 4 subgroups with different biological behavior were identified, taking into account the many expression sequences belonging to both regions of the colon.

In the present study, high or low expressed genes were detected in tumors belonging to the ascending region compared to other colon tumors. The network between these genes as well as the pathways were determined. Accordingly, 4 genes with statistically different expression values in the ascending colon cancer samples are associated with colon cancer based on the OMIM database. These genes are *APC* (Adenomatous polyposis coli), *BAX*, *PMS2* and *MLH3*.

APC gene is one of the most critical genes that affect colon cancer formation. The *APC* gene is used as a negative regulator for the Wnt signaling pathway involved in colon cancer development. It also takes part in phosphory-

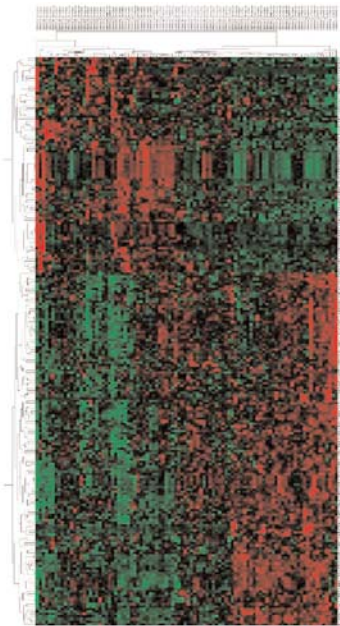


Figure 3. Hierarchical clustering of 224 statistically significant genes between groups. Genes highlighted in green represent genes with low expression, while red colored groups represent high expression.

lation occurring in cells. Studies show that the *APC* gene increases the expression of the *MMP9* gene using the JNK signaling pathway. Importantly, this indicates that the

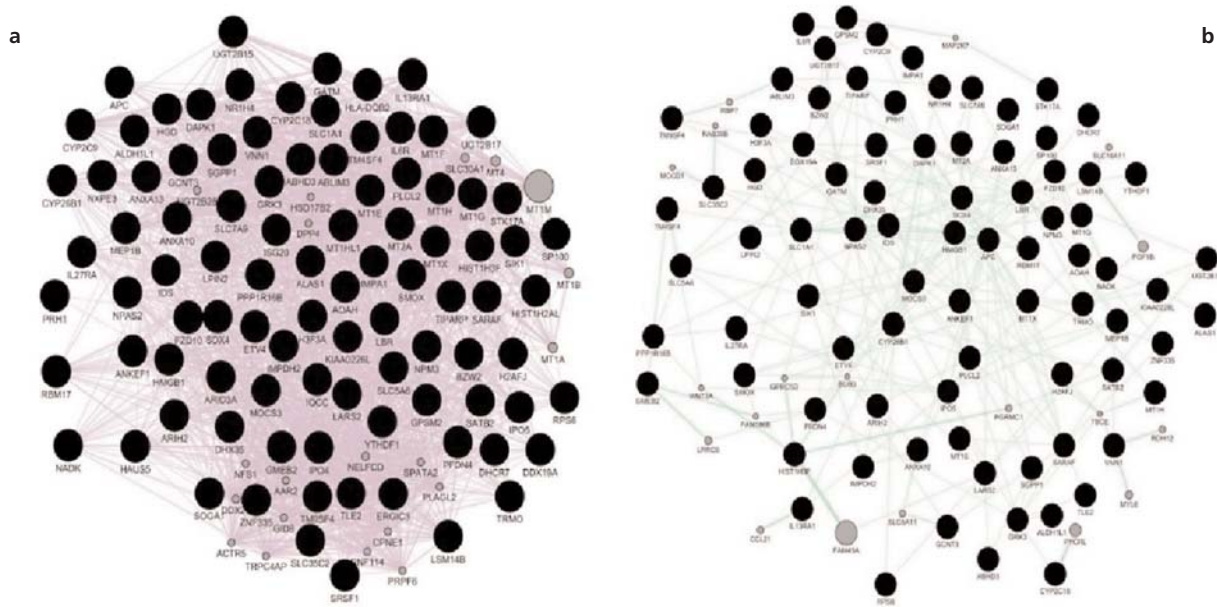


Figure 4. Representation of the co-expression and interactions of 100 genes. (a) statistically significant co-expression of 100 genes both among themselves and between other genes; (b) Representation of the genetic interactions of 100 genes that have statistically significant expression, both among themselves and between other genes.

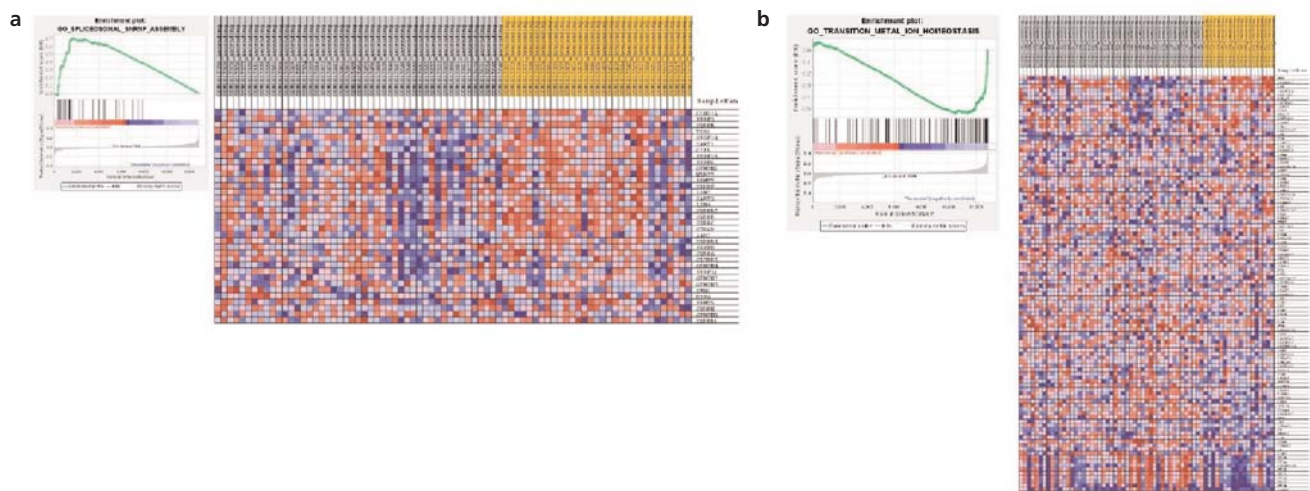


Figure 5. The graph and heat map of the SPLICEOSOMAL_SNRNP_ASSEMBLY and TRANSITION_METAL_ION_HOMEOSTASIS pathways. **(a)** SPLICEOSOMAL_SNRNP_ASSEMBLY enriched as a result of GSEA in ascending colon cancer. **(b)** TRANSITION_METAL_ION_HOMEOSTASIS enriched as a result of GSEA in transverse and descending colon cancer.

change in gene expression pattern is critical for the development of colorectal tumor cells. In other words, mutations in the *APC* gene play a role in the course of sporadic colorectal cancers, indicating that this gene is not only responsible for familial adenomatous polyposis (FAP). As a result of the researches, colorectal tumor formation occurs with the gradual occurrence of histological changes triggered by genetic changes and “adenoma-carcinoma” sequence as a result of mutation from tumor suppressor or oncogenic genes. These changes are known to occur as a result of loss of function resulting from mutation in the *APC* gene. In order to inactivate the critical function of the *APC* gene and trigger the formation of cancer cells, genetic instability and clonal expansion must basically occur. Because, these two changes can enable the activation of genes that support malignant transformation and tumor progression.^[26-28]

In parallel with the results we obtained, Du et al.^[29] showed that high expression of the *APC* gene is associated with poor prognosis in gastritis cancer. In our results, we determined that this gene has a higher expression in the ascending colon samples. This may be one of the reasons why colon cancers occurring in the right region have a worse prognosis than the left side.

In another study, it was shown that the *APC* gene is associated with a poor prognosis in microsatellite-stable proximal colon cancer supports the findings we obtained.^[30]

Our results show that the *BAX* gene has significantly less expression in colon tumors. Basically, *BAX* protein is known to promote cell death. Thus, it can inactivate the

expression of cancer cells. Studies on the importance of the *BAX* gene have shown that mutations in the *BAX* gene reduce the apoptotic index of colorectal cancer cells. It has been determined that this situation is seen in 50% of colorectal cancer cases. In addition, in similar studies, high expression of the *BAX* gene shows that it can be a good prognostic marker for colon cancer patients, except for the ascending colon.^[31,32]

One of the four basic sensitivity genes in Lynch syndrome (LS), the most common cancer syndrome in the world, is the *PMS1* Homologous 2, Mismatch Repair System Component (*PMS2*) gene. However, unfortunately it is not known whether the decrease in the gene expression value of the *PMS2* gene has an effect on the repair mechanism and, critically, how this effect may occur.

The study by Kasela et al.^[33] shows that MMR activity is significantly reduced in cells in which the *PMS2* gene is knocked out. These findings suggest that low expression of the *PMS2* gene in colon tumors that rise in parallel with the findings we obtained as a result of our analysis causes a decrease in DNA mismatch repair (MMR), leading to poor prognosis of the colon.

Another gene that we found to have higher expression in the colon cancer samples compared to other types of colon cancer is the *MLH3* gene. Although many studies show that descending colon cancer cases have a better survival rate, it is known that colon tumors in the right region have a worse prognosis than the left.^[34,35] Although not statistically significant, a study by Zhao et al.^[36] on ovarian can-

cer showed that higher expression of the *MLH3* gene is associated with lower survival. In addition, *MLH3* (MutL homolog 3), *MSH2* (MutS homolog 2) and *MSH3* (MutS homolog 3) genes are also known to be frequently seen in colorectal cancer. These genes have also been identified as potential genetic markers for personalized therapy, showing that they are associated with chemo-resistance.

As a result of GSE analysis, important gene sets associated with colorectal cancer progression and metastasis were determined. The enrichment of spliceosomal snRNP assembly gene sets in the ascending colon suggests that spliceostatin A, which has the capacity to target pladienolide compounds and spliceosome of these types of colon cancers, may be anticancer potential drugs.^[37] Based on the fundamental role of DNA methylation in colon cancer development, the application of DNMT inhibitors for the treatment of colon cancer patients, especially patients with DNA hypermethylation, is recommended as a result of studies.^[38]

Our results showed that the gene sets of Methyl transferase activity are enriched in ascending colon tumors. This suggests that such agents may be more effective in the treatment of this type of colon cancer subgroups especially. On the other hand, our analysis showed that Transition metal ion homeostasis gene sets enriched in other colon types except for ascending colon tumors. This suggests the use of drugs that target transition metal homeostasis such as ferristatin II, clioquinol, and omeprazole in colon cancers other than ascending colon cancers.^[39]

In addition to the characteristic features of tumors that occur in different parts of the colon, many studies have shown that their response to treatment can be very different. In this study, differently expressed genes and pathways were determined by comparing the whole genome profiles of tumors in different regions of the colon. A better understanding of the biology of the tumor allows more effective treatment. This may provide more effective treatment choices in the future. Importantly, it is crucial to validate the results of this study *in vitro* and clinically.

Conflict of Interest

No conflicts declared.

Ethics Approval

No ethics approval needed.

Funding

This research did not receive any specific grant from funding agencies in the public or commercial.

References

- Cappell MS. Pathophysiology, clinical presentation, and management of colon cancer. *Gastroenterol Clin North Am* 2008;37:1–24.
- Colussi D, Brandi G, Bazzoli F, Ricciardiello L. Molecular pathways involved in colorectal cancer: implications for disease behavior and prevention. *Int J Mol Sci* 2013;14:16365–85.
- Hisamuddin IM, Yang VW. Molecular genetics of colorectal cancer: an overview. *Curr Colorectal Cancer Rep* 2006;2:53–9.
- Tariq K, Ghias K. Colorectal cancer carcinogenesis: a review of mechanisms. *Cancer Biol Med* 2016;13:120–35.
- Ogino S, Odze RD, Kawasaki T, Brahmandam M, Kirkner GJ, Laird PW, Loda M, Fuchs CS. Correlation of pathologic features with CpG island methylator phenotype (CIMP) by quantitative DNA methylation analysis in colorectal carcinoma. *Am J Surg Pathol* 2006;30:1175–83.
- Peltomäki P, Lothe RA, Aaltonen LA, Pylkkänen L, Nyström-Lahti M, Seruca R, David L, Holm R, Ryberg D, Haugen A, Brøgger A, Børresen AL, de la Chapelle A. Microsatellite instability is associated with tumors that characterize the hereditary non-polyposis colorectal carcinoma syndrome. *Cancer Res* 1993;53:5853–5.
- Haggard FA, Boushey RP. Colorectal cancer epidemiology: incidence, mortality, survival, and risk factors. *Clin Colon Rectal Surg* 2009;22:191–7.
- Meyer B, Are C. Current status and future directions in colorectal cancer. *Indian J Surg Oncol* 2018;9:440–1.
- Rawla P, Sunkara T, Barsouk A. Epidemiology of colorectal cancer: incidence, mortality, survival, and risk factors. *Prz Gastroenterol* 2019;14:89–103.
- White A, Ironmonger L, Steele RJC, Ormiston-Smith N, Crawford C, Seims A. A review of sex-related differences in colorectal cancer incidence, screening uptake, routes to diagnosis, cancer stage and survival in the UK. *BMC Cancer* 2018;18:906.
- Carethers JM. Risk factors for colon location of cancer. *Transl Gastroenterol Hepatol* 2018;3:76.
- Church JM. Colon cancer screening update and management of the malignant polyp. *Clin Colon Rectal Surg* 2005;18:141–9.
- Li F-Y, Lai M-D. Colorectal cancer, one entity or three. *J Zhejiang Univ Sci B* 2009;10:219–29.
- Tamas K, Walenkamp AM, de Vries EG, van Vugt MA, Beets-Tan RG, van Etten B, de Groot DJA, Hospers GAP. Rectal and colon cancer: Not just a different anatomic site. *Cancer Treat Rev* 2015;41:671–9.
- Lee L, Erkan A, Alhassan N, Kelly JJ, Nassif GJ, Albert MR, Monson JR. Lower survival after right-sided versus left-sided colon cancers: is an extended lymphadenectomy the answer? *Surg Oncol* 2018;27:449–55.
- Turk S, Turk C, Temirci ES, Malkan UY, Ucar G, Ozguven SV. Assessing the genetic impact of *Enterococcus faecalis* infection on gastric cell line MKN74. *Ann Microbiol* 2021;71:Article 8.
- Barrett T, Wilhite SE, Ledoux P, Evangelista C, Kim IF, Tomashevsky M, Marshall KA, Phillippy KH, Sherman PM, Holko M, Yefanov A, Lee H, Zhang N, Robertson CL, Serova N, Davis S, Soboleva A. NCBI GEO: archive for functional genomics data sets—update. *Nucleic Acids Res* 2013;41:D991–D5.
- Irizarry RA, Bolstad BM, Collin F, Cope LM, Hobbs B, Speed TP. Summaries of Affymetrix GeneChip probe level data. *Nucleic Acids Res* 2003;31:e15.

19. de Hoon MJL, Imoto S, Nolan J, Miyano S. Open source clustering software. *Bioinformatics* 2004;20:1453–4.
20. Shannon P, Markiel A, Ozier O, Baliga NS, Wang JT, Ramage D, Amin N, Schwikowski B, Ideker T. Cytoscape: a software environment for integrated models of biomolecular interaction networks. *Genome Res* 2003;13:2498–504.
21. Franz M, Rodriguez H, Lopes C, Zuberi K, Montojo J, Bader GD, Morris Q. GeneMANIA update 2018. *Nucleic Acids Res* 2018;46:W60–W4.
22. Huang da W, Sherman BT, Lempicki RA. Systematic and integrative analysis of large gene lists using DAVID bioinformatics resources. *Nature protocols* 2009;4(1):44–57.
23. Huang da W, Sherman BT, Lempicki RA. Bioinformatics enrichment tools: paths toward the comprehensive functional analysis of large gene lists. *Nucleic Acids Res* 2009;37:1–13.
24. Subramanian A, Tamayo P, Mootha VK, Mukherjee S, Ebert BL, Gillette MA, Paulovich A, Pomeroy SL, Golub TR, Lander ES, Mesirov JP. Gene set enrichment analysis: a knowledge-based approach for interpreting genome-wide expression profiles. *Proc Natl Acad Sci USA* 2005;102:15545–50.
25. Guinney J, Dienstmann R, Wang X, de Reyniès A, Schlicker A, Soneson C, Marisa L, Roepman P, Nyamundanda G, Angelino P, Bot BM, Morris JS, Simon IM, Gerster S, Fessler E, De Sousa E Melo F, Missiaglia E, Ramay H, Barras D, Homicsko K, Maru D, Manyam GC, Broom B, Boige V, Perez-Villamil B, Laderas T, Salazar R, Gray JW, Hanahan D, Tabernero J, Bernards R, Friend SH, Laurent-Puig P, Medema JP, Sadanandam A, Wessels L, Delorenzi M, Kopetz S, Vermeulen L, Tejpar S. The consensus molecular subtypes of colorectal cancer. *Nat Med* 2015;21:1350–6.
26. Fodde R. The APC gene in colorectal cancer. *Eur J Cancer* 2002;38:867–71.
27. Fodde R, Smits R, Clevers H. APC, signal transduction and genetic instability in colorectal cancer. *Nat Rev Cancer* 2001;1:55–67.
28. Zhang L, Shay JW. Multiple roles of apc and its therapeutic implications in colorectal cancer. *J Natl Cancer Ins* 2017;109:djw332.
29. Du W-B, Lin C-H, Chen W-B. High expression of APC is an unfavorable prognostic biomarker in T4 gastric cancer patients. *World J Gastroenterol* 2019;25:4452–67.
30. Jorissen RN, Christie M, Mouradov D, Sakthianandeswaren A, Li S, Love C, Xu ZZ, Molloy PL, Jones JT, McLaughlin S, Ward RL, Hawkins NJ, Ruzkiewicz AR, Moore J, Burgess AW, Busam D, Zhao Q, Strausberg RL, Lipton L, Desai J, Gibbs P, Sieber OM. Wild-type APC predicts poor prognosis in microsatellite-stable proximal colon cancer. *Br J Cancer* 2015;113:979–88.
31. Katkooori VR, Suarez-Cuervo C, Shanmugam C, Jhala NC, Callens T, Messiaen L, Posey J 3rd, Bumpers HL, Meleth S, Grizzle WE, Manne U. Bax expression is a candidate prognostic and predictive marker of colorectal cancer. *J Gastrointest Oncol* 2010;1:76–89.
32. Prczynicz A, Gryko M, Niewiarowska K, Cepowicz D, Ustymowicz M, Kemona A, Guzinska-Ustymowicz K. Bax protein may influence the invasion of colorectal cancer. *World J Gastroenterol* 2014;20:1305–10.
33. Kasela M, Nyström M, Kansikas M. PMS2 expression decrease causes severe problems in mismatch repair. *Hum Mutat* 2019;40:904–7.
34. Lim DR, Kuk JK, Kim T, Shin EJ. Comparison of oncological outcomes of right-sided colon cancer versus left-sided colon cancer after curative resection: which side is better outcome? *Medicine (Baltimore)* 2017;96:e8241–e.
35. Nahas SC, Nahas CS, Bustamante-Lopez LA, Pinto RA, Marques CF, Campos FG, Ceconello I. Prognostic factors of surgically-treated patients with cancer of the right colon: a ten years' experience of a single university institution. *Arq Bras Cir Dig* 2017;30:103–7.
36. Zhao C, Li S, Zhao M, Zhu H, Zhu X. Prognostic values of DNA mismatch repair genes in ovarian cancer patients treated with platinum-based chemotherapy. *Archives Gynecol Obstet* 2018;297:153–9.
37. van Alphen RJ, Wiemer EAC, Burger H, Eskens FALM. The spliceosome as target for anticancer treatment. *Br J Cancer* 2009;100:228–32.
38. Cervena K, Siskova A, Buchler T, Vodicka P, Vymetalkova V. Methylation-based therapies for colorectal cancer. *Cells* 2020;9:1540.
39. Weekley CM, He C. Developing drugs targeting transition metal homeostasis. *Curr Opin Chem Biol* 2017;37:26–32.

ORCID ID:

C. Türk 0000-0003-1514-7294

**Correspondence to:** Can Türk, PhD

Department of Medical Microbiology, Faculty of Medicine, Lokman Hekim University, 06510, Ankara, Turkey

Phone: +90 542 457 18 55

e-mail: can.turk@lokmanhekim.edu.tr

Conflict of interest statement: No conflicts declared.

This is an open access article distributed under the terms of the Creative Commons Attribution-NonCommercial-NoDerivs 4.0 Unported (CC BY-NC-ND4.0) Licence (<http://creativecommons.org/licenses/by-nc-nd/4.0/>) which permits unrestricted noncommercial use, distribution, and reproduction in any medium, provided the original work is properly cited. *How to cite this article:* Türk C. *In silico* transcriptomic analysis of ascending colon cancer unearths known and novel genes and gene sets regard to characteristic features of colon cancer. *Anatomy* 2021;15(1):11–25.

Appendix 1

Sample codes and anatomic locations of colon cancer patients.

Sample code	Anatomic location	Sample code	Anatomic location
GSM1012286_00620AR1	Ascending colon	GSM1012591_C0194AR1	Ascending colon
GSM1012308_02500AR1	Ascending colon	GSM1012592_C0194HR1	Ascending colon
GSM1012320_03283AR1	Ascending colon	GSM1012627_C0323AR1	Ascending colon
GSM1012326_03519AR2	Ascending colon	GSM1012628_C0323H	Ascending colon
GSM1012327_03519HR2	Ascending colon	GSM1012631_C0330AR3	Ascending colon
GSM1012350_04276AR2	Ascending colon	GSM1012634_C0334AR3	Ascending colon
GSM1012351_04276HR2	Ascending colon	GSM1012645_C0487AR3	Ascending colon
GSM1012358_04800AR4	Ascending colon	GSM1012646_c0487hr3	Ascending colon
GSM1012359_04800hr4	Ascending colon	GSM1012307_02308AR1	Descending colon
GSM1012361_05025AR4	Ascending colon	GSM1012325_03465AR3	Descending colon
GSM1012366_05629AR4	Ascending colon	GSM1012336_03706AR2	Descending colon
GSM1012368_05786AR2	Ascending colon	GSM1012337_03706HR2	Descending colon
GSM1012369_05786hr3	Ascending colon	GSM1012346_04176AR2	Descending colon
GSM1012371_05885AR2	Ascending colon	GSM1012347_04176HR3	Descending colon
GSM1012384_06840AR2	Ascending colon	GSM1012374_06220AR2	Descending colon
GSM1012399_08018AR2	Ascending colon	GSM1012381_06706AR2	Descending colon
GSM1012416_09468AR2	Ascending colon	GSM1012385_06997AR3	Descending colon
GSM1012423_10194AR2	Ascending colon	GSM1012389_07427AR2	Descending colon
GSM1012426_10264AR3	Ascending colon	GSM1012408_09054AR2	Descending colon
GSM1012447_14475AR3	Ascending colon	GSM1012421_09811AR2	Descending colon
GSM1012461_A1516AR4	Ascending colon	GSM1012429_10630AR3	Descending colon
GSM1012463_A1716AR4	Ascending colon	GSM1012445_13321AR3	Descending colon
GSM1012468_A2367AR4	Ascending colon	GSM1012446_13357AR3	Descending colon
GSM1012494_A5135AR2	Ascending colon	GSM1012456_A0702AR4	Descending colon
GSM1012495_A5135AR2_ez	Ascending colon	GSM1012469_A2434AR3	Descending colon
GSM1012496_A5135DR2	Ascending colon	GSM1012474_A3536AR4	Descending colon
GSM1012499_A5320AR3	Ascending colon	GSM1012478_A4248AR4	Descending colon
GSM1012539_C0123AR3	Ascending colon	GSM1012544_C0128AR3	Descending colon
GSM1012540_C0123HR1	Ascending colon	GSM1012545_C0128BR1	Descending colon
GSM1012547_C0134AR1	Ascending colon	GSM1012565_C0151AR1	Descending colon
GSM1012548_C0134HR1	Ascending colon	GSM1012577_C0168AR3	Descending colon
GSM1012549_C0136AR1	Ascending colon	GSM1012580_C0172AR1	Descending colon
GSM1012550_C0136HR1	Ascending colon	GSM1012581_C0172HR1	Descending colon
GSM1012551_C0136KR1	Ascending colon	GSM1012595_C0200AR3	Descending colon
GSM1012552_C0136UR1	Ascending colon	GSM1012603_C02308H	Descending colon
GSM1012572_C0157AR1	Ascending colon	GSM1012615_C0273A	Descending colon
GSM1012573_C0157H	Ascending colon	GSM1012617_C0283AR3	Descending colon
GSM1012589_C0193AR1	Ascending colon	GSM1012629_C0329AR1	Descending colon
GSM1012590_C0193HR1	Ascending colon	GSM1012630_C0329HR1	Descending colon

Appendix 1 [Continued]

Sample codes and anatomic locations of colon cancer patients.

Sample code	Anatomic location	Sample code	Anatomic location
GSM1012297_00990AR1	Sigmoid colon	GSM1012561_C0147AR1	Sigmoid colon
GSM1012303_02184AR2	Sigmoid colon	GSM1012562_C0147AR3	Sigmoid colon
GSM1012304_02184HR2	Sigmoid colon	GSM1012563_C0147HR1	Sigmoid colon
GSM1012310_02679AR1	Sigmoid colon	GSM1012569_C0154AR1	Sigmoid colon
GSM1012311_02679BR1	Sigmoid colon	GSM1012576_C0159AR3	Sigmoid colon
GSM1012314_02815AR1	Sigmoid colon	GSM1012578_C0170AR1	Sigmoid colon
GSM1012315_02815HR1	Sigmoid colon	GSM1012579_C0171AR1	Sigmoid colon
GSM1012317_03023AR1	Sigmoid colon	GSM1012584_C0180AR1	Sigmoid colon
GSM1012318_03023HR1	Sigmoid colon	GSM1012585_C0180HR1	Sigmoid colon
GSM1012319_03156AR1	Sigmoid colon	GSM1012586_C0181AR3	Sigmoid colon
GSM1012354_04494AR4	Sigmoid colon	GSM1012587_C0186AR3	Sigmoid colon
GSM1012355_04494HR4	Sigmoid colon	GSM1012588_C0192A	Sigmoid colon
GSM1012367_05708AR2	Sigmoid colon	GSM1012593_C0198AR1	Sigmoid colon
GSM1012375_06265AR2	Sigmoid colon	GSM1012594_C0198HR1	Sigmoid colon
GSM1012379_06657AR2	Sigmoid colon	GSM1012611_C0257AR3	Sigmoid colon
GSM1012380_06657HR3	Sigmoid colon	GSM1012618_C0285AR1	Sigmoid colon
GSM1012386_07061AR2	Sigmoid colon	GSM1012619_C0295AR3	Sigmoid colon
GSM1012387_07145AR2	Sigmoid colon	GSM1012620_C0297AR1	Sigmoid colon
GSM1012397_07930AR2	Sigmoid colon	GSM1012621_C0297HR1	Sigmoid colon
GSM1012401_08061AR2	Sigmoid colon	GSM1012624_C0312AR3	Sigmoid colon
GSM1012405_08168AR2	Sigmoid colon	GSM1012625_C03156H	Sigmoid colon
GSM1012407_08792AR2	Sigmoid colon	GSM1012316_02832AR1	Transverse colon
GSM1012409_09077AR2	Sigmoid colon	GSM1012328_03531AR2	Transverse colon
GSM1012411_09297AR2	Sigmoid colon	GSM1012334_03657AR2	Transverse colon
GSM1012413_09394AR2	Sigmoid colon	GSM1012335_03657HR2	Transverse colon
GSM1012424_10216AR3	Sigmoid colon	GSM1012344_03862AR2	Transverse colon
GSM1012428_10512AR3	Sigmoid colon	GSM1012345_03862HR2	Transverse colon
GSM1012439_12292AR3	Sigmoid colon	GSM1012352_04388AR2	Transverse colon
GSM1012442_12847AR3	Sigmoid colon	GSM1012364_05424AR4	Transverse colon
GSM1012462_A1644AR4	Sigmoid colon	GSM1012392_07632AR2	Transverse colon
GSM1012492_A4947AR4	Sigmoid colon	GSM1012393_07662AR2	Transverse colon
GSM1012502_A5627AR3	Sigmoid colon	GSM1012396_07925AR2	Transverse colon
GSM1012503_A5627BR3	Sigmoid colon	GSM1012410_09185AR2	Transverse colon
GSM1012526_C0101AR3	Sigmoid colon	GSM1012437_12237AR3	Transverse colon
GSM1012527_C0104AR3	Sigmoid colon	GSM1012467_A2226AR4	Transverse colon
GSM1012531_C0112AR1	Sigmoid colon	GSM1012507_A6141AR	Transverse colon
GSM1012535_C0115AR3	Sigmoid colon	GSM1012529_C0111AR1	Transverse colon
GSM1012541_C0124AR3	Sigmoid colon	GSM1012530_C0111HR1	Transverse colon
GSM1012553_C0137AR1	Sigmoid colon	GSM1012570_C0155AR3	Transverse colon
GSM1012554_C0137HR1	Sigmoid colon		

Appendix 2

T-test p-values which expressed statistically significant ($p < 0.05$).

Probe set	Gene symbol	T-test of ascending vs transverse colon	T-test of ascending vs descending colon
201888_s_at	<i>IL13RA1</i>	0.00016271505536615	0.00521747486476386
205844_at	<i>VNN1</i>	0.000385136080291112	0.00776739644507052
47530_at	<i>C9orf156</i>	0.00081241732984075	0.0365888700564041
206122_at	<i>SOX15</i>	0.000939632286890665	0.0319002678319461
212665_at	<i>TIPARP</i>	0.00109740862530723	0.0149345738624881
210219_at	<i>SP100</i>	0.00129941458167625	0.0294511216230853
216300_x_at	<i>RARA</i>	0.00151063853838347	0.0208808293029783
209937_at	<i>TM4SF4</i>	0.00151545886589597	0.00353593901875218
213664_at	<i>SLC1A1</i>	0.0015657003068625	0.00415570175875679
215427_s_at	<i>ZCCHC14</i>	0.00169179299291247	0.0129502331872678
210651_s_at	<i>EPHB2</i>	0.00191836064222717	0.00348119288028227
213823_at	<i>HOXA11</i>	0.00207814621070703	0.0121059077242761
214191_at	<i>ICA1</i>	0.00223163799888523	0.0268164312486215
205730_s_at	<i>ABLIM3</i>	0.00237677641741103	0.0110983916886486
209320_at	<i>ADCY3</i>	0.0024290420211383	0.0413257100128183
217415_at	<i>POLR2A</i>	0.00269575520034894	0.0443829653243419
219021_at	<i>RNF121</i>	0.00270128512746877	0.0241668884728377
204843_s_at	<i>PRKAR2A</i>	0.00270329662456024	0.022956823964002
202459_s_at	<i>LPIN2</i>	0.00296337853260737	0.0195009066395492
203139_at	<i>DAPK1</i>	0.00298573846223663	0.00816942350979891
217165_x_at	<i>MT1F</i>	0.00324876323465622	0.00396035427170252
218529_at	<i>CD320</i>	0.00351895978865357	0.0180499499266918
210143_at	<i>ANXA10</i>	0.00361453883148403	0.0221704734694777
208559_at	<i>PDX1</i>	0.00369666604226198	0.0122623122943415
221268_s_at	<i>SGPP1</i>	0.00378110101356417	0.0102610200115258
202693_s_at	<i>STK17A</i>	0.00384950815651231	0.00391428186084062
206330_s_at	<i>SHC3</i>	0.00394389390077759	0.0245753599746245
209415_at	<i>FZR1</i>	0.00402400242963556	0.0182118711074509
219508_at	<i>GCNT3</i>	0.00422343917924779	0.047898599428003
217661_x_at	<i>SIX5</i>	0.00425011261287881	0.0137974636654496
220220_at	<i>LRRC37A2</i>	0.00439560705223552	0.00836802539554393
220017_x_at	<i>CYP2C9</i>	0.00444735128361806	0.00134303329341892
204326_x_at	<i>MT1X</i>	0.00519304170186292	0.00834774838935453
220631_at	<i>OSGEPL1</i>	0.00526809783102296	0.00553805125320832
207245_at	<i>UGT2B17</i>	0.00550011172873036	0.000207098444077029
211837_s_at	<i>PTCRA</i>	0.0055415215807438	0.00671054670922654
208323_s_at	<i>ANXA13</i>	0.00558331241550815	0.000689024383137067
211612_s_at	<i>IL13RA1</i>	0.00567959161179234	0.00361028639239372
206396_at	<i>SLC1A1</i>	0.00595593858849176	0.00220879457656152
215536_at	<i>HLA-DQB2</i>	0.00630638948511806	0.0111442131330687
213629_x_at	<i>MT1F</i>	0.00635435696241856	0.0060779585920024
218902_at	<i>NOTCH1</i>	0.00657731256094427	0.0373357125780496
33304_at	<i>ISG20</i>	0.00679460592547953	0.0470076157248008
215741_x_at	<i>AKAP8L</i>	0.00680810240983979	0.0241477714028368
216671_x_at	<i>MUC8</i>	0.00688053299616361	0.0383618636348532
204487_s_at	<i>KCNQ1</i>	0.00695196777896742	0.0267287721809296
207392_x_at	<i>UGT2B15</i>	0.00701467429678188	0.0000402790708368557
210126_at	<i>PSG9</i>	0.00708607742512625	0.0125502556385473
206461_x_at	<i>MT1H</i>	0.00740990648227567	0.00664244458624349
216025_x_at	<i>CYP2C9</i>	0.0081014424105605	0.00278353975836334

Appendix 2 [Continued]

T-test p-values which expressed statistically significant ($p < 0.05$).

Probe set	Gene symbol	T-test of ascending vs transverse colon	T-test of ascending vs descending colon
209150_s_at	<i>IPO4</i>	0.00813333467021513	0.0291253365640916
208478_s_at	<i>BAX</i>	0.00842647383645954	0.0180985713492701
208581_x_at	<i>MT1X</i>	0.0084498408519362	0.0069586322696345
204745_x_at	<i>MT1G</i>	0.00878185719233833	0.00825222817999293
205945_at	<i>IL6R</i>	0.00903050180890933	0.0155618323765579
209938_at	<i>TADA2A</i>	0.00945544955869718	0.00309026125623243
207484_s_at	<i>EHMT2</i>	0.00948494012139873	0.00219893832066608
217144_at	<i>UBBP1</i>	0.00958596978462974	0.0145424696521897
212349_at	<i>POFUT1</i>	0.00973930667339722	0.000617553707937332
208141_s_at	<i>DOHH</i>	0.00983615661677668	0.011910985340121
215481_s_at	<i>PEX5</i>	0.0103438282376347	0.00804466303700721
219705_at	<i>QSER1</i>	0.0104459036229018	0.00676393361084865
213017_at	<i>ABHD3</i>	0.0105440609903702	0.00476599658264377
222048_at	<i>CRYBB2P1</i>	0.0108152465635539	0.0282968004426767
210267_at	<i>NIPAL3</i>	0.0109010197875034	0.00856582555555673
214509_at	<i>HIST1H3I</i>	0.0109945017669423	0.00339083291753431
211165_x_at	<i>EPHB2</i>	0.0110917447081954	0.0447733383125438
200847_s_at	<i>SARAF</i>	0.0121362657717354	0.0419230207567175
216336_x_at	<i>MT1E</i>	0.0125092393886943	0.019407065285516
215090_x_at	<i>LOC440434</i>	0.0127541655551143	0.0147145577512873
201269_s_at	<i>NUDCD3</i>	0.0128524197409381	0.0446016814176866
212185_x_at	<i>MT2A</i>	0.0130672353402319	0.00649540715033966
216661_x_at	<i>CYP2C9</i>	0.0131555450446433	0.00263835552758308
220135_s_at	<i>SLC7A9</i>	0.0132174575878814	0.0186779975671967
211217_s_at	<i>KCNQ1</i>	0.0133533618305394	0.0372855960451213
213235_at	<i>KNOP1</i>	0.0134177122427596	0.0111546975489925
213084_x_at	<i>RPL23A</i>	0.0135588704208067	0.0190007343585758
203178_at	<i>GATM</i>	0.0139109285622442	0.0150692618903142
202840_at	<i>TAF15</i>	0.0141517073353498	0.000826256415493992
206342_x_at	<i>IDS</i>	0.0151931991872957	0.0495167710834829
214421_x_at	<i>CYP2C9</i>	0.0152940141134296	0.0045228127940653
206340_at	<i>NR1H4</i>	0.0154381593388525	0.00527264108358479
213880_at	<i>LGR5</i>	0.0155320771240081	0.0258575028455203
218952_at	<i>PCSK1N</i>	0.0156360941687803	0.0490248292471147
207532_at	<i>CRYGD</i>	0.0157250215466018	0.0015745823661968
203525_s_at	<i>APC</i>	0.0160199606611479	0.00654979599151522
203011_at	<i>IMPA1</i>	0.0161134843221806	0.0212973706856163
212859_x_at	<i>MT1E</i>	0.0162127222474829	0.0344523189650514
217540_at	<i>NXPE3</i>	0.0162353616457161	0.0287143614578353
216256_at	<i>GRM8</i>	0.0165960997424514	0.00285899797251689
217476_at	<i>NR1D1</i>	0.0166520787088074	0.0298478241776261
208720_s_at	<i>RBM39</i>	0.0167777891030138	0.00599829409632798
211456_x_at	<i>MT1HL1</i>	0.0168212757278422	0.0178286194911081
217696_at	<i>FUT7</i>	0.0168766608008016	0.0120566924445446
221270_s_at	<i>QTRT1</i>	0.0172160800745213	0.00221405955547414
212221_x_at	<i>IDS</i>	0.0172437073161689	0.0219544554849409
216842_x_at	<i>AC007967.3</i>	0.0175720344954194	0.036529406495752
216218_s_at	<i>PLCL2</i>	0.0176936200023459	0.00309755282910636
200051_at	<i>SART1</i>	0.0178721328287539	0.0192476105409923
207545_s_at	<i>LOC101928143</i>	0.0179519211554138	0.0301148107716804

Appendix 2 [Continued]

T-test p-values which expressed statistically significant ($p < 0.05$).

Probe set	Gene symbol	T-test of ascending vs transverse colon	T-test of ascending vs descending colon
205208_at	ALDH1L1	0.0183667929138689	0.00415250332330587
205221_at	HGD	0.0184049090852041	0.00271285945641777
221820_s_at	KAT8	0.0186851086363686	0.028753409045594
203655_at	XRCC1	0.0195552969036288	0.0400589045965037
212750_at	PPP1R16B	0.0195646183353	0.0492377107044371
221506_s_at	TNPO2	0.0196184627564618	0.00174457407733694
209805_at	PMS2	0.019825195471822	0.00486316399502379
215064_at	SC5D	0.0199954612067164	0.0440091445857484
207849_at	IL2	0.0207176895788813	0.0276467525952765
205906_at	FOXJ1	0.0207563339586082	0.0179806461888217
219825_at	CYP26B1	0.0209583654715191	0.00881670793732234
214223_at	PTP4A3	0.0217386685680162	0.0479893913605289
208126_s_at	CYP2C18	0.0217932781609716	0.000177625442325609
219931_s_at	KLHL12	0.0218840059415327	0.0117095765515496
213829_x_at	RTEL1	0.0219376081160701	0.00440303070992156
215720_s_at	NFYA	0.0221274789124913	0.0312210491487658
215152_at	MYB	0.02264495177855	0.000756885454908027
211526_s_at	RTEL1	0.0233096492986428	0.0285190925053854
213683_at	ACSL6	0.0234069662080029	0.00120288150344804
208918_s_at	NADK	0.0234457136397553	0.0248146569085601
213866_at	SAMD14	0.0238234367565757	0.0393396874739623
205633_s_at	ALAS1	0.0239382239270208	0.00821418634889686
202695_s_at	STK17A	0.0243135715265882	0.00152227814059241
206918_s_at	CPNE1	0.0244699526788544	0.00345312532742211
220143_x_at	LUC7L	0.0247428675222006	0.0219049685866196
208078_s_at	SIK1	0.0248000872538751	0.041063891774819
216255_s_at	GRM8	0.0249146761499734	0.0157547724656726
212057_at	GSE1	0.0249589897515221	0.0484698192948672
204600_at	EPHB3	0.0253505027616503	0.0147809814079668
211207_s_at	ACSL6	0.0255396431283917	0.00395698612756328
200647_x_at	EIF3C	0.0255607837170601	0.0483723632307421
207251_at	MEP1B	0.0257354358177781	0.009189242444587496
207839_s_at	TMEM8B	0.0258093361300557	0.0196095035480556
213588_x_at	RPL14	0.0260872509286091	0.0111475221873574
212486_s_at	FYN	0.0261078855626755	0.00428508777172897
213052_at	PRKAR2A	0.0264065924349971	0.0021970152350812
202453_s_at	GTF2H1	0.0265095800665638	0.0346504801267993
211082_x_at	MARK2	0.0268829025992098	0.0425854689163323
216076_at	L3MBTL1	0.0272017509712494	0.00398324397474508
203692_s_at	E2F3	0.0272445128841317	0.0156576760326496
203060_s_at	PAPSS2	0.027895144467807	0.00389786074898919
205316_at	SLC15A2	0.0279885836431827	0.0326919567585641
220544_at	TSKS	0.0287006492697387	0.00509790839600052
221309_at	RBM17	0.0290725433318261	0.0268887155853216
201418_s_at	SOX4	0.0292023385814225	0.0126185253830067
206092_x_at	RTEL1	0.0293869362376055	0.00113860086201966
78330_at	ZNF335	0.0294480246483918	0.0171741697532607
205272_s_at	PRH1	0.0299220129135875	0.0369958217690242
217702_at	IL27RA	0.0299544046093803	0.0401086359899183
209589_s_at	EPHB2	0.0311842634624996	0.0123654229209086

Appendix 2 [Continued]

T-test p-values which expressed statistically significant ($p < 0.05$).

Probe set	Gene symbol	T-test of ascending vs transverse colon	T-test of ascending vs descending colon
211955_at	<i>IPO5</i>	0.0315578723564607	0.0176122286833458
211682_x_at	<i>UGT2B28</i>	0.0318354648805484	0.00648649431682457
204087_s_at	<i>SLC5A6</i>	0.0321670692191126	0.0122490683721897
203526_s_at	<i>APC</i>	0.0328761174866492	0.0212298366801329
200679_x_at	<i>HMGB1</i>	0.0329526572600519	0.00917422818239894
213435_at	<i>SATB2</i>	0.0330632523557303	0.00922901315374263
200680_x_at	<i>HMGB1</i>	0.0332268565706552	0.00579719881939093
214554_at	<i>HIST1H2AL</i>	0.0337259349634992	0.0327594672367312
204016_at	<i>LARS2</i>	0.0337866327513232	0.00764014221799583
201741_x_at	<i>SRSF1</i>	0.0337921106182684	0.0072445228268078
219017_at	<i>ETNK1</i>	0.0339975156635643	0.0481914664756225
221803_s_at	<i>NRBF2</i>	0.034042693873365	0.000847266509728566
207470_at	<i>BC113958</i>	0.0340739924012714	0.0176655520428064
200721_s_at	<i>ACTR1A</i>	0.0341968526622086	0.0189529433666907
209130_at	<i>SNAP23</i>	0.0343722782076268	0.0124604330970823
219471_at	<i>KIAA0226L</i>	0.0348646305671111	0.00420770437161399
208209_s_at	<i>C4BPB</i>	0.0351031049245856	0.0153006465554325
204109_s_at	<i>NFYA</i>	0.0354670905518342	0.0188479934829926
201229_s_at	<i>ARIH2</i>	0.0356977568922814	0.0403156245301037
216032_s_at	<i>ERGIC3</i>	0.0361625187029235	0.0122220223853168
201556_s_at	<i>VAMP2</i>	0.036315069181276	0.00326733016642116
205459_s_at	<i>NPAS2</i>	0.0363568240584999	0.0275010969600155
201892_s_at	<i>IMPDH2</i>	0.0368418931444874	0.0164254058840621
217809_at	<i>BZW2</i>	0.0370411672528593	0.0111530894359189
219316_s_at	<i>FLVCR2</i>	0.0371526563664439	0.0182386046049849
215930_s_at	<i>CTAGE5</i>	0.0372737894038448	0.0098514878384589
201716_at	<i>SNX1</i>	0.0374101133631535	0.0390882393411317
205460_at	<i>NPAS2</i>	0.0377153078107637	0.00438955957285321
212198_s_at	<i>TM9SF4</i>	0.0377980018920065	0.0315153804333592
201791_s_at	<i>DHCR7</i>	0.037836973883822	0.0105566885301129
220354_at	<i>MCF2L-AS1</i>	0.0382621296936618	0.0194122145451439
212322_at	<i>SGPL1</i>	0.0382890186278431	0.0269948479228522
215852_x_at	<i>SOGA1</i>	0.0384830960234485	0.038601969455771
219447_s_at	<i>SLC35C2</i>	0.0390051865506059	0.00838972207178568
208506_at	<i>HIST1H3F</i>	0.0393787505015506	0.00327565992567932
204183_s_at	<i>ADRBK2</i>	0.0393973730972733	0.000287600062011398
219764_at	<i>FZD10</i>	0.0394147921859214	0.0334876991591887
205639_at	<i>AOAH</i>	0.0395018367342232	0.00311265333171492
206407_s_at	<i>CCL13</i>	0.0397475278576177	0.043343940220237
213828_x_at	<i>H3F3A</i>	0.0400145315327654	0.0353596437251339
205141_at	<i>ANG</i>	0.0403289905997115	0.0159352728259481
206141_at	<i>MOCS3</i>	0.0404920863485373	0.0182643063304355
201795_at	<i>LBR</i>	0.0406052479067525	0.00100262931231705
204838_s_at	<i>MLH3</i>	0.0409725162323634	0.0104570300276411
220936_s_at	<i>H2AFJ</i>	0.0409742871889988	0.00740207154862594
209134_s_at	<i>RPS6</i>	0.0411455819895845	0.0143108121353305
220144_s_at	<i>ANKEF1</i>	0.0412498731136823	0.00869022109987666
213053_at	<i>HAUS5</i>	0.0412932176220598	0.0150984897605612
41577_at	<i>PPP1R16B</i>	0.0414980406250487	0.0484377414685173
220211_at	<i>FLJ13224</i>	0.0416850414369416	0.0435986596500468

Appendix 2 [Continued]T-test p-values which expressed statistically significant ($p < 0.05$).

Probe set	Gene symbol	T-test of ascending vs transverse colon	T-test of ascending vs descending colon
204438_at	MRC1	0.0418464706452934	0.00992848027255271
40837_at	TLE2	0.0423156766188777	0.00626333011427297
215103_at	CYP2C18	0.0423707724064298	0.00559948063703009
218579_s_at	DHX35	0.0427011211748617	0.0436691935495297
222251_s_at	GMEB2	0.0430124806537605	0.00725566828019381
210357_s_at	SMOX	0.0433172855060324	0.0338207181600041
205129_at	NPM3	0.0436309133780782	0.0384625268226612
205240_at	GPSM2	0.0439793027972249	0.000631561331351521
202576_s_at	DDX19A	0.0440814208639885	0.018256407713014
206650_at	IQCC	0.0449944650713525	0.0121751394207934
214107_x_at	LOC440434	0.0450720367479637	0.0265633412274562
204613_at	PLCG2	0.0454915719075093	0.0229035737853801
216508_x_at	HMGB1P4	0.0461980573409067	0.0143328712291447
205865_at	ARID3A	0.0463046577532617	0.00292335880810168
203909_at	SLC9A6	0.0466752587281775	0.0473501198857895
221741_s_at	YTHDF1	0.0473235099369472	0.0161402553890302
211603_s_at	ETV4	0.0473890117318017	0.0057997801630521
219653_at	LSM14B	0.0476370621810747	0.000580206292203339
206170_at	ADRB2	0.0476421232283042	0.0154418296902453
221922_at	GPSM2	0.0476880097134143	0.000657071637689071
210393_at	LGR5	0.0490924051065539	0.0138545969031669
213975_s_at	LYZ	0.0496410825350101	0.0216348586636666
209588_at	EPHB2	0.0498298092972293	0.0316158601621646
205362_s_at	PFDN4	0.0498825900877403	0.000926938401448077

Appendix 3

Result of GSEA showed that a total of 11 gene sets were enriched in the ascending tumor type, while 6 gene sets were not enriched in the same group.

Enriched in ascending colon	Diminished in ascending colon
HP_POSTAXIAL_FOOT_POLYDACTYLY	GO_CARBOHYDRATE_BINDING
GO_REGULATION_OF_TELOMERE_CAPPING	GO_REGULATION_OF_EXOCYTOSIS
HP_ABNORMALITY_OF_THE_5TH_TOE	GO_NEGATIVE_REGULATION_OF_GLUCOSE_TRANSMEMBRANE_TRANSPORT
GO_N_METHYLTRANSFERASE_ACTIVITY	GO_DEAMINASE_ACTIVITY
GO_NEGATIVE_REGULATION_OF_GENE_EXPRESSION_EPIGENETIC	GO_POSITIVE_REGULATION_OF_BLOOD_CIRCULATION
GO_REGULATION_OF_GENE_EXPRESSION_EPIGENETIC	GO_TRANSITION_METAL_ION_HOMEOSTASIS
GO_TELOMERE_CAPPING	
GO_S_ADENOSYLMETHIONINE_DEPENDENT_METHYLTRANSFERASE_ACTIVITY	
GO_SPLICEOSOMAL_SNRNP_ASSEMBLY	
GO_SNRNA_PROCESSING	
GO_PROTEIN_DNA_COMPLEX	

Three-dimensional muscle architecture of the infant and adult trapezius: a cadaveric study

Mikaela L. Stiver^{1,2} , Luke R. Bradshaw³ , Ethan M. Breinhorst³ , Anne M. R. Agur^{1,2} ,
S. Ali Mirjalili³ 

¹Division of Anatomy, Department of Surgery, Faculty of Medicine, University of Toronto, Toronto, Ontario, Canada

²Rehabilitation Sciences Institute, Faculty of Medicine, University of Toronto, Toronto, Ontario, Canada

³Department of Anatomy and Medical Imaging, University of Auckland, Auckland, New Zealand

Abstract

Objectives: The elaborate morphometry of the human trapezius muscle facilitates its involvement in numerous active movements of the shoulder girdle and passive stabilization of the upper extremity. Despite its functional importance throughout the lifespan, little is known about the 3D architecture of trapezius at any post-natal timepoints. Accordingly, the aim of this preliminary cadaveric study was to digitize, quantify, model, and compare the 3D architecture of trapezius at two temporal extremes: infancy and adulthood.

Methods: We examined trapezius in two female formalin-embalmed cadavers, aged 6 months and 72 years, respectively. We meticulously dissected each muscle, allowing us to digitize and model the comprehensive muscle architecture *in situ* at the fiber bundle level. We quantified standard architectural parameters to facilitate comparison between each functional partition of trapezius (*i.e.*, descending, transverse, ascending) and proportionally between the infant and adult specimens.

Results: We found markedly different patterns in fiber bundle length range, physiological cross-sectional area, and muscle volume within and between muscles. Notably, the proportional physiological cross-sectional area of the ascending and descending partitions was equal (1:1) in the infant, in contrast to 3:1 in the adult. The transverse partitions were proportionally similar, accounting for over half of the whole muscle physiological cross-sectional area in both specimens.

Conclusion: This study provides preliminary insights into infant and adult trapezius architecture at an unparalleled level of detail and precision. The quantifiable architectural differences appear to coincide with functional development—a notion that warrants further investigation in larger samples and with longitudinal approaches.

Keywords: cadaver; digitization; infant; muscle architecture; skeletal muscle; trapezius

Anatomy 2021;15(1):26–35 ©2021 Turkish Society of Anatomy and Clinical Anatomy (TSACA)

Introduction

The trapezius is a morphometrically complex muscle that is conventionally divided into three distinct partitions: ascending, transverse, and descending. Functionally, the trapezius is involved in voluntary movement of the scapulae (depression, retraction, elevation, and upward rotation) and clavicles (elevation), as well as postural stability and upper extremity support via suspension of the shoulder girdle.^[1] This large superficial muscle is frequently implicated in a wide range of pathologic conditions,

including fibromyalgia,^[2,3] cerebral palsy,^[4] and facioscapulothoracic muscular dystrophy.^[5] Morphological changes present in these conditions include reduction of muscle mass due to atrophy leading to functional changes such as altered excursion (range of motion) or reduced relative force generating capacity.^[6]

Despite its common involvement in pathologic conditions, very little is known about both the detailed architecture of the trapezius and its developmental trajectory. Without this foundational knowledge, assessment of the

This study was presented as an oral presentation at the 36th Annual Meeting of the American Association of Clinical Anatomists, June 11th–15th 2019, Tulsa, OK, USA.

etiology, pathophysiology, rehabilitation, and management of trapezius pathologies are inherently limited.

A recent study by Badura et al.^[7] reported preliminary quantitative data regarding pre-natal growth dynamics of the human trapezius. This study offers vital insights into fetal trapezius development; however, fetal development patterns are not influenced by external functional demands and therefore cannot be generalized to post-natal growth. Post-natal data are essential for understanding how functionality may affect the morphometry and growth dynamics of muscles like the trapezius.

In early post-natal development, the trapezius (in tandem with the sternocleidomastoid) generates a head thrust movement that is essential to infant breastfeeding mechanics.^[8] Moreover, it has been demonstrated that stabilization of the head and shoulder are facilitated by increases in trapezius and deltoid activity. These muscular changes provide increased postural stability to enable the development of functional reaching patterns.^[9] Nevertheless, to the best of our knowledge, no studies to date have investigated or documented the morphometry of the infant trapezius.

The adult trapezius has been examined in greater detail than that of the infant. Numerous *in vivo* imaging studies (e.g., ultrasound and magnetic resonance) have been used to quantify various morphometric parameters, including cross-sectional area, fiber bundle length (FBL), and muscle thickness.^[10-13] Yet, a lack of thorough understanding of the fundamental anatomy in this region poses a significant challenge to imaging optimization and interpretation. Several cadaveric studies have investigated adult trapezius morphometry;^[14-17] however, the architectural parameters quantified in these studies are often overgeneralized and inaccurate due to limited fiber bundle (FB) sampling, lack of volumetric data, and 2D manual measurements of 3D parameters. Recently, our lab has begun digitizing the 3D architecture of the adult trapezius in cadaveric specimens using the same methods presented in this paper;^[18] however, data analysis is still in progress.

Accordingly, this study had two primary objectives; (1) to capture and quantify three-dimensional (3D) trapezius architecture in an infant and adult cadaveric specimen, and (2) to document morphometric differences between the infant and adult trapezius.

Materials and Methods

This study examined two lightly formalin-embalmed cadaveric specimens: one female infant (age: 6 months) and one female adult (age: 72 years). Neither specimen had discernable evidence of structural abnormality,

pathology, or previous surgery in the back, neck, or shoulder regions.

The digitization and modeling techniques used in this study were developed in our laboratory and have been used previously to examine the morphometry of other muscles, including supraspinatus,^[19] pectoralis major,^[20] and soleus.^[21]

Prior to data collection, we obtained full body computerized tomography (CT) scans of the infant cadaver on an Aquilion ONE™ 320 scanner (Toshiba Medical Systems Corporation, Tokyo, Japan) with a voxel size of 0.62 mm × 0.62 mm × 0.3 mm. While the bony attachments of the adult trapezius have been studied in detail, no studies to our knowledge have characterized the attachments of the infant trapezius with respect to the progressive ossification of bones such as the scapula and clavicle. Next, each cadaver was stabilized in a prone position with the scapulae fixed in a neutral position against the rib cage. In the adult specimen, both humeri were in anatomical position, while in the infant the right humerus was slightly abducted (<30°). Only the right trapezius was studied in the infant specimen due to positional limitations of the left upper extremity resulting from the tissue fixation process; both the left and right trapezius were analyzed in the adult specimen.

The skin and subcutaneous tissues were carefully removed to expose each trapezius muscle in its entirety. Beginning on the superficial surface of the trapezius, each FB was meticulously delineated *in situ* between its lateral and medial attachment sites (**Figure 1**). FBs were digitized in 3–5 mm increments, from origin to insertion, using a MicroScribe® G digitizer (Immersion Corp.; San Jose, CA, USA). Digitized FBs were then removed to reveal underlying FBs, and the process of serial digitization and dissection was repeated through the entire volume of the muscle. The surfaces of aponeuroses that provided attachment for FBs to bone were digitized in a grid pattern as they were exposed during dissection. The resultant point cloud data were segmented into the three functional partitions of the trapezius based on individual FB attachments to lateral bony landmarks examined in 3D: ascending partition—FBs with lateral attachment to the base of the scapular spine (end of the deltoid tubercle); transverse partition—FBs with lateral attachment to the scapular spine or acromion; and descending partition—FBs with lateral attachment to the clavicle. Subsequently, the data were reconstructed as 3D models of the connective and contractile elements of each trapezius using Autodesk® Maya® 2019 (Autodesk Inc.; San Rafael, CA, USA).

Digitized data were imported into a custom program developed in the laboratory to quantify FBL, FBL range,

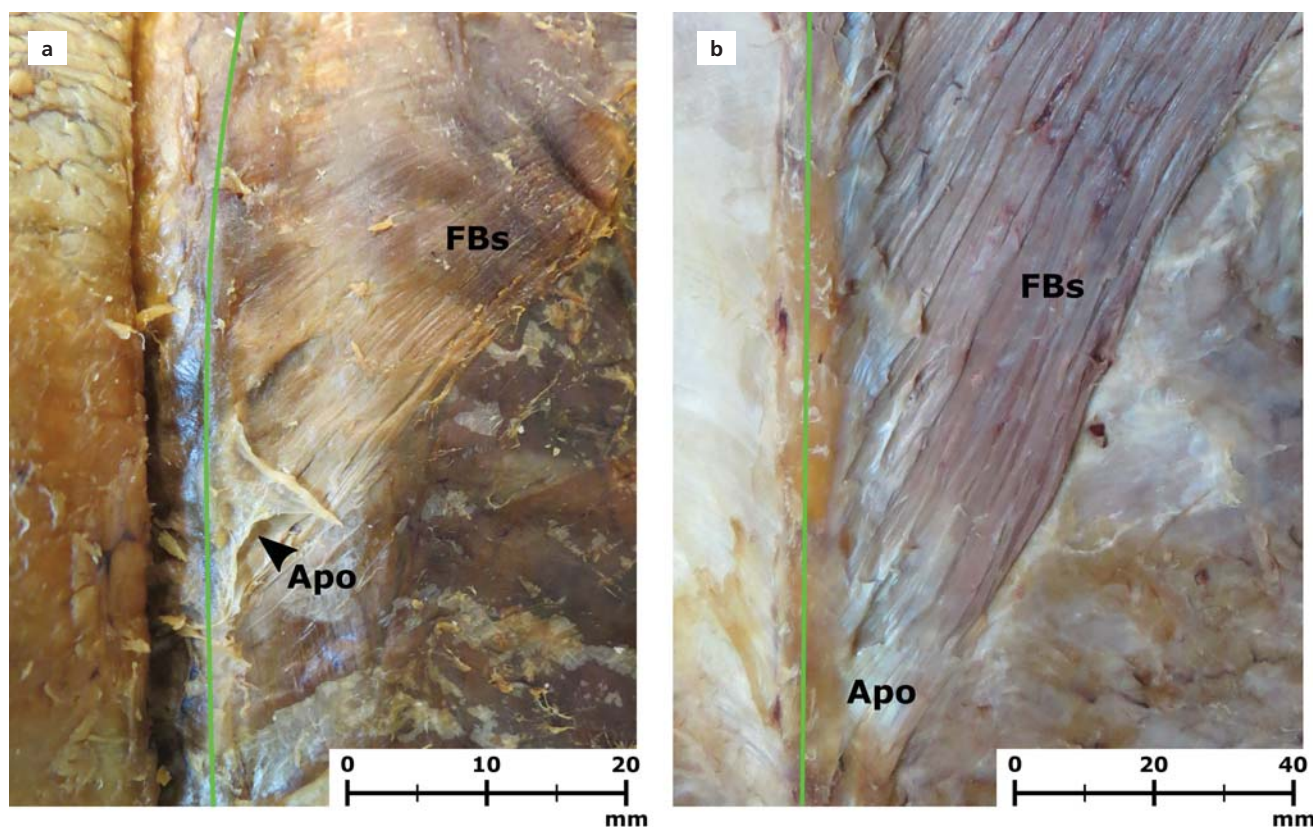


Figure 1. Dissection photographs of fiber bundles in the ascending partition of the infant (a) and adult (b) specimens. The green line shows the spinous processes of the thoracic vertebrae. Apo: Aponeurosis; FBs: fiber bundles.

muscle volume (MV), and physiological cross-sectional area (PCSA) for each functional partition according to the method described in Lee et al.^[22] Each muscle parameter is defined as follows: (a) FBL: the length of a single FB between its attachment sites and is a measure of excursion; (b) MV: the volume of a muscle or partitions thereof and is a component of PCSA; and (c) PCSA: MV accounting for the internal architecture of a muscle and represents relative force generating capability of a muscle or a functional partition. Proportional values were also calculated for PCSA and MV (% of whole muscle) and FBL range (% of whole muscle range) to facilitate comparison between muscles.

Descriptive statistics (mean, standard deviation, range) were calculated for FBL. One-way analysis of variance (ANOVA) was conducted to assess significant differences in FBL between functional partitions for each trapezius. All statistical analyses were conducted in SPSS® Statistics v.26.0 (IBM®, Armonk, NY, USA) using a significance level of $\alpha=0.05$. If a one-way ANOVA demonstrated statistical significance, data were tested for normality and homogeneity of variance and appropriate post-hoc inde-

pendent-samples t-tests were used to explore differences. Significance levels were adjusted using the Bonferroni correction where appropriate. Relative PCSA and MV for each partition were compared between the infant and adult muscles.

Results

Contractile tissues of the trapezius in the infant and adult spanned between wide, flat connective tissue elements (*i.e.*, aponeuroses) both medially and laterally. These aponeuroses were more extensive in the adult, attaching medially to the thoracic spinous processes, nuchal ligament, and superior nuchal line and laterally to the scapular spine, acromion, and lateral part of the clavicle. In the infant these tissues were less developed, and some bony features were still cartilaginous, as seen in the CT scans onto which the infant trapezius model was superimposed (Figure 2). We also found a rhomboidal aponeurosis extending inferomedially from the base of the scapular spine in both the infant and adult specimens.

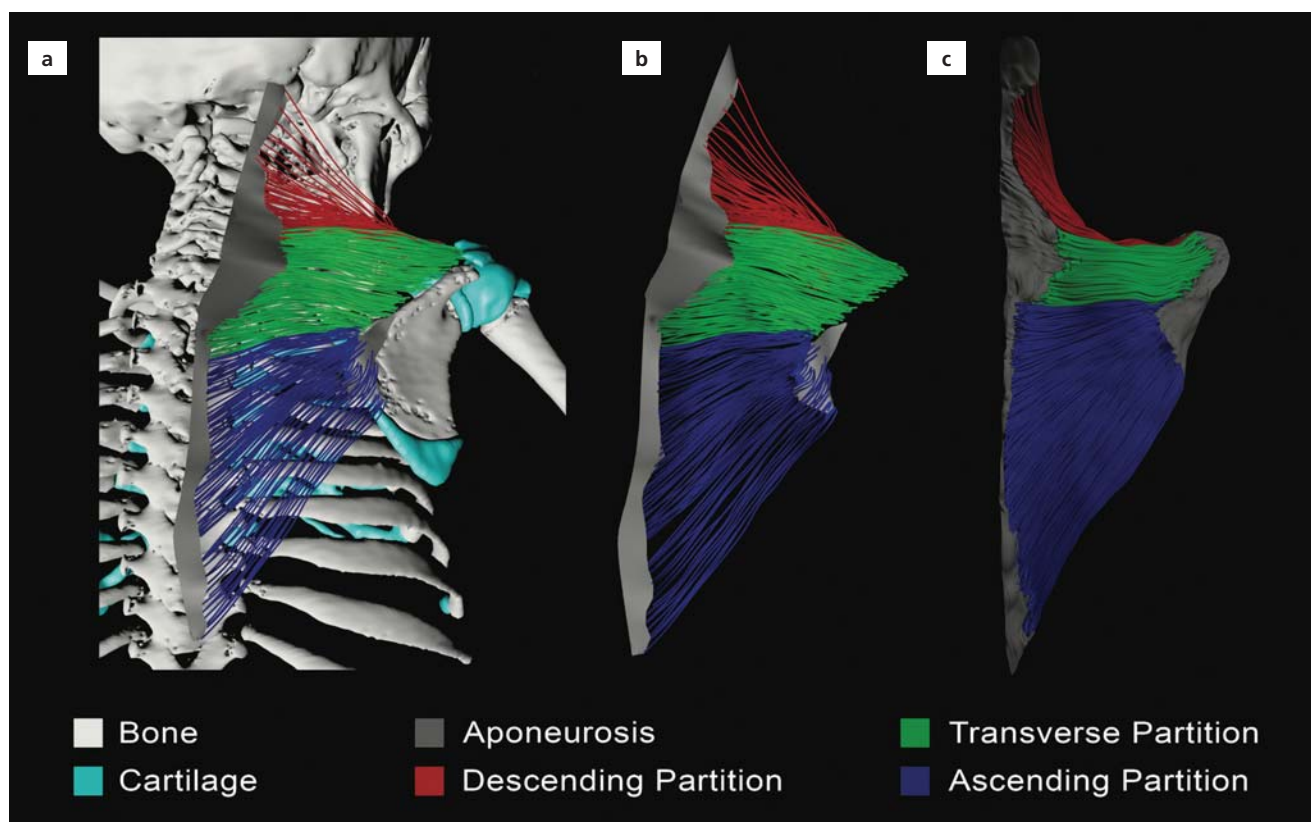


Figure 2. Three-dimensional models of the infant and adult trapezius rendered in Autodesk® Maya® from the digitized cadaveric data. (a) Right infant trapezius registered onto computerized tomography-scanned skeletal and cartilaginous elements; (b) right infant trapezius; and (c) right adult trapezius.

Infant Trapezius Architecture

The infant trapezius had a mean FBL of 37.64 ± 6.72 mm. Each functional partition (descending, transverse, and ascending) exhibited distinct morphometric characteristics (Figure 3). The ascending partition had the largest range of FBLs and the transverse partition had the shortest average FBL (Table 1).

A one-way ANOVA revealed significant differences in FBL between partitions in the infant trapezius ($F_{(2,313)} = 58.700$, $p < 0.001$). *Post hoc* independent-samples t-tests indicated that the mean FBL in the transverse partition was significantly smaller than in both the descending partition ($t = 13.096$, $p < 0.001$; 95% confidence interval [CI]: 6.23–8.43) and the ascending partition ($t = 7.594$, $p < 0.001$; 95% CI: 5.07–8.63). There was no significant difference between the descending and ascending FBL ($p = 0.601$).

The PCSA for the infant trapezius was 147.88 mm^2 and the MV was 7.51 cm^3 (Table 1). In the infant, the proportional PCSA and MV values differed markedly in the descending and transverse partitions. Conversely, the transverse partition had the largest proportional PCSA,

but a similar MV to the descending partition. The relative PCSA and MV in the ascending partition were almost identical (Figure 4).

Adult Trapezius Architecture

The left adult trapezius had a mean FBL of 93.06 ± 25.01 mm. As with the infant, functional partitions of the adult

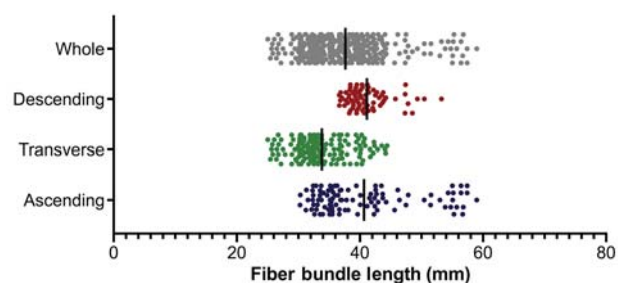


Figure 3. Infant trapezius: fiber bundle lengths. Each point represents the length of one fiber bundle in the whole muscle and each functional partition. The vertical black line indicates the mean fiber bundle length. Additional numerical details are provided in Table 1.

Table 1
Architectural parameters: infant trapezius.

Muscle partition	n	Mean FBL±SD (mm)	FBL range (Min.–max.)	% Whole FBL range	PCSA (mm²)	% Whole PCSA	MV (cm³)	% Whole MV
Whole	314	37.64±6.72	25.04–58.98	-	147.88	-	7.51	-
Descending	71	41.14±3.46	36.65–53.25	48.91%	31.89	21.25%	2.90	38.66%
Transverse	144	33.82±4.53	25.04–44.41	57.08%	85.11	57.56%	2.98	39.68%
Ascending	99	40.66±8.15	30.28–58.98	84.55%	31.34	21.19%	1.63	21.65%

FBL: fiber bundle length; MV: muscle volume; n: number of fiber bundles; PCSA: physiological cross-sectional area; SD: standard deviation.

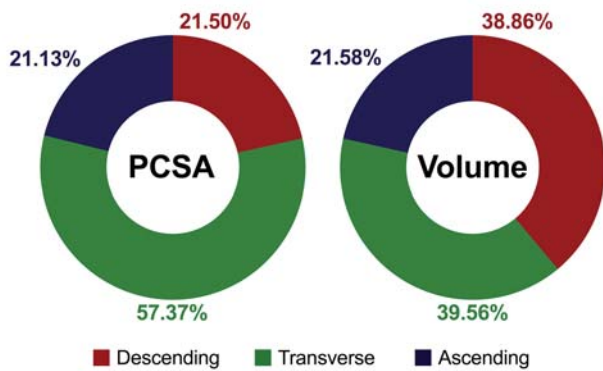


Figure 4. Infant trapezius: proportional physiological cross-sectional area and muscle volume. This figure illustrates the proportional physiological cross-sectional area (labeled: PCSA) and muscle volume (labeled: Volume) for each functional partition of the right infant trapezius. The percentage of whole muscle values are printed around each chart in the corresponding color for each partition. Additional numerical details are provided in Table 1.

trapezius muscles were morphometrically distinct (Figure 5). The ascending partition included both the shortest and longest FBLs in the muscle while the transverse partition had both the shortest mean FBL and the smallest range of FBLs (Table 2).

The right trapezius was slightly smaller than the left but had a similar range of FBLs. The mean FBLs for each partition exhibited a similar pattern to those in left trapezius. As found in the left trapezius, the ascending partition of the right trapezius also included 100% of the range of FBLs documented in the whole muscle (Table 2).

One-way ANOVAs for both left and right adult muscles indicated significant differences between partitions (left: $F_{(2,998)}=193.034$, $p<0.001$; right: $F_{(2,1445)}=204.834$, $p<0.001$). *Post hoc* independent-samples t-tests of the left trapezius revealed that the mean FBL in the transverse partition was significantly smaller than in the descending partition ($t=20.157$, $p<0.001$; 95% CI: 24.10–29.32) and in the ascending partition ($t=15.634$, $p<0.001$; 95% CI: 23.05–29.68). Average FBLs in the ascending and descending partitions were not significantly different in the left trapezius ($p=0.864$). Analyses of the right trapezius revealed the same differences between the descending and transverse mean FBLs ($t=18.779$, $p<0.001$; 95% CI: 18.73–23.13) as well as between the ascending and transverse mean FBLs ($t=17.849$, $p<0.001$; 95% CI: 24.29–30.30); however, the ascending and descending partition average FBLs were also significantly different ($t=3.486$, $p=0.001$; 95% CI: 2.78–9.95).

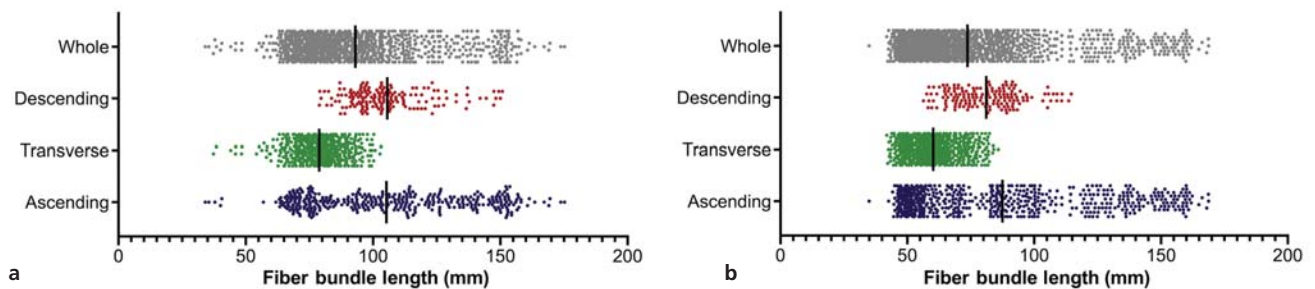


Figure 5. Adult trapezius: fiber bundle lengths. Each point represents the length of one fiber bundle in the whole muscle and each functional partition of the left trapezius (a) and right trapezius (b). The vertical black line indicates the mean fiber bundle length. Additional numerical details are provided in Table 2.

Table 2

Architectural parameters: adult trapezius.

Muscle partition	n	Mean FBL±SD (mm)	FBL range (Min.–max.)	% Whole FBL range	PCSA (mm ²)	% Whole PCSA	MV (cm ³)	% Whole MV
Whole: Left	1001	93.06±25.01	34.12–175.23	-	811.77	-	79.48	-
Descending	164	105.60±15.83	78.90–150.80	50.95%	95.25	11.73%	11.15	14.03%
Transverse	465	78.89±10.30	37.34–103.16	46.64%	408.12	50.28%	33.21	41.78%
Ascending	372	105.25±31.19	34.12–175.23	100.00%	308.40	37.99%	35.13	44.20%
Whole: Right	1448	73.75±27.90	34.97–168.80	-	874.13	-	73.34	-
Descending	157	81.14±13.25	56.36–114.66	43.56%	94.58	10.82%	13.01	17.73%
Transverse	693	60.21±9.26	41.93–85.87	32.83%	481.41	55.07%	31.30	42.68%
Ascending	598	87.50±36.40	34.97–168.80	100.00%	298.13	34.11%	29.03	39.59%

FBL: fiber bundle length; MV: muscle volume; n: number of fiber bundles; PCSA: physiological cross-sectional area; SD: standard deviation.

The PCSAs for the left and right adult trapezius muscle were 811.77 and 874.13 mm², respectively (Table 2). In both adult muscles, the transverse partitions accounted for over half of the whole muscle PCSA while the proportional MVs of this partition were slightly lower. In contrast, the proportional PCSA was lower than the proportional MV in both the descending and ascending partitions (Figure 6).

Morphometric Comparison

On the surface, the infant and adult trapezius were fairly similar in terms of shape and attachment to skeletal elements. Some bony elements (e.g., acromion) were not yet fully developed in the infant and were instead cartilaginous in composition. Morphometrically, the variability in FBL throughout the muscle, and within each functional partition, was comparable between the infant and adult muscles. The FBL range in the descending partitions were just under half of the whole muscle range (48.91% in the infant vs 47.26% in the adult). The ascending partitions had the largest range of FBLs in both the infant and adult muscles, while the transverse partitions had the smallest range of FBLs (Table 3).

The trapezius in infancy and adulthood exhibited several other notable disparities. The infant trapezius MV was about one tenth that of the adult trapezius. MV was evenly distributed between the descending and transverse partitions in the infant, with the ascending partition being markedly smaller. In the adult, nearly 85% of the MV was divided between the transverse and ascending partitions, while the descending partition was strikingly smaller (Table 3).

Compared to the infant trapezius PCSA, the average adult muscle PCSA was 5.7 times greater. The transverse

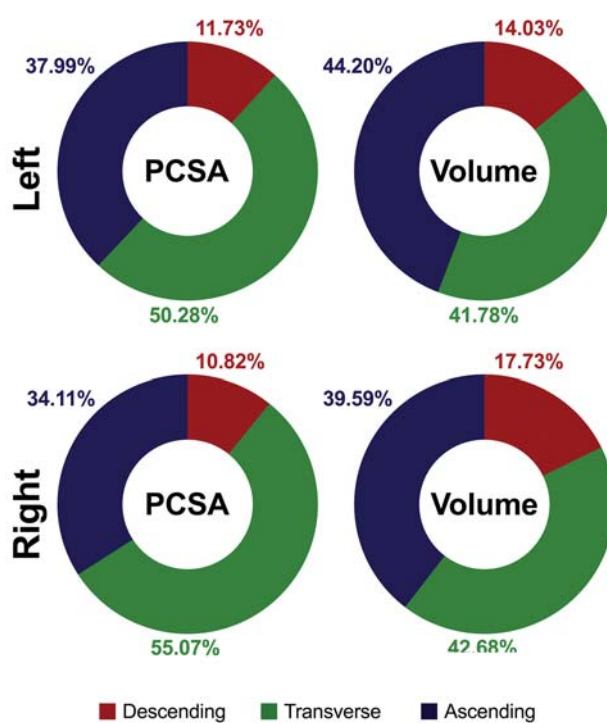


Figure 6. Adult trapezius: proportional physiological cross-sectional area and muscle volume. This figure illustrates the proportional physiological cross-sectional area (labeled: PCSA) and muscle volume (labeled: Volume) for each functional partition of the left and right adult trapezius. The percentage of whole muscle values are printed around each chart in the corresponding color for each partition. Additional numerical details are provided in Table 2.

partitions of the infant and adult muscles were proportionally similar, accounting for just over half of the whole muscle PCSA. In the infant, PCSA was equally distributed between the ascending and descending partitions; on the contrary, the ascending partition PCSA in the adult was

Table 3
Morphometric changes: infancy to adulthood.

Muscle partition	% Whole FBL range		% Whole PCSA		% Whole MV	
	Infant	Adult	Infant	Adult	Infant	Adult
Descending	48.91%	47.26%	21.25%	11.28%	38.66%	15.88%
Transverse	57.08%	39.74%	57.56%	52.68%	39.68%	42.23%
Ascending	84.55%	100%	21.19%	36.05%	21.65%	41.90%

FBL: fiber bundle length; MV: muscle volume; PCSA: physiological cross-sectional area.

approximately three times greater than that of the descending partition (Table 3).

The proportional adult MV and PCSA were comparable, with a slightly higher MV than PCSA in the descending and ascending partitions and vice versa in the transverse partition. Proportional MV and PCSA in the infant trapezius partitions were noticeably incongruent. For example, while the descending and transverse partitions had almost identical proportional MVs, the PCSA in the transverse partition was over 170% greater than the descending partition PCSA.

Discussion

To the best of our knowledge, this is the first study to document and quantify the comprehensive 3D architecture throughout the muscle volume of the infant and adult trapezius. The preliminary results presented in this paper offer an unprecedented level of precision and detail regarding the trapezius muscle. Likewise, our findings support the long-held pediatric dogma that, from the perspective of muscle architecture, “children are not little adults”.

Trapezius Morphology

One of the major confounds in musculoskeletal literature involving trapezius is a lack of consensus regarding the precise definitions of anatomical or functional partitions within the muscle. While most sources divide trapezius into three partitions—ascending, transverse, and descending—there are inconsistencies in how each partition is defined. In particular, FBs that attach laterally to the medial border of the acromion are variably included in either the descending partition^[23] or the transverse partition.^[24,25] Several electromyographical studies have divided trapezius into four partitions;^[26,27] however, there is currently no clear evidence to support this further subdivision. The partitioning of trapezius is believed to have been derived from non-human literature,^[28] further substantiat-

ing the need for detailed studies of this muscle in humans. As a result, it is currently challenging to compare between studies in which different criteria have been used to partition trapezius.

The broad morphological characteristics of trapezius observed in this study are mostly in agreement with those presented in the existing cadaveric literature. Similar to Kamibayashi and Richmond,^[16] we observed that the FBs throughout the muscle volume span the full width of the muscle, from medial origin to lateral insertion. We also noted a similar expansive aponeurosis extending laterally from the spinous processes in the transverse partition; however, in the infant there were no markedly shorter FBs present in the deep transverse partition, and it lacked the substantial thickness seen in the adult. The common aponeurotic tendon attaching to the base of the scapular spine was consistent with that described by Johnson et al.^[15] We observed that all FBs in the ascending partition of both the infant and adult trapezius inserted onto this rhomboidal aponeurosis, in contrast to Johnston et al.^[15] in which this aponeurosis was described as the lateral attachment only for fascicles originating from T2 through T5. Similar levels of qualitative detail regarding trapezius morphometry were not reported in other cadaveric literature, and we did not find any non-adult cadaveric studies including trapezius.

Muscle Architecture

We also compared the quantitative results of our pilot study to existing adult literature; there were no quantitative studies of pediatric trapezius architecture with which to compare our findings. Of the four cadaveric studies of adult trapezius architecture that included numerical data,^[15–17,29] only one presented data divided into three distinct muscle partitions. In general, the proportional relationships reported by Kamibayashi and Richmond^[16] are similar to those in our adult cadaver: the ascending partition had the largest average FBL of the three partitions (right muscle only in the current study)—including both

the shortest and longest FBLs recorded in the whole muscle, the descending partition PCSA was the smallest, and the transverse partition PCSA was the largest. In the current study, the FBL values were slightly smaller (*e.g.*, overall FBL range of 34.12–175.23 mm compared to 56.0–225.0 mm [converted from cm]), as were the PCSA values. These differences may be attributable to numerous factors including donor height and weight, measurement methodology, and FB sampling. In the current study, every FB throughout the muscle volume is included in the dataset, compared to a mere 5–20 FBs pseudo-randomly sampled from each muscle.

A more extensive literature has been published on the adult trapezius using *in vivo* magnetic resonance imaging and ultrasound; however, the majority of these studies are focused on pathological conditions and rarely include values for baseline or asymptomatic trapezius architectural parameters. Those that do typically report parameters with limited functional value—such as muscle thickness,^[13,29,30] MV,^[31] or anatomical cross-sectional area (*i.e.*, measured in standard anatomical planes)^[10,11,31]—as opposed to FBL or PCSA. Compared to the adult MVs calculated in the current study, the trapezius MVs reported by Li et al.^[31] from serial MRI scans were much larger, ranging from 170–530 cm³; however, this is consistent with a study that reported MV estimated from MRI were an average of 64% larger than those estimated from cadaveric dissection.^[29] Nonetheless, studies suggest that FBL does not change as long as tissue is fixed while remaining intact with bony attachments^[32] and that relative or proportionate values for PCSA are consistent between computed tomography images and cadaveric data.^[33]

Functional Implications

Pre-natal data, such as those reported by Badura et al.,^[7] provide insight into fetal muscle developmental trajectories. Nevertheless, pre-natal muscle growth is not influenced by the same types of external forces and functional demands present during post-natal development and adulthood. The morphometric differences between the infant and adult trapezius muscles documented in this study suggest that external forces and functional demands during post-natal development change the muscle architecture in favour of postural stability and functional upper limb movement.

At six months of post-natal age, an infant is typically able to elevate their head and chest off the ground by extending their arms from a prone position and may begin to maneuver themselves along the floor with their arms and legs.^[34] These developmental milestones are consistent

with the patterns of PCSA (relative force generating capability) observed within the infant trapezius: the transverse partition—which functionally is associated with scapular retraction and, to a lesser extent, depression—accounts for over half of the whole muscle PCSA. These scapular movements are integral to the sequential activity of raising the head and chest in a prone position using the upper limbs. Without scapular retraction and depression, this functional task would not be possible.

The remaining PCSA is equally distributed between the ascending and descending partitions of the trapezius, in stark contrast to the approximate 3:1 ratio seen in the adult. This may be explained by the considerable increases in muscle tone required during the development of voluntary head and neck movement during early infancy, such as the head thrust movement required for productive breastfeeding. When the scapulae are stabilized, the descending partition of trapezius assists with head/neck extension, ipsilateral flexion, and contralateral rotation.^[25] In the adult, the ascending partition may have greater force generating capabilities due to functional demands associated with upright posture and positioning of the upper limb; in contrast, the descending partition may remain more functionally analogous to that of the infant in terms of gross motor activity, resulting in the unbalanced PCSA ratio observed in the adult.

Furthermore, electromyographical studies of the adult trapezius have reported that “the greatest activity in trapezius appears during abduction of the limb and chiefly in the lower two-thirds of the muscle”.^[35] This is in keeping with our findings that the ascending and transverse partitions jointly contained nearly 90% of the whole muscle PCSA and 85% of the whole MV.

Limitations and Strengths

The most notable limitation of this study is the small sample size: one infant and one adult. This is largely attributable to strict regulations regarding non-adult body donation resulting in a dearth of cadaveric data during key developmental timepoints. Adult data is more widely available; however, due to the preliminary nature of this study we chose to include data from a single female adult cadaver for the purposes of comparison. Moreover, previous cadaveric studies conducted in our laboratory using similar digitization techniques, including preliminary data collected from adult trapezius muscles,^[18] have reported consistent patterns of muscle architecture between specimens.^[19,20] It is also worth noting the limitation presented by the use of embalmed cadaveric specimens. Neither tissue properties nor architectural parameters are directly

comparable between cadaveric and *in vivo* imaging studies;^[36] however, the use of proportional values will help facilitate comparisons between the data presented in this study and future *in vivo* studies.^[33]

Despite a small sample size, we strongly believe that these preliminary results warrant further investigation into the changing morphometry of trapezius throughout post-natal development and adulthood. While longitudinal studies are not possible in cadaveric research, patterns of morphometry between specimens at different developmental timepoints have the potential to provide valuable insights into how muscles adapt to functional demands and how structure is associated with pathologic conditions. Likewise, a better understanding of the underlying anatomy of trapezius will provide an essential foundation upon which to create new imaging protocols for the collection of *in vivo* longitudinal developmental data.^[37] Future studies should focus on collecting detailed anatomical data to better understand the internal structure of trapezius, ideally from a range of development timepoints.

Conclusion

This is the first pilot study to digitize and quantify the complete 3D architecture of the infant and adult trapezius and offer preliminary evidence of how the morphology and architecture of trapezius differ between infancy and adulthood. Literature describing the detailed anatomy of trapezius is sparse, particularly before adulthood, leaving a notable gap in our understanding of how structure informs function during post-natal development. Future longitudinal studies should build upon the findings presented in this paper to document the post-natal developmental trajectory of trapezius using *in vivo* imaging techniques.

Acknowledgements

We would like to acknowledge and thank the individuals who donated their bodies for the advancement of education and research through the University of Toronto Willed Body Program. We would also like to thank William Wood and Harun Bola for their valuable technical assistance.

Conflict of Interest

The authors have no conflicts of interest.

Author Contributions

MLS: project development, data collection & analysis, manuscript writing & editing; LRB: data collection & analysis, manuscript editing; EMB: data collection & analysis, manuscript editing; AMRA: project development,

manuscript writing & editing; SAM: project development; manuscript editing.

Ethics Approval

Ethics approval was obtained from the Research Ethics Board at the University of Toronto (#32679 & #27210). Donor consent was obtained in accordance with the Anatomy Act and The Trillium Gift of Life Network Act of the Province of Ontario, Canada.

Funding

The study was funded by Canadian Institute of Health Research (CIHR) Vanier Canada Graduate Scholarship [MLS].

References

1. Moore KL, Dalley AF, Agur AMR. Clinically oriented anatomy. 8th ed. Philadelphia: Lippincott Williams & Wilkins; 2018. 1168 p.
2. Lindman R, Hagberg M, Bengtsson A, Henriksson KG, Thornell LE. Changes in trapezius muscle structure in fibromyalgia and chronic trapezius myalgia. In: Jacobsen S, Danneskiold-Samsøe B, Lund B, editors. Musculoskeletal pain, myofascial pain syndrome and the fibromyalgia syndrome. New York (NY): Haworth Medical Press; 1993. p. 171–6.
3. Olsen NJ, Park JH. Skeletal muscle abnormalities in patients with fibromyalgia. *Am J Med Sci* 1998;315:351–8.
4. Boyd RN, Morris ME, Graham HK. Management of upper limb dysfunction in children with cerebral palsy: a systematic review. *Eur J Neurol* 2001;8(Suppl 5):150–66.
5. Tasca G, Monforte M, Iannaccone E, Laschena F, Ottaviani P, Leoncini E, Boccia S, Galluzzi G, Pelliccioni M, Masciullo M, Frusciantè R, Mercuri E, Ricci E. Upper girdle imaging in facioscapulohumeral muscular dystrophy. *PLoS One* 2014;9:e100292.
6. Powers SK, Lynch GS, Murphy KT, Reid MB, Zijdwind I. Disease-induced skeletal muscle atrophy and fatigue. *Med Sci Sports Exerc* 2016;48:2307–19.
7. Badura M, Grzonkowska M, Baumgart M, Szpinda M. Quantitative anatomy of the trapezius muscle in the human fetus. *Adv Clin Exp Med* 2016;25:605–9.
8. Wallden M. The trapezius-clinical & conditioning controversies. *J Body Mov Ther* 2014;18:282–91.
9. Thelen E, Spencer JP. Postural control during reaching in young infants: a dynamic systems approach. *Neurosci Biobehav Rev* 1998;22:507–14.
10. Elliott JM, Jull GA, Noteboom JT, Durbridge GL, Gibbon WW. Magnetic resonance imaging study of cross-sectional area of the cervical extensor musculature in an asymptomatic cohort. *Clin Anat* 2007;20:35–40.
11. Stemper BD, Baisden JL, Yoganandan N, Pintar FA, Paskoff GR, Shender BS. Determination of normative neck muscle morphometry using upright mri with comparison to supine data. *Aviat Space Environ Med* 2010;81:878–82.
12. Debernard L, Robert L, Charleux F, Bensamoun SF. Characterization of muscle architecture in children and adults using magnetic resonance elastography and ultrasound techniques. *J Biomech* 2011;44:397–401.

13. Adigozali H, Shadmehr A, Ebrahimi E, Rezasoltani A, Naderi F. Ultrasonography for the assessment of the upper trapezius properties in healthy females: a reliability study. *Muscles Ligaments Tendons J* 2016;6:167–72.
14. Mayoux-Benhamou MA, Barbet JP, Bargy F, Vallée C, Revel M. Method of quantitative anatomical study of the dorsal neck muscles. *Surg Radiol Anat* 1990;12:181–5.
15. Johnson G, Bogduk N, Nowitzke A, House D. Anatomy and actions of the trapezius muscle. *Clin Biomech* 1994;9:44–50.
16. Kamibayashi LK, Richmond FJ. Morphometry of human neck muscles. *Spine* 1998;23:1314–23.
17. Borst J, Forbes PA, Happee R, Veeger D. Muscle parameters for musculoskeletal modelling of the human neck. *Clin Biomech* 2011; 26:343–51.
18. Stiver ML, Käärilä K, Kumbhare D, Agur AM. Comprehensive 3D architecture of the adult human trapezius: a cadaveric study. *The FASEB Journal* 2019;33:77.2–77.2.
19. Kim SY, Boynton EL, Ravichandiran K, Fung LY, Bleakney R, Agur AM. Three-dimensional study of the musculotendinous architecture of supraspinatus and its functional correlations. *Clin Anat* 2007;20: 648–55.
20. Fung L, Wong B, Ravichandiran K, Agur A, Rindlisbacher T, Elmaraghy A. Three-dimensional study of pectoralis major muscle and tendon architecture. *Clin Anat* 2009;22:500–8.
21. Agur AM, Ng-Thow-Hing V, Ball KA, Fiume E, McKee NH. Documentation and three-dimensional modelling of human soleus muscle architecture. *Clin Anat* 2003;16:285–93.
22. Lee D, Ravichandiran K, Jackson K, Fiume E, Agur A. Robust estimation of physiological cross-sectional area and geometric reconstruction for human skeletal muscle. *J Biomech* 2012;45:1507–13.
23. Hamilton WJ. *Textbook of human anatomy*. 2nd ed. London: Macmillan; 1956. 753 p.
24. Gray H. *Anatomy of the human body*. 20th ed. Philadelphia (PA): Lea&Febiger; 1918. 1396 p.
25. Grant JCB. The Musculature. In: Schaeffer JP, editor. *Morris' human anatomy*. 10th ed. Philadelphia (PA): The Blakiston Company; 1942. p. 377–581.
26. Holtermann A, Roeleveld K, Mork PJ, Grönlund C, Karlsson JS, Andersen LL, Olsen HB, Zebis MK, Sjøgaard G, Søgaard K. Selective activation of neuromuscular compartments within the human trapezius muscle. *J Electromyogr Kines* 2009;19:896–902.
27. Zanca GG, Oliveira AB, Anselmo W, Barros FC, Mattiello SM. EMG of upper trapezius-electrode sites and association with clavicular kinematics. *J Electromyogr Kines* 2014;24:868–74.
28. Reighard J, Jennings H. *Anatomy of the cat*. New York (NY): H. Holt and Company; 1901. 498 p.
29. Van Ee CA, Nightingale RW, Camacho DL, Chancey VC, Knaub KE, Sun EA, Myers BS. Tensile properties of the human muscular and ligamentous cervical spine. *Stapp Car Crash J* 2000;44:85–102.
30. O'Sullivan C, Meaney J, Boyle G, Gormley J, Stokes M. The validity of rehabilitative ultrasound imaging for measurement of trapezius muscle thickness. *Man Ther* 2009;14:572–8.
31. Li F, Laville A, Bonneau D, Laporte S, Skalli W. Study on cervical muscle volume by means of three-dimensional reconstruction. *J Magn Reson Imaging* 2014;39:1411–6.
32. Cutts A. Shrinkage of muscle fibres during the fixation of cadaveric tissue. *J Anat* 1988;160:75–8.
33. Cutts A, Seedhom BB. Validity of cadaveric data for muscle physiological cross-sectional area ratios: a comparative study of cadaveric and in-vivo data in human thigh muscles. *Clin Biomech* 1993;8:156–62.
34. Gerber RJ, Wilks T, Erdie-Lalena C. Developmental milestones: motor development. *Pediatr Rev* 2010;31:267–77.
35. Basmajian JV, De Luca CJ. *Muscles alive: their functions revealed by electromyography*. 5th ed. Baltimore (MD): Williams & Wilkins; 1985. 561 p.
36. Martin DC, Medri MK, Chow RS, Oxorn V, Leekam RN, Agur AM, McKee NH. Comparing human skeletal muscle architectural parameters of cadavers with *in vivo* ultrasonographic measurements. *J Anat* 2001;199:429–34.
37. Kim S, Bleakney R, Boynton E, Ravichandiran K, Rindlisbacher T, McKee N, Agur A. Investigation of the static and dynamic musculotendinous architecture of supraspinatus. *Clin Anat* 2010;23:48–55.

ORCID ID:

M. L. Stiver 0000-0002-8045-7291; L. R. Bradshaw 0000-0002-8722-8440;
E. M. Breinhorst 0000-0002-7535-1361; A. M. R. Agur 0000-0002-2303-3628;
S. A. Mirjalili 0000-0002-1599-3573

**Correspondence to:** Mikaela Stiver, MSc, PhD(c)

Division of Anatomy, Department of Surgery, Faculty of Medicine,
University of Toronto, Toronto, Ontario, Canada
Phone: +1 226 9793366
e-mail: mikaela.stiver@mail.utoronto.ca

Conflict of interest statement: No conflicts declared.

This is an open access article distributed under the terms of the Creative Commons Attribution-NonCommercial-NoDerivs 4.0 Unported (CC BY-NC-ND4.0) Licence (<http://creativecommons.org/licenses/by-nc-nd/4.0/>) which permits unrestricted noncommercial use, distribution, and reproduction in any medium, provided the original work is properly cited. *How to cite this article:* Stiver ML, Bradshaw LR, Breinhorst EM, Agur AMR, Mirjalili SA. Three-dimensional muscle architecture of the infant and adult trapezius: a cadaveric study. *Anatomy* 2021;15(1):26–35.

Perforator flaps based on the deltoid branch of the thoracoacromial artery: anatomical study

Philippe Manyacka Ma Nyemb^{1,2} , Christian Fontaine³ , Véronique Duquenois-Martinot⁴ ,
Xavier Demondion^{3,5} 

¹Department of Anatomy and Organogenesis, School of Medicine, Gaston Berger University, Saint-Louis, Senegal

²Department of General Surgery, Regional Hospital, Saint-Louis, Senegal

³Department of Anatomy and Organogenesis, Henri Warembourg Faculty of Medicine, Université de Lille 2, Lille, France

⁴Department of Plastic, Esthetic and Reconstructive Surgery, Roger Salengro Hospital, Lille University Hospital, Lille, France

⁵Department of Musculoskeletal Imaging, Roger Salengro Hospital, Lille University Hospital, Lille, France

Abstract

Objectives: Tissue defects in the lateral triangle of the neck and the anterior cervical region represent a high demand for plastic and reconstructive surgery. Their management most often requires regional or free flaps. The perforator flap based on the deltoid branch of the thoracoacromial artery (TAA) may be a good solution for these indications. The objective of this work is to propose anatomical landmarks to raise perforator flaps pedicled on the deltoid branch of the TAA.

Methods: We carried out dissection of 24 perforator flaps based on the deltoid branch of the TAA, in body donor specimens preserved in a glycerin-rich, formalin-free solution. The TAA was first injected with methylene blue. The vascular territory, location of perforators relative to known landmarks, along with the flap's potential amplitude and arc of rotation were studied.

Results: The main perforating arteries of the flap were located in the middle of the deltopectoral groove, often surrounded by adipose tissue in 18 out of 24 dissections. In 22 out of 24 dissections, there were at least 2 perforator arteries originating from the deltoid branch. The average diameter of the perforator arteries was 1 mm. The flap's amplitude of movement made it possible to reach in all cases the lateral triangle of the neck and the anterolateral cervical region.

Conclusion: The thoracoacromial artery has already been used for perforator flaps. However, the individualization of its deltoid branch offers to practitioners new surgical options. This anatomical study of the perforator flap based on the deltoid branch of the TAA made it possible to review the anatomical bases for the raising of this flap, and to fix useful landmarks for the surgeon in order to propose an easily feasible surgical technique.

Keywords: deltoid branch; perforator flap; thoracoacromial artery; vascular territory

Anatomy 2021;15(1):36–43 ©2021 Turkish Society of Anatomy and Clinical Anatomy (TSACA)

Introduction

For many years, covering the tissue defects of the lateral triangle of the neck and the anterior cervical region has required complex techniques because these two regions are limited by the course of the sternocleidomastoid muscle.^[1,2] The deltoid region has never been exploited to fill in for these tissue defects. Indeed, in the deltoid region, muscular and musculocutaneous flaps are mostly

used in other indications.^[3] In this case the morbidity on the deltoid muscle is high, even when the donor site can be primarily closed.^[3] More recently, the advent of perforator flaps marked a turning point in the reconstruction of tissue defects of the neck. Besides, in the indications of loss of substances from the lateral triangle of the neck and the anterior cervical region, the perforator flap of the cervical transverse artery can provide an efficient solution.^[4] The perforator flaps are based on the muscu-

This study was a poster presentation at the 102nd Congress of the French Association of Morphologists, 11th-12th March 2021, Montpellier, France.

locutaneous perforators which cross the muscle and end on a skin pallet without participating in the muscular vascularization.^[5] They therefore better match for filling (or repairing) the loss of substance in question, with reduced morbidity and a wider choice of donor sites.

The thoracoacromial artery (TAA) originates below the lateral half of the clavicle. It is a big artery located on the anterior face of the axillary artery; its initial portion is located behind the cranial margin of the pectoralis minor muscle.^[6-9] The deltoid and pectoral branches are the two permanent voluminous arteries arising from the TAA. It is also found inconstantly two other variable branches: a clavicular branch (arising from the TAA) and an acromial branch arising from the deltoid branch (when present).^[6-9] These four arteries (and their satellite veins) come out of the TAA just below the clavicle. They meet on their way the pectoralis major muscle which they cross from inside out below the clavicle.^[6-9] The clavicular branch medially supplies the pectoralis major muscle, which is laterally irrigated by the deltoid and acromial branches.^[6-9] The deltoid and acromial branches provide musculocutaneous perforators for the subcutaneous tissue and skin of the upper portion of the pectoral wall. It is common for the acromial branch to arise directly from the deltoid branch; this acromial branch also provides a musculoskeletal perforator for the subcutaneous tissue and skin above the deltoid muscle and the clavicle (acromial end).^[6-9] The deltoid branch crosses the upper part of the deltopectoral groove and ramifies into a superficial and a deep branch.^[10,11] The duplication of the fascia houses a small canal in which the deep branch travels inside the deltopectoral groove. This deep branch crosses superficial planes of its fascial canal, at the level of the intermuscular space. It reaches the subcutaneous tissue and irrigates the skin overlying both the pectoralis major tendon and the insertional portion of the deltoid.^[10,11]

In the literature, the perforator flap based on the deltoid branch of the TAA has not yet been the subject of anatomical study, this work therefore represents a pioneer study in this area. The aim of this study was to highlight the feasibility of a perforator flap based on the deltoid branch of the TAA, in covering tissue defects with cervical regions.

Materials and Methods

Prior to our work, all the institutional procedures concerning cadaveric dissection were respected, as well as the ethical framework. From an ethical point of view, our work was based on the legislation at the time of the study. We dissected 24 anatomical regions belonging to 12 cadavers (12 right and 12 left upper limbs). The 12 non-

formalin fixed cadavers consisted of 9 males and 3 females. The mean age was 69 years (range 47–88). No history of surgery or deformity was reported on the cadavers. The areas targeted for dissection were supraclavicular, pectoral and deltoid regions. For embalming we used a glycerin-rich, formalin-free solution. Such a solution is used in the laboratory of anatomy of Lille to preserve tissue suppleness.

Our dissections were carried out in several phases. For the first phase, the cadaver was placed in a supine position, the lateral triangle of the neck was dissected and the clavicle removed. We dissected, identified and marked the subclavian artery and its branches. The origin of the TAA was exposed on the anterior side of the first segment of the axillary artery. A mixture (gelatin, methylene blue and iron powder) was used for infecting the TAA (**Figures 1a and b**). The cadaver was then refrozen for 24 hours for hardening the injected mixture.

In the second phase, the cadaver was thawed out at room temperature and then placed in dorsal decubitus to dissect the subcutaneous tissue and skin. For this phase, the dissection made it possible to completely circumscribe the cutaneous perforasome, and to detach it while sparing the muscular layer. The superficial plane was then dissected and separated from the muscle layer over the entire surface of the perforasome. Special care was taken at this phase of the dissection to prevent damaging veins accompanying each perforating artery (**Figures 2, 3a and b**). During this procedure, the perforating arteries were dissected, inventoried and listed according to their characteristics (location, dimensions, orientation, frequency and size of the cutaneous perforasome). Perforasome area was calculated based on a circular shape (radius \times radius \times π) or elliptical shape (long radius \times small radius \times π). Dissection of perforators was then continued through the muscle while preserving the integrity of the pectoralis major muscle. The superficial layer of the perforator flap was then completely harvested with its pedicle. All measurements were made by the same operator. The following equipment was used for the various measurements: felt pen, metal rulers graduated in millimeters, surgical suture, caliper, thumbtacks, and magnifying glasses.

Results

The TAA had an average diameter of 2 mm. An average of 2.4 perforators (range: 1–3) were found on the perforasome corresponding to the territory of the TAA's deltoid branch. The average diameter of these perforators was 0.9 (range: 0.5–1.5) mm. The perforators of the deltoid branch are mainly observed over an area of 4 cm² project-

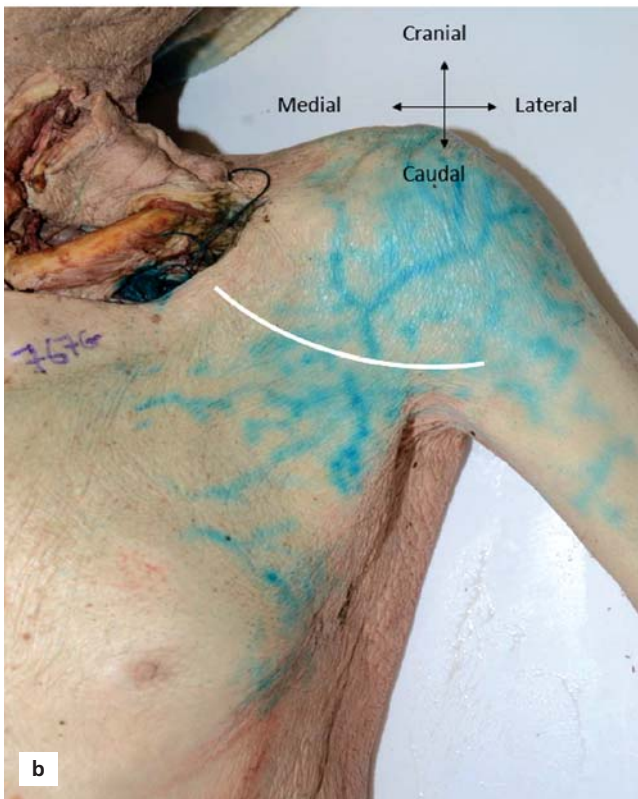
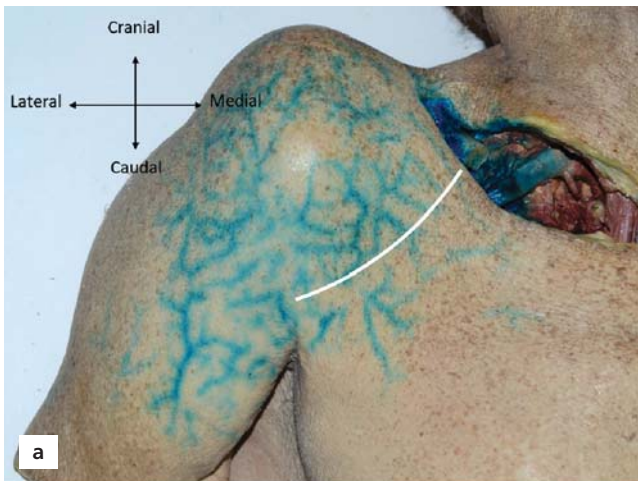


Figure 1. Injection of dye on the right (a) and left (b) sides into the deltopectoral and pectoral branches of the thoracoacromial artery in two subjects. The deltopectoral groove is represented as a white line (specimen numbers 17 and 2).

ing near the middle third of the deltopectoral groove (Figure 4). The average dimensions of the perforasome were 6×7 cm, corresponding to a mean area of 33 (range: 23.5–50) cm². Its general orientation was descending on the ventral side of the deltoid muscle and slightly oblique infero-laterally (Figure 5). The extramuscular pedicle had

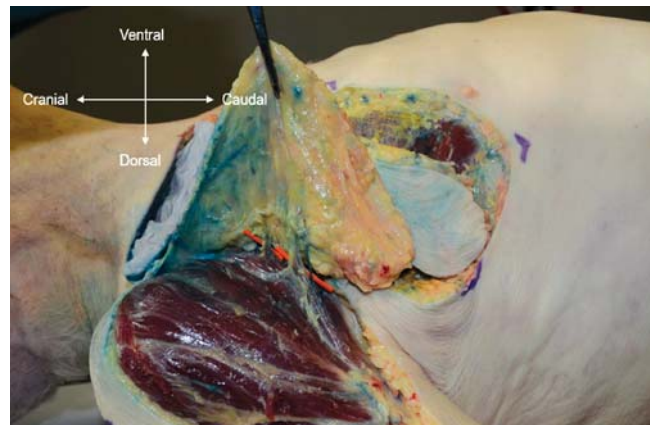


Figure 2. Dissecting the vascular territory of the deltoid branch of the thoraco-acromial artery (specimen number 13).

an average length of 1.8 (range: 10–30) cm and the transmuscular pedicle had an average length of 7 (range: 5–10) cm. A 180° arc of rotation was possible from the pivot point (Figure 6). In 19 of the 24 specimens, the deltoid branch of the TAA and its perforators converged over the middle third of the deltopectoral groove (pivot point). It also appears that the acromial branch is always a daughter branch from the deltoid branch.

The following topographic boundaries can be used when dissecting this flap, although the perforasome area often extends beyond these boundaries: caudally the horizontal line passing through the nipple and the 4th intercostal space, laterally the vertical line passing through the insertion of the deltoid muscle, medially the anterior edge of the deltoid, the apex of the perforating flap lying near its pedicle, along the deltopectoral groove. The more detailed results are presented in Table 1 and Figures 1–3.

Discussion

Several anatomical and surgical series have already proposed the musculocutaneous flaps of the thoracic muscles in the indications of tissue defects in the lateral triangle of the neck and the anterior cervical region.^[1,2] More recently the fasciocutaneous and perforator flaps of pectoral region have been studied in the same indications.^[1,2] In the loss of substance of the supraclavicular area, the needs for soft tissue often require the harvesting of local, regional or distant flaps. In these indications, it is often the musculocutaneous flaps such as the flap of the pectoralis major muscle or the flap of the trapezius muscle which are preferred to conventional propeller perforator flaps. Traditionally, the musculocutaneous flap of the pectoralis major and the deltopectoral flap

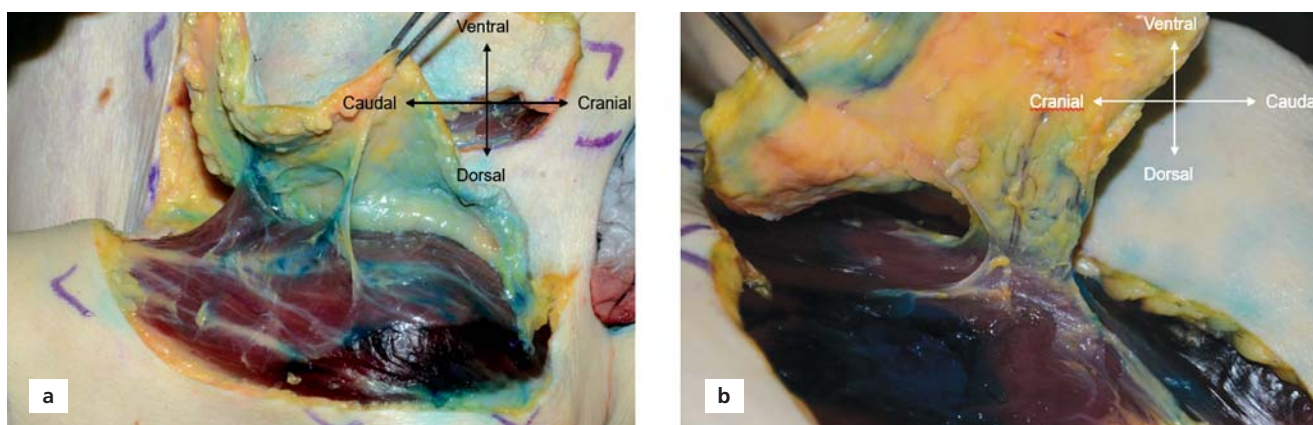


Figure 3. Identification and dissection of the vascular territory (a) and perforators (b) of the deltoid branch of the thoracoacromial artery.

were the first choices in terms of reconstruction of the head and neck.^[13,14] Unfortunately, functional and aesthetic requirements limit their use today. Indeed, research is increasingly directed towards the flaps corresponding exactly to the characteristics of the recipient

site, with a lower morbidity of the donor site. The main disadvantages of these two flaps concern a high rate of necrosis, the need for a skin graft to cover the donor site, and a low rotation angle due to the short length of the pedicle.^[13,14] We also believe that these two flaps are not

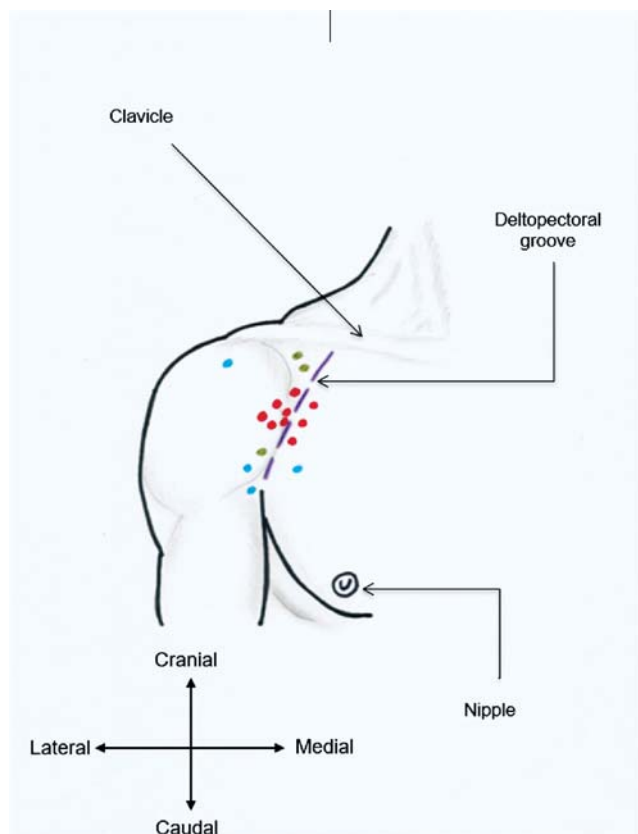


Figure 4. Distribution of the perforator of the deltoid branch of the thoracoacromial artery based on incidence. Blue: <40%; green: between 40 and 70%; red: >70%.

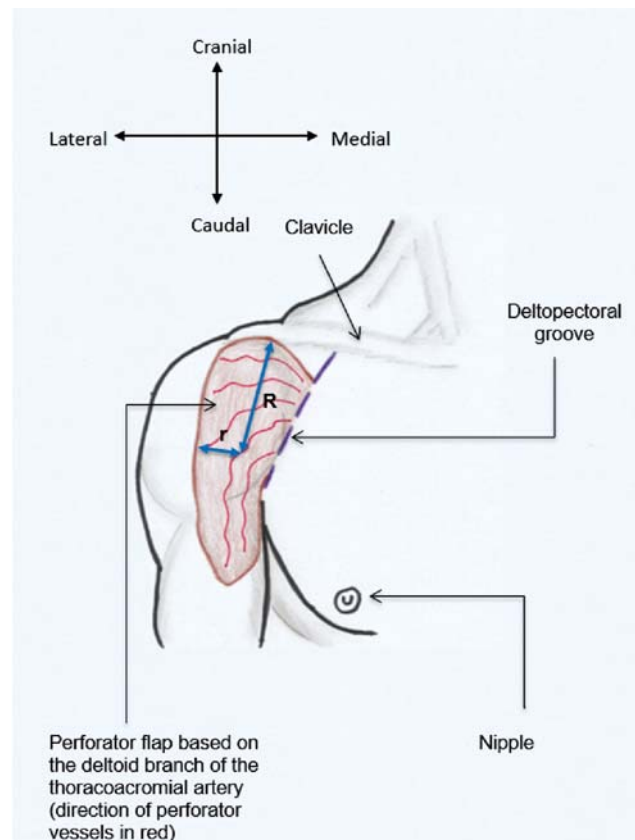


Figure 5. Drawing of the perforator flap (range, 6-7 cm) based on the deltoid branch of the thoracoacromial artery. R: long radius; r: small radius.

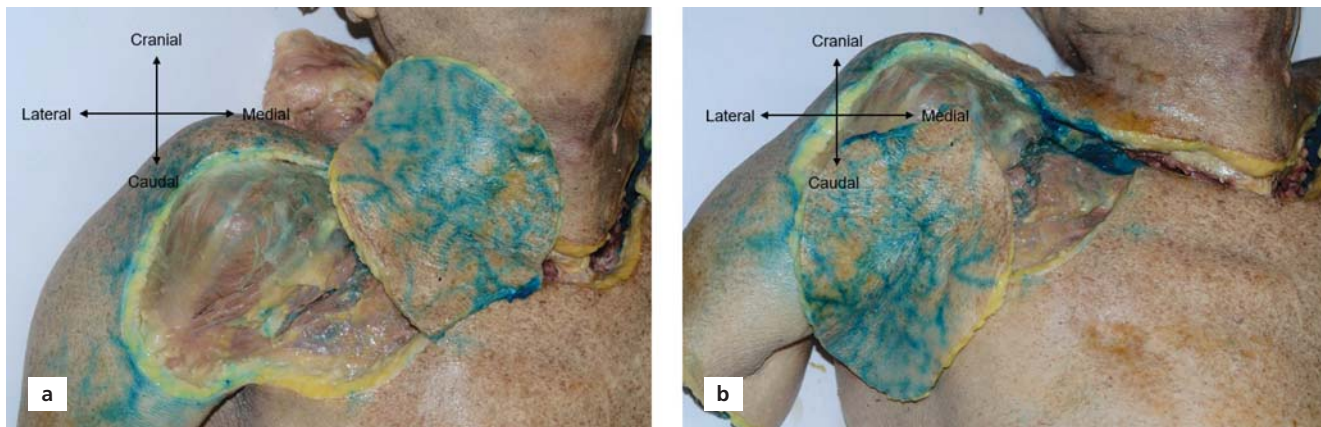


Figure 6. Skin flap pedicled on the perforators of the thoracoacromial artery can be used to reach axillary (a) and cervical (b) regions.

Table 1

Summary of the findings in the 24 dissected specimens.

No	Age	Sex	Diameter of TAA (mm)	Number of deltoid perforators found	Min. diameter of deltoid perforators (mm)	Max. diameter of deltoid perforators (mm)	Average diameter of deltoid perforators (mm)	Dimensions of deltoid branch's perforasome (cm)	Length of extrafascial pedicle (cm)	Length of pedicle after transmuscular dissection (cm)	Arc of rotation from pivot point (°)	Side
1	72	M	2	2	0.8	1.2	1	9 × 5	1.5	6	180	L
2	72	M	2	3	0.5	1.5	1	7 × 5	1.5	9	180	R
3	58	M	2	3	1	1	1	7 × 5	1.5	10	180	L
4	58	M	1.5	2	0.8	1.3	1	5 × 9	2	8	180	R
5	63	M	2	2	1	1	1	7 × 5	1.5	5	180	L
6	63	M	2.5	2	0.5	1	0.8	6 × 7	1.5	6	180	R
7	88	M	1	1	0.5	0.5	0.5	5 × 7	2	10	180	L
8	88	M	1	3	0.6	1.5	1.1	5 × 7	1.5	8	180	R
9	67	M	2	2	0.8	1.2	1	6 × 8	1.5	5	180	L
10	67	M	2	3	0.7	1	0.9	6 × 9	2	7	180	R
11	64	M	2	2	0.6	1	0.8	5 × 9	1.5	9	180	L
12	64	M	1.5	3	0.8	1	0.9	5 × 7	1	8	180	R
13	75	M	1.5	2	1	1.2	1.1	6 × 9	2	6	180	L
14	75	M	1.5	3	0.8	1.2	1	5 × 8	1.5	6	180	R
15	87	F	2	3	0.8	1.2	1	6 × 9	2.5	5	180	L
16	87	F	2	1	0.8	0.8	0.8	8 × 5	2.5	6	180	R
17	82	M	2.5	2	0.5	0.9	0.7	6 × 8	2	7	180	L
18	82	M	2.5	2	0.9	1.3	1.1	6 × 7	1.5	8	180	R
19	69	F	2.5	3	0.8	1.2	1	6 × 8	2	9	180	L
20	69	F	2	3	0.5	1	0.7	5 × 7	1.5	8	180	R
21	57	M	3	2	0.8	1	0.9	6 × 9	3	5	180	L
22	57	M	3	3	0.5	0.9	0.7	8 × 7	2.5	6	180	R
23	47	F	1.5	3	0.8	1.2	1	6 × 9	1.5	6	180	L
24	47	F	2	3	0.6	1.5	1.1	5 × 9	1.5	5	180	R

TAA: thoracoacromial artery.

suitable for the most superficial tissue defect in the cervical region, because of their excessive thickness.

The pedicled flaps on the musculocutaneous perforator arteries have several advantages compared to conventional musculocutaneous flaps, in particular during reconstructions in soft tissue defects of head and neck.^[5,6] The proximity of these flaps to the head and neck gives them an additional advantage in filling tissue defects of these regions (**Figure 6**). The absence of hair is also a positive point. In this region, the pedicled flap on the transverse cervical artery is the most used.^[4] For many years, the perforator flap of the transverse cervical artery made easier filling in soft tissues defects of neck and face. Indeed, it fulfills several reconstruction criteria including proximity to the head, good technical flexibility during its harvesting, as well as similarities with head and neck in terms of hairiness, texture, coloring and thickness.^[4] Compared to the perforator flap of the transverse cervical artery, our work shows that the perforator flap of the deltoid branch of the TAA has excellent quality in addition to a long transmuscular pedicle (**Figure 6**). It spares the deltoid muscle in all cases, which decreases the morbidity of the donor site. The donor site can sometimes be primarily closed (according to the flap size and shape) or grafted. However, the perforator flap of the deltoid branch of the TAA has not yet been the subject of important anatomical studies to date.

According to Salmon,^[10,11] the TAA is the main integumentary artery in the anterior portion of the deltoid region. It is divided in depth into two branches: one acromial (the deltopectoral artery) and the other thoracic (or pectoral). Our results are similar to those reported by Thomas et al.^[15] According to their study, the upper limb presents on average 15 territories irrigated by 48 perforators. The average caliber of the perforators is 0.7 mm and the perforasomes cover an average surface of 35 cm². Our work shows that the general orientation of the perforators in the adipose tissue is oblique laterocaudally, parallel to the deltopectoral groove, as stated by Salmon.^[10] However, for dissected specimens presenting 2 or 3 perforators, even if the small branches have different orientations, they are close to the oblique orientation described above. In our dissection experience, the perforator flap based on the deltoid branch of the TAA can be lifted craniocaudally on the proximal part of the upper limb and placed on a recipient site in a lateromedial position within the lateral triangle of the neck, or in a caudocranial position within the anterior cervical region (**Figure 5**). However, harvesting and placing the flap must respect its original orientation (craniocaudal or slightly oblique below and laterally according to

Salmon), the anatomical limits and the average flap dimensions.

The drawing of the flap is therefore possible while respecting the general orientation of the perforators of the deltoid branch of the TAA, the anatomical limits of the perforasome, and the point of origin of the terminal branches of the TAA at the deltopectoral groove. When we perform a retrograde dissection of the perforasome and then the perforator while respecting the middle third of the deltopectoral groove as a landmark, the pedicle obtained from the deltoid branch of the TAA to its axillary origin can measure up to 10 cm long. Despite the fact that the deltoid branch of the TAA gives a constant number of perforators which irrigate the subcutaneous tissue and skin of the supero-anterior region of the upper limb, none of these perforators is observed below the horizontal line passing through the nipple and extending over the arm. The perforasome irrigated by the deltoid branch of the TAA is limited by: the horizontal line passing through the nipple caudally, the vertical line passing through the insertion of the deltoid muscle laterally, the anterior margin of the deltoid muscle medially, and the apex of the flap lying near its pedicle, up to the middle third of the deltopectoral groove. When dissecting this flap, it is better to include the acromial branch of the TAA and the territory assigned to it. Because the acromial branch is always a daughter branch from the deltoid branch as proved by our study. In addition, when it is born early (a few millimeters after the birth of the deltoid branch) it projects like its original branch against the middle third of the deltopectoral groove. During dissections, our experience of harvesting and placing flaps shows that, even if the vascular territory of the deltoid branch covers in all cases the lateral triangle of the neck, in 19 dissections out of 24 the anterior region of the neck is easily accessible by this flap. In 5 cases the pedicle's length is insufficient. To reach cervical regions, a slow and careful transmuscular dissection of the pedicle should be performed.

The work of Hue et al.^[16] shows that the deltoid flap is taken from a vascular transition zone. In fact, the deltoid muscle flap receives three vascular pedicles dividing it into three regions. These pedicles are represented by the deltoid branch of the TAA and the posterior and anterior humeral circumflex arteries. In fact, it is common during the preparation of the deltoid muscle flap to injure the collaterals of the TAA.^[16] The arterial vascularization of the deltoid muscle is organized as follows:^[3,16] the posterior humeral circumflex artery provides the main vascular source, followed by the anterior

humeral circumflex artery, then by the deltoid branch of the TAA. The posterior humeral circumflex artery has the largest caliber and constitutes the vascular base of the muscular and musculocutaneous flaps of the deltoid.^[3,16] However, in our work it appears that the deltoid branch represents an important vascular source for the anterior surface of the deltoid muscle.

For all our injections, the perforasome corresponding to the deltoid branch of the TAA occupies only a part of the skin corresponding to the deltoid muscle. For this reason, the surgeon must take precautions when harvesting this perforator flap.

We might think that the perforator flap based on the deltoid branch of the TAA represents the perforator variant of the deltoid muscle flap. Actually, the deltoid branch of the TAA is only the smallest arterial source of the deltoid muscle.^[3] Besides, the cutaneous perforasome corresponding to this deltoid branch covers only the anterior part of the deltoid subcutaneous tissue and skin. It would therefore be interesting to complete our work with another anatomical study focusing on cutaneous perforasomes from perforator branches of the posterior and anterior humeral circumflex arteries. Another limitation of our study lies in the fact that all the dissected subjects are of Caucasian type. It would be interesting to make our sample more consistent, by including other races in order to compare these first results.

Despite the popularity of the perforator flap of the transverse cervical artery in the correction of cervicofacial tissue defects, the perforator flap of the deltoid branch of the TAA can be used for the same indications. But that requires a careful pedicle dissection. In our experience, it could even be used for loss of pectoral or back tissues. In practice, the surgeon has to perform a preoperative localization of the perforators, using a CT scan or a Doppler ultrasound.

Conclusion

The deltoid branch of the TAA gives several perforators which supply the subcutaneous tissue and skin of the anterior part of the deltoid region. These branches can be used as a vascular base for harvesting perforator flaps within the deltoid muscle, in order to fill in tissue defect from the lateral triangle of the neck and the anterior cervical region.

Acknowledgments

The authors are grateful for the contribution of the entire staff of the Lille University Anatomy Laboratory (France) to this work, along with the staff of the Radiology

Department of the Lille University Hospital. The authors of this work thank all the donors for their contribution.

Conflict of Interest

All authors declare no conflict of interest.

Author Contributions

PMMN: protocol, project development, data collection, data analysis, and manuscript writing; CF: protocol development, data analysis, and manuscript editing; VD-M: protocol development, data analysis, and manuscript editing; XD: protocol development, data analysis, and manuscript editing.

Ethics Approval

All the institutional procedures concerning cadaveric dissection were respected, as well as the ethical framework.

Funding

No funding received.

References

- Ross RJ, Baillieu CE, Shayan R, Leung M, Ashton MW. The anatomical basis for improving the reliability of the supraclavicular flap. *J Plast Reconstr Aesthet Surg* 2014;67:198–204.
- Alves HR, Ishida LC, Ishida LH, Besteiro JM, Gemperli R, Faria JCM, Rereira MC. A clinical experience of the supraclavicular flap used to reconstruct head and neck defects in late-stage cancer patients. *J Plast Reconstr Aesthet Surg* 2012;65:1350–6.
- Munnich DA, Morris AM, Herbert KJ. The deltoid muscle flap: anatomical studies and case reports. *Br J Plast Surg* 1996;49:310–4.
- Kneser U, Beier JP, Dragu A, Arkudas A, Horch RE. Transverse cervical artery perforator propeller flap for reconstruction of supraclavicular defects. *J Plast Reconstr Aesthet Surg* 2011;64:952–4.
- Morris SF, Tang M, Almutkari K, Geddes C, Yang D. The anatomical basis of perforator flaps. *Clin Plast Surg* 2010;37:553–70.
- Manyacka Ma Nyemb P, Fontaine C, Demondion X, Demeulaere M, Descamps F, Ndoye J-M. Anatomical variations of the trunk of origin and terminal branches of the thoraco-acromial artery. *MOJ Anat Physiol* 2018;5:57–61.
- Geddes CR, Tang M, Yang D, Morris SF. An assessment of the anatomical basis of the thoracoacromial artery perforator flap. *Can J Plast Surg* 2003;11:23–7.
- Hallock GG. The island thoracoacromial artery muscle perforator flap. *Ann Plast Surg* 2011;66:168–71.
- Reid CD, Taylor GI. The vascular territory of the acromiothoracic axis. *Br J Plast Surg* 1984;37:194–212.
- Salmon M, Grégoire R. *Artères de la peau* (Vol. 4). Paris (France): Masson; 1936. p. 123–31.
- Salmon M, Dor J. *Les artères des muscles des membres et du tronc*. Paris (France): Masson; 1933. p. 238
- Liu R, Gullane P, Brown D, Irish J. Pectoralis major myocutaneous pedicled flap in head and neck reconstruction: retrospective review of

- indications and results in 244 consecutive cases at the Toronto General Hospital. *J Otolaryngol* 2001;30:34–40.
13. Wei WI, Chan YW. Pectoralis major flap. In: Wei FC, Mardini S, editors. *Flaps and reconstructive surgery*. Philadelphia (PA): Saunders; 2009. p. 175–192.
 14. Nishi Y, Rikimaru H, Kiyokawa K, Watanabe K, Koga N, Sakamoto A. Development of the pectoral perforator flap and the deltopectoral perforator flap pedicled with the pectoralis major muscle flap. *Ann Plast Surg* 2013;71:365–71.
 15. Thomas BP, Geddes CR, Tang M. The vascular supply of the integument of the upper extremity. In: Blondeel PN, Morris SF, Hallock GG, Neligan PC, editors. *Perforator flaps: anatomy, technique and clinical applications*. St Louis (MO): QMP; 2006. p. 129–246.
 16. Hue E, Gagey O, Mestdagh H, Fontaine C, Drizenko A, Maynou C. The blood supply of the deltoid muscle. Application to the deltoid flap technique. *Surg Radiol Anat* 1998;20:161–5.

ORCID ID:

P. Manyacka Ma Nyemb 0000-0002-3339-4312;
 C. Fontaine 0000-0001-9280-7546;
 V. Duquennoy-Martinot 0000-0003-4296-9736;
 X. Demondion 0000-0003-2418-4396



Correspondence to: Philippe Manyacka Ma Nyemb, MD, PhD, MBA
 Department of Anatomy and Organogenesis, School of Medicine, Gaston
 Berger University, P.O. box 234, Saint-Louis, Senegal
 Phone: +221 77 445 43 13
 e-mail: phil_manyacka@yahoo.fr

Conflict of interest statement: No conflicts declared.

This is an open access article distributed under the terms of the Creative Commons Attribution-NonCommercial-NoDerivs 4.0 Unported (CC BY-NC-ND4.0) Licence (<http://creativecommons.org/licenses/by-nc-nd/4.0/>) which permits unrestricted noncommercial use, distribution, and reproduction in any medium, provided the original work is properly cited. *How to cite this article:* Manyacka Ma Nyemb P, Fontaine C, Duquennoy-Martinot V, Demondion X. Perforator flaps based on the deltoid branch of the thoracoacromial artery: anatomical study. *Anatomy* 2021;15(1):36–43.

Morphometry of the hyoid bone: a radiological anatomy study

Ahmet Dursun¹ , Mehtap Ayazoğlu¹ , Veysel Atilla Ayyıldız² , Yadigar Kastamoni¹ ,
Kenan Öztürk¹ , Soner Albay¹ 

¹Department of Anatomy, School of Medicine, Süleyman Demirel University, Isparta, Turkey

²Department of Radiology, School of Medicine, Süleyman Demirel University, Isparta, Turkey

Abstract

Objectives: The hyoid bone occupies a strategic position and participates in vital functions. The aim of this study was to examine the morphometry of the hyoid bone and define its location according to the vertebral level on 3D computed tomography (CT) images.

Methods: This study was conducted using 3D–CT images of 216 patients (104 males, 112 females) aged between 10–98 years. The vertebral level of the hyoid bone was determined for each decade. Furthermore, the anterior-posterior length of the hyoid bone, the length and height of the greater horn, the height and width of the body, the distance between the posterior ends of the greater horn, and the distance of the hyoid bone to the vertebral column and the angle between right and left greater horn was measured.

Results: The hyoid bone was most commonly located at C3 and C2–C3 vertebral level in females (35.7%) and C3 in males (38.5%). No statistically significant difference was found between right and left sides concerning the length and height of the greater horn.

Conclusion: Knowing the radiological anatomy, morphometric properties and vertebral levels of the hyoid bone will contribute to the surgical planning of this region and the hyoid bone. In addition, our study will provide data on the morphometric properties of hyoid bone in forensic and anthropological research.

Keywords: greater horn; lesser horn; morphometry; computed tomography

Anatomy 2021;15(1):44–51 ©2021 Turkish Society of Anatomy and Clinical Anatomy (TSACA)

Introduction

The neck involves vital anatomical structures such as the respiratory tract, arteries, veins, and nerves. Even a slight blow to the neck region may threaten one's health and life. Neck injuries may lead to hemorrhage in the neck muscles to fractures in the laryngeal cartilage and hyoid bone that can cause sudden death.^[1]

The hyoid bone is located between the thyroid cartilage and the mandible in the anterior region of the neck, usually at the level of the C3 vertebra.^[2] It does not directly make articulation with any bone. It has a body and two protrusions called the greater and the lesser

horns.^[3] The hyoid bone occupies a strategic position and participates in important vital functions. It is intimately connected to the larynx and plays a part in phonation, respiration, speech, and swallowing.^[4] The hyoid bone also serves as an insertion point for swallowing and respiratory muscles due to its position.^[3] During the pharyngeal phase of swallowing, the suprahyoid muscles contract, and the hyoid bone moves forward under the base of the tongue. Dysphagia, aspiration, and swallowing disorders can be seen as a side effect of the treatment of head and neck cancer with chemoradiotherapy resulting in decreased movement of the hyoid bone during swallowing. This can cause impaired closure of airway

This study was an oral presentation in the 20th National Anatomy Congress, 27th–31st August 2019, İstanbul, Turkey.

increasing the risk of aspiration.^[5] Therefore, it is important to know the morphometric characteristics and topography of the hyoid bone to provide an ideal surgical approach and plan radiotherapy.^[3]

The hyoid bone syndrome is characterized by sensitivity and pain around the greater horn of the hyoid bone. The surgical removal of the greater horn is used for treatment of hyoid bone syndrome.^[6] Knowledge of the morphometric characteristics and variations of the hyoid bone is essential for the treatment of this syndrome.^[7]

The hyoid bone fractures are regarded as the evidence of drowning or hanging in forensic medicine.^[8] The hyoid bone fractures have been associated with other injuries such as thyroid and cricoid cartilage fractures, and cervico-spinal fractures. The hyoid bone fractures are more common in males compared to females since blunt trauma, firearm injuries, sports-related injuries, falls, and attacks are more commonly seen in males. However, the incidence of the hyoid bone fractures is higher in females in relation to suicide attempts by hanging. The hyoid bone fractures, which occur with other bone fractures within head and neck fractures, are observed at a rate of 1.15%. The ratio of isolated hyoid bone fractures is as low as 0.002% among all head and neck fractures. This ratio increases to 27–50% in cases such as suicide by hanging.^[9]

Since the topography of the hyoid bone varies in between individuals, the location and morphometric characteristics of the hyoid bone should be known while evaluating this bone. Therefore, in this study, it was aimed to determine the location of the hyoid bone according to vertebral level, to examine its morphometry, to determine its distance to the vertebral column and to make a comparison between decades on three-dimensional computed tomography (3D-CT) images.

Materials and Methods

This study was conducted on 3D-CT images of 216 patients (104 males, 112 females) between 10 and 98 years of age. The patients were admitted to the hospital for any other reason rather than complaints or pathologies in the neck region. The age groups were divided into decades, including 2nd decade (10–19 years), 3rd decade (20–29 years), 4th decade (30–39 years), 5th decade (40–49 years), 6th decade (50–59 years), 7th decade (60–69 years), 8th decade (70–79 years), 9th decade (80–89 years), and 10th decade (90–98 years). The cases in the first decade (0–9 years) were not included in the study because the hyoid bone ossification was not completed yet and could be misleading for measurements.

The images were obtained from our hospital's "Image Picture Archiving and Communication System." Multislice spiral CT scans were obtained with a multidetector 128 slice SOMATOM Definition AS Siemens (Siemens Healthcare, Erlangen, Germany) CT using the following parameters: 120 kV, effective mAs=143 mAs, slice thickness=1 mm, matrix=512×512, collimation=128×0.6 slice increment=0.7 pitch=0.8 FOV (Field of View) (250–300). A 3D reconstruction was created from scanned images using RadiAnt DICOM Viewer (Version 2020.1; Swansea, UK) programme.

The landmarks and parameters used for the measurements are presented in **Table 1**. While the angle between right and left greater horn was measured by the ImageJ program (Public Domain, BSD-2), other parameters were measured by RadiAnt DICOM Viewer (Version 2020.1; Swansea, UK) program. Our measurements were performed from the superior for the A, B, C, H, and α parameters, from the anterior for the F and G parameters, from the right lateral for the D parameter, and from the left lateral for the E and I parameters (**Figures 1, 2 and 3**).

While determining the vertebral level of the hyoid bone, we draw two lines parallel to the long axis of the hyoid bone from the top and bottom points on the left lateral side of the hyoid bone to the vertebral column so that the position of the head would not change the vertebral level. The point where these lines corresponded to the body of the vertebra was considered as the vertebral level (**Figure 3**). While measuring the distance of the hyoid bone to the vertebral column, we measured the shortest distance of the hyoid bone to the left lateral side of the vertebral column (**Figure 3**). Finally, we measured the angle

Table 1

Landmarks and parameters used for measurements.

Landmark/parameter	
A	Anterior-posterior length of the hyoid bone
B	Length of the greater horn (right)
C	Length of the greater horn (left)
D	Height of the greater horn (right)
E	Height of the greater horn (left)
F	Width of the body of the hyoid bone
G	Height of the body of the hyoid bone
H	The distance between the midpoints of the posterior ends of the greater horn of the hyoid bone
I	The distance of the hyoid bone to the vertebral column (The distance from the greater horn's posterior end to the vertebral column on the line drawn parallel to its long axis)
α (°)	Angle of right and left greater horn (The angle between greater horn by connecting the lines passing through the midpoints of the anterior and posterior ends of the greater horn)

' α ' symbolizes angle, other measurements are in millimeters.

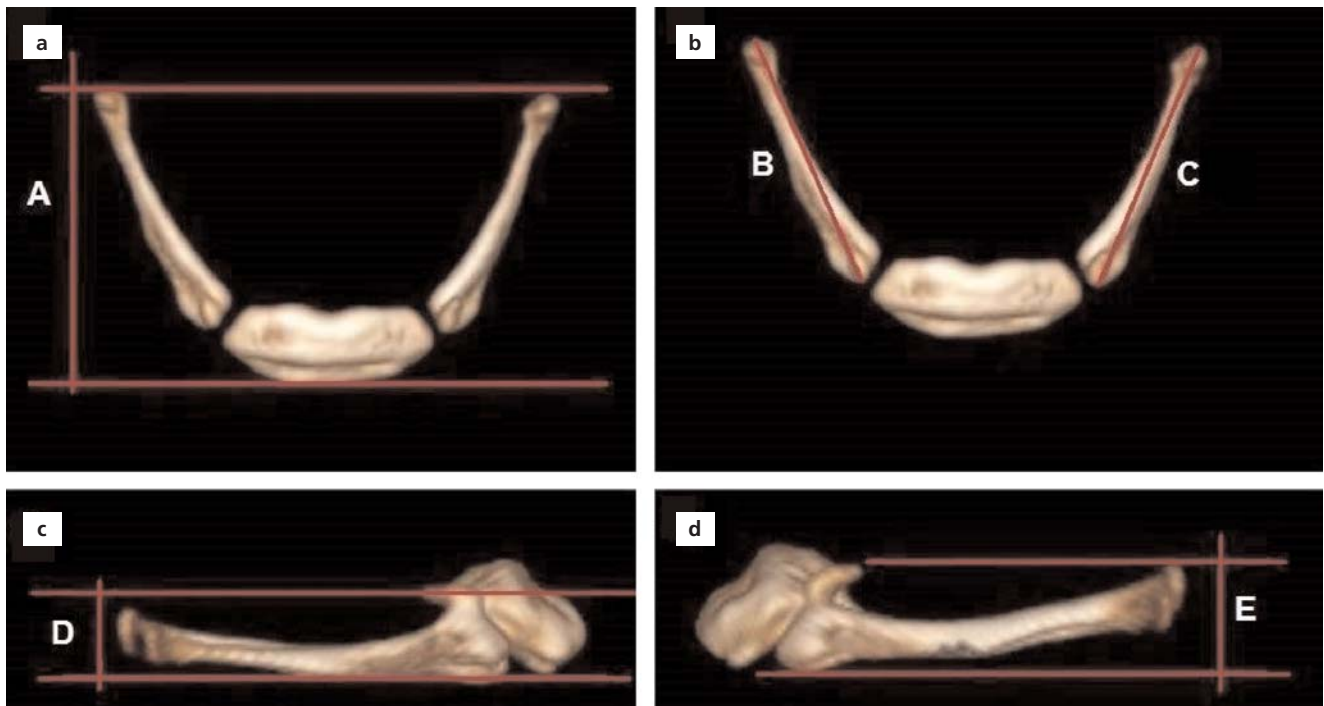


Figure 1. (a, b) Superior views. (c) Right lateral view. (d) Left lateral view. A: anterior-posterior length of the hyoid bone; B: length of the greater horn (right); C: length of the greater horn (left); D: height of the greater horn (right); E: height of the greater horn (left).

between right and left greater horn by connecting the lines passing through the midpoints of the anterior and posterior ends of the greater horn (Figure 2c). In order to

increase the sensitivity for the measurements, the parameters were measured twice by two different researchers and the average of the two values was reported.

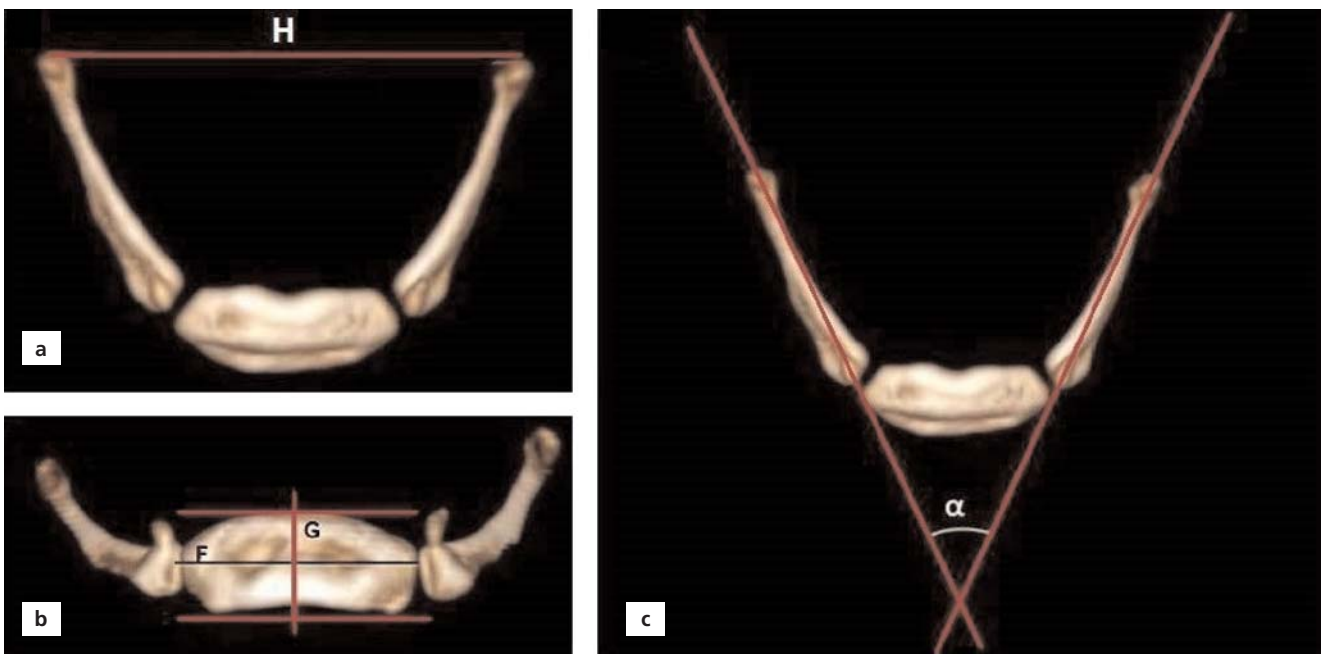


Figure 2. (a, c) Superior views. (b) Anterior view. F: width of the body of the hyoid bone; G: height of the body of the hyoid bone; H: the distance between the posterior ends of the greater horn; α : angle between right and left greater horns.

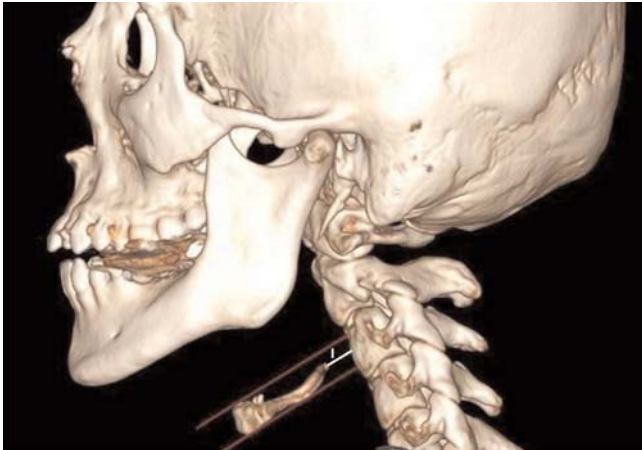


Figure 3. Left lateral view. I: the distance of the hyoid bone to the vertebral column. The lines used to determine the vertebral level of the hyoid bone are shown in red.

Statistical analyses were performed using the IBM SPSS Statistics for Windows (Version 20.0, Armonk, NY, USA). Frequency analysis was performed to determine the frequency of the vertebra level for each decade and both genders. The averages and standard deviations of all parameters by decades and genders were determined. In pairwise comparisons, the independent samples T-test was used for normally distributed data, while the Mann–Whitney U test was used for non-normally distributed data. Kruskal–Wallis test was used for comparison between the decades, because more than two independent groups were which were not normally distributed. The significance level was taken as $p < 0.05$.

Results

The vertebral level of the hyoid bone among genders are presented in **Table 2**, and the minimum, maximum values,

and averages of the measurements are presented in **Table 3**. The most common vertebral levels were C3 and C2–C3 in females by 35.7% and C3 in males by 38.5%, respectively, and the rarest vertebral levels were between C1–C2 and C4–C5 in females by 0.9% and C5 in males by 0.9%. The average distance of the hyoid bone to the vertebral column was higher in males compared to females, although it was not statistically significant. No statistically significant difference was found between genders concerning the angle between right and left greater horns (α) and the distance of the hyoid bone to the vertebral column (I) (**Figure 3**). In other parameters, the values in males were statistically significantly higher ($p < 0.05$) (**Table 4**). The length and height of the greater horn on the right and left sides had no statistically significant difference.

The frequency of vertebral levels by decades is presented in **Table 5**, and the comparison of morphometric measurements by decades is presented in **Table 6**. The vertebral level of the hyoid bone was getting lower as the age increased. In the comparison between the decades, a statistically significant difference was found between some decades for other parameters except for the parameters of the distance of the hyoid bone to the vertebral column (I) and the angle between right and left greater horn (α) (**Table 6**).

Discussion

There is a limited number of studies examining the morphometry and position of the hyoid bone according to the vertebral level. The possibility that the hyoid bone fractures may damage vital anatomical structures due its position, thus, any study on hyoid bone will be important.^[10] The hyoid bone fracture is a clinical condition that is difficult to diagnose and can usually be overlooked. If the hyoid bone fracture is clinically suspected in a patient with

Table 2
Frequency and percentages of vertebral levels by gender.

Vertebral level	Frequency (female)	Percentage (%) (female)	Frequency (male)	Percentage (%) (male)	Frequency (total)	Percentage (%) (total)
C1–C2	1	0.9	-	-	1	0.5
C2	4	3.6	-	-	4	1.9
C2–C3	40	35.7	18	17.3	58	26.9
C3	40	35.7	40	38.5	80	37.0
C3–C4	18	16.1	30	28.9	48	22.2
C4	8	7.1	10	9.6	18	8.3
C4–C5	1	0.9	5	4.8	6	2.8
C5	-	-	1	0.9	1	0.5
Total	112	100 (%)	104	100 (%)	216	100 (%)

C: cervical vertebra.

Table 3

Minimum-maximum and average values of the measurements.

Measurements	n	1st researcher (mean)	2nd researcher (mean)	min	max	mean±SD
A	216	37.4	35.5	23.9	49.7	36.45±4.71
B	216	29.14	27.3	15.4	40.8	28.22±3.87
C	216	29.36	26.4	16.2	39.0	27.88±3.84
D	216	8.02	8	1.00	10.73	8.01±2.20
E	216	8.22	7.8	1.02	10.77	8.01±1.84
F	216	22.61	23.03	12.3	33.8	22.82±3.77
G	216	9.96	9.9	7.13	10.59	9.93±0.61
H	216	40.3	39.5	22.4	58.0	39.9±5.79
I	216	4.45	4.65	.00	10.74	4.55±3.22
α (°)	216	37.31	37.45	.00	64.04	37.38±9.30

'α' symbolizes angle, other measurements are millimeters.

Table 4

Comparison of parameters by gender.

Gender	n	A	B	C	D	E	F	G	H	I	α (°)
Male	104	39.01±4.54	29.64±3.93	29.34±3.99	8.68±2.04	8.55±1.48	25.08±3.29	10.18±0.34	42.45±5.87	4.78±3.22	36.42±9.24
Female	112	34.08±3.47	26.90±3.32	26.52±3.15	7.38±2.17	7.51±2.01	20.73±2.88	9.70±0.61	37.52±4.59	4.34±3.21	38.27±9.31
p		<0.001	<0.001	<0.001	<0.001	<0.001	<0.001	<0.001	<0.001	0.315	0.143

'α' symbolizes angle, other measurements are millimeters.

a neck injury, the diagnosis should be confirmed by CT, laryngoscopy, and surgical examination.^[11]

In previous studies, it has been reported that the vertebral level of the hyoid bone is generally between the C2–C3 vertebra until the age of 10 and between the C3–C4 vertebra in adulthood. However, some studies

reported that the position of the hyoid bone did not differ between genders.^[12,13]

In this study, the vertebral level of the hyoid bone was getting lower as the age increased (Table 5). The most common vertebral levels were C3 and C2–C3 in females by 35.7% and C3 in males by 38.5%, respectively, and the

Table 5

Vertebral level frequency according to decades.

Decade	Frequency								n
	C1–C2	C2	C2–C3	C3	C3–C4	C4	C4–C5	C5	
2nd	-	2	10	17	10	-	1	-	40
3th	-	-	3	7	1	-	-	-	11
4th	-	1	9	14	6	2	-	-	32
5th	1	-	7	14	9	2	1	-	34
6th	-	1	5	10	8	5	1	-	30
7th	-	-	10	6	4	1	2	-	23
8th	-	-	6	6	4	3	1	-	20
9th	-	-	7	3	5	3	-	-	18
10th	-	-	1	3	1	2	-	1	8
Total	1	4	58	80	48	18	6	1	216

C: cervical vertebra.

Table 6
Comparison of measurements by decades.

Decade	N (216)	A	B	C	D	E	F	G	H	I	α (°)
2nd	40	33.34±4.83	24.73±4.19	24.02±3.65	6.92±1.50	6.87±1.39	19.69±3.01	9.45±0.85	38.01±5.64	5.20±2.96	38.19±8.78
3th	11	35.41±4.05	27.75±2.93	27.82±3.15	7.70±1.49	7.32±1.82	21.94±3.20	9.38±0.78	38.89±5.56	3.86±3.47	34.75±8.67
4th	32	36.69±4.03	28.54±3.34	28.43±3.10	7.66±2.83	8.25±1.40	22.82±3.51	9.93±0.53	38.74±5.44	4.18±3.12	34.07±10.67
5th	34	37.25±4.78	29.33±3.84	28.62±3.39	8.91±1.36	8.59±1.53	23.57±3.85	10.05±0.46	41.30±5.48	3.76±2.84	38.78±7.62
6th	30	38.59±4.18	29.57±2.62	29.62±3.25	8.38±2.49	8.23±1.98	24.63±3.78	10.08±0.37	41.86±5.61	4.85±3.33	36.92±10.84
7th	23	36.52±5.27	28.71±3.25	28.51±3.75	8.13±2.33	7.77±2.73	24.08±3.74	10.09±0.54	39.95±4.95	4.12±2.97	38.08±8.75
8th	20	39.01±3.91	30.52±2.65	30.68±2.99	8.47±2.77	9.11±1.58	24.62±3.28	10.23±0.18	41.57±7.64	5.46±3.81	38.27±8.60
9th	18	35.05±3.38	27.81±3.25	27.30±3.10	7.72±2.07	8.41±1.64	21.70±1.92	10.19±0.09	38.24±4.57	5.14±3.69	39.96±8.00
10th	8	37.72±3.70	28.96±2.16	27.85±2.51	9.12±0.93	7.49±1.18	24.20±3.50	10.23±0.17	41.42±6.83	3.66±3.53	35.90±12.63
p		<0.001	<0.001	<0.001	<0.001	<0.001	<0.001	<0.001	0.028	0.472	0.313

'α' symbolizes angle, other measurements are milimeters. A: difference between groups (2.-5., 2.-6., 2.-8. decades); B: difference between groups (2.-4., 2.-5., 2.-6., 2.-7., 2.-8. decades); C: difference between groups (2.-4., 2.-5., 2.-6., 2.-7., 2.-8. decades); D: difference between groups (2.-5., 2.-6., 2.-8. decades); E: difference between groups (2.-4., 2.-5., 2.-6., 2.-8. decades); F: difference between groups (2.-4., 2.-5., 2.-6., 2.-7., 2.-8. decades); G: difference between groups (2.-5., 2.-6., 2.-7., 2.-8., 2.-9., 3.-8. decades); H: difference between groups (2.-6. decades).

rarest vertebral levels were between C1–C2 and C4–C5 in females by 0.9% and C5 in males by 0.9% (**Table 2**).

The respiratory pattern and orthodontic treatments change the normal position of the head and the position of the hyoid bone. These changes in the position of the hyoid bone bring swallowing and respiratory problems. The hyoid bone is said to be more distant from the vertebral column in individuals with swallowing disorders.^[13,14] It was indicated that the distance of the hyoid bone to the cervical vertebra remained constant until puberty and that the hyoid bone moved away from the vertebra with age.^[15] Sahin Sağlam and Uydas,^[16] found a significant difference between genders in the distance of the hyoid bone to the vertebral column. In this study, we did not find a significant difference between the decades and genders in the distance of the hyoid bone to the vertebral column.

As a result of our measurements, the average distance of the hyoid bone to the vertebral column was higher in males compared to females, although it was not statistically significant. We consider that the reason for this may be the fact that the laryngeal prominence is more prominent in males and slightly brings the hyoid bone forward through the thyrohyoid ligament. Studies have shown that the size of the hyoid bone is statistically significantly smaller in women than in men.^[17,18] The differentiation of the hyoid bone morphometry between genders contributes to the determination of gender in forensic medicine.^[2,19] The present study revealed that the size of the hyoid in females is significantly smaller, except for the distance of the hyoid bone to the vertebral column and the angle between right and left greater horns (**Table 4**). We observed that there were statistically significant differ-

ences in some parameters when compared between the decades (**Table 6**). We consider that the reason why 3rd and 4th decades were the decades when the angle between right and left greater horn was the narrowest was the consequent ossification of the laryngeal cartilage with age resulting in narrowing of the thyroid angle (**Table 6**).

The studies on the morphometric characteristics of the hyoid bone and comparisons of the studies between genders are presented in **Table 7**. The fact that we obtained very close results with the studies using cadaver as a material also indicates that the measurements performed on 3D-CT images are very close to reality. We suggest that 3D-CT can make a significant and detailed contribution to morphological and morphometric analysis in the evaluation of the hyoid bone, especially in forensic medicine.

This study had several limitations. First, the nature of the study was retrospective. Second, because the study was retrospective, the movement of the hyoid bone in situations such as breathing, speech, and swallowing could not be defined and the parameters could not be measured in these positions. Thirdly, the study had a relatively small sample size.

Conclusion

Although the importance of the hyoid bone has been understood over the years, the studies examining its radiological anatomy and vertebral level are limited. CT is a useful imaging method to evaluate the normal anatomy of the bone and to recognize complications that may occur after the hyoid bone fracture and radiotherapy, both in forensic medicine and in clinical practice.

Table 7
Studies on morphometric properties of hyoid bone and comparison of gender.

Study	Material	Year	n	A	B	C	D	E	F	G	H	I	α
Leksan et al. ^[20]													
M (mm)	Dry bone	2005	70	-	29.4±3.6	29.3±3.8	-	-	-	-	45.8±6.7	-	25.27±13.57
F (mm)	Dry bone	2005	70	-	23.6±5.0	23.7±4.2	-	-	-	-	40.5±6.4	-	24.20±14.68
Kim et al. ^[21]													
M (mm)	Cadaver	2006	85	39.7±3.2	34.8±6.0	33.5±7.3	-	-	26.0±2.5	7.8±1.6	42.8±12.3	-	37.8±14.0
F (mm)	Cadaver	2006	85	33.9±6.6	27.6±10.7	28.0±9.3	-	-	22.4±2.4	7.1±1.2	31.6±16.2	-	29.3±19.2
Kindschuh et al. ^[19]													
M (mm)	Dry bone	2010	398	37.60±3.62	30.98±3.02	-	-	10.72±1.16	-	24.14±2.37	-	-	-
F (mm)	Dry bone	2010	398	33.02±3.62	27.36±3.07	-	-	12.18±1.16	-	20.70±2.20	-	-	-
Mukhopadhyay ^[2]													
M (mm)	Cadaver	2012	50	37.42±2.95	30.00±2.47	-	-	11.34±0.74	42.86±4.28	26.97±2.17	-	-	-
F (mm)	Cadaver	2012	50	31.92±2.11	25.92±1.50	-	-	9.75±1.22	35.58±3.11	23.42±1.93	-	-	-
Balseven-Odabaşı et al. ^[22]													
M (mm)	Cadaver	2013	85	44.6 ± 5.03	35.39±3.82	33.71±3.40	-	-	22.50±3.41	-	45.50 ± 7.31	-	45.45±8.86
F (mm)	Cadaver	2013	85	38.66 ± 5.07	31.32±4.44	31.56±4.15	-	-	20.71±3.96	-	38.47 ± 10.17	-	43.63±11.48
Fakhry et al. ^[3]													
M (mm)	Cadaver	2013	180	39.08±3.96	-	-	-	-	22.27±2.76	-	42.29±7.56	-	38.78±13.93
F (mm)	Cadaver	2013	180	32.50±3.15	-	-	-	-	18.95±2.25	-	38.61±5.69	-	44.09±10.97
Kopuz ve Ortug ^[23]													
M (mm)	Cadaver	2016	60	39.45±4.71	25.61±4.53	25.44±4.50	-	-	26.52±4.22	15.35±2.85	41.31±6.03	-	-
F (mm)	Cadaver	2016	60	38.98±6.54	24.79±4.11	24.79±4.11	-	-	25.28±2.84	14.16±3.08	37.56±4.36	-	-
Our study													
M (mm)	CT	2020	216	39.01±4.54	29.64±3.93	29.34±3.99	8.68±2.04	8.55±1.48	25.08±3.29	10.18±0.34	42.45±5.87	4.78±3.22	36.42±9.24
F (mm)	CT	2020	216	34.08±3.47	26.90±3.32	26.52±3.15	7.38±2.17	7.51±2.01	20.73±2.88	9.70±0.61	37.52±4.59	4.34±3.21	38.27±9.31

' α ' symbolizes angle, other measurements are millimeters; F: female, M: male.

Conflict of Interest

The authors declare that they have no conflict of interest.

Author Contributions

AD: project development, data collection, data analysis, manuscript writing; MA: data collection, data analysis, manuscript writing; VAA: data collection, data analysis, manuscript writing; YK: data analysis, manuscript writing, manuscript editing; KÖ: data analysis, manuscript writing, manuscript editing; SA: manuscript writing, manuscript editing.

Ethics Approval

Approval was obtained from the Clinical Research Ethics Committee of Süleyman Demirel University, Faculty of Medicine (Date: 06/25/2019, Decision No: 200).

Funding

This research received no specific grant from any funding agency in the public, commercial, or not-for-profit sectors.

References

- Soerdjbalie-Maikoe V, Van Rijn RR. Embryology, normal anatomy, and imaging techniques of the hyoid and larynx with respect to forensic purposes: a review article. *Forensic Sci Med Pathol* 2008;4:132–9.
- Mukhopadhyay PP. Determination of sex from an autopsy sample of adult hyoid bones. *Med Sci Law* 2012;52:152–5.
- Fakhry N, Puymeraill L, Michel J, Santini L, Lebreton-Chakour C, Robert D, Giovanni A, Adalian P, Dessi P. Analysis of hyoid bone using 3D geometric morphometrics: an anatomical study and discussion of potential clinical implications. *Dysphagia* 2013;28:435–5.
- Auvenshine RC, Pettit NJ. The hyoid bone: an overview. *Cranio* 2020;38:6–14.
- Kraaijenga SAC, van der Molen L, Heemsbergen WD, Remmerswaal GB, Hilgers FJM, van den Brekel MWM. Hyoid bone displacement as parameter for swallowing impairment in patients treated for advanced head and neck cancer. *Eur Arch Otorhinolaryngol* 2017;274:597–606.
- Stern N, Jackson-Menaldi C, Rubin AD. Hyoid bone syndrome: a retrospective review of 84 patients treated with triamcinolone acetate injections. *Ann Otol Rhinol Laryngol* 2013;122:159–62.
- Bhide AR, Dehadray AY. Excision of the greater cornu of the hyoid in hyoid syndrome. *Auris Nasus Larynx* 1980;7:1–6.
- Kasprzak H, Podbielska H, von Bally G, Fechner G. Biomechanical investigation of the hyoid bone using speckle interferometry. *Int J Legal Med* 1993;106:132–4.
- Sawatari Y, Alshamrani Y. Oral and maxillofacial surgery cases concurrent hyoid bone fracture associated with multiple facial fractures secondary to assault: case report and review of literature. *Oral and Maxillofacial Surgery Cases* 2019;5:100119.
- Bolath G, Dogan NÜ, Fazlougullari Z, Kıvrak AS, Uysal İİ, Karabulut AK, Paksoy Y. The evaluation of variations of the hyoid bone with multidetector computerized tomography. *Tropical Health and Medical Research* 2020;2:1–8.
- Samieirad S, Rayeni AS, Tohidi E. A rare case of hyoid bone fracture concomitant with a comminuted mandibular fracture. *J Maxillofac Oral Surg* 2020;19:40–3.
- Bibby RE, Preston CB. The hyoid triangle. *Am J Orthod* 1981;80:92–7.
- Ceylan I, Gunnar A. The Study of the natural head and hyoid bone positions of the subjects having different vertical facial development. *Turkish Journal of Orthodontics* 1995;8:165–71.
- Cleal CF. Deglutition: a study of form and function. *Am J Orthod* 1965;51:566–94.
- Durzo CA, Brodie AG. Growth behavior of the hyoid bone. *Angle Orthod* 1962;32:193–204.
- Sahin Sağlam AM, Uydaz NE. Relationship between head posture and hyoid position in adult females and males. *J Craniomaxillofac Surg* 2006;34:85–92.
- Pollanen MS, Ubelaker D. Forensic significance of the polymorphism of hyoid bone shape. *J Forensic Sci* 1997;42:890–2.
- Shimizu Y, Kanetaka H, Kim YH, Okayama K, Kano M, Kikuchi M. Age-related morphological changes in the human hyoid bone. *Cells Tissues Organs* 2005;180:185–92.
- Kindschuh SC, Dupras TL, Cowgill LW. Determination of sex from the hyoid bone. *Am J Phys Anthropol* 2010;143:279–84.
- Lekšan I, Marcikić M, Nikolić V, Radić R, Selthofer R. Morphological classification and sexual dimorphism of hyoid bone: new approach. *Coll Antropol* 2005;29:237–42.
- Kim DI, Lee UY, Park DK, Kim YS, Han KH, Kim KH, Han SH. Morphometrics of the hyoid bone for human sex determination from digital photographs. *J Forensic Sci* 2006;51:979–84.
- Balseven-Odabasi A, Yalcinozan E, Keten A, Akcan R, Tumer AR, Onan A, Canturk N, Odabasi O, Dinc AH. Age and sex estimation by metric measurements and fusion of hyoid bone in a Turkish population. *J Forensic Leg Med* 2013;20:496–501.
- Kopuz C, Ortug G. Variable morphology of the hyoid bone in Anatolian population: clinical implications – a cadaveric study. *International Journal of Morphology* 2016;34:1396–403.

ORCID ID:

A. Dursun 0000-0003-4568-8761; M. Ayazoğlu 0000-0001-9027-7633; V. A. Ayyıldız 0000-0003-0252-9023; Y. Kastamoni 0000-0002-3504-5853; K. Öztürk 0000-0002-5552-8684; S. Albay 0000-0001-8438-8628

deomed®

Correspondence to:

Mehtap Ayazoğlu, PhD(c)
Department of Anatomy, Faculty of Medicine, Süleyman Demirel University,
Isparta, 32260, Turkey
Phone: +90 246 211 33 07
e-mail: ayazoglumehtap@outlook.com

Conflict of interest statement: No conflicts declared.

This is an open access article distributed under the terms of the Creative Commons Attribution-NonCommercial-NoDerivs 4.0 Unported (CC BY-NC-ND4.0) Licence (<http://creativecommons.org/licenses/by-nc-nd/4.0/>) which permits unrestricted noncommercial use, distribution, and reproduction in any medium, provided the original work is properly cited. *How to cite this article:* Dursun A, Ayazoğlu M, Ayyıldız VA, Kastamoni Y, Öztürk K, Albay S. Morphometry of the hyoid bone: a radiological anatomy study. *Anatomy* 2021;15(1):44–51.

Protective role of sildenafil citrate in isoniazid-rifampicin induced histomorphological changes in liver of albino mice

Najma Hameed¹ , Khalid Farooq² 

¹Department of Anatomy, Khyber Girls Medical College, Peshawar, Pakistan

²Department of Urology, Lady Reading Hospital, Peshawar, Pakistan

Abstract

Objectives: The objective of the study was to reveal the reversal of histo-morphological changes in mice liver induced by combined isoniazid-rifampicin (INH-RIF) therapy with sildenafil treatment.

Methods: Twenty-one mice weighing between 25–35 g were enrolled in the study. Randomisation was carried out by simple balloting method. The selected mice were sorted into three groups with 7 mice, each group. In group C (n=7) control group, mice were administered 0.4ml of saline per kg body weight daily intra peritoneally for 21 days. In group R (n=7) INH-RIF group, rifampicin (50 mg/kg) and isoniazid (50 mg/kg), dissolved in 4 ml/kg isotonic saline, were administered intra-peritoneally (ip) daily for 21 days. In group S (n=7) sildenafil administered group, 10 mg/kg sildenafil was given orally by gastric gavage on daily basis along with the intraperitoneal injection of INH-RIF (50 mg/kg each) daily for 21 days.

Results: Histopathology revealed hepatotoxicity in group R (INH-RIF), while significant improvement was observed in group C (INH-RIF-sildenafil).

Conclusion: Sildenafil citrate possesses hepatoprotective role against INH-RIF induced hepatotoxicity.

Keywords: hepatotoxicity; histomorphology; INH-RIF; oxidative stress; sildenafil citrate

Anatomy 2021;15(1):52–58 ©2021 Turkish Society of Anatomy and Clinical Anatomy (TSACA)

Introduction

Tuberculosis (TB) remains one of the leading causes of illness and death worldwide including Pakistan.^[1] WHO still considers isoniazid-rifampicin (INH-RIF) combination therapy as a basic pillar of anti-tuberculous therapy.^[2] INH when administered in an inactive form is activated by the catalase-peroxidase enzyme in *Mycobacterium tuberculosis* known as KatG which results in mycolic acid synthesis inhibition. Toxic effects of INH are mediated by its metabolites hydrazine and acetyl hydrazine produced by acetyltransferase followed by oxidation by cytochrome p450 to form hepatotoxic metabolites.^[3,4] RIF causes unconjugated hyperbilirubinemia. When given in combination, RIF accelerates INH metabolism producing toxic metabolites resulting in pathological changes in mice liver.^[3]

As per literature antitubercular drug induced hepatotoxicity varies from 2–28%, and 11% of patients. About 20% of patients receiving combined therapy results in

asymptomatic elevation of liver enzymes. Studies have shown raised levels of alanine aminotransferase (ALT) and aspartate transaminase (AST) as markers of hepatotoxicity. A rise in ALT and AST values 3–4 times of the normal range with nausea, vomiting, pain abdomen, tiredness and jaundice is considered as evidence of acute hepatic toxicity.^[5,6] Hepatic histologic alterations were revealed in a qualitative histological animal study treated by INH-RIF.^[4–7] Hepatocytes were enlarged having an abundance of eosinophilic cytoplasm and signs of vacuolization. Sinusoids were dilated with a large number of erythrocytes in the lumen. Central veins showed dilatation and congestion. In another study, the mechanism of liver injury secondary to combination therapy of INH-RIF was studied in rats in which the liver showed portal triaditis and microvascular fat deposition.^[8]

The literature revealed increase oxidative stress in INH-RIF therapy which was evident from a decrease in

the levels of glutathione superoxide dismutase, glutathione peroxidase, and glutathione-S-transferases. Both the altered profile of antioxidant enzymes and increased lipid peroxidation pointed towards the pathogenesis. Fulminant hepatic failure can be one of the worst complications of combination therapy.^[9]

Sildenafil citrate is a phosphodiesterase inhibitor that was approved initially for erectile dysfunction and pulmonary hypertension.^[10] Recently literature revealed that sildenafil inhibits oxidative stress as well as lessens inflammatory changes.^[11] The hepatoprotective role of sildenafil has been observed in thioacetamide-induced liver fibrosis as well as deranged liver function tests.^[12] Paracetamol is one of the known hepatotoxic drugs and was administered in Wister rats along with sildenafil it was found that phosphodiesterase 5 inhibition has a preventive role in paracetamol-induced liver injury.^[13] In another related study by Ayman et al.,^[14] the protective role of sildenafil in cisplatin-induced nephrotoxicity was manifested by improvement in renal function tests (RFTs) as well as reversal of histological changes in rats kidneys. There is evidence that sildenafil has an important protective role in oxidative stress-related cardiac, lung, and kidney injuries, but data is very much scarce regarding the role of sildenafil in liver injury in both biochemical as well as histological aspects, therefore this experimental study has been designed in a mouse model to find out the hepatoprotective role of sildenafil, in the face of combined INH-RIF therapy.

Materials and Methods

This study was conducted in Anatomy Department of Khyber Girls Medical College Peshawar in collaboration with Pakistan Council of Scientific and Industrial Research (PCSIR) laboratories of Peshawar. Total duration of study was six months. Thirty-one healthy male albino mice seven mice in each group of 6–8 weeks age were bought from Veterinary and Research Laboratories of Khyber Pakhtunkhwa Peshawar. Sample size was calcu-

lated by a formula which is $E = \frac{\text{total number of animals} - \text{total number of groups}}{\text{total number of groups}}$, where E is the degree of freedom and its value should lie between 10 and 20. So, $E = \frac{21 - 3}{3} = 18$. The surplus 10 mouse were kept as a reserve using attrition formula. Simple random sampling was performed by balloting method into three different groups. Mice of 6–8 weeks age having 25 to 30 g weight were included whereas inactive and deformed mice were excluded. The mice were purchased from Veterinary Research laboratories Peshawar, weighing 25–35 g and housed in the animal house of PCSIR. They were kept in 12 hours light / 12 hours dark cycle at temperature of $(23 \pm 2^\circ\text{C})$ for one week to be acclimatized. The mice in each group were numbered. The dosage was standardized according to international protocols of study of drugs in the animals. At the commencement of the research, the general physical examination (GPE) of the mice were done and it was ensured that all the mice were healthy and without any apparent deformity. All the animals were weighed by electronic animal weighing scale before the commencement and before culling of mice. All the weights of mice were recorded.

Two groups of drugs that are INH-RIF and Sildenafil citrate dose calculation and solution preparation was done in the Anatomy Department of Khyber Girls Medical College (**Table 1**).

The groups were as follows:

Group C (n=7): The control group were administered 0.4 ml of saline per kg of body weight daily intra peritoneal for 21 days.

Group R (n=7): In group R, rifampicin (50 mg/kg) and isoniazid (50 mg/kg), dissolved in 4 ml/kg isotonic saline, was administered intraperitoneally (i.p.) daily for 21 days.

Group S (n=7): In group S 10 mg/kg sildenafil was given orally by gastric gavage on daily basis along with the intraperitoneal injection of INH-RIF (50 mg/kg each) daily for 21 days.

Table 1

Details of administered antitubercular drugs (dosage, strength and supplier).

Chemical	Physical state	Strength	Supplier	Use	Dose
Saline	Solution	500 ml	Otsuka	Group C	4 ml/kg
Sildenafil	Tablets	50 mg	Pfizer	Group S	10 mg/kg
INH	Tablets	300 mg	TB control board	Group R Group S	50 mg/kg
RIF	Tablets	300 mg	TB control board	Group R Group S	50 mg/kg

Table 2

Necrosis and inflammation scores by modified Knodellar index.

Piecemeal necrosis(A)	Score	Confluent necrosis (B)	Score	Focal lytic necrosis, apoptosis (C)	Score	Portal inflammation (D)	Score
Absent	0	Absent	0	Absent	0	None	0
Mild (focal, few portal areas)	1	Focal confluent necrosis	1	One focus or less per 10x objective	1	Mild, some or all portal areas	1
Mild/moderate (focal, most portal areas)	2	Zone 3 necrosis in some areas	2	2–4 foci per 10x objective	2	Moderate, some or all portal areas	2
Moderate (cont around <50% of tracts or septa)	3	Zone 3 necrosis in most areas	3	5–10 foci per 10x objective	3	Moderate/marked, all portal areas	3
Severe (cont around >50% of tracts or septa)	4	Zone 3 necrosis+occasional portal-central bridging	4	More than ten foci per 10x objective	4	Marked, all portal areas	4
		Zone 3 necrosis + multiple portal-central bridging/panacinar necrosis		5/6			

Animals were culled on day 21. Anaesthesia was administered by chloroform-soaked cotton, placed in 50ml conical plastic tube. As per laboratory animals dissection protocols, all the animals were dissected by central incision. Livers were retrieved and weighed one by one. The livers from mice were preserved in 10% neutral buffered formalin solution. The tissue samples were transported to the histopathology section of PCSIR labs.

After fixation in 10% formalin solution, the cassettes of cut liver were placed in the tissue processor. Tissue sections were cut. Liver tissue was stained with hematoxylin eosin stain. All the slides were studied under the light microscope according to modified Knodellar criteria to observe quantitative and qualitative histological features of the mouse liver to differentiate the changes occurred in different groups of mice (Table 2). Microscopy was done for each group of mice with 10× and 40× lenses of microscope for the detailed observation.

Results

Before the start of research all the mice in groups C, R and S were completely active having sharp response to touch

stimuli whereas at the completion of 21 days, the mice in group R were having sluggish response to touch stimuli as compare to other two groups (groups C and S).

The mean weight of mice before and after experiment was calculated and t test was applied (Table 3). There was no statistically significant change in between weights before treatment and after treatment in any of the three groups (Df=6, $p < 0.05$; 2-tailed). When Tukey post hoc test was applied there was no significant weight change in between groups C, R and S (Table 3).

The mean absolute weight of liver ranged from minimum 1.5 g for group C to maximum 1.86 g for group R (Figure 1). No statistical significant difference between absolute liver weights was found in different groups except groups C and R ($p = 0.02$).

Histological variables

Mean Knodellar score was calculated, ranging from minimum 5 in groups C and S to maximum score 10 in group R (Figure 2). One-way ANOVA evaluated the degree of variance between groups and within groups, which was significant ($p = 0.000$). Post-hoc Tukey test showed the signifi-

Table 3

Mean weight of mice before and after treatment.

Groups	Mortality (n)	Body weight before treatment	Body weight after treatment	Paired sample test	Anova/Post-hoc Tukey
Control	0/7	28.7±2 g	28.1±2 g	0.231	C=R
INH-RIF	0/7	27.5±2 g	27.1±1 g	0.289	R=S
INH-RIF-sildenafil	0/7	28.7±2 g	28.1±3 g	0.231	C=S

Paired t test $p \geq 0.05$; Post-hoc Tukey $p \geq 0.05$.

cant difference between the mean Knodellar score in all three treated groups. Significant increase was found in the mean Knodellar score in group R as compare to group C, whereas a significant decrease was noted in group S as compare to group R. The score was equal in between groups C and S, which potentiates our alternate hypothesis.

In order to check qualitative variables (ordinal data) Kruskal Wallace test was applied to show association between histological changes in liver like piece meal necrosis, confluent necrosis, focal lytic necrosis and portal inflammation with type of administered drugs assuming significant ($p \leq 0.05$) (Table 4).

Moreover, the histological changes occurred in all the three groups were compared individually with each other in order to see whether the effect of sildenafil on histomorphological changes in liver is significant or not. For this reason, Mann-Whitney U test was applied. When group C was compared with group R significant histological changes (Piece meal necrosis, focal lytic necrosis and Portal inflammation) were observed in R group ($p \leq 0.05$) (Figures 3a and 3b). In group S versus R there was less degree of piecemeal necrosis and portal inflammation ($p \leq 0.05$) (Figures 4a and 4b).

Significant improvement was observed in overall Knodellar score in group S as compare to group R. There was also significant improvement in histological parameters like piece meal necrosis and portal inflammation, when INH-Rifampicin was administered along with Sildenafil citrate.

Discussion

The most striking finding of our research study was that INH-RIF had established hepatotoxic effects and sildenafil citrate had antioxidant properties which proved to be hepatoprotective against the toxic effects. In the era of laparoscopic and robotic surgery, one cannot precede regarding the management without a histopathological picture of the tissue. Every drug has its manifestations in the body that appear either in form of the biochemical changes at the enzymatic level or histopathological changes at the tissue level.

One of the established mechanisms of drug-induced hepatotoxicity in literature is oxidative stress. It is also a fact that diets, as well as drugs having antioxidant properties, have a hepatoprotective role in countering the toxic effects of drugs.^[15,16]

Bodyweight is one of the benchmark tools to check the toxic effects of a specified drug. In our study, there was no significant difference in body weights either before or after

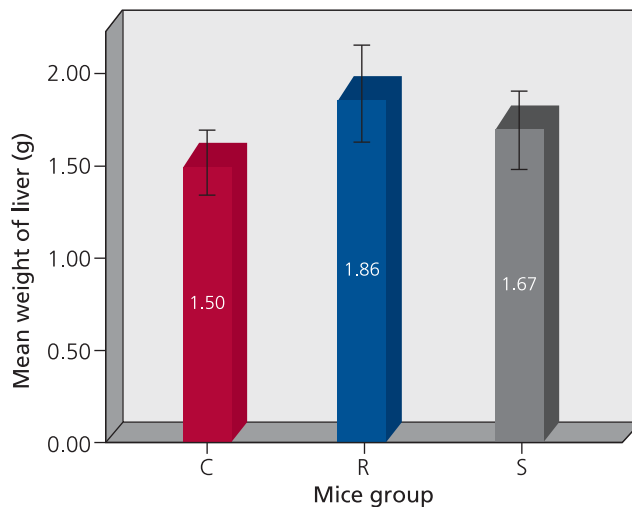


Figure 1. Comparison of mean weight of mice livers (error bars $\pm 2SD$).

Table 4

Comparison of histological parameters in mice liver by applying Kruskal Wallice and Mann-Whitney U tests.

Histological parameters	Overall group comparisons (Kruskal-Wallis test)	Pair wise significant comparisons (Mann-Whitney U test)
Piecemeal necrosis	0.000	C ↔ R R ↔ S
Confluent necrosis	0.119	
Focal lytic necrosis	0.168	C ↔ R
Portal inflammation	0.000	C ↔ R R ↔ S C ↔ S

↔ shows $p \leq 0.05$

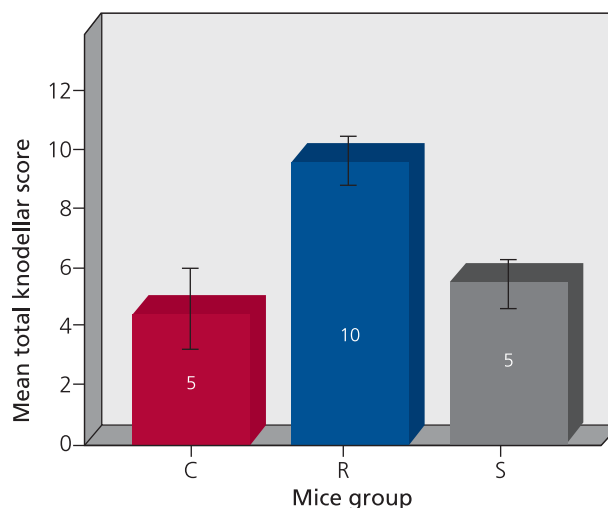


Figure 2. Mean difference of Knodellar score in between groups C, R and S (error bars 95% CI).

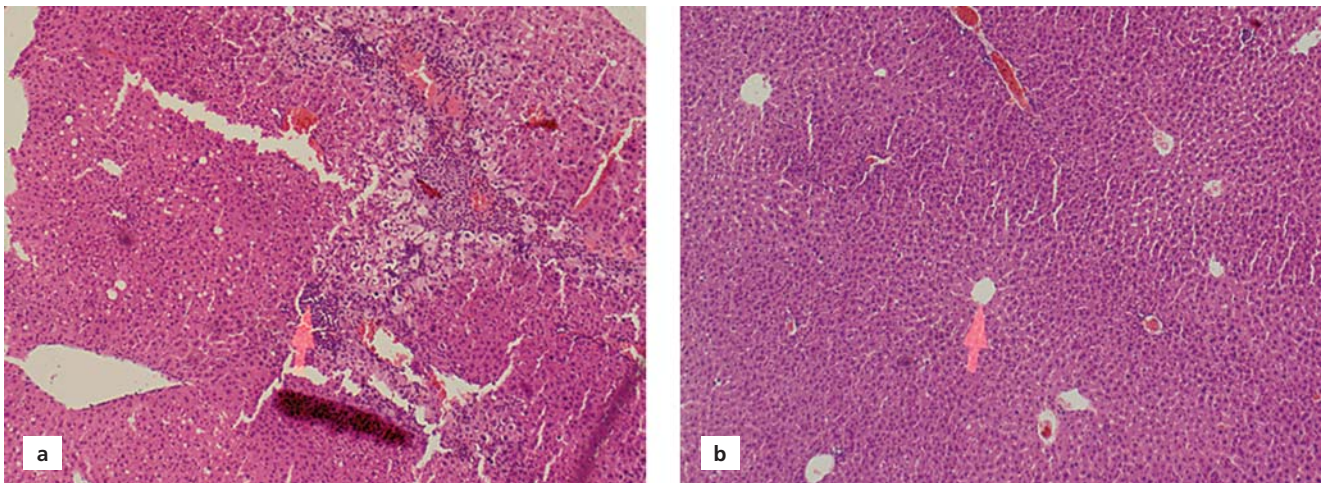


Figure 3. (a) Liver histology in group R showing grade 3 focal lytic necrosis and portal inflammation. (b) Normal liver histology in group C.

treatment. In a study on INH-RIF by Pal et al.,^[17] hepatotoxic model was produced by injecting 50 mg/kg INH-Rifampicin and garlic was administered as a hepatoprotective agent showing no significant change between the three groups. In another study by Pal et al.,^[18] carotenoids effects were observed in INH-RIF hepatotoxicity, there was no significant change in body weights. Overall, our results are following the literature.

In our study a significant increase in absolute liver weight was observed in-between groups C and R as well as the significant increase was found in relative liver weight in group R as compared to group C which was per the study conducted by Wang et al.,^[19] where the protective effects of naranginin were studied against INH-RIF induced hepa-

totoxicity. In group S, the liver weight decreased but that was not significant and the same was the case in the above-mentioned study where the decrease in liver weight in naranginin 50 mg/kg administered group was not significant. On the other side in another group of mice where naranginine was administered in 100 mg/kg, the decrease in the liver weight was significant $p < 0.05$. Based on these facts we can also presume that if sildenafil citrate is given in increased dosage in future research there may be a significant decrease in liver weight. In a very detailed research study conducted by Yang et al.,^[20] protective effects of diallyl trisulfide (DATS) were studied against the histomorphological and biochemical effects of INH-RIF. The mice were divided into six groups and DATS (10 mg/kg, 20 mg/kg, and 40 mg/kg) were administered two hours before

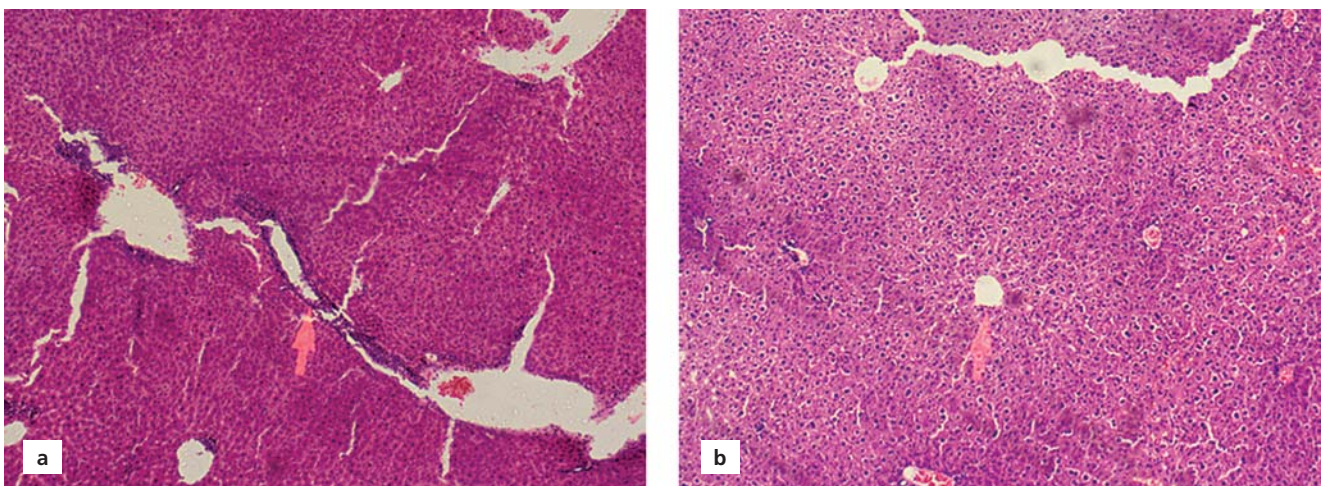


Figure 4. (a) Portal inflammation in group R. (b) Group S showing improved liver histology.

administration of INH-RIF (100 mg/kg & 100 mg/kg) respectively. The levels of AST, ALP, liver weight, and histological parameters were studied. In similarity to our study where the mean Knodellar score was the same in the control and sildenafil administered group, they observed significant improvement in the histological parameters of liver induced by INH-RIF. In our study control and sildenafil group had more or less normal lobar architecture with normal cell morphology while in the INH-RIF group there was focal lytic necrosis, piecemeal necrosis and portal inflammation which was also observed in a study by Yang et al.^[20] DATS have an anti-oxidant effect like sildenafil citrate that's why significant improvement was observed in liver morphology.

Reactive oxygen and nitrogen species are one of the main causes of the initiation and progression of liver injury. Free radicals have unpaired electrons which is highly reactive. These reactive species activate lipid peroxidation, breakage of DNA strands and ultimately oxidize all molecules in cell membrane resulting in cell injury. Normally in a healthy person, there is a balance between oxidative agents and the production of antioxidants.^[21]

It is a known fact that some of the non-toxic herbs are having reverse activities in the form of membrane stabilization, anti-oxidant, and having CYP2E1 inhibitory effects. Literature review suggests that decreased levels of lipid peroxide content in tissue and an increase in superoxide dismutase, catalase, glutathione, and glutathione peroxidase activities help to maintain liver cell coherence and control the derangement in the level of liver enzymes.^[22]

The comprehensible mechanism of hepatotoxicity is not clear, but the proposed mechanism for INH and RIF-induced damage involve lipid peroxidation and oxidative stress resulting in lowering of phospholipids protein synthesis with modifications in cell wall layout, reduced glutathione level, and activation of CYP2E1.^[21,22] PDEs play a vital role in the control of normal and pathological cellular signalling mechanisms. Mainly the PDE5 family inhibition increases cGMP levels as it hydrolyses specifically cGMP. Sildenafil, a PDE5 inhibitor, is mainly used for treating erectile dysfunctions and pulmonary hypertension. It also induces protective effects during ischemia-reperfusion injury in several organs like lungs and kidneys.^[23] Based upon these facts, sildenafil was used as an anti-oxidant and observed its protective role in the liver. Our limitations in this research study were very small data and no guidelines can be changed based upon this data, however this study opens up new avenues to climb further upon the shoulders of this research and randomized trials should be done to establish the protective role of sildenafil in INH-RIF induced hepatotoxicity.

Conclusion

In the light of this study, it is concluded that INH and RIF exhibit hepatotoxic potentials as observed in this study from the derangements in hepatic histological parameters. We suggest that sildenafil has a hepatoprotective role against INH-RIF-induced hepatotoxicity if administered along with it, as evident by significant improvement in histological parameters.

Acknowledgement

We formally thank PCSIR for their support with this study.

Conflict of Interest

All authors declare no potential conflicts of interest.

Author Contributions

NM: conceived the idea, designed the study and wrote initial manuscript; KF: helped in executing the plan after going through the study protocol, data collection, interpretation and revising the manuscript. NM, and KF, reviewed the draft critically, carried out corrections and supervised the whole study. All authors contributed significantly to the submitted manuscript.

Ethics Approval

Study was approved by Graduate Study Committee, and advanced study and research board, Khyber Medical University vide notification no DIR/KMU-AS and RB/TS/001126 dated 31/12/2019.

Funding

The study did not have a funding source.

References

1. Laghari M, Sulaiman SA, Khan AH, Memon N. Epidemiology of tuberculosis and treatment outcomes among children in Pakistan: a 5-year retrospective study. *PeerJ* 2018;6:e5253.
2. D'Ambrosio L, Dara M, Tadolini M, Centis R, Sotgiu G, Van Der Werf MJ, Gaga M, Cirillo D, Spanevello A, Raviglione M, Blasi F. Tuberculosis elimination: theory and practice in Europe. *Eur Respir J* 2014;43:1410–20.
3. Pan Y, Cao M, You D, Qin G, Liu Z. Research progress on the animal models of drug-induced liver injury: current status and further perspectives. *Biomed Res Int* 2019;2019:1283824
4. Humayun F, Tahir M, Lone KP. Histological effects of isoniazid on the liver of albino mice. *Khyber Medical University Journal* 2017;30:85–91.
5. Schaberg T, Rebhan K, Lode H. Risk factors for side-effects of isoniazid, rifampin and pyrazinamide in patients hospitalized for pulmonary tuberculosis. *Eur Respir J* 1996;9:2026–30.
6. Ramappa V, Aithal GP. Hepatotoxicity related to anti-tuberculosis drugs: mechanisms and management. *J Clin Exp Hepatol* 2013;3:37–49.

7. Čustović S, Muzika V, Mornjaković Z, Čosović E, Kapić D. Qualitative histological study of isoniazid-rifampicin induced liver injury in rats. *Folia Medica Facultatis Medicinae Universitatis Saraeviensis* 2015;50:2.
8. Sodhi CP, Rana SV, Mehta SK, Vaiphei K, Attari S, Mehta S. Study of oxidative-stress in isoniazid-rifampicin induced hepatic injury in young rats. *Drug Chem Toxicol* 1997;20:255–69.
9. Bigoniya P, Singh CS, Shukla A. A comprehensive review of different liver toxicants used in experimental pharmacology. *International Journal of Pharmaceutical Sciences and Drug Research* 2009;1:124–35.
10. Hatzimouratidis K. Sildenafil in the treatment of erectile dysfunction: an overview of the clinical evidence. *Clin Interv Aging* 2006;1: 403–14.
11. Sheweita S, Salama B, Hassan M. Erectile dysfunction drugs and oxidative stress in the liver of male rats. *Toxicol Rep* 2015;2:933–8.
12. Said E, Said SA, Gameil NM, Ammar EM. Modulation of thioacetamide-induced liver fibrosis/cirrhosis by sildenafil treatment. *Can J Physiol Pharmacol* 2013;91:1055–63.
13. Ekor M, Odewabi AO, Kale OE, Bamidele TO, Adesanoye OA, Farombi EO. Modulation of paracetamol-induced hepatotoxicity by phosphodiesterase isozyme inhibition in rats: a preliminary study. *J Basic Clin Physiol Pharmacol* 2013;24:73–9.
14. Rizk AA, Shawky YM, Motawie AG. Can sildenafil citrate ameliorate cisplatin-induced nephrotoxicity? Crosstalk between the possible mechanisms. *Eur J Anat* 2019;23:113–9.
15. Vitaglione P, Morisco F, Caporaso N, Fogliano V. Dietary antioxidant compounds and liver health. *Crit Rev Food Sci Nutr* 2005;44: 575–86.
16. Alía M, Horcajo C, Bravo L, Goya L. Effect of grape antioxidant dietary fiber on the total antioxidant capacity and the activity of liver antioxidant enzymes in rats. *Nutrition Research* 2003;23: 1251–67.
17. Pal R, Vaiphei K, Arbab Sikander KS, Rana SV. Effect of garlic on isoniazid and rifampicin-induced hepatic injury in rats. *World J Gastroenterol* 2006;12:636–9.
18. Pal R, Rana S, Vaiphei K, Singh K. Effect of different doses of carotenoids in isoniazid-rifampicin induced hepatotoxicity in rats. *Trop Gastroenterol* 2010;29:153–9.
19. Wang C, Fan RQ, Zhang YX, Nie H, Li K. Naringenin protects against isoniazid-and rifampicin-induced apoptosis in hepatic injury. *World J Gastroenterol* 2016;22:9775–83.
20. Yang Y, Jiang L, Wang S, Zeng T, Xie K. Diallyl trisulfide protects the liver against hepatotoxicity induced by isoniazid and rifampin in mice by reducing oxidative stress and activating Kupffer cells. *Toxicol Res* 2016;5:954–62.
21. Li S, Tan HY, Wang N, Zhang ZJ, Lao L, Wong CW, Feng Y. The role of oxidative stress and antioxidants in liver diseases. *Int J Mol Sci* 2015;16:26087–124.
22. Adhvaryu MR, Reddy NM, Vakharia BC. Prevention of hepatotoxicity due to anti tuberculosis treatment: a novel integrative approach. *World J Gastroenterol* 2008;14:4753–62.
23. Tetsi L, Charles AL, Georg I, Goupilleau F, Lejay A, Talha S, Maumy-Bertrand M, Lugnier C, Geny B. Effect of the phosphodiesterase 5 inhibitor sildenafil on ischemia-reperfusion-induced muscle mitochondrial dysfunction and oxidative stress. *Antioxidants (Basel)* 2019;8:93.

ORCID ID:

N. Hameed 0000-0003-2537-1759;
K. Farooq 0000-0003-1985-0235

**Correspondence to:** Khalid Farooq, FCPS

Department of Urology, Lady Reading Hospital,
Peshawar, Pakistan
Phone: +902 0345 5908751
e-mail: drkhalid846@gmail.com

Conflict of interest statement: No conflicts declared.

This is an open access article distributed under the terms of the Creative Commons Attribution-NonCommercial-NoDerivs 4.0 Unported (CC BY-NC-ND4.0) Licence (<http://creativecommons.org/licenses/by-nc-nd/4.0/>) which permits unrestricted noncommercial use, distribution, and reproduction in any medium, provided the original work is properly cited. *How to cite this article:* Hameed N, Farooq K. Protective role of sildenafil citrate in isoniazid-rifampicin induced histomorphological changes in liver of albino mice. *Anatomy* 2021;15(1):52–58.

Numerical variations and localization of foramen spinosum in 3D-CT images

Yadigar Kastamoni¹ , Ahmet Dursun¹ , Veysel Atilla Ayyıldız² , Kenan Öztürk¹ 

¹Department of Anatomy, School of Medicine, Süleyman Demirel University, Isparta, Turkey

²Department of Radiology, School of Medicine, Süleyman Demirel University, Isparta, Turkey

Abstract

Objectives: The structures passing through the foramen spinosum and its neurovascular relationships are of great importance for surgical approaches directed to middle cranial fossa. The aim of the present study was to examine the number and location of the foramen spinosum (FS) in 3D-CT images.

Methods: The study was retrospectively conducted on 3D-CT images of 177 adults. Firstly, the transverse section passing through the upper edge of the orbit, extending parallel to the Frankfurt plane was chosen. Then, the x and y-axes were determined on that transverse section. The coordinates, number, and location of the FS with respect to the foramen ovale (FO) were identified accordingly on x and y-axes.

Results: While 1 FS was present in 90.96% of a total of 354 sides of 177 heads, there were 2 FS and 3 FS in 8.76% and 0.28% of the sides, respectively. The FS was located posterolaterally in 97.68%, posteriorly in 2.06%, and laterally in 0.26% with respect to the FO. In terms of FS coordinates, there was no statistically significant difference between gender and sides in the distance of the FS to the x-axis, but there was a statistically significant difference between gender and sides in the distance of the FS to the y-axis.

Conclusion: Evaluation of the number of the FS and its location would help identifying and preserving neighbouring neurovascular structures during surgical interventions directed to the middle cranial fossa.

Keywords: computed tomography; middle cranial fossa; middle meningeal artery; skull base; sphenoid bone

Anatomy 2021;15(1):59–63 ©2021 Turkish Society of Anatomy and Clinical Anatomy (TSACA)

Introduction

The skull base is divided into three cranial fossae: anterior, middle, and posterior. The region located between the small wing of the sphenoid bone and the petrous part of the temporal bone is known as the middle cranial fossa.^[1] The middle cranial fossa is clinically very significant due to the foramina it contains and the structures passing through these foramina. The complex anatomy of this region, the diversity and aggressiveness of its tumors, and the complex reconstruction process make operations on the region requiring a multidisciplinary approach difficult. Important surgical landmarks allow surgeons to have a good understanding of the anatomy, which makes it easier to plan and perform the surgical procedure.^[2]

The foramen spinosum (FS) is one of the foramina located in the infratemporal surface of the great wing of

the sphenoid bone and is usually located posterolateral to the foramen ovale (FO).^[3,4] The FS is one of the structures providing the connection between the infratemporal fossa and the middle cranial fossa. The middle meningeal artery, middle meningeal vein, and the meningeal branch of the mandibular nerve pass through it.^[5,6] The FS derives from the first pharyngeal arch, also known as the mandibular arch. It starts to ossify eight months after birth, and it may take up to seven years for it to develop into a bony ring-shaped formation.^[7,8]

Due to its proximity to other cranial foramina, the FS is an important landmark, especially in skull base traumas involving the middle cranial fossa and infratemporal fossa. The clinical significance of this foramen is better understood in bypass surgeries involving the petrous segment of the internal carotid artery and the posterior cerebral artery, in which the middle meningeal artery is

used as a graft.^[4] The FS is important for various diagnostic and treatment techniques such as electroencephalographic analysis, percutaneous trigeminal rhizotomy, and percutaneous biopsy of cavernous sinus tumors. During such procedures, the middle meningeal artery can be iatrogenically injured since the FS is very close to the FO.^[4] Therefore, knowledge about the location and variations of this foramen is important for neurosurgeons, radiologists, and anatomists due to the techniques available nowadays.

Different bony landmarks on 2D and 3D radiological images and dry bones used to determine the location of the foramina in previous studies.^[9-11] The developments in 3D imaging have largely improved the visualization of craniofacial structures. This imaging method allows the 3D coordinates of the foramina to be known.^[12]

Considering the clinical significance of the FS, we aimed to examine the morphometric properties of the FS upon 3D reconstruction CT images since it helps to understand the 3D location of the FS in interventions to be performed in this region.

Materials and Methods

Our study was retrospectively conducted on head and neck computed tomography (CT) images. The morphometric and morphological characteristics of the FS belonging to 177 individuals (94 females, 83 males) aged between 20 and 92 years (mean age 55.06 ± 18.83) were examined.

Head and neck CT images were obtained from the hospital's "Picture Archiving and Communication System" (PACS) in the Radiology Department. Patients with any tumors or fractures on head-neck CT were not included in the study. Metabolic bone conditions that might affect bone tissue in patients, such as osteoporosis, were not questioned. CT images were obtained by a multidetector 128 slice SOMATOM Definition AS Siemens (Siemens Healthcare, Erlangen, Germany) CT device using the following parameters: 120 kV, slice thickness=1 mm, matrix=512x512, collimation=128x0.6 slice increment=0.7 pitch =0.8 FOV (Field of View) (250–300). A 3D reconstruction was created from the scanned axial images using the RadiAnt DICOM Viewer (Version 2020.2; Swansea, UK) program. After the 3D-CT image of the cranium was obtained, the calvaria was removed by taking a transverse section passing through the upper edge of the orbit, extending parallel to the Frankfurt plane. Then, the following axes were determined by looking at the cranium from the top.

y-axis: the sagittal axis passing through the middle of the dorsum sellae and connecting the frontmost and backmost points of the cranium (**Figure 1**).

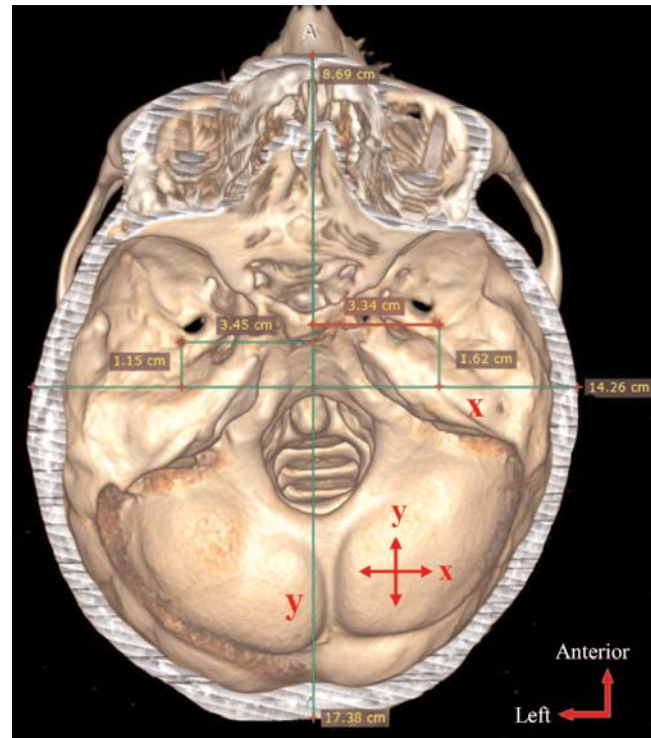


Figure 1. Distances of the foramen spinosum to the x- and y-axes.

x-axis: the axis extending from the middle of the y-axis in the transverse direction on the transverse plane (**Figure 1**).

The following FS morphometry-related parameters were measured:

- Coordinates of the FS (distance to x and y-axes) (**Figure 1**)
- Number of the FS
- Location of the FS with respect to the FO

Statistical analysis was performed using SPSS for Windows 20.0 program (SPSS Inc., Armonk, NY, USA). The arithmetic means and standard deviations of all parameters were calculated according to the sides and sex. In pairwise comparisons, the independent samples t-test was used for the normally distributed parameters, and the Mann-Whitney U test was used for the non-normally distributed parameters.

Results

While 1 FS was present in 90.96% (n=322) of 354 sides of 177 heads, 2 FS and 3 FS were present in 8.76% (n=31) and 0.28% (n=1) of them, respectively. When the location of the FS with respect to the FO was examined, it was observed that the FS was located posterolaterally

Table 1

Averages and p values of foramen spinosum according to sex and sides.

Parameters	Sex	n	Mean±SD	p	Side	n	Mean±SD	p
Distance of the FS to the x-axis (cm)	F	94	0.95±0.39	0.670	R	177	0.92±0.40	0.310
	M	83	0.93±0.41		L	177	0.96±0.40	
Distance of the FS to the y-axis (cm)	F	94	3.08±0.20	<0.001*	R	177	3.19±0.25	0.020*
	M	83	3.24±0.26		L	177	3.12±0.22	

*p<0.05. F: female; FS: foramen spinosum; L: left; M: male; R: right; SD: standard deviation.

in 97.68% (n=379), posteriorly in 2.06% (n=8), and laterally in 0.26% (n=1) with respect to the FO.

The distance of the FS to the x and y-axes was compared by giving averages according to sex and sides (Table 1). Accordingly, there was no statistically significant difference between gender (p=0.670) and sides (p=0.310) in the distance of the FS to the x-axis parameter. In the distance of the FS to the y-axis parameter, a statistically significant difference was found between gender (p<0.001) and sides (p=0.020) (Figure 2).

Discussion

Due to the advantages of 3D imaging, it is recommended for clinicians to learn to use 3D reconstruction imaging sources effectively and move away from conventional 2D imaging methods.^[12] In light of this information, the FS coordinates in our study were obtained using the 3D imaging method and different landmark points (coordinate system) from previous studies. There are many studies based on measuring the distance between the FS and other anatomical structures.^[6,9,13] However, the variations of other anatomical structures with the measured distances were ignored in these studies. Therefore, the coordinate system, which was considered least affected by the variations, was used in our study.

Some authors indicated that the differences in the skull base foramina could be considered a variation for some populations due to the evolutionary process.^[14,15] Tewari et al.^[4] indicated that the FS-related anatomical variations were associated with ethnic differences, incomplete osteogenesis, or abnormal development of the middle meningeal artery. Some authors reported that the diversity in the knowledge of the FS might be the result of factors such as age, sex, or population and differences in reference points taken as criteria in measurements.^[10]

Many studies have been conducted on the number of the foramen spinosum.^[3,4,7,10,14,16-20] The comparison of the results of those studies with the results of our study is presented in Table 2. Duplication of FS varies between

0–8.76%. We suggest that this variation may be due to the difference in the population on which the study was conducted, the difference in the method used in the study, the number of materials used, and the subjective interpretation of the researchers who conducted the study. The absence rate of FS is 0–2.85%. We had no cases in which FS was absent, as in the studies carried out by Tewari et al.^[4] and Osunwoke et al.^[10] On the other hand, we observed 3 FS in one sample, similar to the findings obtained by Lazarus et al.^[14]

The variations in the presence, absence, and the number of the FS are very important for the supply of the dura mater since they may accompany variations such as; the early branching of the middle meningeal artery, a meningeal artery passing through the foramen ovale, a meningeal artery emerging from the ophthalmic artery, or passing through the superior orbital fissure as a branch of the maxillary artery.^[7,9,20]

The FS is usually known as it is located posterolateral to the FO.^[4] However, as can be seen in our study, the FS location with respect to the FO varies. According to our results, the FS was located posterolateral to the FO by 97.68%, posterior to it by 2.06%, and lateral to it by

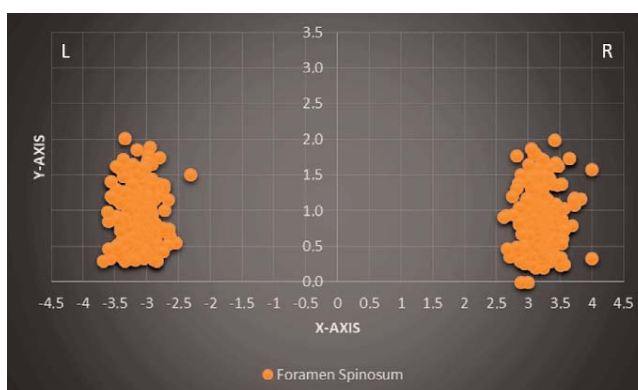


Figure 2. The distribution chart of the localizations of the foramen spinosum according to the x and y-axes (R: right, L: left).

Table 2

Comparison of studies on the number of foramen spinosum.

Authors	Number of sides	Number of foramen spinosum (%)			
		Absent	1	2	3
Our study	354	-	90.96	8.76	0.28
Khaimar and Bhusari ^[3]	186	0.54	96.23	3.23	-
Tewari et al. ^[4]	126	-	100	-	-
Sophia and Kalpana ^[7]	80	2.5	93.75	3.75	-
Osunwoke et al. ^[10]	174	-	100	-	-
Lazarus et al. ^[14]	200	2	95	2.5	0.5
Javed et al. ^[16]	70	1.43	90	8.57	-
Farooq et al. ^[17]	40	2.5	95	2.5	-
Kulkarni and Nikade ^[18]	200	2.5	97.5	-	-
Rai et al. ^[19]	70	2.85	-	2.85	-
Khan et al. ^[20]	50	2	96	2	-

0.26%. Lazarus et al.^[14] reported that the FS was located posterolateral to the FO by 97.53%, posterior to it by 1.97%, and posteromedial to it by 0.5%. The results of both studies are considerably similar. Differently, while no FS located posteromedial to the FO in our cases, no FS located lateral to the FO as revealed Lazarus et al.^[14] Although the location of the FS lateral or posteromedial to the FO is rare, these possible locations should also be taken into account. Particularly, considering the structures passing through the FS and neurovascular structures to which it is adjacent, it is very important to have full knowledge of the FS location in any intervention to be performed to this region.

Boduç and Öztürk^[21] revealed that the FS was symmetrical in 14 of 133 skulls and asymmetrical in the remaining part. Likewise, in our study, a difference was found between the right and left sides in the FS distance to the y-axis. In our samples, the FS was further away from the y-axis on the right side than on the left side. Unlike our study, Somesh et al.^[22] reported that the FS on the left side was far from the midline. We think that the difference in the results of both studies may be due to the difference in the studied population, the different number of samples studied, the difference of the method used, and the lack of knowledge about factors such as age and sex in the study performed by Somesh et al.^[22] Since the difference between the right and left sides of the FS affects the location of the middle meningeal artery, it should be considered, especially in surgical interventions to be performed in this region.

Conclusion

We suggest that our study may contribute to future studies on the FS and the middle meningeal artery passing through it. The knowledge of the normal and variational anatomy of the FS may prevent misinterpretation during imaging procedures such as CT and magnetic resonance imaging. Furthermore, the evaluation of the FS number, its relationship with the FO, and its location will be an important guide for surgeons to identify and protect neurovascular structures, especially during surgical interventions to the middle cranial fossa.

Conflict of Interest

The authors declare that they have no conflict of interest.

Author Contributions

YK: project development, data collection, data analysis, interpretation of the results, manuscript writing; AD: project development, data collection, manuscript editing; VAA: data collection, manuscript reviewing; KO: data analysis, manuscript reviewing.

Ethics Approval

Approval for this study was obtained from the Clinical Research Ethics Committee of Süleyman Demirel University, Faculty of Medicine (Date: 16 April 2020, Decision No: 109).

Funding

This research received no specific grant from any funding agency in the public, commercial, or not-for-profit sectors.

References

- Karthikeyan G, Sankaran PK, Raghunath G, Yuvaraj M, Arathala R. Morphometric study of various foramina in the middle cranial fossa of the human skull. *Indian Journal of Clinical Anatomy and Physiology* 2017;4:574-8.
- Liu Z, Yi Z. A new bony anatomical landmark for lateral skull base surgery. *J Craniofac Surg* 2020;31:1157-60.
- Khairnar KB, Bhusari PA. An anatomical study on the foramen ovale and the foramen spinosum. *J Clin Diagn Res* 2013;7:427-9.
- Tewari S, Gupta C, Palimar V, Kathur SG. Morphometric analysis of foramen spinosum in South Indian population. *Acta Medica Iranica* 2018;56:113-8.
- Krishnamurthy J, Chandra L, Rajanna S. Morphometric study of foramen spinosum in human skulls. *International Journal of Current Research and Review* 2013;5:44-8.
- Saheb SH, Khaleel N, Havaladar PP, Shruthi BN. Morphological and morphometric study of foramen spinosum. *International Journal of Anatomy and Research* 2017;5:4523-6.
- Sophia MM, Kalpana R. A study on foramen spinosum. *International Journal of Health Sciences and Research* 2015;5:187-93.
- White HJ, Reddy V, Mesfin FB. Anatomy, head and neck, foramen spinosum. In: StatPearls [Internet]. Treasure Island (FL): StatPearls Publishing; 2021 [Internet]. Available from: <https://www.ncbi.nlm.nih.gov/books/NBK535432/>
- Krayenbühl N, Isolan GR, Al-Mefty O. The foramen spinosum: a landmark in middle fossa surgery. *Neurosurg Rev* 2008;31:397-402.
- Osunwoke EA, Mbadugha CC, Orish CN, Oghenemavwe EL, Ukash CJ. A morphometric study of foramen ovale and foramen spinosum of the human sphenoid bone of southern Nigerian population. *Journal of Applied Biosciences* 2010;26:1631-5.
- Zhu HY, Zhao JM, Yang M, Xia CL, Li YQ, Sun H, Zhang YQ, Tian Y. Relative location of foramen ovale, foramen lacerum, and foramen spinosum in hertel pathway. *J Craniofac Surg* 2014;25:1038-40.
- Lagravere MO, Gordon JM, Flores-Mir C, Carey J, Heo G, Majorf PW. Cranial base foramen location accuracy and reliability in cone-beam computerized tomography. *Am J Orthod Dentofacial Orthop* 2011;139:e203-10.
- Baur DA, Beushausen M, Leech B, Quereshy F, Fitzgerald N. Anatomic study of the distance between the articular eminence and foramen spinosum and foramen spinosum and petrotympanic fissure. *J Oral Maxillofac Surg* 2014;72:1125-9.
- Lazarus L, Naidoo N, Satyapal KS. An osteometric evaluation of the foramen spinosum and venosum. *International Journal of Morphology* 2015;33:452-8.
- Sharma NA, Garud RS. Morphometric evaluation and a report on the aberrations of the foramina in the intermediate region of the human cranial base: a study of an Indian population. *European Journal of Anatomy* 2011;15:140-9.
- Javed M, Rehman Z, Iftikhar S, Naz F, Junaid SM, Alam A. Anatomical variations of foramen ovale and foramen spinosum in dry human skull. *Journal of Khyber College of Dentistry* 2020;2:Article No20. p.1-3 [Available from: <http://www.jkcd.kcd.edu.pk/issues/PublishedOnline2020Vol01/JKCD-OnlinePub2020-V2-No24.pdf>]
- Farooq B, Gupta S, Raina S. Anatomic variations in foramen ovale and foramen spinosum. *JK Science* 2018;20:112-5.
- Kulkarni SP, Nikade VV. A morphometric study of foramen ovale and foramen spinosum in dried indian human skulls. *International Journal of Recent Trends in Science and Technology* 2013;7:74-5.
- Rai AL, Gupta N, Rohatgi R. Anatomical variations of foramen spinosum. *Innovative Journal of Medical and Health Science* 2012;2:86-8.
- Khan AA, Asari MA, Hassan A. Anatomical variants of foramen ovale and spinosum in human skulls. *International Journal of Morphology* 2012;30:445-9.
- Boduç E, Öztürk L. Morphometric evaluation of foramen spinosum [Article in Turkish]. *Kafkas Journal of Medical Sciences* 2020;10:60-4.
- Somesh MS, Murlimanju BV, Krishnamurthy A, Sridevi HB. An anatomical study of foramen spinosum in South Indian dry skulls with its emphasis on morphology and morphometry. *International Journal of Anatomy and Research* 2015;3:1034-8.

ORCID ID:

Y. Kastamoni 0000-0002-3504-5853; A. Dursun 0000-0003-4568-8761;
V. A. Ayyıldız 0000-0003-0252-9023; K. Öztürk 0000-0002-5552-8684



Correspondence to: Yadigar Kastamoni, PhD

Department of Anatomy, Faculty of Medicine, Süleyman Demirel University, Isparta, 32260, Turkey
Phone: +90 246 211 33 02
e-mail: yadigarkastamoni@hotmail.com

Conflict of interest statement: No conflicts declared.

This is an open access article distributed under the terms of the Creative Commons Attribution-NonCommercial-NoDerivs 4.0 Unported (CC BY-NC-ND4.0) Licence (<http://creativecommons.org/licenses/by-nc-nd/4.0/>) which permits unrestricted noncommercial use, distribution, and reproduction in any medium, provided the original work is properly cited. *How to cite this article:* Kastamoni Y, Dursun A, Ayyıldız VA, Öztürk K. Numerical variations and localization of foramen spinosum in 3D-CT images. *Anatomy* 2021;15(1):59-63.

Morphometric evaluation of nasolacrimal duct

Burcu Erçakmak Güneş¹ , Alper Vatansever² , Deniz Demiryürek¹ , Ekim Gümeler³ 

¹Department of Anatomy, Faculty of Medicine, Hacettepe University, Ankara, Turkey

²Department of Anatomy, Faculty of Medicine, Balıkesir University, Balıkesir, Turkey

³Department of Radiology, Faculty of Medicine, Hacettepe University, Ankara, Turkey

Abstract

Objectives: Obstructions are very commonly seen in nasolacrimal duct before it opens into the inferior nasal meatus. Detailed anatomical knowledge of the nasolacrimal duct is crucial for physicians to understand the etiology of the obstructions, to plan ideal management option and to reduce unexpected iatrogenic injuries during surgeries. The aim of this study was to investigate morphometric properties of the nasolacrimal duct on computed tomography images.

Methods: Three-dimensional computed tomography (3D-CT) of 142 adults (65 females, 77 males) were retrospectively evaluated. Antero-posterior cranial diameter, antero-posterior and transverse diameters and vertical angle of the nasolacrimal duct, distance between distal end of the nasolacrimal duct to anterior surface of the maxilla were measured and the differences evaluated statistically between right and left sides and among females and males and among different ages. All measurements were done using Osirix-Lite version 9 software.

Results: None of the morphometric parameters of the nasolacrimal duct showed significant differences between right and left sides. Antero-posterior cranium and transverse diameter of the nasolacrimal duct were longer in men than women.

Conclusion: Determining to morphometric properties of the nasolacrimal canal has advantages for understanding the etiology of the NLD obstructions, deciding the ideal surgical technique and reducing to unexpected injuries during surgeries related with this region.

Keywords: 3D reconstruction; anatomy; computed tomography; nasolacrimal duct

Anatomy 2021;15(1):64–68 ©2021 Turkish Society of Anatomy and Clinical Anatomy (TSACA)

Introduction

Nasolacrimal duct (NLD) begins from the lacrimal sac and continues as the bony nasolacrimal duct between the lacrimal bone and maxilla. It drains into nasal cavity at the level of inferior nasal meatus. The NLD is entirely surrounded by the maxilla.^[1]

The obstructions of the NLD are seen frequently, due to its shape. The obstructions can be either congenital or acquired. In each instance, the etiology and the prognosis is different.^[2] There are different options for the management of the obstruction; non-surgical or surgical.^[3,4] Detailed anatomical knowledge is of great clinical importance for to understand the etiology of the obstruction and the success of treatment techniques. There are numbers of studies that are evaluating the morphometric properties of the NLD.^[5-7] The NLD has different anthropometric characteristics among populations.^[1,4,7-9] Avdagic et al.^[10] indicated that NLD obstruc-

tions could count as an important etiologic factor of epiphora, and emphasized that selecting criteria for treating these obstructions depends on its anatomical properties.

Considering craniometric features of the NLD during a surgical treatment is of great importance for a successful surgery and improving quality of post-operative period; the aim of this study was to examine detailed morphometric properties of the NLD according to its craniometric characteristics.

Materials and Methods

Computed tomography (CT) images of 142 adults (65 females, 77 males) who admitted to Hacettepe University Hospital without a significant pathology or previous surgery in the head region were retrospectively evaluated in the study. The mean age of participants was 60.02 (range: 27–85) years. DICOM series of CT images were recon-

structed three-dimensionally (3-D) using free licensed Osirix Lite Software v.12.0.1. Participants who undergone the CT for any reason other than trauma or interventional applications in their orbit, nose or paranasal sinuses were included in the study. Participants who had bone disorders, trauma history, and neoplasms in related regions were excluded from the study.

A 64-detector-row dual-source CT scanner (SOMATOM Definition, Siemens Healthcare, Erlangen, Germany) was used for CTA imaging. The protocol was as follows: 64×0.6 collimation, 1.4 pitch, 0.5-s rotation time, 100 kV (peak), and 180 effective mAs. The source images were reconstructed into 1-mm slice thicknesses in axial view, and coronal and sagittal images were reformatted. All CT images were obtained from the Picture Archiving and Communication System

(PACS) of the authors' University Hospital. A 20-year experienced anatomy professor, 14-year and 7-year experienced anatomy specialists and a 10-year experienced radiology specialist using Osirix Lite v.12.0.1 completed all measurements.

CT image series were set in same anatomical planes using 3-D multiplanar reconstruction (MPR) tool of Osirix Lite software. Distance between tip of nasal bone and the external occipital protuberance was calculated as antero-posterior diameter of the cranium in the midsagittal sections (**Figure 1**). Furthermore, in sagittal sections distances from the distal end of NLD to anterior surface of maxilla were measured bilaterally (**Figure 2**). Antero-posterior and transverse diameters of NLD were measured bilaterally on the axial sections where the inferior orbital margins were detected (**Figure 3**). Angle between

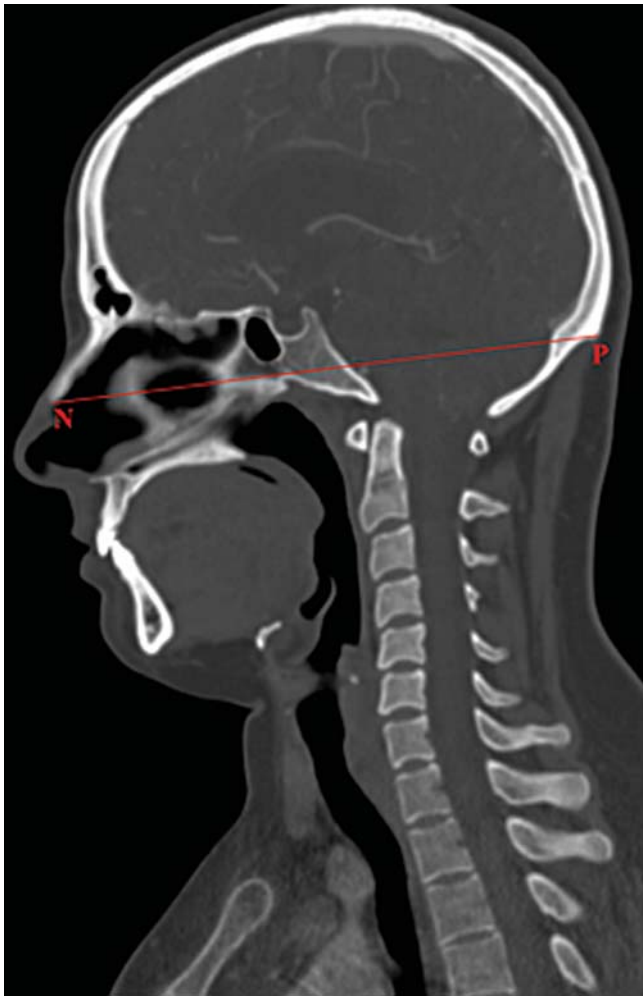


Figure 1. Computed tomography image, midsagittal section. N: tip of the nasal bone; P: external occipital protuberance; red line: distance between tip of nasal bone and external occipital protuberance defining antero-posterior diameter of the cranium.

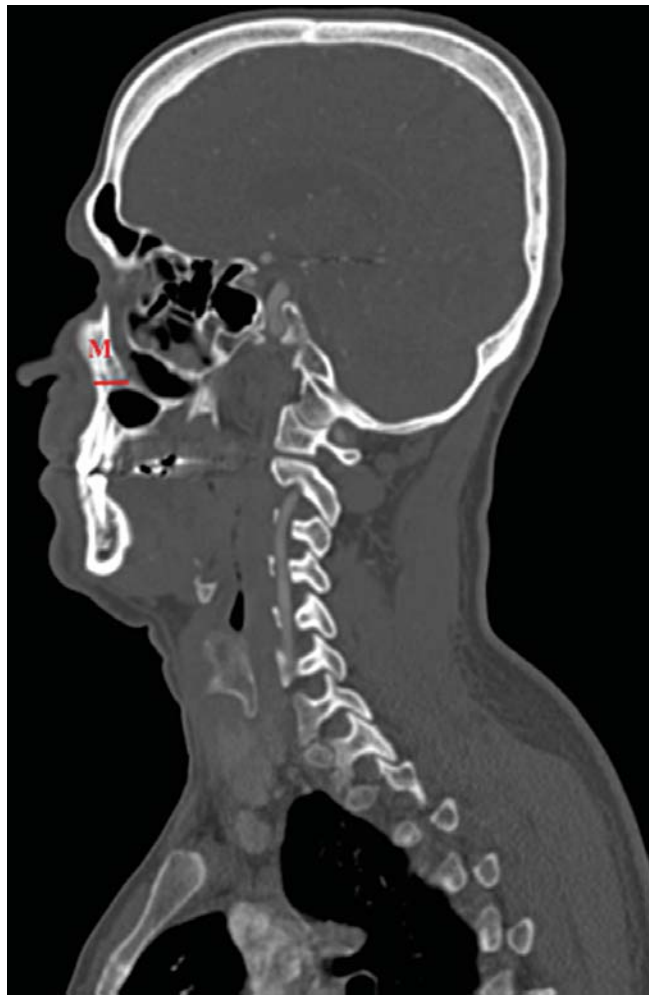


Figure 2. Computed tomography image, sagittal section. M: maxilla; red line: distance between opening of nasolacrimal duct and anterior wall of the maxilla.

proximal and distal ends of the NLD according to vertical axis were also measured bilaterally in sagittal sections.

Statistical analysis were performed using SPSS version 23 (SPSS Inc., Chicago, IL, USA). All morphometric parameters were examined using histograms and probability plots. The Kolmogorov–Smirnov test and the Shapiro–Wilk test used to define normality distribution of the data. Descriptive analyses were used for demonstrating the means and standard deviations of all measurements. The student t-test and the Mann–Whitney U test were utilized for comparison of measured parameters between genders and ages. Paired student's t test and Wilcoxon test was performed for normal and non-normal distributed parameters, respectively to compare measured variables between left and right sides. Pearson test for normally distributed parameters and Spearman's rho test for non-normally distributed parameters were used to investigate associations between parameters with calculating correlation coefficients and their significance at a 5% Type-I error level. Variables with a p value of less than 0.05 were considered statistically significant.

Results

The mean antero-posterior cranium diameter was 17.97 ± 0.07 (range: 15.96–20.15) cm. The narrowest antero-posterior diameter of the NLD was measured as 2.71 mm, while the narrowest transverse diameter of the NLD was 1.99 mm. The angle between the proximal end

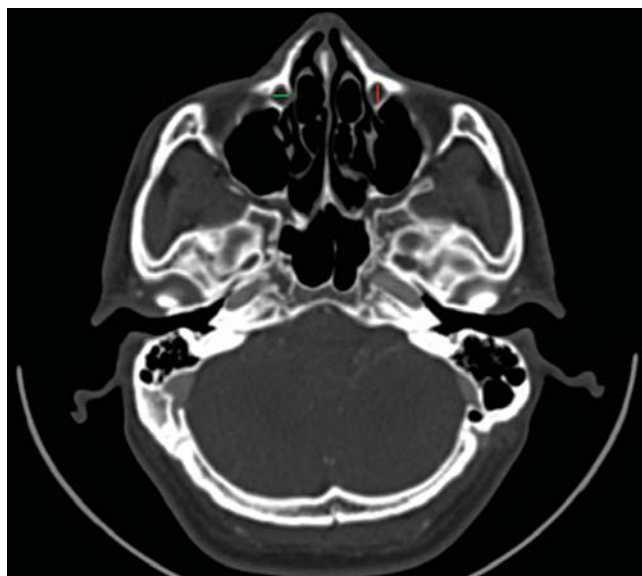


Figure 3. Computed tomography image, axial section. Green line: transverse diameter of the NLD (nasolacrimal duct); red line: antero-posterior diameter of the nasolacrimal duct.

and the distal end of the NLD was 0.87° to 29.14° , varying in a very wide range. Mean values, standard deviations, and minimum-maximum values of all measured parameters were demonstrated in **Table 1**. None of morphometric parameters demonstrated significant difference between right and left sides.

Table 1

Results of the measurements.

Parameters	Sex	Side	Mean \pm SD	Min-max
Antero-posterior diameter of NLD (mm)	F	R	4.67 \pm 0.12	2.83–7.04
		L	4.67 \pm 0.12	2.96–7.51
	M	R	5.09 \pm 0.13	2.71–7.87
		L	4.95 \pm 0.1	2.79–7.29
Transverse diameter of NLD (mm)	F	R	3.81 \pm 0.08	2.43–5.66
		L	3.74 \pm 0.09	1.99–6.43
	M	R	4.2 \pm 0.09	2.03–6.43
		L	4.15 \pm 0.09	2.76–6.34
Angle of NLD (mm)	F	R	13.61 \pm 0.65	5.53–29.14
		L	13.98 \pm 0.61	5.68–27.24
	M	R	12.83 \pm 0.62	0.87–23.92
		L	12.25 \pm 0.59	4.18–27.89
Distance to anterior face of maxilla (cm)	F	R	0.91 \pm 0.02	0.48–1.53
		L	0.89 \pm 0.03	0.33–1.64
	M	R	0.97 \pm 0.03	0.45–1.71
		L	0.97 \pm 0.03	0.35–2.27

F: female; L: left; M: male; NLD: nasolacrimal duct; R: right; SD: standard deviation.

Antero-posterior and transverse diameters of proximal end of NLD had positive and statistically significant correlation with antero-posterior diameter of cranium (right side; antero-posterior diameter, $r=0.226$, $p<0.001$; transverse diameter, $r=0.231$, $p<0.001$). Left side; antero-posterior diameter, $r=0.203$, $p<0.001$; transverse diameter, $r=0.286$, $p<0.001$).

Antero-posterior cranium diameter was longer in men than women ($p<0.001$). Transverse diameters of proximal end of the NLD on both sides were wider in men than women ($p<0.001$). However, the angle between proximal and distal ends of the NLD was wider in women than men ($p=0.02$).

The angle between proximal and distal ends of NLD of the right sides had negative and statistically significant correlation with age ($r=-0.195$, $p=0.02$). Furthermore, distance between distal end of NLD and anterior surface of maxilla on right sides had negative and statistically significant correlation with age, as well ($r=-0.178$, $p=0.03$). The angle between proximal and distal ends of the NLD had negative and statistically significant correlation with age among women ($r=-0.272$, $p=0.02$). In men, the distance between the distal end of the NLD and anterior surface of maxilla on right side had negative and significant correlation with age ($r=-0.305$, $p<0.001$).

Discussion

We evaluated the morphometric properties of the NLD and compared these measured parameters between genders. Furthermore, we investigated the effects of age on these morphometric parameters.

The morphometry of the NLD had been a subject of numerous cadaveric studies.^[4,7,11-14] These studies aimed to evaluate morphometric properties of the NLD in different populations using cadaveric specimens. Computed tomography studies purposed determining the NLD anatomy in different patient groups such as NLD obstructions and craniofacial malformations.^[15-20] A great number of studies focused on the NLD pathologies indicated the importance of anatomical knowledge for increasing quality of surgeries and post-operative period of patients. Besides these clinical studies, there were a few radiologic studies focusing on morphometry of the NLD.^[1,5,6,21] Ela et al.^[6] studied the morphometry of NLD on children, while Czyn et al.^[5] examined the NLD morphometry according to aeration grades in adult participants. However, they could not find any significant differences for morphometric values of the NLD between age and genders. In contrast to their results, our data demonstrated statistically significant differences between gender for antero-posterior diameter of the NLD

in favor of men. Furthermore, our results demonstrated that NLD's vertical angle and distance of the distal end of the NLD to anterior surface of the maxilla on the right side were getting lower with increase in age.

According to our knowledge, there is only one study that evaluated the NLD morphometry according to craniometrical properties.^[22] However, participants included in that study had acquired NLD obstructions, thus, anatomical characteristics may show differences since pathologic condition could affect the other structures. We evaluated the relationship between antero-posterior diameter of cranium and morphometric parameters in healthy adult participants. Our results indicated that only antero-posterior diameter of proximal end of the NLD had significant positive correlation with the antero-posterior cranium diameter.

Craniofacial anomalies, such as thickening of nasal mucosa, septal deviations, hypertrophic concha, immature maxilla, cleft lip/plate could lead nasal airway obstructions. Altun et al.^[15] compared nasolacrimal duct morphometry between patients who had unilateral cleft lip/plate and healthy participants. They revealed that nasolacrimal duct diameters were narrower in craniofacial anomaly patients. However, they did not find any statistical differences in any parameters between gender in both craniofacial anomaly and control groups.^[15] In contrast to their study, our results demonstrated the transverse diameter and vertical angle of the NLD was longer in men. The reason of these differences may be due to the mean age of participants. The main limitation of the study is that it could not be compared with cadaveric evaluation.

Conclusion

In the present study, we evaluated morphometric values of the NLD on healthy adult participants. According to our results, some of the morphometric parameters demonstrated statistically significant differences between genders and age. We suggest that our findings would be helpful to understand the nature of NLD obstructions and to avoid unexpected injuries during surgical approaches.

Conflict of Interest

Authors have no conflict of interest to declare.

Author Contributions

BEG: project development, data analyses, manuscript writing; AV: project development, data collection, data analyses, manuscript writing; DD: project development, data analyses, manuscript editing; EG: data collection, data analyses, manuscript writing.

Ethics Approval

Ethics approval for this study was obtained from Institutional Ethical Board (Decree No: 2020/20-16).

Funding

This research did not receive any specific grant from funding agencies in the public, commercial, or not-for-profit sectors.

References

- Lee S, Lee UY, Yang SW, Lee WJ, Kim DH, Youn KH, Kim YS. 3D morphological classification of the nasolacrimal duct: anatomical study for planning treatment of tear drainage obstruction. *Clin Anat* 2021;34:624–33.
- Heichel J, Struck HG, Viestenz A, Hammer T, Viestenz A, Fiorentzis M. Anatomic landmarks in lacrimal surgery from an ophthalmologist's point of view: clinical findings of external dacryocystorhinostomy and dacryoendoscopy. *Clin Anat* 2017;30:1034–42.
- Narioka J, Matsuda S, Ohashi Y. Correlation between anthropometric facial features and characteristics of nasolacrimal drainage system in connection to false passage. *Clin Exp Ophthalmol* 2007;35:651–6.
- Valencia MRP, Takahashi Y, Naito M, Nakano T, Ikeda H, Kakizaki H. Lacrimal drainage anatomy in the Japanese population. *Ann Anat* 2019;223:90–9.
- Czyz CN, Bacon TS, Stacey AW, Cahill EN, Costin BR, Karanfilov BI, Cahill KV. Nasolacrimal system aeration on computed tomographic imaging: sex and age variation. *Ophthalmic Plast Reconstr Surg* 2016;32:11–6.
- Ela AS, Cigdem KE, Karagoz Y, Yigit O, Longur ES. Morphometric measurements of bony nasolacrimal canal in children. *J Craniofac Surg* 2018;29:e282–7.
- Takahashi Y, Nakamura Y, Nakano T, Asamoto K, Iwaki M, Selva D, Leibovitch I, Kakizaki H. The narrowest part of the bony nasolacrimal canal: an anatomical study. *Ophthalmic Plast Reconstr Surg* 2013;29:318–22.
- Okumus O. Investigation of the morphometric features of bony nasolacrimal canal: a cone beam computed tomography study. *Folia Morphol (Warsz)* 2020;79:588–93.
- Shigeta K, Takegoshi H, Kikuchi S. Sex and age differences in the bony nasolacrimal canal: an anatomical study. *Arch Ophthalmol* 2007;125:1677–81.
- Avdagic E, Phelps PO. Nasolacrimal duct obstruction as an important cause of epiphora. *Dis Mon* 2020;66:101043.
- Ali MJ, Schicht M, Paulsen F. Morphology and morphometry of lacrimal drainage system in relation to bony landmarks in caucasian adults: a cadaveric study. *Int Ophthalmol* 2018;38:2463–9.
- Elshaarawy EA. Morphological and morphometrical study of the nasal opening of nasolacrimal duct in man. *Folia Morphol (Warsz)* 2014;73:321–30.
- Takahashi Y, Kakizaki H, Nakano T. Bony nasolacrimal duct entrance diameter: gender difference in cadaveric study. *Ophthal Plast Recons* 2011;27:204–5.
- Park J, Takahashi Y, Nakano T, Asamoto K, Iwaki M, Selva D, Leibovitch I, Yang SW, Kakizaki H. The orientation of the lacrimal fossa to the bony nasolacrimal canal: an anatomical study. *Ophthalmic Plast Reconstr Surg* 2012;28:463–6.
- Altun O, Dedeoglu N, Avci M. Examination of nasolacrimal duct morphometry using cone beam computed tomography in patients with unilateral cleft lip/palate. *J Craniofac Surg* 2017;28:e725–8.
- Bulbul E, Yazici A, Yanik B, Yazici H, Demirpolat G. Morphometric evaluation of bony nasolacrimal canal in a caucasian population with primary acquired nasolacrimal duct obstruction: a multidetector computed tomography study. *Korean J Radiol* 2016;17:271–6.
- Takahashi Y, Nakata K, Miyazaki H, Ichinose A, Kakizaki H. Comparison of bony nasolacrimal canal narrowing with or without primary acquired nasolacrimal duct obstruction in a Japanese population. *Ophthal Plast Recons* 2014;30:434–8.
- Park JH, Huh JA, Piao JF, Lee H, Baek SH. Measuring nasolacrimal duct volume using computed tomography images in nasolacrimal duct obstruction patients in Korean. *Int J Ophthalmol* 2019;12:100–5.
- Choi SC, Lee S, Choi HS, Jang JW, Kim SJ, Lee JH. Preoperative computed tomography findings for patients with nasolacrimal duct obstruction or stenosis. *Korean J Ophthalmol* 2016;30:243–50.
- Zhang C, Yu G, Cui Y, Wu Q, Wei W. Anatomical characterization of the nasolacrimal canal based on computed tomography in children with complex congenital nasolacrimal duct obstruction. *J Pediatr Ophthalmol Strabismus* 2017;54:238–43.
- Lin Z, Kamath N, Malik A. High-resolution computed tomography assessment of bony nasolacrimal parameters: variations due to age, sex, and facial features. *Orbit* 2020;16:1–6.
- Lee JS, Lee H, Kim JW, Chang M, Park M, Baek S. Association of facial asymmetry and nasal septal deviation in acquired nasolacrimal duct obstruction in East Asians. *J Craniofac Surg* 2013;24:1544–8.

ORCID ID:

B. Erçakmak Güneş 0000-0001-6936-0766;
A. Vatansver 0000-0002-3632-1020;
D. Demiryürek 0000-0001-8781-1719;
E. Gümeleler 0000-0003-3783-2372



Correspondence to:

Burcu Erçakmak Güneş, MD
Department of Anatomy, Faculty of Medicine, Hacettepe University,
Ankara, Turkey
Phone: +90 532 493 00 05
e-mail: burcue@hacettepe.edu.tr

Conflict of interest statement: No conflicts declared.

This is an open access article distributed under the terms of the Creative Commons Attribution-NonCommercial-NoDerivs 4.0 Unported (CC BY-NC-ND4.0) Licence (<http://creativecommons.org/licenses/by-nc-nd/4.0/>) which permits unrestricted noncommercial use, distribution, and reproduction in any medium, provided the original work is properly cited. *How to cite this article:* Erçakmak Güneş B, Vatansver A, Demiryürek D, Gümeleler E. Morphometric evaluation of nasolacrimal duct. *Anatomy* 2021;15(1):64–68.

The contribution of plastinates to teaching complex anatomy of the heart

Güneş Aytaç^{1,2} , Eren Öğüt³ , Rahime Şekerci⁴ , Sezgi Gürçay⁵ , Nurettin Oğuz⁴ ,
Muzaffer Sindel⁴ 

¹Department of Anatomy, School of Medicine, TOBB University of Economics and Technology, Ankara, Turkey

²Department of Anatomy, Biochemistry & Physiology, John A. Burns School of Medicine, University of Hawai'i at Mānoa, Hawaii, USA

³Department of Anatomy, School of Medicine, Bahçeşehir University, İstanbul, Turkey

⁴Department of Anatomy, School of Medicine, Akdeniz University, Antalya, Turkey

⁵Department of Anatomy, School of Medicine, Mustafa Kemal University, Hatay, Turkey

Abstract

Objectives: The use of plastination can minimize health risks and cost in anatomy laboratories. Plastinates are easy to handle and can facilitate the learning of complex anatomical structures. Therefore, we aimed to evaluate the contribution of plastinates to teaching complex anatomy of the heart.

Methods: Standard S10 technique was used for heart plastination by fixation, dehydration, impregnation and curing stages. Ninety volunteer first-year medicine students at Akdeniz University, who did not take cardiovascular system anatomy lectures yet, were included. Formalin-fixed heart specimens were used in the lecture of group 1; both formalin-fixed heart specimens and heart plastinates were used in the lecture of group 2. After the lecture, a 10-question exam was administered. Statistical significance between the scores of the two groups was tested with one sample t-test, and post hoc Tukey test was used for multiple comparisons.

Results: The pre-test scores of the groups were compared with the scores obtained after the 2 hours of lecture ($p=0.002$, $p<0.05$). The test scores of both groups increased significantly after the lecture ($p<0.05$). The post-test scores of group 2 were significantly higher than group 1 ($p=0.047$, $p<0.05$). The average test scores of those trained with formalin-fixed specimens increased from 23.78 ± 1.94 to 48.22 ± 3.19 ($p<0.05$). Students gave positive feedback about heart plastinates, and they stated that their rising interest in the anatomy lecture due to the odourless, disinfected and reusable materials.

Conclusion: In conclusion, besides being cost-effective, healthy, long lasting and easy to maintain materials, plastinates are useful tools to teach complex anatomical structures.

Keywords: anatomy; COVID-19; medical education; plastinate; plastination

Anatomy 2021;15(1):69–75 ©2021 Turkish Society of Anatomy and Clinical Anatomy (TSACA)

Introduction

Anatomy as one of the basic medical sciences is fundamental for medical training. In particular, anatomy is necessary for surgical disciplines that the spatial relationships of the structures with one another should be very well known. The basic teaching tools used for teaching anatomy are cadavers, anatomical models, written materials (such as books, atlases, posters), video images and computer programs.^[1] Cadavers have been essential for

physicians to have a through understanding of the human morphology and have played a crucial role in medical education. Dissections of the cadavers provide an excellent opportunity to recognize the three-dimensional structure of the body.^[2] However, some issues make difficult to study with cadavers such as scarcity of cadavers, decreased cadaver donations, and increased number of students.^[3-5] Anatomical models are another commonly used anatomy education material. However,

This study was a poster presentation at 20th National Anatomy Congress, 27th–31st August 2019, İstanbul, Turkey.

anatomical models are not show the variations and they are expensive because of importation. Two-dimensional educational materials such as textbooks, drawings and digital images, may be of limited benefit in understanding the three-dimensional complexity of the anatomy and spatial relationships of the structures.^[1]

Another important issue to highlight is that, although anatomy is essential for diagnosis and treatment, medical school students graduate with inadequate anatomy knowledge.^[6] Various studies evaluating the adequacy of anatomy education have shown that anatomy knowledge of medical graduates is deficient.^[3,4,7] Therefore, it has become compulsory to search effective alternative or supportive tools for teaching anatomy.^[8-10] In the last two decades there has been a growing interest in plastination techniques. Plastination is a great method for long-term preservation of anatomical specimens. With plastination, it is possible to protect the anatomical materials in a durable, aesthetic and realistic manner. In this technique, curable polymers in a special vacuum process replace tissue fluids. The specimens are dry and odorless after this process. Moreover, plastinates can be manipulated without personal protective equipment.^[11] Although plastination could not be replaced by traditional cadaver training, it is an important auxiliary method ensures that the materials remain intact for a long time. Plastinates provide a learning tool that converts two-dimensional textbook images into three-dimensional model.^[5,12,13] Therefore, plastinated specimens are valuable in teaching anatomy.^[10,14,15] Beyond the educational benefits, plastination stops the reactions inside the body and prevents the degradation and dehydration of the materials. In this way, plastinates remain intact much longer than formalin fixed cadavers do. These materials do not deteriorate over time and save dissection hours.

Another important issue is the risk of transmitting SARS-CoV-2, the virus causing COVID-19, from dead bodies is not yet known.^[16] People should be notified not to touch the body if it was recognised or presumed that the deceased was infected with COVID-19; it is not yet understood how long the virus will remain on human tissue and dead bodies. As with other infectious diseases, the cause of death should be communicated to all those who will be handling the body via the medical certificate of death. Equipment and material cleaning, as well as individual hygiene, are essential parts of safety during the pandemic.^[17] Therefore disinfected and sanitised plastinates are alternative options for the anatomical education during the COVID-19 pandemic period when considering their hygienic properties.

One of the most difficult organs for students to understand is the human heart with its complex physiol-

ogy and detailed anatomy. Knowledge of the basic anatomy and physiology of the heart is essential. It is very difficult in formalin fixed specimens to show the detailed anatomy of the heart valves without damaging the structures.^[18] Therefore, in this study, we aimed to investigate if the heart plastinates contribute to anatomy education of the under graduate medical students.

Materials and Methods

Standard S10 technique, which was previously defined in the literature, was used for plastination. Fresh sheep hearts were plastinated by fixation, dehydration, impregnation and curing stages.^[18] Heart specimens have gained light and flexible structure after plastination process and become dry, odourless and resistant to deterioration (**Figure 1**). Structures including chordae tendinea, papillary muscles, right and left atrioventricular orifice, bicuspid (mitral) and tricuspid valves, pulmonary veins, aortae, coronary vessels, and their relations with each other were described in heart plastinates in details (**Figures 1 and 2**).

Ninety volunteer first-year students in the School of Medicine (Akdeniz University), who did not take cardiovascular system anatomy lectures yet, were included in the study. This study was conducted in accordance with the Helsinki Declaration. All protocols were approved by the Clinical Research Ethics Committee of Akdeniz University (Number: 70904504-98). Furthermore, written informed consent was obtained from the students.

A pre-test consisting of ten questions was applied to the students in order to determine their knowledge about cardiac anatomy, and then they divided into two equal groups according to pre-test results. Thus, there was no significant difference between the two groups' knowledge levels. Both groups were given a 2-hour identical lecture regarding the anatomy of the heart by the same instructor. Formalin-fixed heart specimens were used in the lecture of group 1. Formalin-fixed heart specimens and plastinated hearts were used in the lecture of group 2. After the lecture, a 10-question exam was administered to both groups. In this exam, open-ended and multiple-choice questions were prepared in order to test the student's knowledge levels. In this test, questions including atrial and ventricular structures, heart valves, and heart vessels were asked to students. The same anatomy instructor who was blinded to the study evaluated test scores.

The data were analyzed with SPSS (Version 25.0, Armonk; NY, USA). Descriptive statistics of continuous variables, such as test scores of the students, were given with mean, standard deviation, minimum and maximum

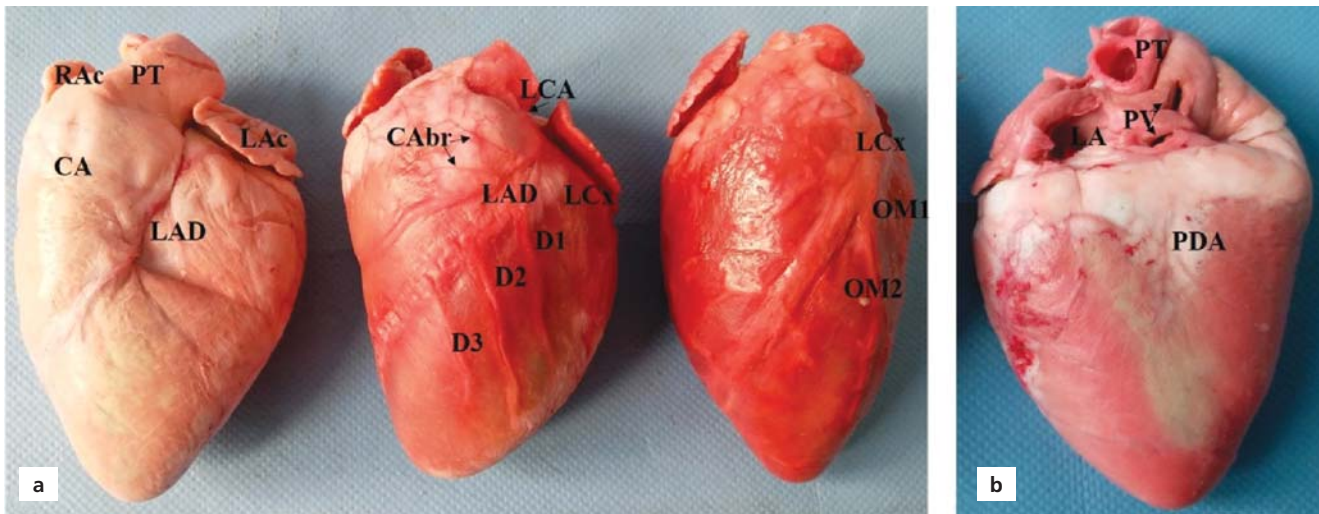


Figure 1. External aspects of the plastinated heart. (a) Anterior long-axis view. (b) Posterior view. CA: conus arteriosus; CABr: branches for conus arteriosus; D: diagonal branches; LA: left atrium; LAc: left auricle; LAD: left descending artery, LCA: left coronary artery; LCx: left circumflex artery; OM: obtuse marginal artery; PDA: posterior descending artery; PT: pulmoner trunk; PV: pulmoner vein; RAc: right auricle.

values, and frequency and percent for categorical variables. The Shapiro-Wilk test was used as a test of normality. The independent samples t-test was used for two independent group comparisons of normally distributed variables, and the Mann-Whitney U test was used for non-normal distributed variables. Statistical significance between the scores of the two groups was tested with one sample paired t-test, and post hoc Tukey test was used for multiple comparisons. A p-value <0.05 was considered significant.

Results

The Kirkpatrick Model was used in the current study for analyzing and evaluating the results of lectures with plastinates. The evaluation model consists of four parts: reaction (level 1), learning (level 2), behavior or transfer (level 3), and results (level 4).^[19] All of the students indicated their feelings about the plastinates (level 1), and their behavior changed because of attending a lecture with plastinates. In level 2, pre-tests and post-tests were conducted to the students to measure the proper amount

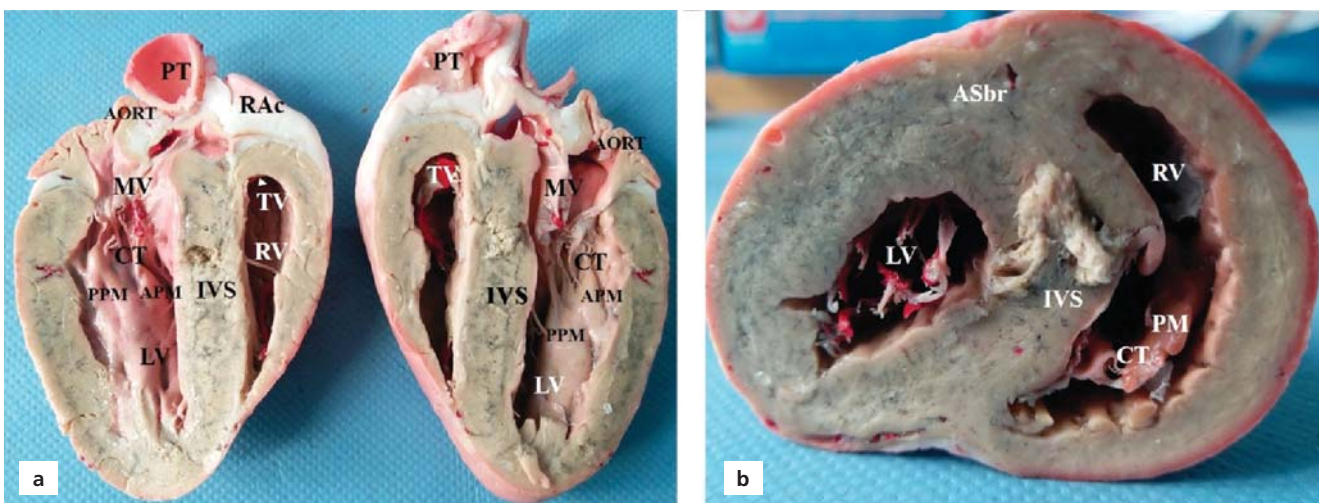


Figure 2. Internal aspect of the plastinated heart. (a) Longitudinal incision. (b) Transverse incision. APM: anterior papillary muscle; ASbr: anterior septal branches; CT: chorda tendinea; IVS: interventricular septum; LV: left ventricle; MV: mitral valve; PPM: posterior papillary muscle; PM: papillary muscle; PT: pulmonary trunk; RAc: right auricle; RV: right ventricle; TV: tricuspid valve.

of learning that has taken place. This level gives students and us for the advancement of knowledge, skills, and attitudes based on their participation. The evaluation by Kirkpatrick's model showed that the use of plastinates in anatomy education improved the learning outcome of medical students, their level of satisfaction and the quality of anatomy education. The implications of the plastinates for anatomy education can add to the appeal and

effectiveness of medical education, and that triggers active learning.

The mean values of group 1 post-test scores were 48.22 ± 3.19 , and the mean value of group 2 was 56.89 ± 3.52 (Table 1). The post-test scores of group 2 were significantly higher than group 1 ($p=0.047$, $p<0.05$). The test scores of the group that received lectures with both formalin-fixed specimens and plastinates were sig-

Table 1
Pre-test and post-test scores of the groups.

		Descriptives	Statistic	SE
Pre-test	Group 1	Mean	23.78	1.941
		95% CI for mean	Lower bound	19.87
			Upper bound	27.69
		5% trimmed mean	23.58	
		Median	20.00	
		Variance	169.495	
		SD	13.019	
		Minimum	0	
		Maximum	50	
		Range	50	
	Interquartile range	20		
	Skewness	.216	.354	
	Kurtosis	-.623	.695	
	Group 2	Mean	15.56	1.922
		95% CI for mean	Lower bound	11.68
			Upper bound	19.43
		5% trimmed mean	14.57	
		Median	10.00	
		Variance	166.162	
		SD	12.890	
Minimum		0		
Maximum		60		
Range		60		
Interquartile range	10			
Skewness	1.171	.354		
Kurtosis	1.889	.695		
Post-test	Group 1	Mean	48.22	3.199
		95% CI for mean	Lower bound	41.78
			Upper bound	54.67
		5% trimmed mean	47.96	
		Median	40.00	
		Variance	460.404	
		SD	21.457	
		Minimum	10	
		Maximum	90	
		Range	80	
	Interquartile range	35		
	Skewness	.444	.354	
	Kurtosis	-.462	.695	
	Group 2	Mean	56.89	3.522
		95% CI for mean	Lower bound	49.79
			Upper bound	63.99
		5% trimmed mean	57.59	
		Median	60.00	
		Variance	558.283	
		SD	23.628	
Minimum		10		
Maximum		90		
Range		80		
Interquartile range	30			
Skewness	-.313	.354		
Kurtosis	-.689	.695		

CI: confidence interval; SD: standard deviation; SE: standard error.

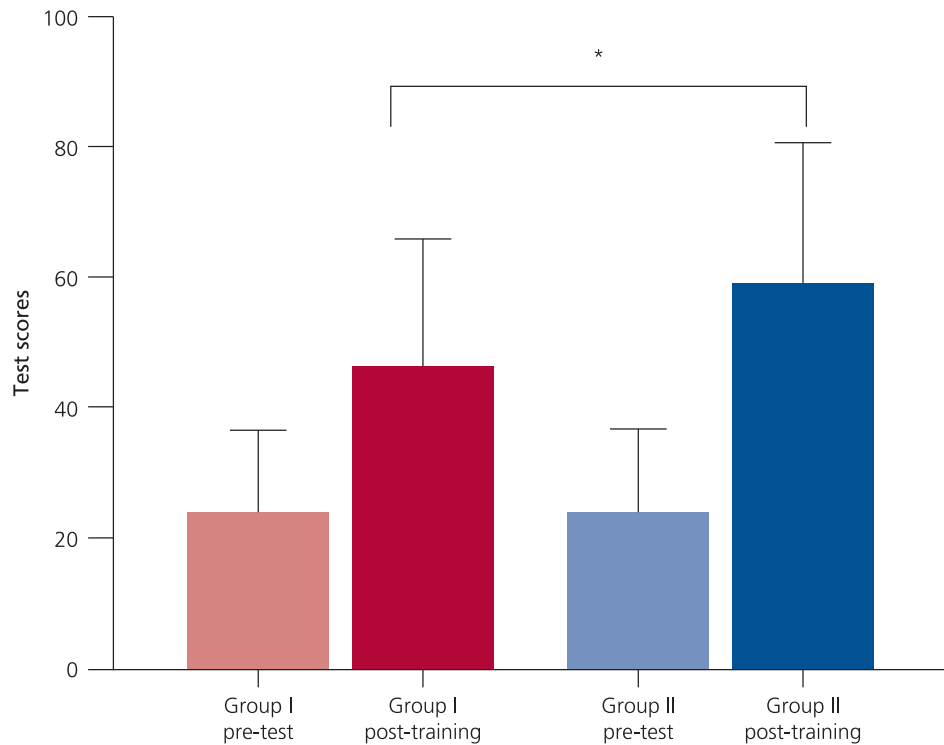


Figure 3. Differences between the groups related to the test scores. Graphs shows pre-test and post-training scores. Group II post-training scores were significantly higher than the group I post-training scores (* $p < 0.05$). The scores of those trained with formalin-fixed specimens and plastinates increased significantly more than the other group ($p = 0.0294$) (One sample paired t test).

nificantly higher than those of the group that received lectures with the only formalin-fixed specimen. The pre-test scores of the groups were compared with the scores obtained after the 2 hours lecture ($p = 0.002$, $p < 0.05$) (Table 2). It was observed that the test scores of both groups increased significantly after the lecture ($p = 0.047$, $p < 0.05$) (Table 2). The average test scores of those trained with formalin-fixed specimens increased from 23.78 ± 1.94 to 48.22 ± 3.19 ($p < 0.05$). The average test scores of those trained with both formalin-fixed specimen and plastinates increased from 15.56 ± 1.92 to 56.89 ± 3.52 ($p < 0.05$) (Figure 3).

Table 2

The comparison between the groups via test scores.

	Test statistics*	
	Pre test	Post test
Mann-Whitney U	642.000	769.000
Wilcoxon W	1677.000	1804.000
Z	-3.087	-1.983
Asymp. sig. (2-tailed)	.002	.047

*Grouping variable: Mann-Whitney U.

Discussion

Plastination has been the focus of many studies for the last two decades. Some of these studies were related to plastination techniques,^[11,12,20] and some of them were related to the importance of plastination in anatomy education.^[10,13-15,21] Our study is the first study so far that evaluate if the heart plastinates contribute to anatomy education of the students. Many anatomists prefer plastinates to formalin-fixed cadavers because they are odorless, durable, effortless and easy to handling.^[13,14,21] Musumeci et al.^[22] indicated that plastination is a good tool for dissection and a complementary educational technique that shows different aspects of human anatomy. Riederer stated that plastinates provide a 3-dimensional vision for complex anatomical areas, and a very useful tool for pre- and post-graduate training.^[10] Our data showed that education with formalin-fixed cadavers increased students test scores, but the addition of plastinates to the education was significantly increased the success rate. These results indicate that plastinates are useful for teaching the anatomy of the heart, which is a very complex region for the undergraduate medical students.

With its complex anatomy and unique function, the heart has been the subject of various plastination studies

over the years.^[18,23-25] In the 1980s, the researchers explored how to optimize heart plastinates and to protect the heart's fine structures by plastination.^[18,23] Since then, the importance, usefulness and benefits of plastinates have been studied.^[24,25] Raoof et al.^[25] have performed plastination to demonstrate the function of cardiac valves during systolic and diastolic phases in their study. In this study, a pilot questionnaire was applied to get opinions of the students about plastinates. The results of the survey have shown that most of the students thought heart plastinates are beneficial in terms of demonstrating structural anatomical relationships, learning the anatomy of the heart, understanding function-structure correlation.^[25] Since the questionnaire in this study was consisted of only three yes/no type questions, it may not reflect the exact views of the students. However, our study has perceptibly shown that plastinates make easier to learn the anatomy of the heart.

Gomez et al.^[24] have compared heart plastinates and echocardiography images and indicated that plastinated slices were corresponded accurately with the echocardiographic images. They stated that their research could be a reference atlas for assisting 2D echocardiography interpretation.^[24]

Plastinates are long lasting, odorless, easy to use, non-toxic and non irritating materials, and these beneficial features have been mentioned in various studies.^[13,14,21,26-28] In our study, besides the increase of success levels, students gave positive feedback about plastinates. They stated that their interest in the lecture increased because plastinates were odorless and easy to handle.

The use of the human body as a cadaver in medical education is a crucial part of anatomy education.^[29] When considered in terms of health, formalin could cause eye and skin irritations, degeneration of the mucous membranes, nasopharynx and nasal cavity tumors.^[30] Another important issue is the high cost of importing the cadavers of certified donors. In Turkey, body donation is very rare due to cultural structure and majority of the universities are failed to meet the cadaver needs for anatomy training. This problem may common in many countries that have similar culture with Turkey.

COVID-19 outbreak has had serious implications on medical education. In many universities, laboratory lectures are planned to be held in small groups. The transmission risk of SARS-CoV-2 from cadavers is not known yet.^[16] Equipment and material cleaning, as well as individual hygiene, are essential parts of safety during the pandemic.^[17] Therefore disinfected and sanitised plastinates could be a good option for the anatomical education during the COVID-19 pandemic when considering their hygienic properties.

Despite all their negative features, formalin fixed cadavers are indispensable for anatomy education. However, it can be beneficial in many ways using plastinates during anatomy education. In their study among medical educators in the USA, Klaus et al.^[26] investigated the use and perception of plastination. According to this study results, 100% of the educators had heard of plastination, 57% of them correctly defined plastination, and 39% of them currently utilize plastinates for anatomy education. This study indicated plastinates are used higher than mentioned in the literature in the U.S., but medical anatomy educators perceived plastination as a useful tool, but not a replacement for cadavers.^[26]

The large scale studies need to investigate the effects of plastinate in anatomy education. Further studies can be supported by plastinates obtained from different regions of the body to improve the quality of anatomy education. The combined evaluation methods can be used to assess the quality of anatomy education with plastinates, or it can be compared using the same techniques for medical students in various schools, regions, or countries.

Conclusion

Findings of this study with undergraduate first-year medical students at Akdeniz University of School of medicine contributed auxiliary grounds in support of credibility of the plastinated specimens in medical education system. In conclusion, besides being cost-effective, healthy, long lasting and easy to maintain materials, plastinates are useful tools in anatomy education.

Conflict of Interest

Authors have no conflict of interest to declare.

Author Contributions

NO, MS and GA: conceived and planned the experiments; GA, EÖ, RŞ and SG: carried out the experiments; GA and EÖ: contributed to figures and preparation of tables. GA and EÖ: writing the manuscript. All authors contributed to the interpretation of the results, provided critical feedback and helped organizing the research, analysis and manuscript.

Ethics Approval

The authors certify that the study was performed in accordance with the ethical standards as laid down in the 1964 Declaration of Helsinki and its later amendments. All protocols were approved by the Clinical Research Ethics Committee of Akdeniz University (Number: 70904504-98).

Funding

The study was funded by the Akdeniz University Scientific Research Projects Coordination Unit, Antalya, TURKEY (Project number: TSA-2015-710).

References

1. Yammine K, Violato C. The effectiveness of physical models in teaching anatomy: a meta-analysis of comparative studies. *Adv Health Sci Educ Theory Pract* 2016;21:883–95.
2. Wilson AB, Miller CH, Klein BA, Taylor MA, Goodwin M, Boyle EK, Brown K, Hoppe C, Lazarus M. A meta-analysis of anatomy laboratory pedagogies. *Clin Anat* 2018;31:122–33.
3. Cottam WW. Adequacy of medical school gross anatomy education as perceived by certain postgraduate residency programs and anatomy course directors. *Clin Anat* 1999;12:55–65.
4. Fitzgerald JE, White MJ, Tang SW, Maxwell-Armstrong CA, James DK. Are we teaching sufficient anatomy at medical school? The opinions of newly qualified doctors. *Clin Anat* 2008;21:718–24.
5. Papa V, Vaccarezza M. Teaching anatomy in the XXI century: new aspects and pitfalls. *ScientificWorldJournal* 2013;2013:310348.
6. Yammine K, Violato C. A meta-analysis of the educational effectiveness of three-dimensional visualization technologies in teaching anatomy. *Anat Sci Educ* 2015;8:525–38.
7. Bhangu A, Boutefnouchet T, Yong X, Abrahams P, Joplin R. A three-year prospective longitudinal cohort study of medical students' attitudes toward anatomy teaching and their career aspirations. *Anat Sci Educ* 2010;3:184–90.
8. Collins JP. Modern approaches to teaching and learning anatomy. *BMJ* 2008;337:a1310.
9. Estai M, Bunt S. Best teaching practices in anatomy education: a critical review. *Ann Anat* 2016;208:151–7.
10. Riederer BM. Plastination and its importance in teaching anatomy. Critical points for long-term preservation of human tissue. *J Anat* 2014;224:309–15.
11. Ottone NE, Cirigliano V, Bianchi HF, Medan CD, Algieri RD, Borges Brum G, Fuentes R. New contributions to the development of a plastination technique at room temperature with silicone. *Anat Sci Int* 2015;90:126–35.
12. Neha, Lalwani S, Dhingra R. Plastinated knee specimens: a novel educational tool. *J Clin Diagn Res* 2013;7:1–5.
13. O'Sullivan E, Mitchell BS. Plastination for gross anatomy teaching using low cost equipment. *Surg Radiol Anat* 1995;17:277–81.
14. Latorre R, Bainbridge D, Tavernor A, Lopez Alborn O. Plastination in anatomy learning: an experience at Cambridge University. *J Vet Med Educ* 2016;43:226–34.
15. Ravi SB, Bhat VM. Plastination: A novel, innovative teaching adjunct in oral pathology. *J Oral Maxillofac Pathol* 2011;15:133–7.
16. Kampf G, Todt D, Pfander S, Steinmann E. Persistence of coronaviruses on inanimate surfaces and their inactivation with biocidal agents. *J Hosp Infect* 2020;104:246–51.
17. WHO Team. Infection prevention and control for the safe management of a dead body in the context of COVID-19. Interim guidance 2020;WHO/2019-nCoV/IPC_DBMgmt/2020.1. CC BY-NC-SA 3.0 IGO, WHO Global. p. 6.
18. Tiedemann K, von Hagens G. The technique of heart plastination. *Anat Rec* 1982;204:295–9.
19. Dorri S, Farahani MA, Maserat E, Haghani H. Effect of role-playing on learning outcome of nursing students based on the Kirkpatrick evaluation model. *J Educ Health Promot* 2019;8:197.
20. Arnts H, Kleinnijenhuis M, Kooloos JG, Schepens-Franke AN, van Cappellen van Walsum AM. Combining fiber dissection, plastination, and tractography for neuroanatomical education: revealing the cerebellar nuclei and their white matter connections. *Anat Sci Educ* 2014;7:47–55.
21. Latorre RM, Garcia-Sanz MP, Moreno M, Hernandez F, Gil F, Lopez O, Ayala MD, Ramirez G, Vazquez JM, Arencibia A, Henry RW. How useful is plastination in learning anatomy? *J Vet Med Educ* 2007;34:172–6.
22. Musumeci E, Lang FJW, Duvoisin B, Riederer BM. Plastinated ethmoidal region: I. Preparation and applications in clinical teaching. *Journal of the International Society for Plastination* 2003;18:23–8.
23. Baptista CAC, Conran PB. Plastination of the heart: preparation for the study of the cardiac valves. *Journal of the International Society for Plastination* 1989;3:3–7.
24. Gomez A, Del Palacio JF, Latorre R, Henry RW, Sarria R, Alborn OL. Plastinated heart slices aid echocardiographic interpretation in the dog. *Vet Radiol Ultrasound* 2012;53:197–203.
25. Raoof A, Marchese L, Marchese A, Wischmeyer A. Demonstration of systolic and diastolic phases of the cardiac cycle in a plastinated human heart. *The Journal of Plastination* 2013;25:18–21.
26. Klaus RM, Royer DF, Stabio ME. Use and perceptions of plastination among medical anatomy educators in the United States. *Clin Anat* 2018;31:282–92.
27. Chaturvedi RK, Singh A, Chaturvedi P, Mishra A, Mishra SP. Advantages of plastinated human body in medical education and its legal & ethical aspects. *Journal of Evolution of Medical and Dental Sciences* 2014;3:2626–31.
28. Sivrev DP, Usovich A. Using of plastinated anatomical preparations in preclinical and clinical education of medical students. *Acta Morphologica et Anthropologica* 2012;19:211–19.
29. Riederer BM. Body donations today and tomorrow: what is best practice and why? *Clin Anat* 2016;29:11–8.
30. Tanaka K, Nishiyama K, Yaginuma H, Sasaki A, Maeda T, Kaneko SY, Onami T, Tanaka M. Formaldehyde exposure levels and exposure control measures during an anatomy dissecting course [Article in Japanese]. *Kaibogaku Zasshi* 2003;78:43–51.

ORCID ID:

G. Aytac 0000-0003-4902-2844; E. Ögüt 0000-0003-2506-9883; R. Şekerci 0000-0002-3253-1186; S. Gürçay 0000-0002-9061-676X; N. Oğuz 0000-0001-6864-8872; M. Sindel 0000-0002-6594-1325



Correspondence to: Muzaffer Sindel, MD, PhD, Prof
Department of Anatomy, School of Medicine, Akdeniz University,
07070, Antalya, Turkey
Phone: +90 532 562 09 00
e-mail: sindelm@akdeniz.edu.tr

Conflict of interest statement: No conflicts declared.

This is an open access article distributed under the terms of the Creative Commons Attribution-NonCommercial-NoDerivs 4.0 Unported (CC BY-NC-ND4.0) Licence (<http://creativecommons.org/licenses/by-nc-nd/4.0/>) which permits unrestricted noncommercial use, distribution, and reproduction in any medium, provided the original work is properly cited. *How to cite this article:* Aytac G, Ögüt E, Şekerci, R Gürçay S, Oğuz N, Sindel M. The contribution of plastinates to teaching complex anatomy of the heart. *Anatomy* 2021;15(1):69–75.

Lungs and hypoxia: a review of the literature

Mustafa F. Sargon 

Department of Anatomy, Faculty of Medicine, Lokman Hekim University, Ankara, Turkey

Abstract

Acute, intermittent or chronic hypoxia have negative effects on lung maturation during the embryological period which has been shown by many experimental models designed on animal studies. The receptors responsible from the development of lungs in fetal period are affected from hypoxia. Hypoxia also affects the morphometry, anatomy and microscopy of lung tissue in the adults. In acute phase of hypoxia; lung parenchyma showed destructive oxidative changes. However, in later phases repair and proliferative processes were observed in the lung tissue. Damage to the lining layer of alveoli, accumulation of alveolar macrophages, oedematous changes in the lung parenchyma, mild oedema, inflammatory cell infiltration, increased number of type II pneumocytes and pulmonary fibrosis are the main findings in cases of hypoxia. Chronic hypoxia accentuates lung growth by increasing the lung parenchyma. Decrease of capillary volume and suppression of elastin repair in lung fibroblasts are other clinically important microscopic findings in hypoxia. Many molecular studies found in the literature revealed micro-RNAs to be involved in modulation of hypoxia-induced pulmonary hypertension. In animal models submitted to acute hypobaric hypoxia; the researchers detected an increase in eNOS mRNA which is responsible of the immediate response, producing nitric oxide that caused vasodilation and bronchodilation in lung tissue. In other molecular studies; suppression of many immune molecules, major changes at the levels of various enzymes and growth factors were detected in the researches. Additionally; hypoxia causes to an increase in the amount of lung cancer cells and therefore; induces the metastases of lung cancer cells to brain tissues.

Keywords: cancer; gross anatomy; hypoxia; lung; microscopy; molecular study

Anatomy 2021;15(1):76–83 ©2021 Turkish Society of Anatomy and Clinical Anatomy (TSACA)

Introduction

Hypoxia describes the inability while using oxygen or it is the case of oxygen deficiency in tissues. Hypoxia itself is not a respiratory disease, but is often a consequence of respiratory diseases. According to its cause; hypoxia is classified in four groups; hypoxemic hypoxia, ischemic hypoxia, anemic hypoxia and histotoxic hypoxia. In hypoxemic hypoxia; the arterial PO₂ is low and it is due to inadequate pulmonary gas exchange in most of the cases. The major causes of hypoxemic hypoxia are respiratory arrest, degenerative lung diseases, atmospheric deficiency of oxygen at high elevations and impaired ventilation. Inadequate circulation of the blood is the cause of ischemic hypoxia. Congestive heart failure is a good example to this condition. Anemic hypoxia occurs in cases of anemia and in this situation; the blood cannot carry adequate amounts of oxygen for the body. If a metabolic poison prevents the usage of oxygen by a tissue; histotoxic hypoxia occurs in these cases.^[1]

Approximately 480 million alveoli are found in the human lungs. 64% of total lung structure is formed by these alveoli. Alveoli provide a surface area of 120–150 m² dedicated for gas exchange. The oxygen diffusion constant and gas exchange surface area are proportional to body weight and oxygen consumption. Exposure to a cold environment, living in high altitudes and physical hyperactivity causes to an increase in oxygen diffusion capacity in proportion to enhanced oxygen consumption. Life-threatening barrier to proper oxygenation occurs in cases of decreased ventilatory drive, airway obstruction, intraalveolar exudate, damages to alveolar capillaries, septal thickening due to edema, inflammation and fibrosis. The alveolar/arterial PO₂ gradient is enhanced if there is a life-threatening barrier to proper oxygenation.^[2]

The aim of this review article is to define the embryological, gross anatomic, histopathological and molecular changes observed in the lung tissue in cases of hypoxia. Additionally; the relation of hypoxia and tumors is also discussed in the study. The manuscripts related to

hypoxia were searched from the literature, from PubMed (<https://www.ncbi.nlm.nih.gov/pubmed>) in between the years of 1945–2019. From these manuscripts; the ones, which were related to lung tissue changes due to hypoxia, were chosen and included to the review. The key words selected for searching the database were “hypoxia and lungs”. In the research of these keywords; totally 15,445 manuscripts were found. From these manuscripts; 43 of them were related with our subject and these studies were included to the review study.

Hypoxia and Development of the Lungs

Schwartz et al.^[3] examined fetal growth in rats exposed to brief and intermittent hypoxia with little change in nutrient intake. In rats exposed to hypoxia for one hour; fetal body weight, length of the fetus and liver weight was decreased. However; the brain/liver weight ratio was increased in these rats, when compared with the control group. In the study; another group of rats were exposed to hypoxia for two hours and results were the decrease of the fetal body weight and fetus length. The lung develops in relative hypoxic conditions if the fetus is exposed to 25% of ambient oxygen levels in utero.^[4] Hypoxic conditions in fetal environment stimulates the developmental stages of embryo, organogenesis and vascularization of the organs.^[5,6] Vascular endothelial growth factor (VEGF) is an important factor in lung development in the fetus. Inhibition of VEGF receptor signaling impairs the branching of airways and blood vessels in lung explants. Regulation of hypoxia-inducible genes and expression levels of hypoxia-inducible factors such as VEGF are necessary for proper lung development.^[7]

The differential effects of hypoxic levels to organ system development of the chicken was studied by Zhang and Burggren.^[8] Hypoxia occurring from day zero to day 10 during incubation had larger effects on embryonic mortality and organ growth than hypoxia occurring from day 10 to day 18. Growth of the heart and chorioallantoic membrane was stimulated by chronic hypoxia in the study. However; the lung, brain, eye, liver, stomach, beak, and toes were most affected from hypoxia. Sustained hypoxia from the beginning of incubation in chicken decreased blood haemoglobin and haematocrit levels. Red blood cell concentration of embryos at day 10 were also affected. At day 18; there was no statistically significant difference in between hypoxic and normoxic groups. In conclusion; modest hypoxia which describes 15% oxygen level during development, or hypoxia at any level during the late stages of development (from day 11 to day 18) increased the weights of the heart and chorioallantoic membrane. The results of this study

showed that the first half of embryonic development contained critical parameters for the detrimental effects of hypoxia and the second half of embryonic development contained critical parameters for the compensatory responses of hypoxia in key organs.

Schmiedl et al.^[9] investigated the influence of prenatal hypoxia and/or postnatal hyperoxia on morphological lung maturation based on stereological parameters in mice. The aim of this study was to find out which model best reflects morphological changes in lung development comparable with alterations observed in bronchopulmonary dysplasia. The authors found that prenatal hypoxia and postnatal hyperoxia differentially influenced the maturation of parenchyma of lungs. After hypoxia and hyperoxia in 14-day old mice, they observed a significant retardation in lung development morphologically which lead to bronchopulmonary dysplasia like alterations.

Hypoxia and Anatomic Studies

Davies et al.^[10] developed a method based on planimetry of elastic laminae in vessel cross sections and determined the reactivity of microvessels of lung tissue. The authors obtained slices from the lungs of six rats exposed to hypobaric hypoxia for 14 days. According to their results; after chronic hypoxia, the regression line shifted which indicated the structural remodeling. After hypoxia, newly muscularized arteries were found and in these vessels; the new internal elastic lamina was always shorter than the external elastic lamina. A complex network of elastin was connecting the two laminae. Sekhon and Thurlback^[11] studied the morphometry of lungs in rats between four and seven weeks of age. They divided the rats into five groups; control, hypobaric normoxic, normobaric hypoxic, hypobaric hypoxic, and weight matched to the hypobaric hypoxic group. In hypobaric hypoxic and normobaric hypoxic rats; the volume of the lungs, alveolar surface area of lungs and total number of alveoli were increased when compared to the weight-matched control group. In normobaric hypoxia group of rats; mean linear intercept, mean chord length of alveoli were increased and the number of alveoli per unit volume were decreased when compared to the weight-matched control animals. In hypobaric hypoxia group; the only change was the increase of mean chord length in rats. In hypobaric normoxia group; alveolar size and lung volume were diminished when compared with the control groups. Lung growth was impaired in weight-matched controls without affecting the dimension of air-spaces. In hypobaric hypoxic and normobaric hypoxic rats; an increase was observed in lung growth which

overcame the nutritional effects. In the rats; Sulkowska^[12] evaluated the effects of hypobaric hypoxia on lung parenchyma and in the surfactant system-forming structures in the lungs. These changes were evaluated basing on ultrastructural analysis by transmission electron microscopy. In the early phase; in three days, destructive-exudative changes predominated. These ultrastructural changes were delamination of type II pneumocytes, oedematous changes in the lungs (**Figure 1**), damage to the lining layer of alveoli and accumulation of alveolar macrophages in the lung tissue. In the later phases, repair-proliferative processes were found to be predominant such as increased number of type II pneumocytes and focal intensification of fibroplasia (**Figure 2**). In hypobaric conditions for 3 and 10 days; the changes within the surfactant system-forming structures were accompanied by the accumulation of granulocytes and monocytes. In hypobaric conditions for 30 days; an accumulation of blood platelets was detected in the vascular bed of the lungs. Clough et al.^[13] used χ -ray microfocal angiographic images of isolated perfused dog lung lobes in order to detect the effects of alveolar hypoxia on pulmonary microvascular volume. Their results showed that the capillary volume was decreased by hypoxia in the dogs' lung lobes. In a scanning electron microscopic study; Gade et al.^[14] examined the effects of bronchial arterial devascularization on the morphological appearance of bronchi in pigs. Bronchial arterial devascularization and bronchial transection were performed in pigs and the ultrastructure of the surfaces of bronchi was

examined. In conclusion; the grooves in between the bronchi were wrinkled in appearance and a large proportion of the epithelial cells were devoid of cilia. New cilia seemed to shoot up from the surface, in the study. On the control side; the ultrastructural morphology was similar with the normal pigs. In another study; Gade et al.^[15] examined the physiological consequences of porcine bronchial transection and reanastomosis with and without bronchial artery blood supply with relation to lung transplantation. In the study; postoperatively, bronchial transection and reanastomosis without bronchial artery blood supply was resulted by a significant decrease in the mucosal blood flow and saturation. Additionally; a significant decrease was detected in the tissue haemoglobin concentration. These findings provided a physiological explanation of histological changes observed in the study. In the microscopic examination of main bronchi and lung parenchyma; oedema (**Figure 1**), slight fibrosis (**Figure 2**) and inflammation were detected. In this study; the most remarkable two findings were the oedematous lung septa with inflammation and beginning of the fibrosis. In an experimental study of chronic hypoxia by Berk et al.;^[16] it was shown that the chronic hypoxia suppressed elastin repair by rat lung fibroblasts. According to their data; it was suggested that regional hypoxia limited lung elastin repair following protease injury at least in part by inhibiting elastin gene expression. In cases of acute hypoxia; Miserocchi^[17] examined the lung interstitial pressure and structure of the lungs. In the study; fragmentation of chondroitin sulphate pro-

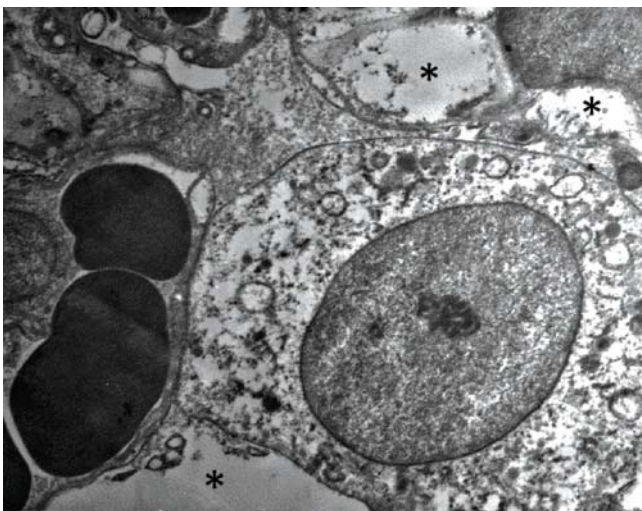


Figure 1. Transmission electron micrograph showing oedematous changes in lung tissue (*) in hypoxia. (Original magnification $\times 5000$) (from the collection of author).

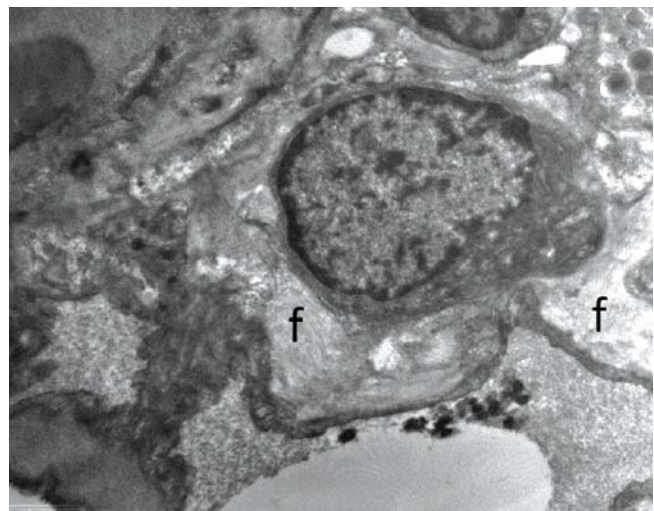


Figure 2. Transmission electron micrograph showing pulmonary fibrosis (f) in hypoxia. (Original magnification $\times 5000$) (from the collection of author).

teoglycans of the extracellular matrix and heparansulphate proteoglycans of the basement membrane were detected in acute hypoxia. There was a decrease in tissue elastance and an increase in the permeability of the endothelial barriers and epithelial barriers. In the study; when the overall proteoglycans fragmentation overcame to a critical threshold, developing of a severe lung edema was observed, in acute hypoxia.

In the adult mice; Reinke et al.^[18] examined the effects of chronic intermittent hypoxia on lung growth. The morphometry of the lungs, mean airspace chord lengths of lungs and alveolar surface areas of lungs were determined. In the study; it was shown that intermittent hypoxia increased the lung volumes and alveolar surface areas in the experimental model. Secondly; intermittent hypoxia induced a 60% increase in cellular proliferation, however; the number of proliferating type II alveolocytes were tripled. The authors could not be able to detect any increase in apoptosis. Other important findings of the study were upregulation of pathways for cellular movement, cellular growth and development in chronic intermittent hypoxia. Key developmental genes, vascular endothelial growth factor A and platelet-derived growth factor B were also upregulated by chronic intermittent hypoxia in adult mice. Zhang et al.^[19] studied the effects of hypoxia on the histological structure of rats' lungs. Their results demonstrated that mild edema and inflammatory cell infiltration appeared in the lung tissue at the third day of hypoxia. As the treated time extended; a gradually aggravated inflammation was observed in the rats. In the rats, due to the increase of the exposure time to normobaric hypoxia; interalveolar septa became thicker and thicker. By using *in vivo* high-resolution computed tomography measurements; Llapur et al.^[20] examined the effects of chronic hypoxia on lung growth. In the study; a number of 19 healthy adults living at 2,000 meters above sea level and a number of 23 healthy adults living in 400 meters above sea level underwent high-resolution computed tomography. In between the two groups; differences in the total lung volume, air volume and lungs' tissue volume were compared. Additionally; the mean lung densities of the two groups, airway lumens and wall areas in anatomically matched airways were compared in between the two groups. The authors detected no significant differences for age, sex, weight or height in between the two groups. Their results showed that the adult lung did not increase its lung volume later in life by expansion of an existing number of alveoli.

Rivolta et al.^[21] developed a hypoxia model by applying 10% of oxygen to Wistar male rats for 30 days and compared the results with the control animals. The

researchers measured: pulmonary interstitial pressure, cardiac and haemodynamic parameters by echocardiography. Additionally; they examined the morphometry of lungs in the lung specimens obtained after fixation *in situ*. After the exposure of hypoxia to rats; mean \pm standard deviation of pulmonary interstitial pressure was increased, air/tissue volume ratio was decreased and capillary vascularity index in the air-blood barrier was increased in hypoxic rats, when compared with the control group. In normal regions of the lung tissue; the density of pre-capillary vessels was increased and their thickness/internal diameter ratios were decreased. In the oedematous regions of the lungs; opposite results were obtained. In chronic hypoxia group of animals; the pulmonary artery pressure was increased, when compared to controls. In oedematous regions of lung tissue, the decrease in capillary vascularity was found to be correlated with the remarkable increase in interstitial pressure. Additionally; the morphometry of pre-capillary vessels suggested an increase in vascular resistance, in chronic hypoxia. In regions of normal lung tissue; the opposite findings were detected. In hypoxic state; an acute inflammatory reaction was observed in some studies found in the literature. The authors of these studies explained this condition by the activation of bone marrow and immigration of inflammatory precursor cells. It was measured by the increase of pulmonary granulocytes and megakaryocytes.^[22-25] In humans; the lack of oxygen resulted in a tremendous increase of perivascular mast cells, being rapidly recruited in the lungs within a few minutes.^[26] In the experimental study of Orth et al.^[27] performed on rats; the duration of hypoxia necessary for mast cell degranulation took only five minutes. Schmiendl et al.^[9] examined the lung parenchyma of 14-day old mice with light microscopy and electron microscopy. In the study; well-developed formed septa, normal alveoli and normal alveolar ducts were observed in the lungs of control group. Prenatal hypoxia induced lungs of mice showed lung parenchyma without clearly visible alterations, when compared to control animals. Postnatal hyperoxia induced lungs of mice indicated more expanded airspaces with fewer septa than the control group. In the microscopic examination; the lungs exposed to prenatal hypoxia and postnatal hyperoxia displayed enlarged parenchymal airspaces surrounded by thick septa. Hypoxia and hypoxia signalling have many negative effects on the lung tissue. Fibroblast proliferation, inflammatory cell infiltration and interstitial thickening are the main pathological findings. These pathological findings are combined with alveolar ventilation defects in order to increase the oxygen consumption and limit the oxygen supply to the injured lung tissues. As a result;

local tissue hypoxia is observed in the lungs. In the lung tissues of patients having idiopathic pulmonary fibrosis or cystic fibrosis, and in the experimental models developed idiopathic pulmonary fibrosis or cystic fibrosis in mice; increased stabilisation of hypoxia-inducible transcription factor (HIF-1 α) had been detected.^[2,28,29] Following exposure to hypoxia; a proliferation was observed in the fibroblasts and these fibroblasts had the highest quantity of excreted collagen; mainly the type-I collagen.^[30] As a result of all these studies; it can be concluded that hypoxia is involved in the development of pulmonary fibrosis (Figure 2). In an experimental study performed on rats; Ge et al.^[31] investigated the pathological changes on upper and lower respiratory tract in chronic intermittent hypoxia. In conclusion; chronic intermittent hypoxia formed irreversible changes both at upper and lower respiratory tracts in the rats. The thickness of the lamina propria of soft palate was significantly increased in hypoxia group. Additionally, in rats; pulmonary interval thickening was detected in the lungs.

Hypoxia and Molecular Studies

In hypoxic human lung fibroblast cell cultures, Shan-Shan Liu et al.^[32] examined the effects and underlying mechanisms of angiotensin II on collagen synthesis. After hypoxic treatment; angiotensinogen, angiotensin converting enzyme, angiotensin II type 1 receptor and angiotensin II type 2 receptor expression levels in human lung fibroblast cell cultures were analysed by using real-time polymerase chain reaction. Secondly; collagen type I, angiotensin II type 1 receptor and nuclear factor kappaB (κ B) protein expression levels were detected by using Western blot analysis. In addition to all these analyses; nuclear factor κ B nuclear translocation was measured by using immunofluorescence localization analysis. Angiotensin II levels in human lung fibroblast cell cultures were measured by using enzyme-linked immunosorbent assay (ELISA) method. The authors found that hypoxia increased collagen type I mRNA and protein expression levels in human lung fibroblast cells. According to the results of the study; it has been shown that these effects could be inhibited by an angiotensin II type 1 receptor or angiotensin II type 2 receptor inhibitor. After exposure to hypoxia; the levels of nuclear factor κ B, renin-angiotensin system components and angiotensin II production in human lung fibroblast cell cultures were significantly increased. Tsao and Wei^[33] developed a prenatal hypoxia model in mice experimentally. In these animals; the authors examined the role of vascular endothelial growth factor (VEGF) and VEGF receptors in fetal lung development and maturation. In the study; prenatal hypoxia resulted in fetal mice body

weight gain impairment and the authors observed delayed fetal pulmonary aeration and maturation in mice. Pulmonary surfactant proteins SP-A, SP-B, SP-C, and SP-D mRNA were all decreased in the prenatal hypoxia group in mice. In addition, the authors demonstrated that prenatal hypoxia inhibited the developmental increase of pulmonary hypoxia-inducible factors HIF-1 α and HIF-2 α expression and resulted in decreasing VEGF and its receptors (Flt-1 and Flk-1) at the mRNA expression level. Secondly; the VEGF protein levels in fetal lungs were also found to be decreased.

Primary murine alveolar epithelial cells were exposed to 1% of oxygen for 24 hours in order to develop a hypoxia model in wild-type mice. In the study; a significant suppression of key innate immune molecules was observed. These key innate molecules included granulocyte-macrophage colony stimulating factor, CCL2, and IL-6. Any toxicity finding was not observed in the experimental model, however; it induced stabilization of hypoxia inducible factor 1 α protein and shift to glycolytic metabolism. The researchers found that hypoxia greatly decreased the rate of granulocyte-macrophage colony stimulating factor transcription. In another experimental model; the mice were exposed to hypoxia *in vivo* by the application of 12% oxygen for two days. In this model; the lung granulocyte-macrophage colony stimulating factor protein expression was reduced and *in vivo* phagocytosis of fluorescent beads by alveolar macrophages was suppressed. In conclusion of all these studies; it can be suggested that in critically ill patients; local hypoxia may contribute to the susceptibility of poorly ventilated lung units to infection through complementary effects on several pathways reducing alveolar epithelial cell expression of granulocyte-macrophage colony stimulating factor and other key innate immune molecules.^[34] Many studies found in the literature revealed micro-RNAs to be involved in modulation of hypoxia-induced pulmonary hypertension.^[35-37] Blissenbach et al.^[38] examined the plasma micro-RNA levels in order to make a correlation with hypoxia induced pulmonary hypertension. In the study; plasma micro-RNAs were evaluated in a model of hypoxia-related pulmonary hypertension in humans exposed to extreme altitude. Plasma levels of micro-RNA -17, -21, and -190 were measured by real-time quantitative PCR method. The obtained results were correlated with systolic pulmonary artery pressure, which was assessed by echocardiography. In the study; a significant altitude-dependent increase in circulating micro-RNAs expression was detected.

Four hours of exposure to a simulated altitude of 31,000 feet; Martinez-Romero et al.^[39] studied compar-

tively the effects of pharmacological inhibitors of nitric oxide production or Poly (ADP-ribose) polymerase activity in the response of the mouse cerebral cortex. The researchers analysed nitric oxide and reactive oxygen species production, the expression of nitric oxide synthase isoforms, Poly (ADP-ribose) polymerase-1 activity, hypoxia-inducible factor-1 alpha expression and hypoxia-inducible factor-1 transcriptional activity, the protein level of the factor inhibiting hypoxia inducible factor, and at last beclin-1 and fractin expression, as markers of cellular damage. According to their results; the reduction of nitric oxide level did not affect reactive oxygen species production. However; significantly dampened the post hypoxic increase in neuronal nitric oxide synthase and inducible nitric oxide synthase expression without altering endothelial nitric oxide synthase protein level; prevented Poly (ADP-ribose) polymerase activation; decreased hypoxia-inducible factor-1 alpha response to hypoxia; achieved a higher long-term hypoxia-inducible factor-1 transcriptional activity by reducing factor inhibiting hypoxia-inducible factor expression and reduced hypoxic damage. Their results provided an important data about the molecular mechanisms underlying the beneficial effects of controlling nitric oxide production under hypobaric hypoxic conditions. Singh et al.^[40] examined the roles of activator protein-1 (AP-1) transcription factor; mitogen activated protein kinases (MAPKs) which are the c-Jun N-terminal kinase (JNK), extracellular-signal regulated kinase (ERK) and p38 in the hypobaric hypoxia induced changes in lung tissue. In rats; immediate response to hypobaric hypoxia induced c-Jun:c-Fos subunits of AP-1; responsible for proliferation that might cause inhomogeneous vasoconstriction leading to vascular leakage and inflammation at increased duration of hypobaric hypoxia exposure. Secondly; hypoxia resulted in significant increase in reactive oxygen species (ROS), vascular endothelial growth factor (VEGF) and decreased nitric oxide (NO) in hypobaric hypoxia conditions. These act as signaling molecules for activation of MAPK and also contribute in development of vascular leakage which was an indicator of pulmonary edema.

In rats submitted to acute hypobaric hypoxia; Rus et al.^[41] measured endothelial and inducible nitric oxide synthase (eNOS, iNOS) mRNA and protein expression, location, and in situ Nitric Oxide Synthase activity as well as nitrated protein expression and location. In addition, nitric oxide levels were indirectly quantified (NOx) as well as the apoptosis level. The researchers detected an increase in eNOS mRNA, protein activity and eNOS positive immunostaining at 0 h posthypoxia which coincided with raised NOx levels. However; the iNOS, nitrated pro-

tein expression and apoptosis level augmented during the final reoxygenation times. The authors concluded that eNOS was responsible of the immediate response, producing nitric oxide, which caused vasodilation and bronchodilation in lung tissue. Secondly; iNOS was related to the second late response, which seemed to be involved in some of the deleterious consequences that hypoxia induced in the lung. In another study; by using a nitric oxide synthase (NOS) inhibitor, Rus et al.^[42] searched to clarify the current controversy concerning the double protective/toxic role of endogenous nitric oxide under hypoxia/reoxygenation situations. The study was conducted in rats submitted to hypoxia/reoxygenation with or without prior treatment using the nonselective NOS inhibitor L-NAME. Their results showed that after L-NAME administration, in situ NOS activity was almost completely eliminated and consequently, NOx levels fell. Lipid peroxidation and the percentage of apoptotic cells rose at the earliest reoxygenation time, but decreased in the later periods, in the study.

Hypoxia and Tumors

Hypoxia occurs frequently in solid tumors and this condition is a poor prognostic factor for the outcome of the patients. Hypoxia promotes tumor cell proliferation, invasion of tumor cells, angiogenesis, resistance to therapeutic agents and occurrence of metastasis. In a growing tumor; two forms of hypoxia can be observed: Chronic hypoxia caused by abnormal tumor vasculature and intermittent hypoxia caused by transient perfusion facilitated by tumor-supplying blood vessels. In the presence of intermittent hypoxia; many genetic, molecular, biochemical, and cellular changes are detected. All of these changes facilitate the survival of tumor cells and their colonization. Depending upon to all these results; metastatic growth rate of the cancer cells increases.^[43]

In order to reveal the possible mechanisms of brain metastases of lung cancers; Wei et al.^[44] studied the relationships in between hypoxia and hypoxia inducible factor-1 α (HIF-1 α) in lung cancer cells. The hypoxia model of A549 lung cancer cells was established in the study. After the hypoxia culture of A549 cells for 0.5, 2, 4, 8, 12 and 24 hours; the concentration of HIF-1 α in A549 lung cancer cell culture medium were determined by ELISA test. In conclusion; hypoxia induced the increase of HIF-1 α in lung cancer cells. Due to the increase of HIF-1 α in A549 lung cancer cells; a decrease was detected in Claudin-5 expression. These changes increased blood-brain barrier permeability which lead to the metastases of lung cancer cells into the brain tissue.

Conclusion

Clinical manifestations of acute, intermittent or chronic hypoxia have negative effects on lung maturation during the embryological period which has been shown by many experimental models designed on animal studies. Hypoxia also affects the morphometry, anatomy and microscopy of lung tissue in the adults. Chronic hypoxia accentuates lung growth by increasing the lung parenchyma. However; the airways in the lung tissue were found to be normal in hypoxic cases. Histology of lung tissue shows microscopic changes due to hypoxia. Mild edema and inflammatory cell infiltration appear in the lung tissue in experimental studies performed on animal models. In cases of hypoxia; the lung parenchyma shows destructive exudative changes in the early phase; in the later phases repair and proliferative processes are dominant. Decrease of capillary volume, suppression of elastin repair in lung fibroblasts and pulmonary fibrosis are other clinically important findings of hypoxia. Due to hypoxia; the receptors responsible from fetal lung development are also affected. In molecular studies; hypoxia induced pulmonary hypertension, suppression of many immune molecules, major changes at the levels of various enzymes and growth factors were detected in the researches. Additionally; hypoxia causes to an increase in the amount of lung cancer cells and therefore; induces the metastases of lung cancer cells to brain tissues.

Exposure to hypoxia during embryological period must be avoided for normal lung maturation in the fetus. In the adult; if morphometric, anatomic or microscopic changes are observed in the lung tissue; exposure to hypoxia must also be remembered in differential diagnosis. If pulmonary hypertension, suppression of immune molecules, changes in the levels of enzymes or growth factors are detected in molecular studies of lung tissue; the possibility of the exposure to hypoxia must also be remembered. Additionally, in cases of lung cancers, in order to control the over increase of cancer cells or spread of metastases; a great care should be taken to keep patients away from hypoxic environment.

Conflict of Interest

The author declares that he has no conflict of interest.

References

- Saladin KS. Anatomy and physiology. The unity of form and function. 8th ed. New York (NY): Mc Graw Hill Education; 2018. 878 p.
- Tuder RM, Yun JH, Bhunia A, Fijalkowska I. Hypoxia and chronic lung disease. *J Mol Med* 2007;85:1317–24.
- Schwartz JE, Kovach A, Meyer J, McConnell C, Iwamoto HS. Brief, intermittent hypoxia restricts fetal growth in Sprague-Dawley rats. *Biol Neonate* 1998;73:313–19.
- Van Tuyl M, Liu J, Wang J, Kuliszewski M, Tibboel D, Post M. Role of oxygen and vascular development in epithelial branching morphogenesis of the developing mouse lung. *Am J Physiol Lung Cell Mol Physiol* 2005;288:L167–78.
- Tufro-McReddie A, Norwood VF, Aylor KW, Botkin SJ, Carey RM, Gomez RA. Oxygen regulates vascular endothelial growth factor-mediated vasculogenesis and tubulogenesis. *Dev Biol* 1997;2: 139–49.
- Maltepe E, Simon MC. Oxygen, genes, and development: an analysis of the role of hypoxic gene regulation during murine vascular development. *J Mol Med (Berl)* 1998;6:391–401.
- Groenman FA, Rutter M, Wang J, Caniggia I, Tibboel D, Post M. Effect of chemical stabilizers of hypoxia-inducible factors on early lung development. *Am J Physiol Lung Cell Mol Physiol* 2007;3: L557–67.
- Zhang H, Burggren WW. Hypoxic level and duration differentially affect embryonic organ system development of the chicken (*Gallus gallus*). *Poult Sci* 2012;91:3191–201.
- Schmiedl A, Roolfs T, Tutdibi E, Gortner L, Monz D. Influence of prenatal hypoxia and postnatal hyperoxia on morphologic lung maturation in mice. *PLoS One* 2017;12:e0175804.
- Davies P, Maddalo F, Reid L. Effects of chronic hypoxia on structure and reactivity of rat lung microvessels. *J Appl Physiol* 1985;58: 795–801.
- Sekhoni HS, Thurlbeck WM. Lung morphometric changes after exposure to hypobaric and/or hypoxia and undernutrition. *Respir Physiol* 1996;106:99–107.
- Sulkowska M. Morphological studies of the lungs in chronic hypobaric hypoxia. *Pol J Pathol* 1997;48:225–34.
- Clough AV, Haworth ST, Ma W, Dawson CA. Effects of hypoxia on pulmonary microvascular volume. *Am J Physiol Heart Circ Physiol* 2000;279:H1274–82.
- Gade J, Qvortrup K, Andersen CB, Thorsen S, Svendsen UG, Olsen PS. Bronchial arterial devascularization. An experimental study in pigs. *Scand Cardiovasc J* 2001;35:212–20.
- Gade J, Greisen G, Larsen IK, Bibby BM, Olsen PS. Tissue hypoxaemia causes oedema, inflammation and fibrosis in porcine bronchial transection. *Scand Cardiovasc J* 2012;46:286–94.
- Berk JL, Hatch CA, Morris SM, Stone PJ, Goldstein RH. Hypoxia suppresses elastin repair by rat lung fibroblasts. *Am J Physiol Lung Cell Mol Physiol* 2005;289:L931–6.
- Miserocchi G. Lung interstitial pressure and structure in acute hypoxia. *Adv Exp Med Biol* 2007;618:141–57.
- Reinke C, Bevans-Fonti S, Grigoryev DN, Drager LF, Myers AC, Wise RA, Schwartz AR, Mitzner W, Polotsky VY. Chronic intermittent hypoxia induces lung growth in adult mice. *Am J Physiol Lung Cell Mol Physiol* 2011;300:L266–73.
- Zhang X, Xie M, Gao Y, Wei HH, Zheng JQ. Study on the effect and mechanism of hypoxia on the histological structure of rat's lung [Article in Chinese]. *Sichuan Da Xue Xue Bao Yi Xue Ban* 2012;43: 1–5.
- Llapur CJ, Martínez MR, Grassino PT, Stok A, Altieri HH, Bonilla F, Caram MM, Krowchuk NM, Kirby M, Coxson HO, Tepper RS. Chronic hypoxia accentuates dysanaptic lung growth. *Am J Respir Crit Care Med* 2016;194:327–32.
- Rivolta I, Lucchini V, Rocchetti M, Kolar F, Palazzo F, Zaza A, Miserocchi G. Interstitial pressure and lung oedema in chronic hypoxia. *Eur Respir J* 2011;37:943–9.

22. Brinkmann B. Vital reactions of the pulmonary circulation in fatal strangulation. *Z Rechtsmed* 1978;81:133–46.
23. Brinkmann B, Püschel K. Histomorphological alterations of lung after strangulation. A comparative experimental study. *Z Rechtsmed* 1981;86:175–94.
24. Du Chesne A, Cecchi-Mureani R, Püschel K, Brinkmann B. Macrophage subtype patterns in protracted asphyxiation. *Int J Legal Med* 1996;109:163–6.
25. Strunk T, Hamacher D, Schulz R, Brinkmann B. Reaction patterns of pulmonary macrophages in protracted asphyxiation. *Int J Legal Med* 2010;124:559–68.
26. Muciaccia B, Sestili C, De Grossi S, Vestri A, Cipolloni L, Cecchi R. Are mast cells implicated in asphyxia? *Int J Legal Med* 2016;130:153–61.
27. Orth T, Allen JA, Wood JG, Gonzalez NC. Plasma from conscious hypoxic rats stimulates leukocyte-endothelial interactions in normoxic cremaster venules. *J Appl Physiol* (1985) 2005;99:290–7.
28. Urquhart DS, Montgomery H, Jaffé A. Assessment of hypoxia in children with cystic fibrosis. *Arch Dis Child* 2005;90:1138–43.
29. Tzouveleakis A, Harokopos V, Paparountas T, Oikonomou N, Chatziioannou A, Vilaras G, Tsiambas E, Karameris A, Bouros D, Aidinis V. Comparative expression profiling in pulmonary fibrosis suggests a role of hypoxia-inducible factor-1 α in disease pathogenesis. *Am J Respir Crit Care Med* 2007;176:1108–19.
30. Ahmedat A, Warnken M, Seemann W, Mohr K, Kostenis E, Juergens U, Racké K. Profibrotic processes in human lung fibroblasts are driven by an autocrine/paracrine endothelinergetic system. *Br J Pharmacol* 2013;168:471–87.
31. Ge L, Ming T, Hou J, Yan J, Zhao L, Gong N, Jiang J, Wang F. Pathological changes of upper and lower respiratory tissue in rats with chronic intermittent hypoxia [Article in Chinese]. *Zhonghua Er Bi Yan Hou Tou Jing Wai Ke Za Zhi* (Chinese Journal of Otorhinolaryngology Head and Neck Surgery) 2015;50:939–43.
32. Liu SS, Wang HY, Tang JM, Zhou XM. Hypoxia-induced collagen synthesis of human lung fibroblasts by activating the angiotensin system. *Int J Mol Sci* 2013;14:24029–45.
33. Tsao PN, Wei SC. Prenatal hypoxia downregulates the expression of pulmonary vascular endothelial growth factor and its receptors in fetal mice. *Neonatology* 2013;103:300–7.
34. Sturrock A, Woller D, Freeman A, Sanders K, Paine R. Consequences of hypoxia for the pulmonary alveolar epithelial cell innate immune response. *J Immunol* 2018;201:3411–20.
35. Li Q, Zhou X, Zhou X. Downregulation of miR 98 contributes to hypoxic pulmonary hypertension by targeting ALK1. *Mol Med Rep* 2019;20:2167–76.
36. Liu T, Zou XZ, Huang N, Ge XY, Yao MZ, Liu H, Zhang Z, Hu CP. miR-27a promotes endothelial-mesenchymal transition in hypoxia-induced pulmonary arterial hypertension by suppressing BMP signaling. *Life Sci* 2019;227:64–73.
37. Liu A, Liu Y, Li B, Yang M, Liu Y, Su J. Role of miR-223-3p in pulmonary arterial hypertension via targeting ITGB3 in the ECM pathway. *Cell Prolif* 2019;52:e12550.
38. Blissenbach B, Nakas CT, Krönke M, Geiser T, Merz TM, Pichler Hefti J. Hypoxia-induced changes in plasma micro-RNAs correlate with pulmonary artery pressure at high altitude. *Am J Physiol Lung Cell Mol Physiol* 2018;314:L157–64.
39. Martínez-Romero R, Cañuelo A, Siles E, Oliver FJ, Martínez-Lara E. Nitric oxide modulates hypoxia-inducible factor-1 and poly (ADP-ribose) polymerase-1 cross talk in response to hypobaric hypoxia. *J Appl Physiol* 2012;112:816–23.
40. Singh M, Yadav S, Kumar M, Saxena S, Saraswat D, Bansal A, Singh SB. The MAPK-activator protein-1 signaling regulates changes in lung tissue of rat exposed to hypobaric hypoxia. *J Cell Physiol* 2018;233:6851–65.
41. Rus A, Peinado MA, Castro L, Del Moral ML. Lung eNOS and iNOS are reoxygenation time-dependent upregulated after acute hypoxia. *Anat Rec* 2010;293:1089–98.
42. Rus A, Molina F, Peinado MA, Del Moral ML. Endogenous nitric oxide can act as beneficial or deleterious in the hypoxic lung depending on the reoxygenation time. *Anat Rec* 2010;293:2193–201.
43. Chen A, Sceneay J, Gödde N, Kinwel T, Ham S, Thompson EW, Humbert PO, Möller A. Intermittent hypoxia induces a metastatic phenotype in breast cancer. *Oncogene* 2018;37:4214–25.
44. Wei DF, Tang MK, Liu Y, Zhang CY, Qin LJ. Effect of hypoxia inducible Factor-1 α on brain metastasis from lung cancer and its mechanism [Article in Chinese]. *Sichuan Da Xue Xue Bao Yi Xue Ban* 2019;50:188–92.

ORCID ID:

M. F. Sargon 0000-0001-6360-6008

**Correspondence to:** Mustafa F. Sargon, MD, PhD.

Department of Anatomy, Faculty of Medicine,
Lokman Hekim University, Ankara, Turkey
Phone: +90 505 365 81 96
e-mail: mustafa.sargon@lokmanhekim.edu.tr

Conflict of interest statement: No conflicts declared.

This is an open access article distributed under the terms of the Creative Commons Attribution-NonCommercial-NoDerivs 4.0 Unported (CC BY-NC-ND4.0) Licence (<http://creativecommons.org/licenses/by-nc-nd/4.0/>) which permits unrestricted noncommercial use, distribution, and reproduction in any medium, provided the original work is properly cited. *How to cite this article:* Sargon MF. Lungs and hypoxia: a review of the literature. *Anatomy* 2021;15(1):76–83.

Communicating vein between the right external and internal jugular veins: a case report

Eleni Patera , Abdelmenem Alashkham 

Anatomy, School of Biomedical Sciences, Edinburgh Medical School, University of Edinburgh, Edinburgh, UK

Abstract

The external jugular vein is a superficial vein that has a relatively diagonal to vertical course in the neck region and runs superficial to the sternocleidomastoid muscle. This vein is formed by the union of the posterior division of the retromandibular vein with the posterior auricular vein and it is responsible for draining most of the scalp and face as well. Sound knowledge of variations of the external jugular veins and the internal jugular veins, is important as these veins are used or targeted in specific medical procedures such as external jugular vein cannulation or radical neck dissection, respectively. During routine postgraduate dissection of the neck region in a 58-year-old female cadaver, the right external jugular vein was seen communicating with the right internal jugular vein via a communicating vein. The communicating vein was located approximately at the lower border of the thyroid cartilage and the upper border of the cricoid cartilage. A thorough understanding of anatomical variations is important in various medical disciplines and more specifically to anatomists, radiologists, and surgeons. This case report does not solely aim to increase awareness regarding variations of the jugular veins that can be possibly encountered during a neck endovascular procedure, but also contribute to the identification of the prevalence rate of this variation.

Keywords: anatomical variation; anatomy; communicating vein; jugular veins

Anatomy 2021;15(1):84–87 ©2021 Turkish Society of Anatomy and Clinical Anatomy (TSACA)

Introduction

The external jugular vein is a superficial vein in the lateral cervical region which is responsible for draining most of the scalp and side of face. It begins near the angle of the mandible, inferior to the auricle and is formed by the union of the posterior division of the retromandibular vein with the posterior auricular vein.^[1] The external jugular vein descends from the angle of the mandible to the middle of the clavicle. Through its course the external jugular vein crosses the sternocleidomastoid muscle obliquely and superficial to it. The external jugular vein is deep to the platysma and eventually enters the anteroinferior part of the lateral cervical region. The external jugular vein pierces the investing layer of the deep cervical fascia at the posterior border of the sternocleidomastoid muscle, descends to the inferior part of the lateral cervical region and terminates in the subclavian vein lateral or anterior to the scalenus anterior muscle.^[1,2]

The internal jugular vein receives blood from the brain, scalp, superficial parts of the face, and neck. The internal jugular vein is a continuation of the sigmoid sinus and it begins at the cranial base in the posterior compartment of the jugular foramen from which it passes through and descends in the carotid sheath where it unites with the subclavian vein posterior to the sternal end of the clavicle to drain into the brachiocephalic vein.^[1,2]

Awareness of jugular veins variations is significant during the conduction of endovascular procedures taking place in the neck region. The aim of this study was to report an anatomical variation of the right jugular veins that is different from the anatomical variations of the jugular veins that have been currently described in the literature and to contribute into the identification of the rate of which this anatomical variation is encountered.

This study has been presented as a poster at the BACA Winter Conference at New Castle University, United Kingdom in December 17, 2019.

Case Report

This study was conducted in Anatomy, University of Edinburgh on five formalin fixed adult human cadavers aging between 58–101 years of which 2 were male and 3 were female. A full dissection of the thorax and neck regions was performed. The body was in the supine position and the neck was rested on a rubber neck rest allowing slight head extension and access to the neck structures. The platysma muscle and the sternal and clavicular heads of the sternocleidomastoid muscle were detached from their origin. The sternohyoid, sternothyroid and omohyoid muscles were removed from their origin and reflected upwards. Sharp dissection was performed by using a 15mm scalpel to remove the carotid sheath of the deep cervical fascia that covered the carotid vessels and the internal jugular veins and to expose the jugular veins.

In a 58-year-old female cadaver, the right and left external jugular veins were normally formed by the union of the posterior division of the retromandibular vein and the posterior auricular vein. The right external jugular vein was seen communicating with the right internal jugular vein via a communicating vein (**Figure 1**). This variation occurred only in one out of the five cadavers. The communicating vein was posterior to the sternocleidomastoid muscle and was located approximately at the lower border of the thyroid cartilage and the upper border of the cricoid cartilage. The communicating vein was approximately 1.5 cm in length and its diameter was around 3.82 mm. The right internal jugular vein was larger in diameter compared with the right external jugular vein. The right external and internal jugular veins drained normally into the right subclavian and right brachiocephalic vein, respectively. No variations were encountered in the jugular veins of the left side of the neck.

Discussion

Classical anatomical textbooks describe the external jugular vein being formed by the posterior division of the retromandibular vein and the posterior auricular vein.^[1–3] The internal jugular vein is often described to be formed by the union of the sigmoid and inferior petrosal venous sinuses. Classically, there is one external and one internal jugular vein on each side of the neck and no communication between these veins.

In the current literature, variations of the jugular veins have been well reported. Paraskevas et al.^[4] reported a rare case where three external jugular veins were found to co-exist with two anterior jugular veins. In contrast, another case report reported absence of the left EJV. As the EJV was absent, the posterior division of the

retromandibular vein drained directly into the IJV.^[5] Kayiran et al.^[6] reported absence of the right IJV which was identified primarily by ultrasonography, CT, and MRI scans, after the patient presented with a painless cervical mass on the lateral side of the neck. The left IJV was observed to be significantly thicker. The authors attributed this case as a congenital agenesis event.

In the literature, there are currently three published case reports that describe communication between the external and internal jugular veins. Uemura et al.,^[7] published a rare case report of a right partial and double IJVs. Initially, authors reported in their abstract that the right IJV was found to bifurcate into a medial and a lateral branch at the middle of the fifth cervical vertebral body

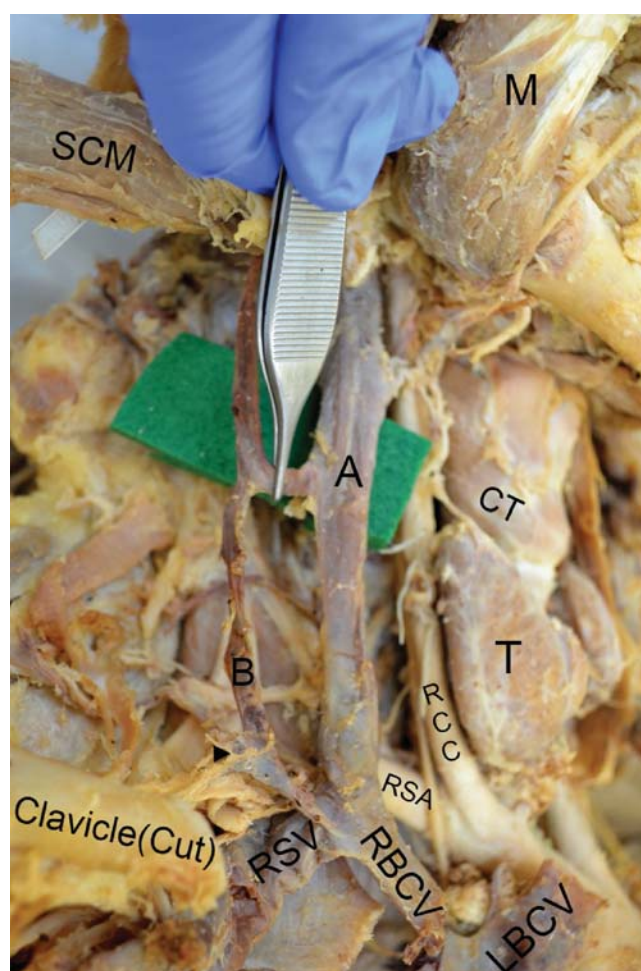


Figure 1. Lateral view of the right side of the neck region showing the variation of the jugular veins. The communicating vein held by the forceps is found between the right internal jugular vein (A) and the right external jugular vein (B). CT: cricothyroid muscle; LBCV: left brachiocephalic vein; M: masseter; RBCV: right brachiocephalic vein; RCC: right common carotid artery; RSA: right subclavian artery; RSV: right subclavian vein; SCM: sternocleidomastoid muscle (reflected); T: thyroid gland.

with both branches draining into the right subclavian vein. Subsequently in their results, authors mentioned that the lateral branch of the right IJV joined the right EJV whereas the medial branch of the right IJV drained directly into the right subclavian vein. The medial and lateral branches of the IJV ran parallel during their descending course in the neck. In addition, the authors reported that the EJV was formed by the confluence between the right superficial temporal and maxillary veins which then divided into a medial and lateral branch, at the level of the superior margin of the right SCM muscle. The medial and lateral branches of the right EJV joined again at the inferior border of the SCM and drained into the distal portion of the right EJV. The right EJV along with the lateral branch of the right IJV eventually drained into the right subclavian vein. Authors concluded that the medial branch of the right IJV was in fact the right IJV and that the lateral branch of the right IJV has in fact developed from the right EJV because the anterior jugular vein drained into it. Hence, they concluded that the lateral branch of the right EJV was a communicating branch between the right EJV and IJV. Overall, there is some ambiguity in this case report as authors primarily mentioned that the right IJV gave a medial and a lateral branch which they then concluded that it was instead a branch of the right EJV that communicated the right EJV and IJV. Further ambiguity toward our understanding over this anatomical variation is present, as the cadaveric images provided in this article do not allow the reader to have a clear view over the course of the veins described and their drainage pathway as well.

Lalwani et al.^[8] reported an abnormal communication between the EJV and the IJV. The authors reported that a venous channel arose from the EJV, traversing the anterior border of the sternocleidomastoid muscle ultimately descending to drain into the IJV. Authors failed to show an image of this venous channel emptying in the IJV as deep dissection to remove the SCM muscle to expose the IJV was not performed. No information was provided regarding the length of the venous channel that was found between the EJV and IJV. In contrast, results from our case report, report a communicating vein between the right EJV and IJV that was identified after performing deep neck dissection (**Figure 1**).

Another rare case report by Karapantzos et al.^[9] reported an anastomosis between the right EJV and IJV. Authors mentioned that this shunt seemed to come off the right EJV, passed through the sternocleidomastoid muscle eventually leading to the IJV where it drained into eventually allowing authors to conclude that this shunt was an extra EJV. The figure showing this anastomosis between

the EJV and IJV hinders our understanding over this variation, as adjacent anatomical structures including the sternocleidomastoid muscle and thyroid cartilage were not indicated. Additionally, by looking at the figure, it seems that the shunt was posterior to the sternocleidomastoid muscle, it ran obliquely eventually draining into the left IJV and not the right IJV as authors reported.

In contrast to the aforementioned studies that reported a communication between the EJV and IJV, results from our case report, report a communicating vein between the right EJV and IJV that was posterior to the sternocleidomastoid muscle and was located approximately at the level of the upper border of the cricoid cartilage. Its length was approximately 1.5 cm, its diameter was around 3.82 mm and its course was horizontal. The communicating vein between the right EJV and IJV described in our current case report, differs significantly from the communicating vein between the jugular veins that has been previously described in the literature by Uemura et al.,^[7] Lalwani et al.,^[8] and Karapantzos et al.^[9] Such anatomical variation has not been previously described in the current literature to the best of our knowledge.

Knowledge of variations of the jugular veins is indispensable prior the conduction of surgical endovascular procedures within the neck region including radical neck dissection surgeries. Radical neck dissection is a surgical oncology procedure that is being conducted for the management of metastatic nodal disease in the neck.^[10] As the neck is a region that is rich in lymph nodes, radical neck dissection is performed in individuals with certain types of head and neck cancer.^[11] In the past, Conley described radical neck dissection as the most effective surgical procedure for controlling suspected or gross metastasis in the neck region via the removal of lymph nodes in the neck.^[12] Despite this, Harish highlighted that when extracapsular spread or perineural invasion due to lymph node metastasis is present, radical neck dissection is not adequate for the removal of the tumour thus, the use of radiation in addition to the radical neck dissection might be necessary for specific patients.^[13]

In radical neck dissection, the internal jugular vein undergoes removal along both the sternocleidomastoid muscle and the spinal accessory nerve. In modified radical neck dissection type I, the internal jugular vein and the sternocleidomastoid muscle undergo removal. In modified radical neck dissection type II, the internal jugular vein is preserved.^[10]

Knowledge of variations of the jugular veins such as a communicating vein between the external and internal

jugular veins is indispensable prior the conduction of radical neck dissection and modified radical neck dissection type I as the EJV is ligated prior the IJV. Therefore, unawareness of such variation can eventually lead to excessive bleeding.

Conclusion

Overall, a thorough understanding of variations of the jugular veins is indispensable prior the conduction of surgical endovascular procedures within the neck region. Additionally, the documentation of anatomical variations contributes to the identification of the actual prevalence rate of specific anatomical variations within a body region. Once, an anatomical variation has been reported in the literature to a great extent by numerous studies, then, it can be included as a frequently encountered anatomical variation in the anatomical variation section in anatomical textbooks.

Acknowledgments

The authors would like to express their sincere gratitude to the donors and their families. Special thanks to the Anatomy department at the University of Edinburgh.

Conflict of Interest

None.

Author Contributions

EP: Dissection, data collection, image acquisition, analysis and writing up; AA: Analysis, editing and proofreading.

Ethics Approval

The specimens were obtained from the Centre for Anatomy, which is regulated by the Anatomy Scotland Act (2006).

Funding

None.

References

1. Moore KL, Dalley AF, Agur AMR, editors. Clinically oriented anatomy clinical anatomy. 7th ed. Philadelphia (PA): Wolters Kluwer; 2017. p. 995–1004.
2. Standring S, editor. Gray's anatomy: The anatomical basis of clinical practice. 41st ed. London: Churchill Livingstone Elsevier; 2015. p. 406–14.
3. Wineski L, editor. Snell's clinical anatomy by regions. 10th ed. London: Wolters Kluwer; 2018. p. 1617–46.
4. Paraskevas G, Natsis K, Ioannidis O, Kitsoulis P, Anastasopoulos N, Spyridakis I. Multiple variations of the superficial jugular veins: case report and clinical relevance. *Acta Medica (Hradec Kralove)* 2014;57:34–7.
5. Abhinitha P, Rao MKG, Kumar N, Nayak SB, Ravindra SS, Aithal PA. Absence of the external jugular vein and an abnormal drainage pattern in the veins of the neck. *OA Anatomy* 2013;1:1–3.
6. Kayiran O, Calli C, Emre A, Soy FK. Congenital agenesis of the internal jugular vein: an extremely rare anomaly. *Case Rep Surg* 2015;2015:637067.
7. Uemura M, Takemura A, Tamada Y, Toda I, Ike H, Suwa F. A case of right partial and double internal jugular veins. *Anat Sci Int* 2006;81:65–8.
8. Lalwani R, Rana K, Das S, Khan R. Communication of the external and internal jugular veins: a case report. *International Journal of Morphology* 2006;24:721–2.
9. Karapantzos I, Zarogoulidis P, Charalampidis C, Karapantzos C, Kioumis I, Tsakiridis K, Mpakas A, Sachpekidis N, Organtzis J, Porpodis K, Zarogoulidis K, Pitsiou G, Zissimopoulos A, Kosmidis C, Fouka E, Demetriou T. A rare case of anastomosis between the external and internal jugular veins. *Int Med Case Rep J* 2016;9:73–5.
10. Gogna S, Gupta N. Cancer, neck resection and dissection. In: *StatPearls* [Internet]. Treasure Island (FL): StatPearls Publishing; 2021. Available from: <https://www.ncbi.nlm.nih.gov/books/NBK536998/>
11. Koroulakis A, Jamal Z, Agarwal M. Anatomy, head and neck, lymph nodes. In: *StatPearls* [Internet]. Treasure Island (FL): StatPearls Publishing; 2021. Available from: <https://www.ncbi.nlm.nih.gov/books/NBK513317/>
12. Conley J. Radical neck dissection. *Laryngoscope* 1975;85:1344–52.
13. Harish K. Neck dissections: radical to conservative. *World J Surg Oncol* 2005;3:21.

ORCID ID:

E. Patera 0000-0001-6154-4069;
A. Alashkham 0000-0003-2959-5039



Correspondence to: Abduelmenem Alashkham, PhD, MSc, MBBCh
University of Edinburgh, Old Medical School, Doorway 3, Teviot Place,
Edinburgh, EH8 9AG, UK
Phone: +44 131 650 2924
e-mail: abduelmenem.alashkham@ed.ac.uk

Conflict of interest statement: No conflicts declared.

This is an open access article distributed under the terms of the Creative Commons Attribution-NonCommercial-NoDerivs 4.0 Unported (CC BY-NC-ND4.0) Licence (<http://creativecommons.org/licenses/by-nc-nd/4.0/>) which permits unrestricted noncommercial use, distribution, and reproduction in any medium, provided the original work is properly cited. *How to cite this article:* Patera E, Alashkham A. Communicating vein between the right external and internal jugular veins: a case report. *Anatomy* 2021;15(1):84–87.

Fireproof plastinates

Okan Bilge , Servet Çelik 

Department of Anatomy, School of Medicine, Ege University, İzmir, Turkey

Abstract

Plastination is a method that has grown in popularity over time, used for the preparation of educational and exhibition samples. We have created many and various anatomical samples to be used in the education of our students in the plastination laboratory we have established since 2010. In this article, it is aimed to explain how our 10-year plastination collection was affected by the fire that broke out in our laboratory building in June 2020 and to bring this information to the literature.

Keywords: anatomy; education; fire; plastination

Anatomy 2021;15(1):88–90 ©2021 Turkish Society of Anatomy and Clinical Anatomy (TSACA)

Plastination has been developed and diversified with numerous studies published over the years since the first introduction of Von Hagens' technique.^[1,2] In recent years, studies that reveal the importance and value of plastination, especially with its contribution to health sciences education, come to the fore.^[3–7] With real tissue-based samples prepared with the plastination method, students are provided to learn anatomy in hygienic and safe environments, especially at the undergraduate level. Plastination also made it possible to enrich educational materials by creating samples dissected at different stages, coloring important structures, or cross-section samples prepared in different thicknesses from different planes.^[8–12] In addition to these, resistance to physical factors (such as ultraviolet or impact), no need for special storage conditions, and long-term usage of the plastinates provide economic use and sustainability of cadavers, which can be difficult to obtain in some countries.^[13]

In our department, we have been using plastinates, which we have produced with various techniques since 2010, together with embalmed samples in our students' practical anatomy lessons. While we prefer silicone plastination (Biodur Products GmbH, Germany) especially for preparing three-dimensional samples (such as dissected upper and lower extremities, thorax and cranium), we also prepare cross-sectioned samples with epoxy (Biodur Products GmbH, Germany) and polyester (Poliya, Turkey) techniques. However, with the technique we have developed, we can also produce silicone plastinates

from serial sectioned (2–10 mm) materials (such as sagittal foot, sagittal knee joint flexed, coronal hand and head sections).^[14,15] We archive the prepared samples by giving code numbers and store (also exhibit) them in glass-door cabinets at the entrance of the anatomy laboratory. These plastinates are used during the relevant practical lessons and students' positive feedbacks are received.

Unfortunately, most of our macroscopy laboratory was damaged in an unfortunate fire on June 15, 2020. This fire broke out in the entrance of the laboratory and affected the cabinets where the plastinates were stored. The cabinets were partially burned, and the glasses on the cabinet doors exploded and partially melted due to the heat (**Figure 1a**). According to the information received from the fire department, the temperature in the area where the cabinets are located has exceeded 700°C degrees. When we checked the condition of the plastinates inside the cabinets after the quenching and cooling processes, it was found that the plastic bases were completely melted, but surprisingly the plastinates did not suffer any damage. It was seen that the surfaces of the plastinates were coated with adhesive black soot (**Figure 1b**). All the plastinates in the cabinets were removed, the adhesive soot was cleaned twice in warm dishwashing water with a toothbrush and sponge, and the samples were rinsed and placed on blotting papers to dry (**Figures 1c and d**).

It has been observed that even after being exposed to extreme heat, covered with soot, and washed with deter-

gent water, the plastinates are preserved as on the first day and are not adversely affected by the whole process. Our entire collection is saved and usable.

Highly visual anatomical structures obtained by performing detailed and laborious dissections unfortunately lose these properties in long-term formalin fixation.

Thanks to plastination, the first-day characteristics of the detailed structures shown by dissections are preserved and educational materials that can be easily worked with bare hands and used in the same way for many years can be created. In addition, exposure to the negative effects of formalin such as bad odor, skin and mucosal irritation and other



Figure 1. (a) The damage done by fire. (b) Sectional head specimens completely coated with adhesive soot. (c) Cleaning the adhesive soot in warm dishwashing water with sponge, the remaining soot (white arrow heads) was then cleaned with the help of a toothbrush. (d) Rinsed and dried samples are ready for use.

toxic effects during practical lessons are also eliminated.^[3-5,7] It has been shown that not only fresh specimens, but also old formalin-fixed cadavers and organs can be plastinated, and that existing educational materials can be used in a healthier and longer time.^[13]

Today, plastination is carried out in many countries in medical and veterinary faculties and by some private companies.^[2,5] In our country, however, only a few plastination is done in the laboratories of a few faculties with limited facilities. Some universities are imported plastinated samples in limited numbers and at high costs to be used in anatomy lessons. The durability, resistance to physical factors, easy storage conditions, and long-term usage are well known properties of plastinated specimens. This article also deals with their resistance to fire and high temperatures and their ability to be cleaned with detergents.

We think that with the widespread production and use of plastinated materials in education in our country, the cadaver problem experienced in medical faculties will be solved to a certain extent, and the quality of education will be increased with appropriate educational materials and a positive contribution will be made to the economy.

In our literature search, we did not find a study containing direct information about the heat resistance of plastinates. Therefore, we think that the experience we gained as a result of a misfortune is important and should be shared.

Acknowledgements

We would like to thank all our assistants and employees who contributed to the reusability of our plastination collection after the fire. The authors sincerely thank those who donated their bodies to science so that anatomical research could be performed. Results from such research can potentially increase mankind's overall knowledge that can then improve patient care. Therefore, these donors and their families deserve our highest gratitude.

ORCID ID:

O. Bilge 0000-0002-8993-2271;
S. Çelik 0000-0002-1102-4417



Conflict of Interest

The authors declare that there is no conflict of interest.

References

1. von Hagens G. Impregnation of soft biological specimens with thermosetting resins and elastomers. *Anat Rec* 1979;194:247-55.
2. von Horst C, von Hagens R, Sora CM, Henry RW. History and development of plastination techniques. *Anat Histol Embryol* 2019; 48:512-7.
3. Chytas D, Piagkou M, Johnson EO, Tsakotos G, Mazarakis A, Babis GC, Nikolaou VS, Kaseta MK, Natsis K. Outcomes of the use of plastination in anatomy education: current evidence. *Surg Radiol Anat* 2019;41:1181-6.
4. Estai M, Bunt S. Best teaching practices in anatomy education: a critical review. *Ann Anat* 2016;208:151-7.
5. Sora MC, Latorre R, Baptista C, López-Albors O. Plastination-a scientific method for teaching and research. *Anat Histol Embryol* 2019;48:526-31.
6. von Horst C. Multiple polymer plastination: combining different types of polymers in teaching and exhibition plastinates. *Anat Histol Embryol*. 2019;48:577-83.
7. Riederer BM. Plastination and its importance in teaching anatomy. Critical points for long-term preservation of human tissue. *J Anat* 2014;224:309-15.
8. Nader PB, Henry RW, Sui HJ. Plastination of larger and massive specimens-With Silicone. *Anat Histol Embryol* 2019;48:547-51.
9. Steinke H, Pfeiffer S, Spänel-Borowski K. A new plastination technique for head slices containing brain. *Ann Anat* 2002;184:353-8.
10. Latorre R, de Jong K, Sora MC, López-Albors O, Baptista C. E12 technique: conventional epoxy resin sheet plastination. *Anat Histol Embryol* 2019;48:557-63.
11. Baptista CAC, DeJong K, Latorre R, Bittencourt AS. P40 polyester sheet plastination technique for brain and body slices: the vertical and horizontal flat chamber methods. *Anat Histol Embryol* 2019; 48:572-6.
12. Iliff S, Concha I, Chereminskiy V, Henry RW. Coloring plastinated specimens. *Anat Histol Embryol* 2019;48:552-6.
13. Bilge O, Çelik S, Boduc E. Plastination of old fixed locomotor system specimens and usage in education. *Ege Journal of Medicine* 2014;53:84-7.
14. Bilge O, Çelik S, Yörük MD, Koçer IB. Useful materials for cross-sectional anatomy education: silicone plastinated examples of foot and hand. *Austin Journal of Anatomy* 2018;5:1080.
15. Boduç E, Bilge O, Çelik S. Examination of pelvic anatomy by section plastination technique. *Anatomy* 2020;14:227-30.

Correspondence to:

Okan Bilge, MD
Department of Anatomy, School of Medicine, Ege University,
Bornova, 35100, Izmir, Turkey
Phone: +90 232 390 39 95
e-mail: okan.bilge@ege.edu.tr

Conflict of interest statement: No conflicts declared.

This is an open access article distributed under the terms of the Creative Commons Attribution-NonCommercial-NoDerivs 4.0 Unported (CC BY-NC-ND4.0) Licence (<http://creativecommons.org/licenses/by-nc-nd/4.0/>) which permits unrestricted noncommercial use, distribution, and reproduction in any medium, provided the original work is properly cited. *How to cite this article:* Bilge O, Çelik S. Fireproof plastinates. *Anatomy* 2021;15(1):88-90.

Obituary

<https://dergipark.org.tr/tr/pub/anatomy>

Received: March 26, 2021; Accepted: April 6, 2021

doi:10.2399/ana.21.Ob01

In dedication to Doğan Taner (1930–2021)

Deniz Demiryürek 

Department of Anatomy, Faculty of Medicine, Hacettepe University, Ankara Turkey

Anatomy 2021;15(1):91–94 ©2021 Turkish Society of Anatomy and Clinical Anatomy (TSACA)

This article is dedicated to the memory of Prof. Dr. Doğan Taner, the former Dean of Hacettepe University Faculty of Medicine and the head of Department of Anatomy, who passed away on March 12, 2021 in Ankara. He was one of the greatest clinical anatomist many of us are familiar with. It was not only my personal, but also all Turkish Anatomists' grief to learn the decease of Prof. Dr. Doğan Taner.

His contributions to medical education, clinical anatomy and personal supports to the development of academic career of many Turkish anatomists, including myself, will never be forgotten. I had the honor of being a research assistant to him and working together with, at the beginning of my academic life, which was a great privilege.

He was a wonderful mentor, a very knowledgeable person and an irreplaceable figure in Anatomy worldwide. He



Figure 1. Hacettepe Anatomy Family, 2019, Ankara. From left to right, upper row: Seza Arbay, Kübra Yıldırım, Beliz Taşçıoğlu, Emine Özkul, Ergül Ersoy, Tülin Aras; middle row: Doğan Akşit, Bedia Sancak, Doğan Taner, Siddık Karatay, Sezgin İlgi; lower row: Nuran Yener, Meserret Cumhur.

was also one of the honorary members of the Turkish Society of Anatomy and Clinical Anatomy. That is one of the several reasons why I wanted to write this article for his memory. You will have chance to read and learn more about him in this article.

Dr. Doğan Taner was born in Cyprus in 1930. After completing his primary, secondary and high school education in Cyprus, he started his medical education in İstanbul University Faculty of Medicine and graduated as a medical doctor in 1955.

He started his residency program in cardiology at New York Medical College, New York City, United States in 1955 and received his degree in 1960. He worked as a cardiologist at West Hendon Hospital-London and London University St. John's Hospital between 1960 and 1963. Since he was born in Cyprus, he joined the academic staff of Hacettepe University Faculty of Medicine as a foreign lecturer in 1964. He received his Associate Professor title in the Department of Anatomy and after being a Turkish citizen, he received his Professor of Anatomy title in 1971.

Prof. Dr. Doğan Taner was one of the founders of Department of Anatomy at Hacettepe University Faculty of Medicine and he was the head of the department for so many years until his retirement. Additionally, during his professional life at Hacettepe University, Dr. Taner worked as the faculty's Phase 2 medical students coordinator (1965–1966, 1969–1971), Director of Medical Technology High School (1967–1971), General Secretary of Institute of Population Studies (1971–1972), Chief



Figure 2. The board of "Associate Professor Academic Title". From left to right: Meserret Cumhur, Doğan Akşit, Bedia Sancak, Siddik Karatay, İlhan Eralp, Doğan Taner.

Coordinator of Medical Education (1971–1981), Director of Institute of Modern Linguistics (1973–1974), Head of Basic Medical Sciences (1973–1981, 1994–1997), Dean of Health Sciences Faculty (Medicine and Health Sciences Post Graduation Education Faculty) (1975–1981), Dean of Faculty of Medicine (1982–1991) and Editor of Hacettepe Medical Journal (1983–1991).

Dr. Taner was one of the founders of Association of Medical Education in Europe and worked as an advisory board member between 1972 and 1994. He also worked as General Secretary of Education Council of Medical and Health Sciences of Turkish Universities (1978–



Figure 3. New year party, 1994, Ankara. From left to right: Nuran Yener, Doğan Akşit, Bedia Sancak, Doğan Taner, Meserret Cumhur, Engin Kural, Selda Önderoğlu, Alper Atasever.

1994), one of the founders of Turkish Medical Education Presidential (1984–1994), Executive Committee member of Association of Medical Deans in Europe (1990–1993), Membership of The Scientific and Technological Research Council of Turkey-Scientist Education Group (1991–1993), Membership of Interuniversity Board Associate Professor Ethics Board (2002–2004). In 1997 Dr. Taner was appointed as the advisor of President of Higher Education Council.

Prof. Dr. Doğan Taner worked as a consultant for World Health Organization in 1972 and 1976. At several meetings in the field of medical education, he represented his university and country at European Council, OECD and ECFMG many times.

His scientific fields of interest were clinical anatomy and medical education. After a lot of effort and hard work, he founded the first ever-English Faculty of Medicine in Turkey. He also applied the systematic committee learning system in medical education instead of classical medical education, which was a great innovation for Turkey in the field of medicine.

Not only was many international publications, Dr. Taner also the editor of two books; Functional Anatomy and Functional Neuroanatomy. In July 22, 1997 Prof. Dr.

Doğan Taner retired from Hacettepe University after many years of productivity and hard work. He was married to Gudrun Taner for 55 years and they had two daughters, Deniz and Aylin.

He attended the meetings of international associations frequently, also won prizes for 'Medical education'. He remained memorable for his style of lectures, presenting with an easiness and high standard. During his lectures, he used to use a pointer for choosing a student, and then he would ask his questions about the lecture to the student behind or next to him, so that he could keep the attention on the lecture until the end of time.

When I saw him as a presenter for the first time at a lecture of neuroanatomy of at Hacettepe in 1996, I was deeply moved and impressed by the manner of his presentations, the standard and the clinical background of his scientific work. He became an idol for me, to work hard and to my best in presenting our scientific work on national and international platforms. Moreover, he was a respected person with high reputation at that time. In addition, he always highlighted the affiliation to the University of Hacettepe and was proud to be part of the department and faculty. All the upcoming years, he surprised everyone with new investigations and never rested to support young



Figure 4. Hacettepe Anatomy Family, 1992, Ankara. From left to right; upper row: Hakan Öztürk, Mine Ergun, Alper Atasever, Cem Denk, Selda Önderoğlu, Emine Özkul, Mustafa Aldur, Mürvet Tuncer, Demet Zağyapan, Selçuk Sürücü, Mustafa Sargon, Barbaros Durgun, Hamdi Çelik, Engin Yılmaz; lower row: Ruhgün Başar, Doğan Aksit, Bedia Sancak, Doğan Taner, Engin Kural, Sezgin Ilgi, Beliz Taşçıoğlu.

colleagues not only from our department, such as myself, but especially encouraged young scientists to come to Hacettepe. Many visits were enforced by Prof. Taner's support; many of us, nowadays-experienced scientists still remember unforgettable memories at Hacettepe.

The importance of the clinical aspects of anatomy and teaching anatomy in medical field always remained a priority in Professor Taner's scientific and academic career. For him, science was the most important part of the anatomist's work. He always encouraged us for publishing articles in international journals with high impact factors and followed our progress. It was not only a great motivation for us, but also an effective control system of our studies.

Teaching was also the other important part. I was lucky to be able to assist him in his lectures for many years. He was one of the professors, who was able to present almost any topic of the human body without any prior preparation. He was using slides of the anatomical atlases spontaneously during the lecture and he had a wonderful memory about the anatomical details present inside the slide contents.

All his work, his love to study and to teach was alive in him until the very end. He would read anatomy from the latest edition of Gray's during the nights and the day after,

would ask us questions from the things he read the previous night. Although he retired after working so many years in the field of medical and anatomy education, I often took his advice due to his experience and passion for Anatomy. The passion and his spirit influenced so many of us and encouraged us in becoming a better teacher, better scientist and better anatomist daily.

Professor Taner; thank you for all moments; thank you for the time we could share together; thank you for being a personal highlight and unforgettable professor of our anatomical community. Your vision and multifaceted work will remain alive in all of us, to inspire us and therefore extend its light to so many generations to come.

Acknowledgement

Please see video supplemental content, https://drive.google.com/file/d/1c5Dp_9QcHux5cAv9Ma82VYER8TKZ1xH7/view?usp=sharing; which shows the speech of Prof. Bülent Altun (Dean of Hacettepe University Faculty of Medicine) and https://drive.google.com/file/d/1-GH2z2_tgj5VLRXKEhMbfmWPlUe7bIp/view?usp=sharing; which shows the speech of Deniz Taner Gökçe (elder daughter of Prof. Doğan Taner).

ORCID ID:

D. Demiryürek 0000-0001-8781-1719



Correspondence to:

Deniz Demiryürek, MD, PhD
Department of Anatomy, Faculty of Medicine, Hacettepe University,
06100, Sıhhiye, Ankara, Turkey
Phone: +90 312 305 23 59
e-mail: mdeniz@hacettepe.edu.tr

Conflict of interest statement: No conflicts declared.

This is an open access article distributed under the terms of the Creative Commons Attribution-NonCommercial-NoDerivs 3.0 Unported (CC BY-NC-ND3.0) Licence (<http://creativecommons.org/licenses/by-nc-nd/3.0/>) which permits unrestricted noncommercial use, distribution, and reproduction in any medium, provided the original work is properly cited. *Please cite this article as:* Demiryürek D. In dedication to Doğan Taner (1930–2021). *Anatomy* 2021;15(1):91–94.

Eulogy for Professor Doğan Taner

İskender Sayek^{1,2} , Erdal Akalın³ 

¹Department of General Surgery (Emeritus), Faculty of Medicine, Hacettepe University Ankara, Turkey

²Association for Evaluation and Accreditation of Medical Education Programs (TEBDAD), İzmir, Turkey

³Department of Internal Medicine (Emeritus), Faculty of Medicine, Hacettepe University, Ankara, Turkey

Anatomy 2021;15(1):95 ©2021 Turkish Society of Anatomy and Clinical Anatomy (TSACA)

We were fortunate to have been students in the 1960's at Hacettepe University Medical School mainly because there was a spirit of compassion in every educator then. After graduation and specialty training we had a chance to work together as colleagues for many years with these outstanding educators. Among these educators Professor Doğan Taner was in a special position as a role model being a prominent educator, educationalist and administrator for all students.

As an Educator

As an educator Dr. Taner in the mid sixties taught us anatomy very enthusiastically and to learn in depth for our future carrier. He always acted as he preached his principles. He was a very strict educator, with discipline being his priority. But he was very affectionate, tender hearted and sincere to the students. We had always to be alert during his lectures or at the anatomy lab. In his lectures he impressed us as he taught functional anatomy in an interactive manner. Briefly we would like to state that he was a very good "role model" for us as an educator.

As an Educationalist

As a medical educationalist, he was one of the main leaders in Turkey to make a reform in medical education. In the sixties he was the pioneer to implement a system-organ based

curriculum at Hacettepe Medical School. With his efforts system-organ based curriculum gained popularity in Turkish medical schools. He was one of those who implemented the concept of integration into medical education. After his retirement he continued his efforts to improve the quality of medical education in Turkey as a consultant in the Higher Educational Council.



Figure 1. Doğan Taner in his young ages.

As an Administrator

Initially he served as a Dean in the School of Health Sciences and later at Hacettepe University School of Medicine for a period over ten years. He combined his expertise as an educationalist with his administrative ability to improve the quality of medical education. As an administrator he was always devoted, fair and principle oriented.

We would like to stress that Dr. Taner was a good "role model" for us as an educator, educationalist and administrator. His efforts will be profoundly remembered as his students continue to practice or teach medicine.

ORCID ID:

I. Sayek 0000-0001-5951-3511;
E. Akalın 0000-0001-9502-3480

deomed®

Correspondence to:

İskender Sayek, MD
Association for Evaluation and Accreditation of Medical Education Programs (TEBDAD), İzmir, Turkey
Phone: +90 312 305 23 59
e-mail: isayek@gmail.com

Conflict of interest statement: No conflicts declared.

This is an open access article distributed under the terms of the Creative Commons Attribution-NonCommercial-NoDerivs 3.0 Unported (CC BY-NC-ND3.0) Licence (<http://creativecommons.org/licenses/by-nc-nd/3.0/>) which permits unrestricted noncommercial use, distribution, and reproduction in any medium, provided the original work is properly cited. Please cite this article as: Sayek İ, Akalın E. Eulogy for Professor Doğan Taner. Anatomy 2021;15(1):95.

Obituary

<https://dergipark.org.tr/tr/pub/anatomy>

Received: April 2, 2021; Accepted: April 3, 2021

doi:10.2399/ana.21.Ob03

My dear teacher Professor Doğan Taner

Nedim Sezgin İlgi 

Department of Anatomy, Near East University Faculty of Medicine, Nicosia, North Cyprus

Anatomy 2021;15(1):96 ©2021 Turkish Society of Anatomy and Clinical Anatomy (TSACA)

Doğan Taner was one of the strongest representatives of the Hacettepe school ecole. He was disciplined, decisive, fair person abiding by the rules.

He was one of the best person who prepared the bylaws of Hacettepe Faculty of Medicine and put them in practice in its founding years. He always invited myself to help him and contributed me in writing these legislations. I was very young at those times and had got angry with him thinking that these were not my business. But then I realized that his intention was teaching me how to prepare bylaws and regulations, how to interpret them and how important to use even a single word.

Doğan Taner was an excellent manager. He made fair decisions and was equal to everyone. He had own unique features. He obeyed the rules, he did not compromise, but the truth was that he was one of the student-friendly manager ever. Other teachers always used him. Since no one dared to want anything from him, the others would tell as they cannot do anything since he asked.

I learned a lot from him as my teacher and it used this knowledge all through my life. Most of all, I learned how to react without losing manner, to stay calm and not make decisions in anger and be stoical.

My teacher Doğan Taner was a very good educator. He wrote more scientific articles about education than anatomy. Most of his articles were on the integrated system.

Everyone respected him because he was respected and powerful. His friends would trust him and say, "Doğan knows and does it".

He had a very good archive and kept everything. We were preparing a booklet in the 30th anniversary of the University. For this, I had to find the official newspaper of Hacettepe University announcing its foundation; but I couldn't be able to find anywhere. When I told this problem to him, he just took that newspaper from one of his files and gave it to me.

Although he look very serious and seems to keep his distance, he was possessed of both humor and wit.

I wish God's mercy on my teacher. May him rest in peace.



Figure 1. Doğan Taner, before his retirement.

ORCID ID:

N. S. İlgi 0000-0001-7822-8927

deomed®

Correspondence to:

Nedim Sezgin İlgi, DDS, PhD
Department of Anatomy, Faculty of Medicine, Near East University Nicosia,
North Cyprus
Phone: +90 392 223 64 64
e-mail: sezgin.ilgi@neu.edu.tr

Conflict of interest statement: No conflicts declared.

This is an open access article distributed under the terms of the Creative Commons Attribution-NonCommercial-NoDerivs 3.0 Unported (CC BY-NC-ND3.0) Licence (<http://creativecommons.org/licenses/by-nc-nd/3.0/>) which permits unrestricted noncommercial use, distribution, and reproduction in any medium, provided the original work is properly cited. Please cite this article as: İlgi NS. My dear teacher Professor Doğan Taner. Anatomy 2021;15(1):96.

Being students of Professor Doğan Taner

Ayşegül Fırat¹ , İlkan Tatar¹ , Nihal Apaydın²⁻⁵ 

¹Department of Anatomy, School of Medicine, Hacettepe University, Ankara, Turkey

²Department of Anatomy, School of Medicine, Ankara University, Ankara, Turkey

³Department of Multidisciplinary Neuroscience, Institute of Health Sciences, Ankara University, Ankara, Turkey

⁴Brain Research Center (AU-BAUM), Ankara University, Ankara, Turkey

⁵Neuroscience and Neurotechnology Center of Excellence (NÖROM), Ankara, Turkey

Anatomy 2021;15(1):97–98 ©2021 Turkish Society of Anatomy and Clinical Anatomy (TSACA)

Prof. Dr. Doğan Taner held many administrative positions including deanship for the longest period (1981–1998) in Hacettepe Medical School for many years. He shaped the mission and vision of the medical faculty. He always prioritized the qualified graduate and postgraduate education. As medical students that attended his anatomy lectures we were very lucky. He was a very impressive and extraordinary person. He was an idol for many young medical students and fellows of anatomy. It was the first time that he was calling us as ‘doctors’ in second year of the medical school. And we calling him as “Prof. DT” or just “DT”. His name was mentioned a lot by our peers and they were telling that his lectures should not be missed, but it is good to wear black or white, avoiding colorful things. We understood the reason why, once we attended his lectures.

He was one of the unforgettable figures among our lecturers. No-one can forget the entrance moments of him to the amphitheater to give his lecture. Those amphitheatres, at those time; red and green lecture halls, which is now the cultural center of Hacettepe University, were always dark to have good projection inside making the atmosphere even more spiritual. These moments are of like a divine ceremony. With his black long cloak on his shoulders, followed by the research assistants; one carrying his long stick, the other carrying his lanternslides, he was walking in slow steps from back entrance to the front and greeting the students who are sitting at the first seat of each row. He had such a different and special aura that affected everyone. All of the other faculty members and research assistants of Anatomy Department were joining to his lectures and sitting at the front row. Once he has started his lecture,



Figure 1. Prof. Doğan Taner (1930–2021), Professor of Anatomy and Chairman, Department of Anatomy, Faculty of Medicine, Hacettepe University, Ankara, Turkey.

no one would say a word and carefully listen not to lose any word spoken by him. He would tell the upcoming slide number and the page numbers from Carpenter textbook, Netter or Sobotta before the assistant change the slide. Since he was not just telling the structure; he had always had a clinical history or a case to be told related with the subject. We learned anatomy from him in

such a way that we were aware of what we learn and why. There was no way to come to his lectures un-prepared. Because he liked to involve us to his comments and enjoyed discussing and talking with us. He always asked questions making us to analyze and interpret what we learn. He would raise a friend of ours by saying “You; Mr. Doctor, in the red shirt 2 row from the back, can you please answer this question?” After asking his name, where he was from, what his mother and father did, he would ask a very different and difficult question for us at that time, for example about how the proximal and distal parts of a femoral neck fracture would move due to a mid-shaft femoral fracture in a vehicle accident. In the following lessons, most of our classmates preferred to wear unobtrusive colors. However, he would remember our names once he learns, and he would ask by saying “Dr. İlkan even though you are in black t-shirt now, I recognized you and I would like to listen your comments” His questions that he asked in our classical exams were always tricky. It was not possible to answer them without fully understanding the subject. His style may be considered as “scary” at those years when we were young, but we then realized that his approach thought us that “anatomy” forms the basis for the practice of medicine and is much more than just memorization of list of names. We realized at early years of our medical education that the network of information needed to visualize the position of structures and an understanding of anat-

my contributes to all areas of medicine making it far beyond simple memorization.

He was one of the professors that is excited about teaching and integrating the basic sciences with the clinical practices. He had the experience and enthusiasm about planning the clinical anatomy lectures which would be the first among medical faculties. As a mentor he will be remembered with his emphasis on clinically applied interactive anatomy lectures, giving importance to learning a foreign language and studying regularly. Except for the education, he attached great attention to research. His passion about a good medical student was studying regularly and being punctual.

Although he was an academician who studied cardiology in the USA, he chose basic sciences, morphology as it was then called, with the will and insistence of Hocabay (Prof. İhsan Dođramacı M.D., founder of Hacettepe University), and continued his duty as the dean of Hacettepe University Faculty of Medicine as a professor of basic medical sciences for a very long time. Although we never worked with him due to his retirement, he has always been with us as our founding teacher at department’s meetings and gatherings.

We are proud to be his students and more proud to become his colleagues at the end. He was such a great role model and he will always be kept in our memory as an influential mentor and a great anatomist.

ORCID ID:

A. Firat 0000-0001-5105-0057;
I. Tatar 0000-0003-2532-8582;
N. Apaydın 0000-0002-7680-1766

**Correspondence to:** Nihal Apaydın, MD, PhD

Department of Anatomy, Ankara University School of Medicine,
Sıhhiye 06100 Ankara, Turkey
Phone: +90 312 595 82 48
e-mail: napaydin@gmail.com

Conflict of interest statement: No conflicts declared.

This is an open access article distributed under the terms of the Creative Commons Attribution-NonCommercial-NoDerivs 4.0 Unported (CC BY-NC-ND4.0) Licence (<http://creativecommons.org/licenses/by-nc-nd/4.0/>) which permits unrestricted noncommercial use, distribution, and reproduction in any medium, provided the original work is properly cited. *How to cite this article:* Firat A, Tatar İ, Apaydın N. Being students of Professor Dođan Taner. *Anatomy* 2021;15(1):97-98.

Table of Contents

Volume 15 / Issue 1 / April 2021

(Continued from back cover)

Protective role of sildenafil citrate in isoniazid-rifampicin induced histomorphological changes in liver of albino mice	52
Najma Hameed, Khalid Farooq	
Numerical variations and localization of foramen spinosum in 3D-CT images	59
Yadigar Kastamoni, Ahmet Dursun, Veysel Atilla Ayyıldız, Kenan Öztürk	
Morphometric evaluation of nasolacrimal duct	64
Burcu Erçakmak Güneş, Alper Vatansever, Deniz Demiryürek, Ekim Gümeler	
Teaching Anatomy	
The contribution of plastinates to teaching complex anatomy of the heart	69
Güneş Aytaç, Eren Ögüt, Rahime Şekerci, Sezgi Gürçay, Nurettin Oğuz, Muzaffer Sindel	
Review	
Lungs and hypoxia: a review of the literature	76
Mustafa F. Sargon	
Case Report	
Communicating vein between the right external and internal jugular veins: a case report	84
Eleni Patera, Abduelmenem Alashkham	
Viewpoint	
Fireproof plastinates	88
Okan Bilge, Servet Çelik	
Obituaries	
In dedication to Doğan Taner (1930–2021)	91
Deniz Demiryürek	
Eulogy for Professor Doğan Taner	95
İskender Sayek, Erdal Akalın	
My dear teacher Professor Doğan Taner	96
Nedim Sezgin İlgi	
Being students of Professor Doğan Taner	97
Ayşegül Fırat, İlkan Tatar, Nihal Apaydın	

On the Front Cover:

Prof. Doğan Taner (1930–2021), Professor of Anatomy and Chairman, Department of Anatomy, Faculty of Medicine, Hacettepe University, Ankara, Turkey. From Fırat A, Tatar İ, Apaydın N. Being students of Professor Doğan Taner. *Anatomy* 2021;15(1):97-98.

Table of Contents

Volume 15 / Issue 1 / April 2021

Editorial

What 2021 takes and what it brings iii
Nihal Apaydın

Original Articles

Investigation of the moderate toxicity of agricultural pesticides cyantraniliprole, boscalid and spiromesifen *in vitro* using neurotoxicity screening test 1
Emine Müge Karakayalı, Duygu Kekeç, Tuna Önal, İbrahim Tuğlu

***In silico* transcriptomic analysis of ascending colon cancer unearths known and novel genes and gene sets regard to characteristic features of colon cancer** 11
Can Türk

Three-dimensional muscle architecture of the infant and adult trapezius: a cadaveric study 26
Mikaela L. Stiver, Luke R. Bradshaw, Ethan M. Breinhorst, Anne M. R. Agur, S. Ali Mirjalili

Perforator flaps based on the deltoid branch of the thoracoacromial artery: anatomical study 36
Philippe Manyacka Ma Nyemb, Christian Fontaine, Véronique Duquennoy-Martinot, Xavier Demondion

Morphometry of the hyoid bone: a radiological anatomy study 44
Ahmet Dursun, Mehtap Ayazoğlu, Veysel Atilla Ayyıldız, Yedigâr Kastamoni, Kenan Öztürk, Soner Albay

(Contents continued on inside back cover)